

**University of Manchester**  
**Institute of Science and Technology**  
**Department of Instrumentation and Analytical Science**

**Diffraction Efficiency Measurements  
for Liquid Crystals used in  
Spatial Light Modulators**

**By**

**Fraser J. Dickin, B.Sc., M.Sc.**

**A Thesis submitted to the  
UNIVERSITY OF MANCHESTER  
for the Degree of  
Doctor of Philosophy  
in the Faculty of Technology**

**August 1988**

## **Declaration**

**No portion of the work referred to in this thesis has been submitted in support of an application for another degree or qualification of this or any other University or institution of learning.**

## **About the Author**

After graduating from Salford University in July 1983 with a B.Sc. degree in Biomedical Electronics, the author attended U.M.I.S.T. to study for an M.Sc. in Microprocessor Engineering and Digital Electronics. The dissertation part of the M.Sc. was spent in the Department of Instrumentation and Analytical Science (D.I.A.S.) researching Optical Computers, from which some of the ideas for this thesis originated. The research described in this thesis is the product of a two year Total Technology Ph.D. working within D.I.A.S. and the Displays Division at S.T.L. Ltd., Harlow.

## **Acknowledgements**

**I would like to thank the following people for their help with this work :-**

**Professor M.S.Beck, Dr. Neil Collings, and Dr. Bob Green.**

**Gail, my parents, and my grandparents.**

**I would also like to thank :-**

**at D.I.A.S., U.M.I.S.T. :- Cheng Gang Xie, Iain Gregory, Andy Jane, Simon Brown,  
Per Lindstrøm and Richard Taylor.**

**at S.T.L. Ltd., Harlow :- John Brocklehurst, Bill Crossland, Peter Ross, Barbara  
Needham, Pat Gunn, Chris Walker and Avril Boucher.**

**at C.M.I., Norway :- Kåre Lunde, Jeremy Cook, Kåre Villanger, Cliff & Tricia  
Addison, Richard Chamberlain and all at the IBM Bergen  
Scientific Centre.**

## **Dedication**

**This work is dedicated to**

**my wife Gail,**

**my parents Jean and John,**

**and my grandparents Leslie and Ivy.**

## Preface

The work for this Ph.D. was carried out under the auspices of the Total Technology Award Scheme. Through this scheme the author was appointed the Displays Division at S.T.L. Ltd., Harlow, as his collaborating company which was developing specialized liquid crystal devices for use in optical systems. Also, the Displays Division and the Department of Instrumentation and Analytical Science (D.I.A.S.) at U.M.I.S.T. were involved with the J.O.E.R.S. P.A.O.D.A.<sup>†</sup> programme whose collective aim was to develop and demonstrate a working optical correlation system<sup>‡</sup>.

The contributions made by the author with respect to optical correlation systems (see Figure 1.1) were concerned with both the input and the output stages of an optical correlator. At the input stage the liquid crystal measurement techniques, put forward in the thesis, will permit future spatial light modulator (SLM) manufacturers to select an appropriate type of liquid crystal for use in their SLM. Some optical correlation systems use adaptive feedback from the output stage in order to improve system performance (for example, changing the orientation of the input image when recognizing patterns), therefore the performance of the output stage was considered during this project. Specifically, the design and development of the electronic optical correlation peak detector for the J.O.E.R.S. P.A.O.D.A. Demonstrator (I) system promoted ideas for additional, more powerful and flexible output detector systems which will be incorporated into future systems.

The major aims of this work are as follows,

- Measurement of liquid crystal director alignment in experimental cell to ensure a reproducible response.
- Determination of the suitability criteria for a liquid crystal employed in a SLM by measuring its diffraction efficiency properties.
- Comparison of experimental results with mathematical modelling of non-Ronchi diffraction gratings.
- Development of a real-time correlation peak detector for use in the output stage of an optical correlation system.

---

<sup>†</sup> Joint Opto-Electronics Research Scheme—Programmable All-Optical Displays and their Applications

<sup>‡</sup> Further details of the demonstrator system are given in chapter 7

## **Abstract**

The real-time input device used to interface an external stimulus to an optical processor (which utilizes the inherent parallelism and speed of light) is referred to as a spatial light modulator (SLM). In liquid crystal-based SLMs a liquid crystal layer is used to spatially modulate light passing into the optical processor. However, manufacturers of such devices select liquid crystals on the basis of their suitability for use in displays. This thesis proposes a novel measurement technique to enable future SLM manufacturers to determine the optimal parameters of a liquid crystal chosen for use in a SLM.

The technique is based on measuring the diffraction efficiency of a liquid crystal, this being directly proportional to its spatial modulation efficiency. To evaluate the technique, a number of treated experimental cells were filled with nematic liquid crystal and a square wave grating pattern electrically written onto the layer. The voltage across this layer was varied and the diffraction efficiency of the grating, when a coherent laser was shone through it, was measured. The intensities of the diffracted orders were measured initially by a photographic method and subsequently by a computer controlled photometer. The diffraction efficiency results compared favourably with the theoretical predictions for non-Ronchi gratings derived from Sommerfeld's work on diffraction gratings.

The description of a real-time optical correlation peak detector system is given. The detector was used in the output stage of an optical correlation system to locate the position and intensity of a correlation peak. This information was fed back to the input stage of the system enabling the position of the object causing the highest peak to be optimized.

# Contents

Declaration . . . . .	i
About the Author . . . . .	ii
Acknowledgements . . . . .	iii
Dedication . . . . .	iv
Preface . . . . .	v
Abstract . . . . .	vi
Contents . . . . .	vii
List of Figures . . . . .	x
List of Symbols . . . . .	xiii
<b>1 Introduction . . . . .</b>	<b>1</b>
<b>1.1 An Overview of Optical Processing . . . . .</b>	<b>1</b>
<b>1.2 Forms of Spatial Light Modulator . . . . .</b>	<b>2</b>
<b>1.3 Types of SLM—A Summary . . . . .</b>	<b>5</b>
<b>1.4 Direction of Research . . . . .</b>	<b>6</b>
<b>1.5 Aims and Objectives . . . . .</b>	<b>8</b>
<b>1.6 Organisation of Thesis . . . . .</b>	<b>9</b>
<b>2 An Introduction to Liquid Crystals . . . . .</b>	<b>10</b>
<b>2.1 Chapter Summary . . . . .</b>	<b>10</b>
<b>2.2 History of Liquid Crystals . . . . .</b>	<b>10</b>
<b>2.3 Mesophases . . . . .</b>	<b>11</b>
<b>2.4 Classification of Thermotropic liquid crystals . . . . .</b>	<b>11</b>
<b>2.3.1 Nematic Order . . . . .</b>	<b>12</b>
<b>2.3.2 Cholesteric Order . . . . .</b>	<b>12</b>
<b>2.3.3 Smectic Order . . . . .</b>	<b>13</b>
<b>2.4 Physical Properties of Mesophases . . . . .</b>	<b>13</b>
<b>2.5 Use of Liquid Crystals for Displays . . . . .</b>	<b>15</b>
<b>2.6 Mechanisms of Surface Alignment . . . . .</b>	<b>16</b>
<b>2.7 Methods of Liquid Crystal Alignment . . . . .</b>	<b>18</b>
<b>2.8 Alignment of Liquid Crystals on Smooth Surfaces . . . . .</b>	<b>18</b>
<b>2.8.1 Inorganic Substrates . . . . .</b>	<b>18</b>
<b>2.8.2 Organic Polymer Substrates . . . . .</b>	<b>19</b>
<b>2.9 Alignment on Grooved Surfaces . . . . .</b>	<b>19</b>
<b>2.10 Alignment by Surface Active Agents . . . . .</b>	<b>21</b>
<b>2.11 Alignment by Silane treated surfaces . . . . .</b>	<b>21</b>
<b>2.12 Tilted Alignment . . . . .</b>	<b>22</b>
<b>2.13 Summary of Liquid Crystal Alignment Techniques . . . . .</b>	<b>22</b>



2.14	Measurement of Tilt Angles	23
2.14.1	Crystal Rotation Method	23
2.14.2	Capacitance Method	24
2.14.3	Magnetic Null Method	25
2.15	Summary of Tilt Angle measurement methods	25
3	Electro-Optic Phenomena	27
3.1	Chapter Summary	27
3.2	Introduction	27
3.3	Dielectric Effects	28
3.3.1	The Freedericksz Transition	28
3.3.2	Electrically Controllable Birefringence	28
3.3.3	Twisted Nematic Effect	29
3.3.4	Cholesteric to Nematic Transition	30
3.3.5	Absorption Effects	31
3.3.5.1	Guest-Host Effect	31
3.3.5.2	Dyed Phase Change Effect	32
3.4	Conduction Induced Effects	32
3.4.1	Dynamic Scattering	33
3.4.2	Optical Storage	34
3.5	Thermo-Optic Effects	35
3.5.1	Cholesteric Temperature Sensors	35
3.5.2	Thermal Smectic Effects	35
3.6	Summary of Liquid Crystal Electro-Optic Effects	36
3.7	The Elastic Continuum Theory of Liquid Crystals	37
3.8	Electric Field Deformations of various configurations	38
3.8.1	A Parallel homogeneous liquid crystal cell	38
3.8.2	Tilted Homogeneous Cell	43
4	Theory of Phase and Amplitude Diffraction Gratings	45
4.1	Chapter Summary	45
4.2	Introduction	45
4.3	Mathematical Description of a Ronchi Grating	47
4.3.1	Ronchi Phase Grating	47
4.3.2	Ronchi Amplitude Grating	49
4.4	Treatment of Non-Ronchi Gratings	50
4.4.1	Non-Ronchi Phase Grating	51
4.4.2	Non-Ronchi Amplitude Grating	53
5	Experimental Details	55
5.1	Chapter Summary	55
5.2	Introduction	55
5.3	Construction of the Experimental Liquid Crystal Cells	55
5.4	Phase Retardance	58
5.5	Experimental arrangement for measuring Phase retardance	59
5.5.1	Method A	59
5.5.2	Method B	61

5.6	Experimental Arrangement for measuring Diffraction Efficiency . .	62
5.6.1	The Photographic Method . . . . .	62
5.6.1.1	Calibration of 10E75 Film . . . . .	63
5.6.1.2	Diffraction Efficiency Measurement . . . . .	64
5.6.2	Computer Controlled Data Logger . . . . .	65
5.6.2.1	Hardware Components of the Data Logger . .	66
5.6.2.2	Software Components of the Data Logger . . .	67
6	Results . . . . .	69
6.1	Chapter Summary . . . . .	69
6.2	Introduction . . . . .	69
6.3	Discussion of the Phase Retardance results . . . . .	71
6.4	Discussion of the Diffraction Efficiency results . . . . .	73
6.4.1	Explanation of the D.E. versus voltage results . . . . .	74
6.4.1.1	Magnitude variations between cell types . . . .	74
6.4.1.2	Parallel readings > Antiparallel readings . . .	76
6.4.1.3	First order readings > second order readings . .	77
6.4.1.4	Number of Diffraction Efficiency peaks . . . .	78
6.5	Use of the D.E. technique as a suitability criterion . . . . .	79
7	Total Technology Aspects of the Research. . . . .	82
7.1	Chapter Summary . . . . .	82
7.2	Introduction . . . . .	82
7.3	Operational Aims of the Demonstrator . . . . .	83
7.4	Output Detection System . . . . .	84
7.5	Operation of the Peak Detector Circuit . . . . .	85
7.6	Controlling Software . . . . .	86
7.7	Suggestions for improvements to the Peak Detector system . . . .	87
7.8	Conclusion for the Total Technology Aspects . . . . .	88
8	Conclusion & Suggestions for Further Work . . . . .	89
8.1	Conclusion . . . . .	89
8.2	Suggestions for Further Work . . . . .	91
<b>Appendices</b>		
A	References . . . . .	93
B	Data Logger Software . . . . .	98
C	Peak Capture Software . . . . .	109
D	Gaussian Quadrature Programs . . . . .	120
E	Liquid Crystal Parameters . . . . .	128

## List of Figures

- 1.1 General Architecture of an Optical Recognition System.**
- 1.2 Schematic Diagram of an Optically Addressed liquid crystal Spatial Light Modulator.**
- 2.1 Orientation of molecules in the three types of Thermotropic liquid crystal.**
- 2.2 Three elasticity components of a liquid crystal.**
- 2.3 Diagram of a 'standard' liquid crystal experimental cell—cross section.**
- 2.4 Liquid crystal director alignments on treated surfaces.**
- 2.5 Alignment of long molecular liquid crystal axes on grooved surfaces.**
- 2.6 Liquid crystal director orientation induced by evaporated silicon oxide.**
- 2.7 Tilt angle of the liquid crystal nematic director produced by different surface treatments.**
- 2.8 Liquid crystal director orientations in parallel rubbed, antiparallel rubbed and twisted aligned cells.**
- 2.9 Cross section of a liquid crystal cell.**
- 3.1 Electrically controllable birefringence effect above and below the voltage threshold in NDA & PDA nematic liquid crystals.**
- 3.2 Two types of nematic liquid crystal filled SLM.**
- 3.3 Twisted Nematic Effect.**
- 3.4 Graphs showing the transmission and Optical Rotation *vs.* voltage for a nematic liquid crystal with PDA.**
- 3.5 Electric field induced Cholesteric to Nematic phase change.**
- 3.6 Guest-Host effect in nematic liquid crystal cell.**
- 3.7 Induction of fluid flow in a nematic liquid crystal by alternating currents below the critical frequency.**
- 3.8 Optical storage effect of a nematic-cholesteric mixture using high and low frequency signals.**
- 3.9 A parallel homogeneous liquid crystal cell.**
- 3.10 Graph of  $\theta_m$  *vs.*  $U/U_0$  for different values of  $\theta_T$ .**
- 3.11 Graph of  $\theta$  *vs.*  $Z/d$  at various values of  $U/U_0$  for a parallel homogeneous cell.**
- 3.12 Graph of Retardance *vs.*  $U/U_0$  for a parallel homogeneous cell.**
- 3.13 A tilted homogeneous liquid crystal cell.**
- 3.14 Graph of  $\theta_m$  *vs.*  $U$  for different values of  $\theta_T$ .**
- 3.15 Graph of Percentage Retardance *vs.*  $U$  for different values of  $\theta_T$ .**
- 4.1 Graph of D.E. *vs.* Phase Retardance for a Ronchi Phase Grating.**

- 4.2 Graph of D.E. *vs.* Grating Thickness for a Ronchi Amplitude Grating.**
- 4.3 Graph of D.E. *vs.* Phase Retardance for a non-Ronchi Phase Grating.**
- 4.4 Graph of D.E. *vs.* Grating Thickness for a non-Ronchi Amplitude Grating.**
- 5.1 Experimental cell dimensions.**
- 5.2 Schematic diagram of a Soleil Babinet Compensator.**
- 5.3 Experimental arrangement for measuring the Phase retardance of the liquid crystal in the cell.**
- 5.4 Experimental arrangement for measuring the the Diffraction Efficiency of the liquid crystal in the cell.**
- 5.5 Schematic diagram of a dual-beam Joyce Loebel Microdensitometer.**
- 5.6 Characteristic  $D$  *vs.*  $\log E$  curve for the 10E75 Agfa Gevaert Film.**
- 5.7 Typical Diffraction Pattern from experimental cell.**
- 5.8 Microdensitometer trace of the horizontal diffraction pattern along 'X'.**
- 5.9 Sequence of events necessary to produce Diffraction Efficiency *vs.* voltage readings.**
- 5.10 Sequence of events performed by the computer controlled data logger in order to obtain D.E. *vs.* voltage results.**
- 5.11 Circuit Diagrams of Computerized data logger.**
- 5.12 Flowchart for Data Logger.**
- 6.1 Experimental arrangements showing orientations of incident polarized light & liquid crystal cell.**
- 6.2 Overview of the different types of experimental cell used to obtain the results for diffraction efficiency.**
- 6.3 Graph of Phase Retardance *vs.* voltage for Zli1982 and Zli1800 type liquid crystals.**
- 6.4 Three stages of electrically induced director movement in parallel and antiparallel rubbed cells.**
- 6.5 Graph of D.E. *vs.* voltage for First Order antiparallel rubbed cell—Zli1982 liquid crystal**
- 6.6 Graph of D.E. *vs.* voltage for Second Order antiparallel rubbed cell—Zli1982 liquid crystal**
- 6.7 Graph of D.E. *vs.* voltage for First Order parallel rubbed cell—Zli1982 liquid crystal**
- 6.8 Graph of D.E. *vs.* voltage for Second Order parallel rubbed cell—Zli1982 liquid crystal**
- 6.9 Graph of D.E. *vs.* voltage for First Order parallel rubbed cell—Zli1800 liquid crystal**

- 6.10** Graph of D.E. *vs.* voltage for Second Order parallel rubbed cell—Zli1800 liquid crystal
- 6.11** Graph of D.E. *vs.* voltage for First Order antiparallel rubbed cell—Zli1800 liquid crystal
- 6.12** Graph of D.E. *vs.* voltage for Second Order antiparallel rubbed cell—Zli1800 liquid crystal
- 6.13** Enlarged graph of D.E. *vs.* voltage for First Order Undyed @ 0° cells—Zli1982 liquid crystal
- 6.14** Enlarged graph of D.E. *vs.* voltage for First Order Undyed @ 0° cells—Zli1800 liquid crystal
- 7.1** J.O.E.R.S. P.A.O.D.A. Mark(I) Demonstrator System.
- 7.2** Flow diagram of the sequence of events controlled by the output stage.
- 7.3** Flow diagram of the functions performed by the peak detector hardware.
- 7.4** Circuit diagram of the correlation peak detector hardware used in the demonstrator system.

<b>List of Symbols</b>
------------------------

- $\vec{n}$  unit vector
- $L$  Spatial period of a cholesteric helix
- $\sigma$  electrical conductivity of a mesomorphic compound
- $\epsilon$  dielectric constant of a mesomorphic compound
- $\chi$  magnetic susceptibility of a mesomorphic compound
- $\epsilon_{\parallel}$  dielectric constant parallel to the director
- $\epsilon_{\perp}$  dielectric constant perpendicular to the director
- $\Delta\epsilon = \epsilon_{\parallel} - \epsilon_{\perp}$
- $\Delta\chi = \chi_{\parallel} - \chi_{\perp}$
- $n_o$  ordinary refractive index (designated  $n_{\perp}$ )
- $n_e$  extraordinary refractive index (designated  $n_{\parallel}$ )
- $\Delta n$  birefringence ( $= n_{\parallel} - n_{\perp}$ )
- $K_{11}, K_{22}, K_{33}$  Splay, twist and bend elasticity components of a liquid crystal
- $\gamma_C$  critical surface tension of a solid
- $\gamma_L$  surface tension
- $\Delta\gamma = \gamma_L - \gamma_C$
- $F$  Overall free energy of a liquid crystal
- $F_E$  Orientational elastic free energy of a liquid crystal
- $F_P$  Orientational physio-chemical free energy of a liquid crystal
- NDA Negative dielectric anisotropy
- PDA Positive dielectric anisotropy
- $\theta_T$  Tilt angle of liquid crystal director wrt substrate surface.
- $N$  Numerical aperture of lens
- $\rho$  Rotation angle of microscope stage
- $C$  Zero field capacitance of cell
- $C_0$  Capacitance of empty cell
- $C_{null}$  Capacitance of cell in null magnetic field
- $C_{(H)}$  Capacitance of cell in magnetic field strength  $H$
- $\delta$  Angular difference between null orientation and the one at which  $C$  is measured
- $V_{TH}$  Threshold voltage for given dielectric effect
- $\epsilon_0$  permittivity of free space

- $I$  Intensity of transmitted light
- $I_p$  Intensity of light transmitted through parallel polarizers
- $d$  Cell thickness
- $\lambda$  Wavelength of incident light
- $\psi$  Angle between input light optical vector and the projection of the director onto the cell walls
- $\omega$  Twist angle for directors in a twisted nematic cell
- $P_0$  Undeformed helix pitch of cholesteric-nematic mixture
- $f_c$  Critical a.c. frequency in conduction induced effects
- $G$  Increase in free energy of a liquid crystal sample
- $g$  Free energy density change
- $g_D, g_E, g_M$  Components of  $g$
- $\vec{L}$  Vector representing unit director field
- $\vec{E}$  Electric field vector
- $\vec{H}$  Magnetic field vector
- $\nabla$  Vector differential operator
- $\theta$  Tilt angle of the director (depends on  $z$ )
- $\theta_m$  Tilt angle of the director at  $d/2$
- $z$  Distance across cell (variable)
- $G'$  Increase in free energy/unit area
- $\vec{D}$  Dielectric displacement vector
- $C$  Constant of integration (in equations [3.25] & [3.26])
- $U$  Applied voltage
- $U_0$  Threshold
- $R$  Cell retardation
- D.E. Diffraction Efficiency
  - $g$  Thickness of grating element
  - $\Theta$  Phase retardance (voltage dependent)
- $f(\Phi)$  Amplitude distribution of a grating element
- $h$  Order number
- $\Delta/d$  Ratio of interline gap to grating element width
- ITO Indium Tin Oxide
  - $\phi$  Phase retardance of a liquid crystal sample
  - $\phi_E$  Experimental phase retardance
- $\phi_{\max}$  Maximum theoretical phase retardance
- $\Delta\phi$  Phase difference ( $= \phi_{\max} - \phi_E$ )

# Introduction

## 1.1 An Overview of Optical Processing

In the quest for computer architectures that will perform operations ever faster, the potential bandwidth proffered by optical architectures represents a considerable improvement on current electronic techniques. The attraction of the optical processor is its inherent ability to process one and two-dimensional data in a parallel fashion. The term optical processing can be subdivided into two categories, namely, optical image processing (OIP) and optical signal processing (OSP), with optical computing being a further subdivision of OSP. The detailed requirements of these categories are distinct but they have many common features and an underlying theoretical framework. However only OSP will be discussed further.

One-dimensional OSP is already well established in many areas such as linear phased array correlator systems<sup>1a</sup>. However, the two-dimensional processing field, which is dominated at present by electronic technology lies open to the far reaching advantages of optical methods. This is further supported by the fact that the input for two-dimensional OSP in pattern recognition and image subtraction is already in the parallel form required. Pattern recognition and image subtraction encompass many important and wide ranging applications such as word recognition, aerial reconnaissance, and production line quality control. In these situations existing digital computer processing is wasteful and slow because the computer architecture only permits data to be input in a controlled serial fashion to avoid the 'von Neumann' bottleneck.



One area of OSP which is receiving closer attention is that of optical correlation. One of many possible architectures that can perform two-dimensional parallel correlation operations faster than existing electronic circuitry is shown in Figure 1.1.

With reference to Figure 1.1, the optical cross correlator is a system consisting of several high quality optical components which correlate the two incoming beams of coherent light. If identical information is present in each beam then a correlation peak is produced at the output of the correlator. The output peak of light is then analysed using a high resolution video camera and the digitized result presented to the digital computer. This computer is dedicated to the task of locating the brightest spot in the field of view and calculating its position relative to the input scene. The input to the optical correlation system is provided by two spatial light modulators (SLMs). These devices spatially modulate a reference beam of coherent light by reflecting it off a modulating interface containing a two-dimensional picture. In this application one SLM is used to gather the moving or static scene data and the other gathers the reference data.

To realize the real-time and parallel processing advantages of optical data processing systems, real-time and re-usable two-dimensional spatial light modulator transducers are required to convert either the input electrical data or the non-coherent ambient image data into a form suitable for spatial modulation of a coherent laser beam for subsequent input into the Optical Correlator. These SLMs can be constructed and operated in many ways. The following section briefly discusses the main forms of SLMs and their relative merits for optical processing applications.

## **1.2 Forms of Spatial Light Modulator**

The two-dimensional spatial light modulators described below can be divided into two categories; electronically addressable and optically addressable. It must be noted that the suitability of any device to a given situation depends almost completely upon the intended application.

Of the available electronically addressed SLMs (EASLMs), most are an electronically addressable progression from their optically addressed counterparts. They generally employ scanned electron beams, semiconductor transistors or charge coupled devices (CCDs) or matrices of electrodes and access a voltage or current controlled modulating picture element.

In operation, a voltage applied to the sandwich is shunted to the modulating layer by the illuminated photoconductor. The Phototitus,<sup>1</sup> Liquid Crystal Light Valve (LCLV),<sup>2</sup> and PLZT devices<sup>3</sup> are examples of this structure.

Many existing optically-addressed SLMs (OASLMs), a typical example of which is shown in Figure 1.2 employ a sandwich structure consisting of: an input write-beam window with a transparent electrode; a photoconductor; an opaque layer to block the read-beam; a reflecting layer to allow readout by reflection; a voltage-controlled phase, amplitude, and/or polarization modulating material (for example, a liquid crystal); another transparent electrode; and a readout window.

Among other OASLMs is the Ruticon<sup>4</sup> which has a slightly different construction, with an electrostatically deformable elastomer sandwiched on one side by a photoconductor and on the other side by either a conducting liquid ( $\alpha$ -Ruticon), a gas discharge ( $\beta$ -Ruticon), or a reflective coating ( $\gamma$ -Ruticon). The thermoplastic SLM replaces the elastomer in the  $\alpha$ -Ruticon with a plastic which deforms only when heated. The Membrane Light Modulator (MLM)<sup>5</sup> and Deformable Membrane Device (DMD)<sup>6</sup> contain a rigid dielectric with holes, over which a reflective conducting membrane is stretched. This membrane structure is accessed by silicon circuitry or phototransistors in the DMD case, whilst in the MLM case it is accessed by an array of electrodes or silicon photodiodes; electrostatic forces then deflect the membrane into the holes of the dielectric. The micro-mechanical modulators on the other hand employ flexing of cantilevered metal or SiO<sub>2</sub> elements instead of the membrane.

The Pockels Readout Optical Modulator (PROM)<sup>7</sup> does not require a separate photosensor since the modulating electro-optic crystal, Bismuth Silicon Oxide (BSO), is itself photoconductive. The PROM sandwich consists of two transparent electrodes which are isolated from the crystal by thin dielectric layers. Even simpler structures, with many important SLM properties, are possible with such photorefractive ferroelectric materials as BSO,  $\text{FeLiNbO}_3$ , or  $\text{BaTiO}_3$ . By applying only a bias voltage to the ferroelectric material, it is possible to obtain: real-time holography; long-term storage of high resolution holograms; image multiplication and amplification by two-wave mixing (TWM) or degenerate four-wave mixing (DFWM); and photo-refractive incoherent to coherent optical conversion (PICOC) by erasing the photorefractive grating with an incoherent input image.

In the Microchannel SLM (MSLM)<sup>8</sup> and Photo-Emitter Membrane Light Modulator (PEMLM),<sup>9</sup> a photocathode converts the incident addressing image into an electron distribution. This electron image is then amplified by a microchannel plate (MCP), accelerated by a grid, and deposited onto a reflective, deformable membrane array covering the MCP (PEMLM) or onto an electro-optic crystal (MSLM). Both devices are read out in reflection.

Heat generated by absorption of the writing image intensity is an alternative optical sensing method. This heat can cause material phase transitions (for example, in smectic liquid crystals) or deformations of a liquid film.

Comparing realistic performances of SLMs is difficult. The measurement conditions are not always given in the literature nor are they consistently related to actual device applications. Resolution, sensitivity, and speed parameters, for example, are almost completely arbitrary without a specification of the measurement of the depth of modulation. There are also fundamental trade offs in performance, for example, a thinner electro-optic crystal in a sandwich SLM not only tends to increase resolution, but also increases device capacitance and thereby decreases speed.

The time response of photoconductive modulators (such as the LCLV) tends to be limited by slow photoconductive carrier transit and decay lifetimes. In contrast, the ultimate speed of the MCP and silicon addressed devices is often limited only by thermal dissipation constraints on the maximum current available to charge the modulating material.

Electro-optic crystals (e.g. BSO) probably offer the fastest intrinsic time response ( $\approx 1\text{ps}$ ). Deformable membranes ( $\approx 1/2\mu\text{s}$ ), cantilevered beams ( $\approx 1\mu\text{s}$ ), magneto-optic domain switching ( $\approx 1\mu\text{s}$ ), PLZTs ( $\approx 10\mu\text{s}$ ) and ferroelectric liquid crystals ( $\approx 100\mu\text{s}$ ) can also be fast. Particle suspensions ( $\approx 1\text{ms}$ )<sup>10</sup>, deformable elastomers ( $\approx 1\text{ms}$ ), and nematic liquid crystals ( $\approx 10\text{ms}$ ) tend to be slower. The speed of electronic SLMs is limited either by the serial addressing mechanism or the product of pixel response time times the number of serial pixels or lines.

### **1.3 Types of SLM—A Summary**

From the details given in the previous section, it is not easy to outline an ideal 'general-use' type of spatial light modulator as they are application specific. As Fisher<sup>11</sup> suggests, perhaps even more important than the actual performance specifications of a SLM are such issues as: ease of use; reproducibility and reliability of operation; low cost (less than £500); minimal and unsophisticated support electronics and associated equipment; simple low-loss optical readout systems; and a small footprint on the optical table. At present, the only SLM meeting the majority of Fisher's suggestions is the Hughes Aircraft Corporation's Liquid Crystal Light Valve (see Figure 1.2). This device is optically addressable, occupies a small footprint on the table and requires unsophisticated drive electronics. Its price is currently £40,000 due to the low demand and the need to re-coup the high 'one-off' production costs. Thus its use is restricted to well funded establishments. A final consideration is that most of the SLMs mentioned in Section 1.2 are experimental and it would therefore be difficult to 'mass produce' them with the identical specifications.

The author believes that there are many institutions and organizations wishing to make use of parallel optical systems but are prevented from doing so by the high cost of the SLMs. These costs arise in the production of the SLMs due to several factors: the requirement for optical grade flatnesses of reflective or transmissive surfaces ( $\lambda/4$  and better); and high manufacturing tolerances, for example, the modulating layer thickness must be to within fractions of a micron over the entire surface area ( $2-3 \text{ cm}^2$ ) to ensure minimal phase distortions of the transmitted light. However, recent advances have been made towards the mass-production of SLMs by the Marconi Research Laboratories who have produced small batch-quantities of liquid crystal based OASLMs<sup>12</sup>. Further, the Japanese display manufacturers have produced miniature ( $4\text{cm} \times 3\text{cm}$ ) liquid crystal televisions which are retailing for £100 or less. These devices have been analysed by several researchers<sup>13-14</sup> for use as a potential EASLMs and their results are in agreement with previous research carried out by the author, indicating that due to the low number of representable grey levels of the liquid crystal and the 'lattice' arrangement of transparent driving electrodes forming the pixels, these devices can only be used for simple binary-input applications. From these developments it is envisaged that future commercially available SLMs are likely to employ liquid crystals as the light modulating medium and to be either optically or electrically addressable.

#### **1.4 Direction of Research**

When considering the specifications of mass-produced liquid crystal spatial light modulators put forward in Section 1.3, it is clear that further research is required with respect to the technology of manufacturing the SLMs. Listed briefly below are two examples of the types of problem encountered in fabricating the component parts of a liquid crystal SLM,

- a) In a reflective readout SLM (see Figure 1.2) the dielectric mirror has several requirements placed on it,
  - i) It must not react with the material it is in contact with.
  - ii) Its dielectric properties must be good enough to ensure that no electrical

conduction occurs.

- iii) The entire surface area of the mirror has to be optically flat to within fractions of a wavelength of the incident light, otherwise phase distortions will be established in the modulating layer and the reflected light cannot be utilized.
- b) In an optically addressable SLM the linear response to light intensity of the photodetector layer is necessary to ensure that the incident image is accurately reproduced in the liquid crystal layer. This means that the response to light of each photodetector site has to be identical.

The technology of forming dielectric mirrors by evaporation has reached a stage where they are >90% reflective as well as being completely inert. The advances made in the field of fabrication techniques have made it possible for the potential problems in constructing the arrangements described in a) and b) above to be dealt with. Many forms of silicon based photodiode arrays have been built, as too have arrays of charge coupled detectors (CCDs). The photorefractive crystal, bismuth silicon oxide (BSO), can also be used in carefully cut slices as the photodetector layer. However, the techniques employed to measure the operational parameters of the SLMs are still those used to determine the performance of liquid crystal displays. Therefore, with regard to the measurement technology of SLMs further research is necessary to 'update' the measurement techniques.

As mentioned in the preface to this thesis, the author was appointed the Displays Division at S.T.L. Ltd. as his collaborating company. The Displays Division was developing a spatial light modulator and possessed technical expertise in the field of liquid crystal research and their applications. In order to make the best use of the available facilities whilst working in the Displays Division *and* to update the the measurement technology of SLMs, the author chose to research a measurement technique to assess the suitability of the liquid crystal used in a SLM. By developing such a technique, manufacturers would be able to choose a liquid crystal with operating parameters matching the optimum operational parameters of their SLM and hence permit SLMs to be manufactured for use in specific situations.

## **1.5 Aims and Objectives**

The aim of this thesis is to present a discussion on the steps taken in devising and testing a measurement technique which determines the suitability of a liquid crystal. The technique is based on measuring the diffraction efficiency of the liquid crystal in response to an applied voltage. Details are given below of the objectives necessary to establish and verify the measurement technique.

- 1 ■ Choice of a liquid crystal for use in experimental arrangements.
- 2 ■ Establish mechanism(s) for aligning the liquid crystal. (Alignment is employed to encourage a reproducible response of the liquid crystal).
- 3 ■ Measure the alignment produced by 2) above.
- 4 ■ Establish types of electro-optic effect possible in the chosen liquid crystal. The effect(s) most relevant to verify the measurement technique will be chosen.
- 5 ■ In order to 'appreciate' the results a mathematical description of the types of alignment and electro-optic effects has to be derived.
- 6 ■ In order to measure the diffraction efficiency of the liquid crystal, it will be driven in the form of a square wave diffraction grating. Thus, mathematical derivations for square wave diffraction gratings are necessary.
- 7 ■ Fabrication of the experimental liquid crystal cell(s).
- 8 ■ Description of the experimental arrangements for measuring the diffraction efficiency of the liquid crystal cell(s).
- 9 ■ Analysis of the experimental results and comparison with the theoretical results obtained in 5) above.
- 10 ■ Design and development of a real-time correlation peak detector for use in the output stage of an optical correlation system.

## **1.6 Organisation of Thesis**

Further to the objectives put forward in section 1.5, the thesis is organised as follows,

**Chapter 1** ◦ This chapter—Introduction.

**Chapter 2** ◦ An Introduction to Liquid Crystals. Classification and properties of mesophases. Mechanisms and methods of surface alignment of liquid crystals, followed by measurement of tilt angles produced by the alignment process.

**Chapter 3** ◦ Electro-Optic Phenomena. Description of dielectric and thermo-optic effects. Mathematical analysis: the elastic continuum theory for electric field deformations of parallel and tilted homogeneously aligned cells. Also, a brief description of a software package available within STL that performs the mathematical analysis on different aligned and treated cells.

**Chapter 4** ◦ Theory of Phase and Amplitude Diffraction Gratings. Both for square wave and non-square wave gratings.

**Chapter 5** ◦ Experimental Details. Details of the construction of the experimental cells treated and filled with liquid crystal described in chapters 2 & 3. The experimental arrangements used to measure the phase retardance and diffraction efficiency of the liquid crystal in the cell are given, followed by two methods used to obtain the readings.

**Chapter 6** ◦ Results. Analysis of the experimental results and comparison with the theoretical results obtained in chapter 4.

**Chapter 7** ◦ Total Technology chapter. This chapter is included to satisfy the body awarding the Ph.D. studentship. It contains details of research carried out at S.T.L. Ltd., as part of the J.O.E.R.S. P.A.O.D.A. programme.

**Chapter 8** ◦ Conclusion and Suggestions for further work.



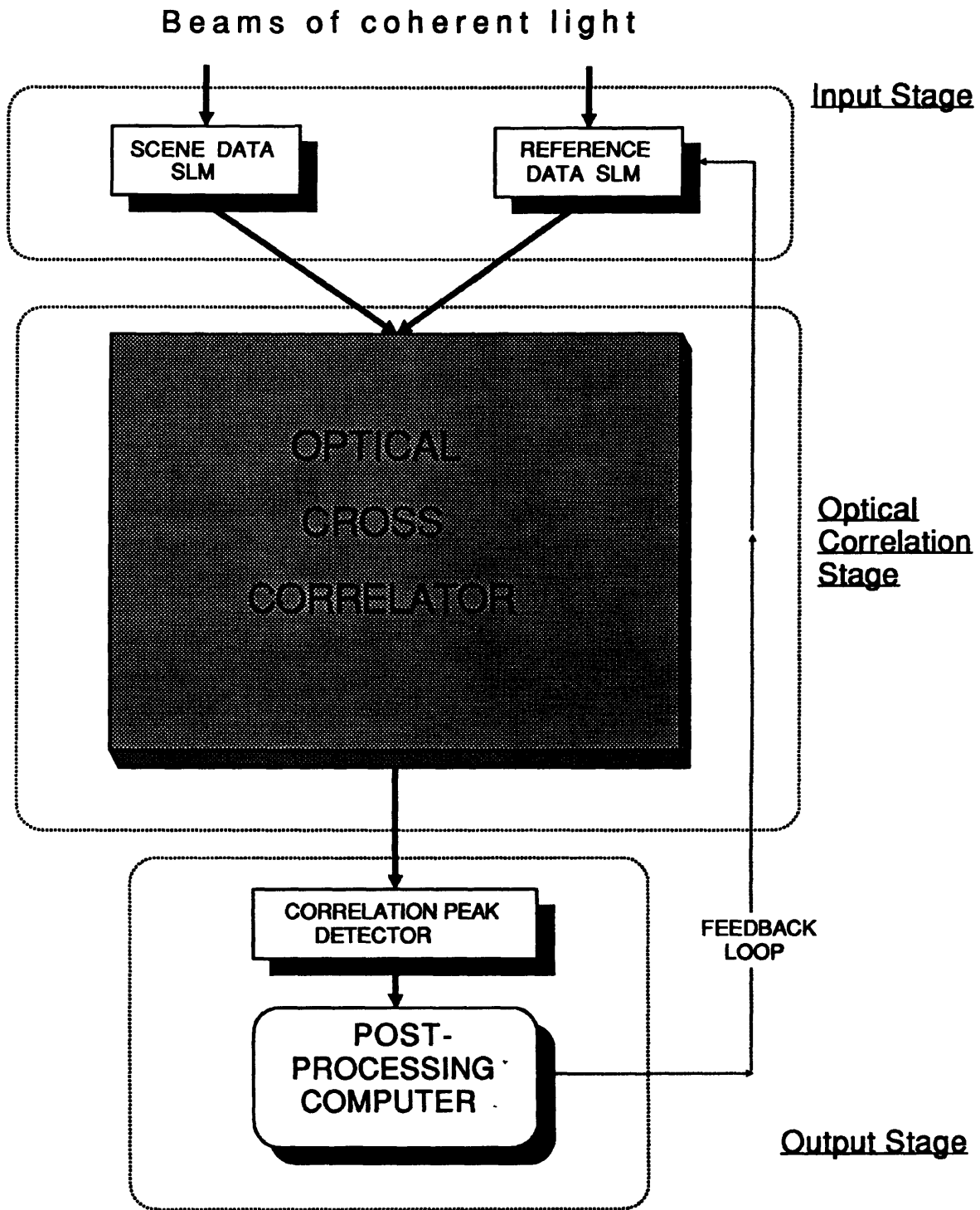


**Figure 1.1**

General Architecture of an Optical Recognition System

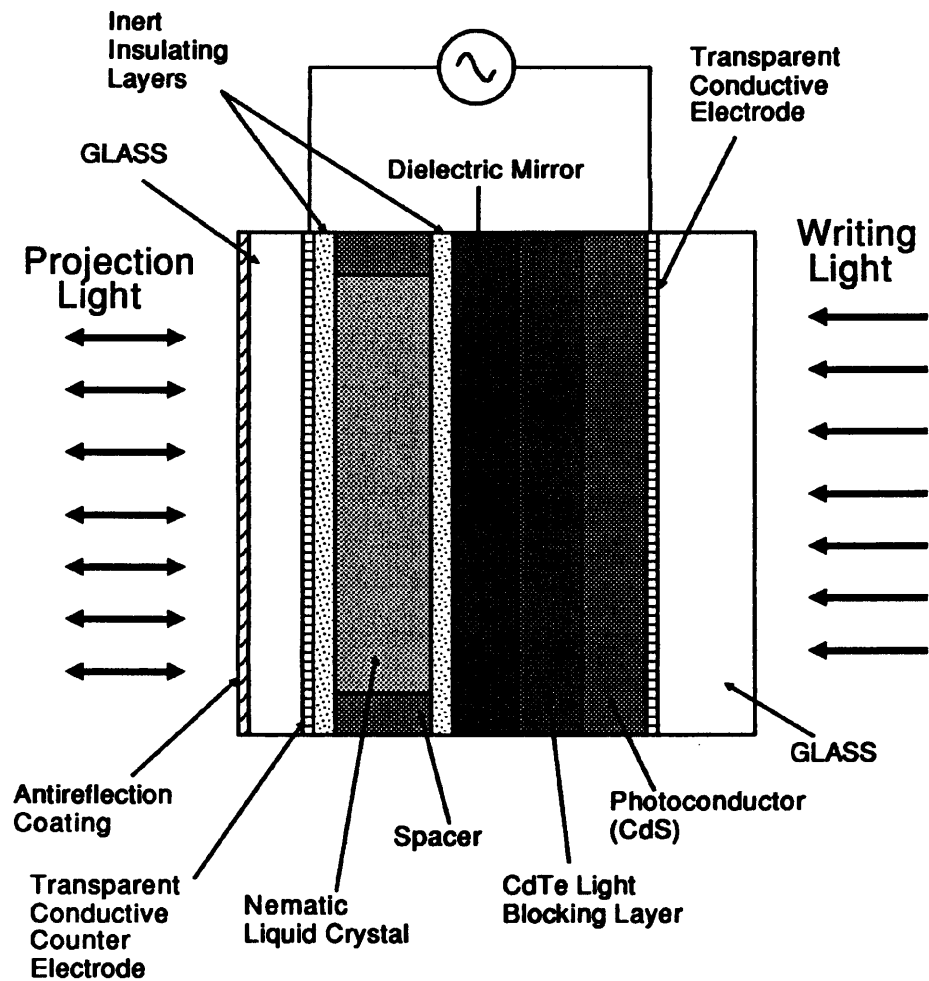


**Figure 1.2**

Schematic Diagram of an Optically Addressed  
Liquid Crystal Spatial Light Modulator.  
(Hughes Liquid Crystal Light Valve - LCLV)

# 2

## An Introduction to Liquid Crystals

### 2.1 Chapter Summary

This chapter begins with a brief account of the history of liquid crystals and the development of a classification system based on three main categories; nematic, cholesteric and smectic. This is then followed by a description of various methods of liquid crystal alignment that may be used during the fabrication of liquid crystal devices: in order to produce such devices with the same characteristics it is first necessary to ensure that the alignment of the liquid crystal's directors is reproducible. From these alignment methods the spin-coated polymer technique was chosen. Finally methods for measuring the angle of liquid crystal director alignment with respect to the bounding substrate, (known as the tilt angle), are described. The conoscopic technique developed by Crossland *et al*<sup>48</sup> at S.T.L. Ltd. was used to measure the experimental cell's tilt angle.

### 2.2 History of Liquid Crystals

The first reference to the term "liquid crystallinity" was made by Reinitzer<sup>15</sup> in 1888. Further workers in the field were Lehmann,<sup>16</sup> the pioneer Friedel<sup>17</sup> who in 1922 made a classification of liquid crystals which is still used today, and Vorländer<sup>17a</sup>, who produced numerous organic compounds with a liquid crystalline phase. Research on these materials greatly intensified in the 1960s due to the discovery of compounds having an anisotropic dielectric constant in the liquid crystalline phase at a reasonable temperature (that is, room temperature). Previously known compounds had their phases at very high temperatures. With the discovery of a profusion of mate-

rials having the required properties, most of the recent research has centred on the application of electro-optic effects, some of which will be described in chapter 3.

### **2.3 Mesophases**

During the melting of a molecular crystal, which in general is composed of anisotropic molecules, there can occur, prior to the formation of the isotropic fluid, a stage involving the formation of intermediate phases (or mesophases). For example, the crystals can lose orientational order in the distribution of the molecules, while still retaining their translational order. In this case the molecules can rotate freely while remaining on their original positional sites in the crystal lattice. Such a mesophase is called a plastic crystal and is characteristic of materials whose molecules do not exhibit pronounced anisotropy. The opposite will occur if a crystal loses translational order while retaining orientational order. In this case the mesophase can flow freely, even if only along certain selected directions, while it retains the anisotropy of almost all its physical properties. Such a mesophase is called a liquid crystal, and is generally characteristic of materials with molecules which are highly anisotropic in shape. Subsequent heating of the mesophase will lead to the break-up of its residual ordering, and the material converts to an isotropic liquid.

If this series of phase transitions in a liquid crystal occurs over a temperature range, the mesophases are termed thermotropic. It is also possible for the mesophases to be formed from isotropic solutions during the increase of their concentration in a suitable solvent. Such mesophases are termed lyotropic. However, this thesis will only be concerned with thermotropic liquid crystals.

### **2.4 Classification of Thermotropic liquid crystals**

Thermotropic liquid crystals can be divided into three groups: nematic, cholesteric, and smectic. Mesophase types are most reliably determined by X-ray diffraction methods, although a quicker identification is often made from the texture as observed under a polarizing microscope. Figures 2.1a–2.1c give a schematic representation of

the orientations of the molecules, depicted as rigid rods, for liquid crystals of the different types.

### 2.3.1 Nematic Order

The word 'nematic' was derived from a Greek word meaning thread by Friedel. Viewed in thin layers, through a polarizing microscope, the nematic texture shows dark 'threads' which are mobile filaments called disclinations where the molecular alignment is discontinuous. As can be seen from Figure 2.1a, there is long range orientational order in the nematic phase, that is, the long axes of the molecules tend to align parallel to each other. The unit vector ( $\vec{n}$ ) referred to as the director, represents the axis of preferred orientation of the molecules. However, there is no long range correlation of the molecular centres of mass.

### 2.3.2 Cholesteric Order

Cholesteric liquid crystals are formed by optically active molecules (until recently they were almost exclusively cholesteryl esters—hence their name). Cholesterics are characterized by the fact that the direction of the long molecular axes in each successive layer (which is made up of molecules which are orientated in parallel and free to move in two directions) forms a given angle with the direction of the axes of molecules in the preceding layer (see Figure 2.1b). In this way a helix is formed, whose pitch is dependent on the nature of the molecules and the external forces.

The helix takes the form,

$$\begin{aligned}n_x &= \cos(q_0 z + \phi) \\n_y &= \sin(q_0 z + \phi) \\n_z &= 0\end{aligned}$$

where both the direction of the helix axis  $z$  in space and the magnitude of the phase angle  $\phi$  are arbitrary. Thus the structure of a cholesteric liquid crystal is periodic with a spatial period ( $L$ ) given by,

$$L = \frac{\pi}{|q_0|}$$

The sign of  $q_0$  distinguishes between left and right helices and its magnitude determines the spatial period.

Also classed with cholesteric liquid crystals are the so-called 'chiral' nematics, whose molecules have a composition which is characteristic of nematic liquid crystal molecules but which are optically active.

### **2.3.3 Smectic Order**

Smectic (from the Greek word for soap) was the name used by Friedel to describe certain mesophases with mechanical properties similar to those of soap solutions. As many as eleven smectic phases have been identified, and are designated smectics *A, B, C, D, E, F, G*, and *H*, (*I, J*, and *K* are more recent) after a classification system by Sackmann & Demus.<sup>18</sup> Structurally all smectics are layered structures with well defined interlayer spacings. Smectics are more ordered than nematics (see Figure 2.1c) and in most of them the molecules are mobile in two directions and can rotate about one axis. Interlayer attractions are weak in comparison to the lateral forces between the molecules, and consequently the layers are able to slide over one another very easily. Low order smectics are unstructured, with the molecules being randomly distributed in the layers. The layers of higher order mesophases are structured however, with the molecules being arranged in a regular two dimensional lattice. The long axes of the molecules may be nearly normal to the layers' planes or inclined, regardless of the structuring of the layers.

## **2.4 Physical Properties of Mesophases**

Almost every tensor property of a mesomorphic compound is anisotropic. These include the electrical conductivity ( $\sigma$ ), the dielectric constant ( $\epsilon$ ), the magnetic susceptibility ( $\chi$ ), the viscosity, the refractive index, and the elastic modulus. They are characterized at any temperature by two constants, one parallel and one perpendicular to the director. The anisotropy of  $\epsilon$  or  $\chi$  permits the director pattern to be

influenced by electric or magnetic fields, and the effect of this on incident light is due to the anisotropy of the refractive index.

The dielectric constant parallel to the director,  $\epsilon_{\parallel}$ , usually differs from that perpendicular to the director,  $\epsilon_{\perp}$ . If  $\Delta\epsilon$  ( $\Delta\epsilon = \epsilon_{\parallel} - \epsilon_{\perp}$ ) is positive, then the mesomorphic material is said to have a positive dielectric anisotropy (PDA), and conversely, if  $\Delta\epsilon < 0$ , then the mesophase has a negative dielectric anisotropy (NDA). If the molecule possesses a permanent dipole moment, then, at zero frequency,  $\Delta\epsilon$  may be positive or negative, depending on whether the dipole lies along or at right angles to the long molecular axes. A consequence of the anisotropy in  $\epsilon$ , is the re-orientation of the director in an electric field. For materials with PDA, the director orientates itself in the direction of the field, whilst for NDA materials the director aligns itself perpendicular to the field.

Most mesogens are diamagnetic, and the largest contribution to the anisotropy of diamagnetism comes from the occurrence of circular electronic currents within the aromatic rings. The effect is greatest when the magnetic field is perpendicular to the director, and hence the perpendicular susceptibility ( $\chi_{\perp}$ ) has the greatest absolute value. Diamagnetic susceptibilities being negative, however, make  $\Delta\chi$  ( $\Delta\chi = \chi_{\parallel} - \chi_{\perp}$ ) positive. In a magnetic field the director is generally aligned preferentially in the direction of the field.

A uniaxial liquid monocrystal has two principal refractive indices,  $n_o$  and  $n_e$  ( $o$  = ordinary,  $e$  = extraordinary). The first,  $n_o$ , holds for linearly polarized light whose electrical vector oscillates at right angles to the director, and is designated  $n_{\perp}$ . The second,  $n_e$ , holds for light where the electric vector is parallel to the director, and is called  $n_{\parallel}$ . In liquid crystals,  $n_{\parallel}$  is always much greater than  $n_{\perp}$ , being directly related to the strong polarizability of the molecules in the longitudinal direction. The birefringence,  $\Delta n$ , ( $\Delta n = n_{\parallel} - n_{\perp}$ ) is approximately 0.2→0.3, which is much higher than well known birefringent solids (e.g. for Quartz  $\Delta n = 0.0091$ ). In bulk nematic

liquid crystals, the director varies from position to position, leading to a marked variation in refractive index and hence to light scattering.

Apart from uniaxial symmetry in nematic systems, and hence the anisotropy in various properties, the tendency of the molecules towards orientational order also appears on a macroscopic scale as an elasticity of the liquid. This tends to make neighbouring director orientations similar. The elasticity is described by three constants:  $K_{11}$ ,  $K_{22}$ , and  $K_{33}$ , which indicate respectively how strong the liquid crystal opposes splay, twist and bend of the director pattern. These properties are depicted in Figure 2.2.

## **2.5 Use of Liquid Crystals for Displays**

Physical properties of liquid crystals such as birefringence, optical activity, viscosity and so on, are all sensitive to weak external stimuli. Electric fields, magnetic fields and heat energy can be used to induce the optical effects. Most of the display related research is centred on the application of the electro-optic effects. This is due to the ease and efficiency by which an electrical stimulus can be applied to the liquid crystal as opposed to say, magnetic excitation. Liquid crystal electro-optic effects are important because instead of relying on light emission, they modify the passage of light through the crystal by either light scattering, modulation of optical density, or colour changes. The most notable features of liquid crystal displays are: low-voltage operation, very low power dissipation, flexibility of size and format, and immunity in high brightness to 'washout'.

For all of the measurements made on the liquid crystal, a 'standard cell' configuration is used to hold the liquid crystal (depicted in Figure 2.3). The cell consists of two treated metallized glass plates about 10–20 microns apart. The liquid crystal is sandwiched between the plates which are then hermetically sealed. By pre-treating the glass plates either chemically or mechanically, the liquid crystal directors can be assigned a definite orientation. The two most common forms of alignment are homo-



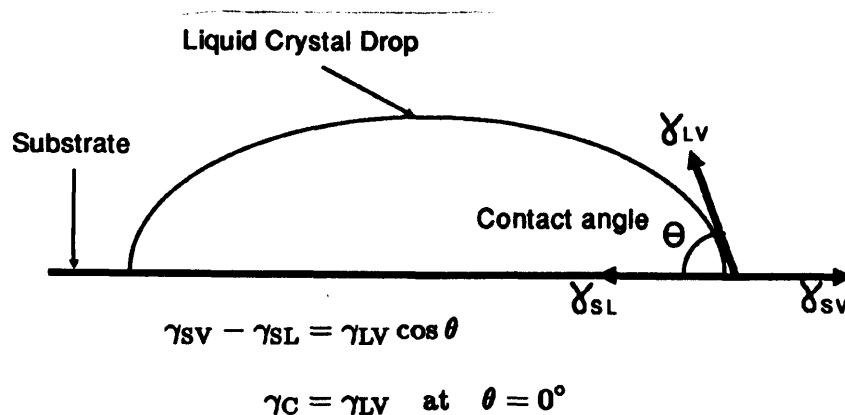
geneous alignment (Figure 2.4a), where the directors align parallel to the cell walls, and homeotropic alignment (Figure 2.4b), where the directors are perpendicular to the cell walls. Recent alignment techniques allow the director to tilt at smaller, controllable angles (Figure 2.4c). The tilted alignment improves the response, contrast uniformity, as well as eliminating defects and disclination lines. The remainder of this chapter discusses the various alignment techniques.

## 2.6 Mechanisms of Surface Alignment

A solid surface can be characterized by a critical surface tension,  $\gamma_C$ , and by a surface tension  $\gamma_L$ . The surface free energy and the critical surface tension are synonymous, that is, surfaces with high  $\gamma_C$  are said to have high surface free energy.

At low substrate surface energies, the intermolecular forces within the liquid crystal are stronger than the forces across the interface, the fluid does not wet the surface and homeotropic alignment results. Here  $\gamma_C < \gamma_L$ .

At high substrate surface energies, the fluid wets the surface to minimize the surface energy and homogeneous alignment results. In general, wetting of the solid by the liquid occurs when  $\gamma_C > \gamma_L$ . In this case the liquid spreads out uniformly on the solid and the contact angle at the liquid/solid interface equals zero. Dubois *et al*<sup>19</sup> obtained the procedure used to obtain values of  $\gamma_C$  for several substrates. This involved measuring the contact angle,  $\theta$ , of drops of liquids having varying surface tensions, and extrapolating to a value of  $\cos \theta = 1$ , that is  $\theta = 0^\circ$  (see diagram).



Therefore Creagh and Kmetz<sup>20</sup> predicted that,

$$\begin{aligned}\gamma_C < \gamma_L &\rightarrow \text{Homeotropic alignment} & (\Delta\gamma > 0) \\ \gamma_C > \gamma_L &\rightarrow \text{Homogeneous alignment} & (\Delta\gamma < 0)\end{aligned}\quad [2.1]$$

In Creagh and Kmetz's model,<sup>20</sup> the effect of grooving was to provide a preferred direction for long range order in the plane of the substrate. Physico-chemical forces primarily determined whether the liquid crystal molecules were parallel or perpendicular to the substrate surface and, when either a high substrate surface or an applied field caused parallel alignment, the elastic energy would be lower if the nematic director lay parallel to the grooves rather than following the surface curvature.

Khan *et al*<sup>21</sup>, although agreeing with the concepts of Creagh and Kmetz, expanded on their ideas. They assumed that the strength of the liquid crystal anchoring increased with increasing absolute value of  $\Delta\gamma$  ( $\Delta\gamma = \gamma_L - \gamma_C$ ). Khan *et al* postulated that on flat, untextured surfaces, the physico-chemical interactions predominated, while for textured surfaces the anisotropic elastic action must also be considered. They discussed alignment processes in terms of  $F_P$  and  $F_E$ , respectively, the physico-chemical and elastic contributions to the overall free energy  $F$ .

The orientational elastic free energy  $F_E$ , of a liquid crystal will be minimized when the nematic director has neither splay, twist or bend. Thus, bounded by a substrate containing parallel grooves, a nematic liquid crystal suffers no elastic deformation if its optical axis lies parallel to the grooves, or perpendicular to the substrate (Figure 2.5a and b). In these configurations, the free energy is minimized, however it is somewhat higher when the nematic molecules are aligned normal to the grooves and parallel to the substrate surface (Figure 2.5c), or normal to both the grooves and the substrate surface (Figure 2.5d).

Discussing these configurations in terms of the  $\Delta\gamma$ : on substrates where  $\Delta\gamma$  was less than zero, the alignments of Figure 2.5a and c have the lowest  $F_P$ , but the

configurations of Figure 2.5a and b have the lowest elastic free energies,  $F_E$ . Hence for  $\Delta\gamma < 0$ , the configuration where molecules lie along the grooves, parallel to the substrate minimized by the total free energy  $F$ , and thus was the orientation produced.

For  $\Delta\gamma > 0$ ,  $F_P$  was minimized by the alignment of Figure 2.5d, but  $F_E$  was minimized by the parallel or perpendicular alignments of Figure 2.5a and b, and thus perpendicular alignment followed for  $\Delta\gamma > 0$ .

Therefore if the cell walls are treated in a certain way, the liquid crystal can be made to align in the preferred direction. In this way cells can be fabricated to exhibit the required electro-optic or magneto-optic effects. The following sections describe different techniques for treating the cell walls.

## **2.7 Methods of Liquid Crystal Alignment**

Historically, Friedel<sup>17</sup> proposed methods by which both homogeneous and homeotropic alignments could be achieved. However, his techniques were somewhat involved and irreproducible. Zocher<sup>22</sup> reported that homogeneous alignment could be obtained by uni-directionally rubbing the surface of the cell with materials such as paper, tissue, and cotton wool. In addition, Dreyer<sup>23</sup> stated that—*“Strong brushing, rubbing or stretching, in one direction of the supporting surface, or any other treatment which affects the surface anisotropy of the support, will result in a definite orientation of the materials applied to the treated surface.”*

## **2.8 Alignment of Liquid Crystals on Smooth Surfaces**

### **2.8.1 Inorganic Substrates**

The surfaces of inorganic substrates such as glasses, oxides and metals exhibit an aligning influence on liquid crystals. However not only is the reproducibility and uniformity of this type of alignment poor as the substrate surface is ill-defined but also the cleaning procedures employed in the substrate preparation also play a rôle, for example, MBBA liquid crystal molecules will align homeotropically

on acid treated glasses<sup>24</sup> or oxides,<sup>25</sup> but nonuniform homogeneous alignment to the substrate surface is obtained with fired<sup>24</sup> or detergent cleaned glasses.<sup>26</sup> The general direction of alignment for cleaved crystals and evaporated layers is a parallel alignment [Note: parallel here implies homogeneous alignment]. It has been reported that reliable homeotropic alignment may not be obtained from such surfaces.<sup>44</sup>

### **2.8.2 Organic Polymer Substrates**

Polymer coatings on glass substrates can be employed to align liquid crystals. A wide variety of methods<sup>27</sup> have been used to form the polymer layer which should preferably be thin in order to avoid an excessive potential drop in the dielectric layer when the cell is electrically driven. The film may be transferred to the surface from a liquid, while polymer casting and thermal or plasma polymerization of the monomer have also been used. The most common method is to form the polymer from partially polymerized solutions by dipping or spin coating followed by curing. Polymer coatings do not withstand high temperatures and displays employing such coatings must be sealed with a carefully chosen adhesive which is compatible with the polymer layers.

In general, smooth layers of glasses, oxides or polymers orientate the nematic director parallel to the substrate but do not induce uniform, reproducible liquid crystal alignment.

### **2.9 Alignment on Grooved Surfaces**

Rubbing, tangential evaporation or shallow angle ion beam etching (SAIBE) produce a wavy surface. It has long been acknowledged that the rubbing of the glass plate induces uniform alignment of liquid crystals,<sup>22&28</sup> with the crystal director nearly parallel to the substrate surface.<sup>29</sup> For some time it was considered that the material used for rubbing determined the efficiency of the process.<sup>30</sup> It is now clear, however, that as proposed many years ago,<sup>22</sup> any rubbing material, for example, paper, tissues,

brushes and polishing powders, gives good results. Some liquid crystals align more easily than others and reproducibility is not very good on substrates that are simply rubbed. The use of polishing powder, such as diamond paste, improves the alignment and is necessary for hard layers of silica or fluoride.

Glass has a surface layer extending one micron in depth which has a higher entropy than the bulk<sup>31</sup> and may easily be deformed by rubbing, producing a wavy surface. Because of its higher energy this surface layer melts 125°C below the softening point of the glass<sup>31</sup> (around 475°C for soda glass) and consequently the effects of rubbing disappear above this temperature. Glass frit sealed cells therefore require the use of layers of high melting point compounds such as silicon dioxide deposited by sputtering or charged vapour deposition (CVD).

Oxides,<sup>32</sup> fluorides and metal layers evaporated obliquely to a substrate generally align the liquid crystal molecules parallel to, or at a slight angle from, the surface<sup>33</sup> but tangentially evaporated calcium fluoride is reported to align the molecules nearly perpendicular.<sup>34</sup> Slant evaporations of a metal and subsequent thermal oxidation or SAIBE produce the same results. Obliquely evaporated  $\text{SiO}_x$  and  $\text{MgF}_2$  layers give reproducible results and are used widely in the fabrication of small displays. These layers are also compatible with any type of sealing.

Where high temperature resistance is not required, as in experimental cells, it is advantageous to coat electrodes with a soft polymeric layer which is rubbed afterwards.<sup>44</sup> The quality of the alignment depends on the polymer layer thickness and the substrate uniformity. Many surfaces tend to align liquid crystal directors in parallel and striations on these surfaces provide uniformity, which has led to the claim<sup>35</sup> that any striated surface, whatever the substrate and the method used to produce them, induces homogeneous alignment.

## **2.10 Alignment by Surface Active Agents**

Haas *et al*<sup>36</sup> observed that surface active agents (known as surfactants) promote liquid crystal alignment. They may be either dissolved in a liquid crystal, deposited on the cell walls, or small amounts dissolved in liquid crystals through a common solvent which is evaporated afterwards. As surfactant induced alignment is complex, depending on the substrate, mode of application and liquid crystal composition, the utilization of this effect requires critical evaluation before use.<sup>37</sup> For example, in displays operating in the field effect mode, the increase in conductivity due to an ionic dopant is a disadvantage and therefore, non-ionic compounds are preferred. Cationic surfactants, which are long chain substituted ammonium salts, are very effective in promoting homeotropic alignment of liquid crystals with both NDA<sup>38-40</sup> and PDA<sup>41</sup> although they increase the liquid crystal conductivity.

The main drawback of this method of alignment is that on filling a cell provided with only one fill port, the preferred construction in industry, the additives absorb strongly in the neighbourhood of the aperture. Consequently, the liquid crystal at the opposite end of the cell contains a lower concentration of additive, producing defects and a conductivity gradient across the cell. Generally, this method of alignment has not found industrial acceptance.

## **2.11 Alignment by Silane treated surfaces**

Alkoxys and chlorosilanes interact strongly with glass surfaces. The proposed mechanisms<sup>42</sup> are either reaction with surface silanol groups, or hydrolysis of the silane to a silanol which further condenses into a linear polysiloxane layer. Thus silanes are often considered as surfactants and sometimes as polymer forming compounds.

Surface treatments with silanes have been effected by dipping (generally for 5 minutes) in a 1%–5% solution of the silane in water, toluene, dilute acetic acid in water, or acetone. Water solutions are only stable for a few hours.<sup>43</sup> It has been noted that most silanes influence the liquid crystal alignment by the in situ formation of

a polysiloxane surface layer. Silyated surfaces degrade upon heating and this precludes the sealing of the cell by the glass frit method. Due to the toxicity of the chlorosilanes the process is rendered hazardous.

### 2.12 Tilted Alignment

As stated by Cognard *et al*,<sup>44</sup> "*Classification of liquid crystal alignment into homeotropic or homogeneous is an over-simplification, as often, non-homeotropic alignment is referred to as homogeneous*". In fact, the nematic director of liquid crystal molecules generally makes an angle  $\theta_T$  with the substrate surface. This 'tilt angle' is required for example, in practical twisted nematic displays in order to obtain a rotation of all the liquid molecules in the same direction on application of an electric field. A careful choice of tilt angle at the surface of each electrode gives rise to a better optical appearance.

In the neighbourhood of a particular surface, tilt angles are distributed around a mean value.<sup>45</sup> The nature of the liquid crystal material, its purity, and its chain length all modify the tilt value  $\theta_T$ . The tilt bias angle is also affected by the rate of evaporation of aligning layers, the pressure, fill-boat temperature, and any subsequent thermal treatment.<sup>46-49</sup> Figure 2.6 illustrates the variation in nematic director orientation for different beam evaporation angles.

There are several well-documented methods<sup>50-59</sup> for obtaining reliable tilt angles ranging from  $0 \rightarrow \pi/2$  radians. Figure 2.7 summarizes the tilt angles of the liquid crystal nematic director produced by different surface treatments.

### 2.13 Summary of Liquid Crystal Alignment Techniques

From the alignment methods described in sections 2.8 to 2.12, the one chosen for use in the experimental cells which will be described in more detail in chapter 5, was the rubbed polymer coating method. The deposition of the polymer by spinning is a simple, reproducible process. The polymerized surfaces are rubbed to give a reproducible tilt angle (of approximately  $2^\circ$ ), these rubbed plates can then be

assembled into three different arrangements; parallel, antiparallel and twisted. Figures 2.8a, b and c show examples of the respective assemblies. The parallel cell in Figure 2.8a is obtained by assembling the rubbed plates so that their directions of rubbing are parallel to each other and facing in the same direction (indicated by the arrows). The antiparallel cell, shown in Figure 2.8b is similar to the parallel case, however the directions of rubbing on each plate are opposite. Finally, the twisted arrangement in Figure 2.8c is obtained by rotating one of the plates through a given angle (usually  $90^\circ$ ) with respect to the other plate. The resultant effect on the directors alignment for a liquid crystal with PDA is also shown in each of these assemblies.

## 2.14 Measurement of Tilt Angles

Having identified a process of alignment for use in the experimental cells, it is necessary to describe the methods by which the tilt angles can be measured. There are three main techniques for measuring the tilt angle of the director across the cell. They are based on electrical or magnetic readings depending on the mode of operation of the liquid crystal.

### 2.14.1 Crystal Rotation Method

Consider the arrangement shown in Figure 2.9. The optical axis of the liquid crystal cell is uniformly orientated within the layer. The nematic material forms a uniaxial monocrystal having its optical axis at an angle  $\theta_T$  with respect to the surface plane, which can be measured using standard crystal optic techniques.<sup>59</sup>

The sample is attached to a moveable stage and viewed under a microscope illuminated with monochromatic light. If the optic axis is approximately parallel or perpendicular to the plane of the sample then it is possible to observe a conoscopic figure. If the axis makes a small angle with the sample, an off-centre uniaxial cross can be seen.

Crossland *et al*<sup>48</sup> described another conoscopic method which does not require



the use of a universal stage and can be applied to untwisted layers when the centre of the uniaxial cross lies outside the field of view. This method was based on the movement of the isogyres (interference figures) when the microscope stage is rotated about the microscope axis. If the optical axis is inclined at a large enough angle, so that the centre of the uniaxial cross lies outside the field of view, then such a rotation causes a single isogyre to move into the field of view, cross it, and then to move out again.

A relationship was obtained between the tilt angle  $\theta_T$  and the rotation angle  $\rho$  of the stage needed to take a centred isogyre to the edge of the field of view. If  $N$  is the numerical aperture of the microscopes objective lens, then the tilt angle is given by the expression,

$$\tan(90^\circ - \theta_T) = \frac{\tan[\sin^{-1}(N/n_o)]}{\sin \rho} \quad [2.2]$$

where  $n_o$  is the ordinary refractive index of the liquid crystal.

#### 2.14.2 Capacitance Method

This is an electrical method based on the measurement of the capacitance of the nematic filled cell. The equation for the zero field capacitance of the cell is given by,

$$C = C_0(\epsilon_{\perp} + \Delta\epsilon \sin^2 \theta_T) \quad [2.3]$$

where,

$C_0$  = capacitance of the empty cell,

$\Delta\epsilon = \epsilon_{\parallel} - \epsilon_{\perp}$  ( $\epsilon_{\parallel}$  and  $\epsilon_{\perp}$  are the parallel and perpendicular dielectric constants of the liquid crystal respectively.)

$\theta_T$  = tilt angle.

Re-arranging [2.3] an expression for  $\theta_T$  is obtained,

$$\theta_T = \sin^{-1} \left[ \frac{(C/C_0 - \epsilon_{\perp})}{\Delta\epsilon} \right]^{1/2} \quad [2.4]$$

To obtain  $\theta_T$ , the four quantities  $C$ ,  $C_0$ ,  $\epsilon_{\perp}$ ,  $\epsilon_{\parallel}$  are required. If errors occur in the measurement of these quantities, the accuracy of  $\theta_T$  is poor. Considerations

as to the magnitude of the measuring voltage have to be made. If the voltage is not small enough, the orientation of the optical axis is altered by the applied voltage (the liquid crystal director moves) giving rise to false readings.

### 2.14.3 Magnetic Null Method

Measurement by means of a magnetic field is generally referred to as a magnetic null method. The method is based on the fact that if the direction of the magnetic field is coincident with the optical axis of the liquid crystal layer, then any measured physical property depending on the molecular alignment is independent of the field strength. A homogeneous nematic layer is rotated in a magnetic field until the above condition occurs, and then the tilt bias angle is identical with the angle between the magnetic field and the sample's  $x$ -axis. Scheffer and Nehring<sup>46</sup> investigated this method using both capacitance and optical phase measurements. They showed that if  $\delta$  was the angular difference, in degrees, between the null orientation and that at which the capacitance is measured, then for small values of  $\delta$ ,

$$\frac{C_{(H)} - C_{null}}{C_{null}} \approx \delta \frac{(\epsilon_{\parallel} - \epsilon_{\perp})}{180} \pi \left\{ \frac{\sin 2\theta}{\epsilon_{\perp} + \epsilon \delta \sin^2 \theta_T} \right\} \quad [2.5]$$

Their results indicated that capacitive detection limited the measurement of tilt angles to materials with large dielectric anisotropies and to cases where the tilt angle is several degrees from 0° and 90°. The alternative optical phase retardation measurements were made by observing the relative intensity of helium neon laser light transmitted through the sample and a polarizer. They (Scheffer & Nehring) reported that the optical method had several advantages over capacitive detection, namely, it could be used on all types of liquid crystals, was sensitive in the 0° and 90° regions, and in addition measured tilt bias angles over smaller regions of the cell.

### **2.15 Summary of Tilt Angle measurement methods**

From the four tilt angle measurement methods described above, the crystal rotation method devised by Crossland *et al*<sup>48</sup> was chosen to measure the tilt angles of the liquid crystal filled experimental cells. The decision was made from the standpoint of convenience—the inventors of the technique worked in the department at S.T.L. Ltd. where the author was carrying out the research, and were available for guidance and consultation. Also the measurement apparatus was readily at hand and did not need to be assembled specially, as would have been the case for the other measurement techniques.

Having considered all of the criteria necessary for the fabrication and testing of liquid crystal filled devices, it only remains to choose the liquid crystal that will produce the required effect. However this is not as straightforward as it sounds and therefore the following chapter is given over to describing the different types of optical phenomena produced by treated liquid crystals in response to an applied voltage.

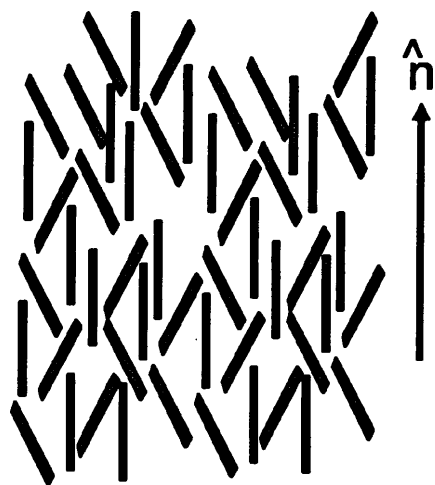


**Figure 2.1a**  
Nematic Mesophase

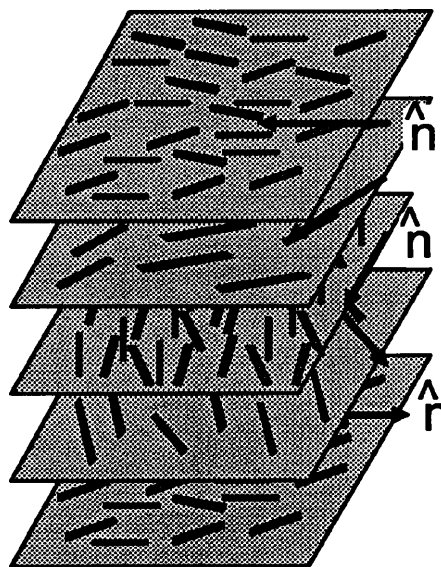


**Figure 2.1b**  
Cholesteric Mesophase

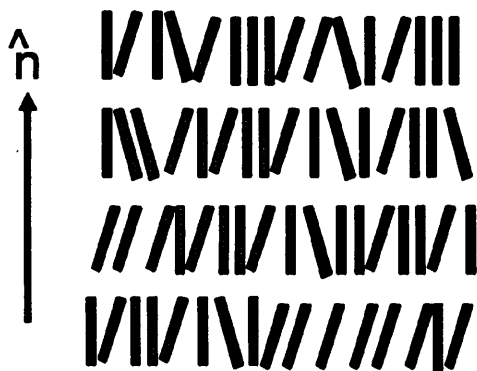


**Figure 2.1c**  
Smectic Mesophase

$\hat{n}$  represents the axis of preferred orientation.  
(That is the average director orientation)

Orientation of molecules in the three types of Thermotropic liquid crystal.

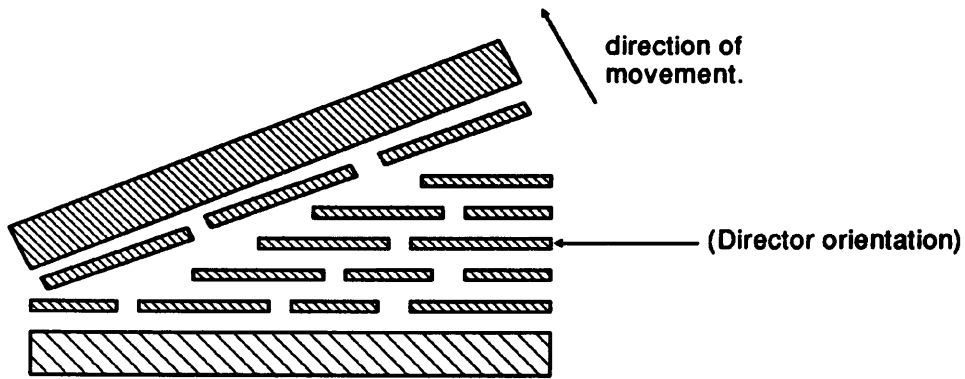


**Figure 2.2a**  
Splay Deformation  $K_{11}$

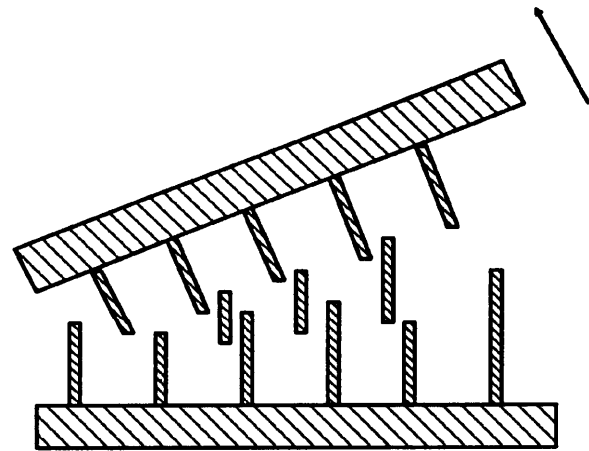


**Figure 2.2b**  
Bend Deformation  $K_{33}$

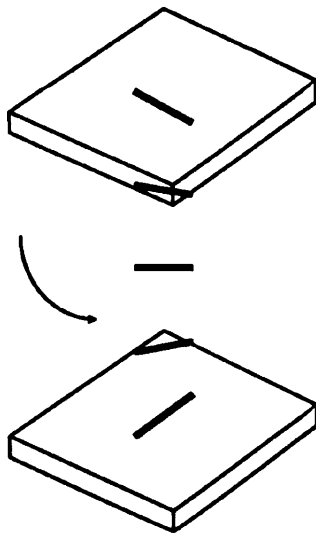


**Figure 2.2c**  
Twist Deformation  $K_{22}$

**Three Elasticity components of a liquid crystal.**

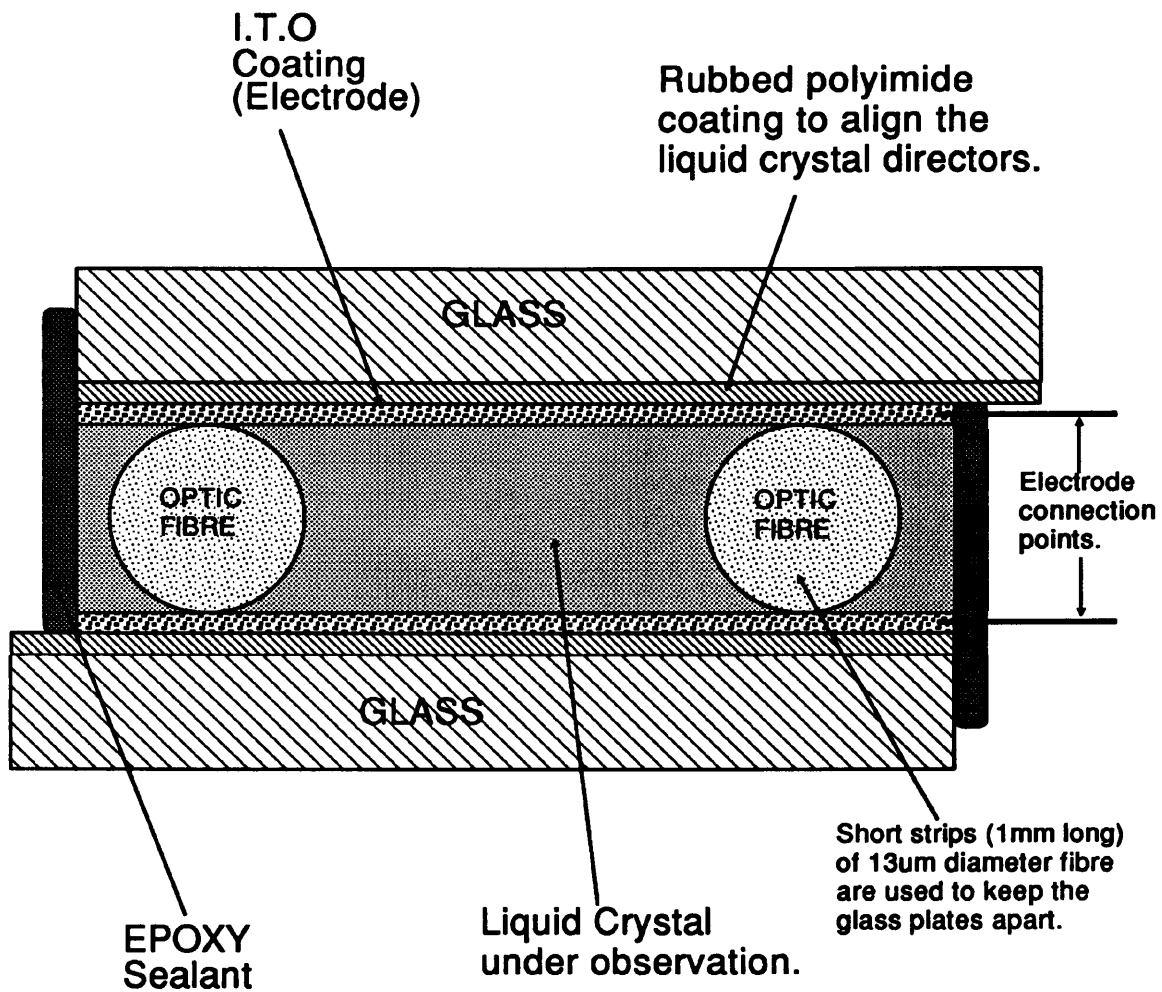


**Figure 2.3**

Diagram of a 'standard' liquid crystal experimental cell - Cross Section.

The cell is used to observe electro- and magneto-optical effects of liquid crystals.

NOT TO  
SCALE

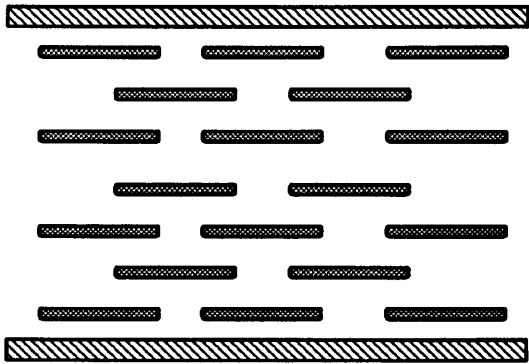


**Figure 2.4a**  
Homogeneous Alignment

**Figure 2.4b**  
Homeotropic Alignment

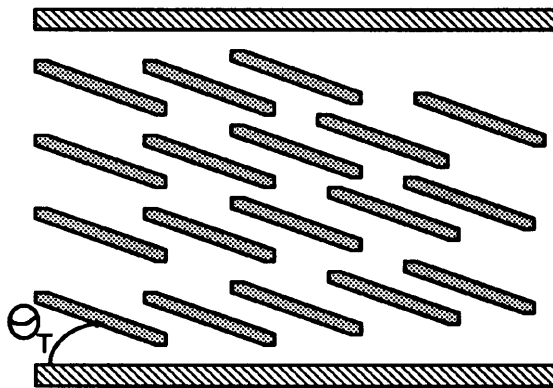
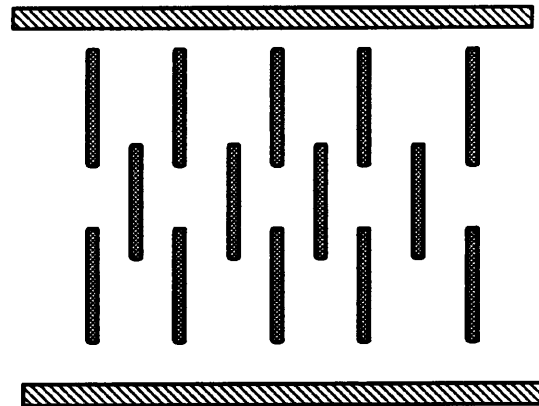
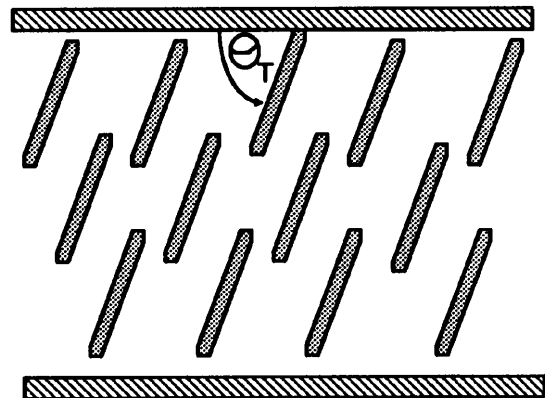


**Figure 2.4c (i)**  
Homogeneous Alignment  
with a tilt.

**Figure 2.4c (ii)**  
Homeotropic Alignment  
with a tilt.



**Liquid crystal director alignments on treated surfaces.**

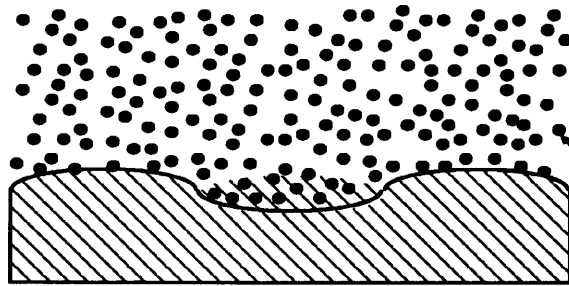


**Figure 2.5a**

low  $F_P$   
low  $F_E$

Long molecular axes of liquid crystal are parallel to surface.

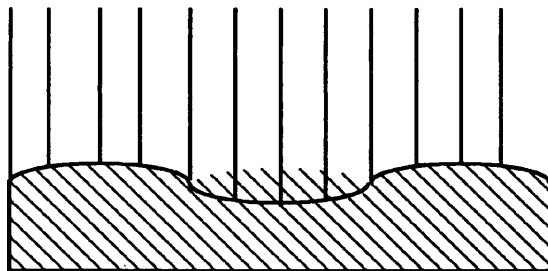


**Figure 2.5b**

high  $F_P$   
low  $F_E$

Long molecular axes of liquid crystal are perpendicular to surface.

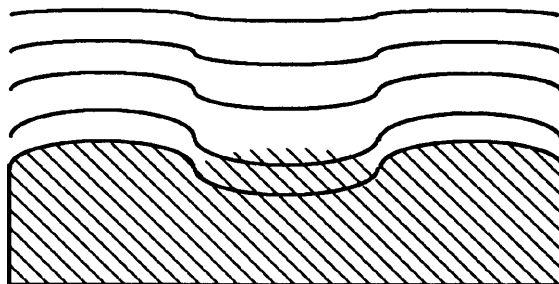


**Figure 2.5c**

low  $F_P$   
high  $F_E$

Long molecular axes of liquid crystal are parallel to surface.

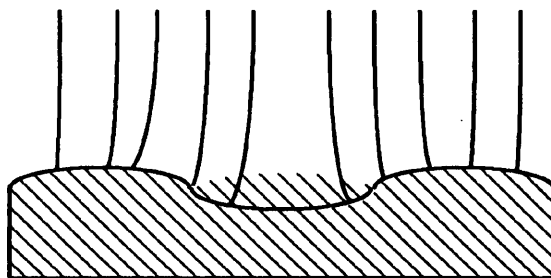


**Figure 2.5d**

low  $F_P$   
high  $F_E$

Long molecular axes of liquid crystal are perpendicular to surface.

### Alignment of long molecular liquid crystal axes on grooved surfaces.

Contributions to the free energy  $F$  are shown:  $F = F_P + F_E$  {  $P$  = physio-chemical free energy.  
 $E$  = elastic free energy. }



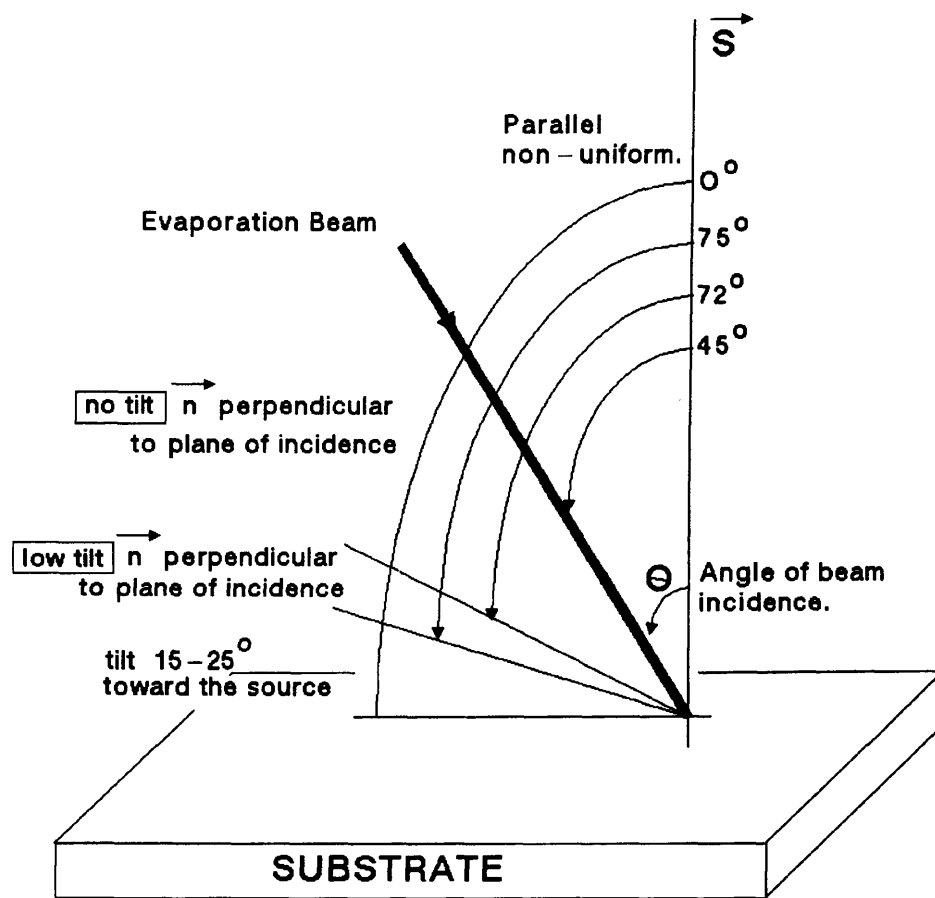


**Figure 2.6**

Liquid Crystal nematic director orientation induced by evaporated silicon oxide. [Depending upon the angle of incidence of the evaporation beam different orientations are observed].

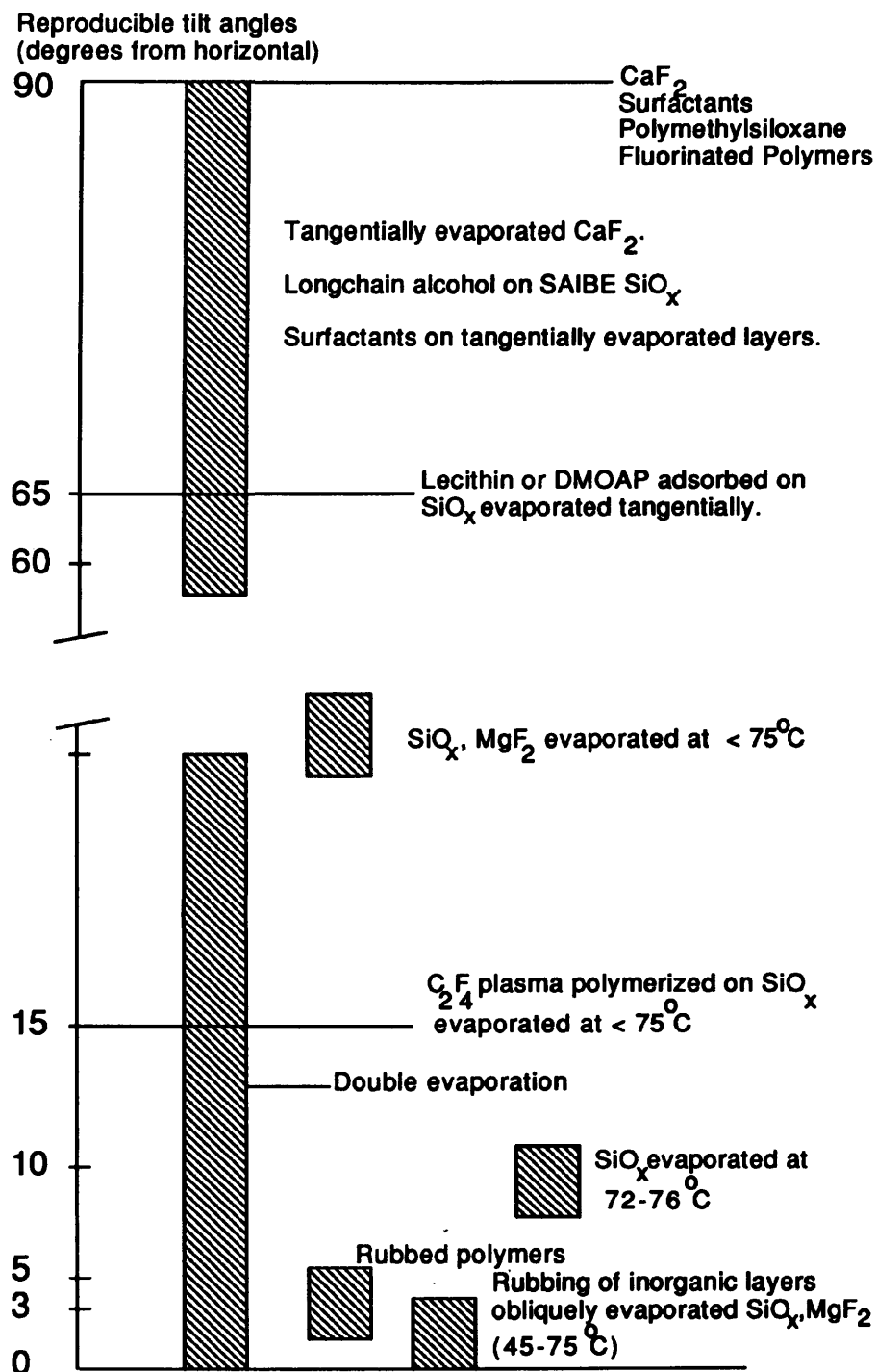


**Figure 2.7**

Tilt angle of the liquid crystal nematic director produced by different surface treatments.

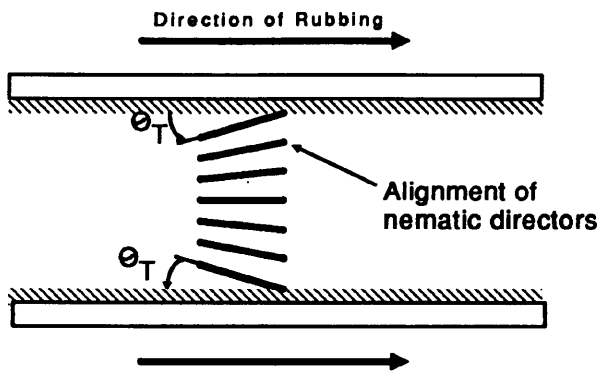


**Figure 2.8a**  
Parallel rubbed cell

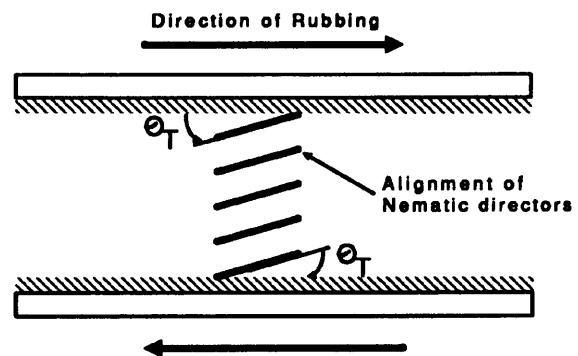


**Figure 2.8b**  
Antiparallel rubbed cell

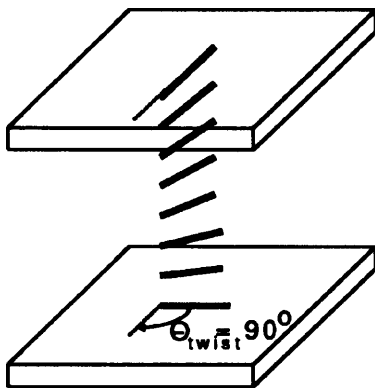


**Figure 2.8c**  
Pi/2 twisted nematic  
(N.B. No pre-tilt is shown)

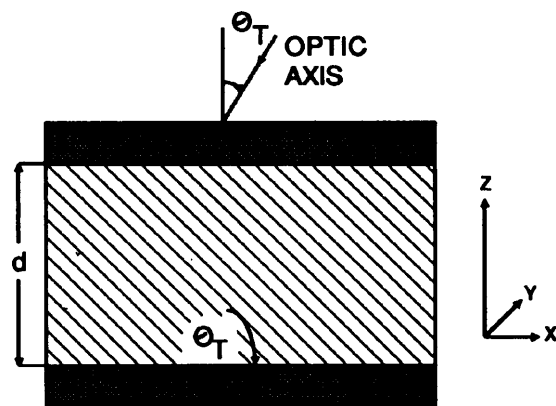


**Figure 2.9**  
Cross section of a liquid crystal cell showing tilt angle and angle of light incidence.

# 3

## Electro-Optic Phenomena

### 3.1 Chapter Summary

The chapter discusses the electro-optic phenomena of liquid crystals with respect to their dielectric- and conduction-induced effects. This information, along with that presented in chapter 2, led the author to choose the nematic liquid crystal family as the most suitable to incorporate into the experimental cells. It was decided that the diffraction efficiency measurements would be made on the cells in three separate modes of operation: 1) electrically controllable birefringence; 2) guest-host dye and 3) phase rotator.

### 3.2 Introduction

One of the simplest and most reliable methods of inducing optical effects in liquid crystals is to apply an electric field to the liquid crystal. This is facilitated in most experimental cells by electrodes which are deposited on the insides of the glass plates and which are in contact with the liquid crystal.

In order to determine the most suitable type of liquid crystal to incorporate into such an arrangement, it is necessary to first consider the different types of electrically inducible effects.

Two types of electro-optic phenomena are considered. Those caused only by dielectric forces, sometimes referred to as field effects, and those induced by the combination of dielectric and conduction forces.

### 3.3 Dielectric Effects

#### 3.3.1 The Freedericksz Transition

The Freedericksz transition effect<sup>60</sup> discovered over 40 years ago, forms the basis of one of the most important dielectric effects that can be utilized in displays: the application of an electric field causes the liquid crystal to deform from its initial equilibrium position. Figures 3.1*a* & 3.1*b* show the effects of an electric field on the two common alignment cases. In Figure 3.1*a*, above the threshold, the majority of molecules rotate until they are parallel with the applied field, apart from the molecules at each boundary, which remain anchored. The same effect can be seen in Figure 3.1*b*, however this time the molecules in the central region align perpendicular to the applied field. The re-alignment process occurs in the material after a threshold voltage has been exceeded. The threshold voltage is given by,<sup>61–62</sup>

$$V_{TH} = \sqrt{\frac{K_{33}}{\epsilon_0 \Delta \epsilon}} \quad [3.1]$$

where  $K_{33}$  is the bend elastic constant and  $\epsilon_0$  is the permittivity of free space.

#### 3.3.2 Electrically Controllable Birefringence

Referring to Figures 3.1*a* and 3.1*b* once more, in Figure 3.1*a*, below the threshold voltage, the birefringence for light at normal incidence to the cell is high ( $\Delta n \approx 0.2 \rightarrow 0.3$ ). As the threshold voltage is reached, the birefringence decreases due to the molecules rotating into a parallel alignment with the incident light. The converse occurs in Figure 3.1*b*: the birefringence is low at zero applied volts and increases as the threshold voltage is reached.

Figure 3.2 shows a NDA nematic liquid crystal SLM in two modes of operation: transmissive and reflective. In the transmissive case, for a liquid crystal with NDA (Figure 3.2*a*), the homeotropic texture is optically isotropic to light propagating perpendicular to the cell walls. Consequently, with crossed polarizers, no light is transmitted through the analyser at the equilibrium state. As

the threshold voltage is reached, the liquid crystal becomes birefringent to the transmitted light, and some of the light passes through the output polarizer. The intensity  $I$  of the transmitted light is expressed by,<sup>63</sup>

$$I = I_p \sin^2 2\psi \sin^2 \frac{\delta}{2} \quad [3.2]$$

where,

$I_p$  is the light transmitted through the two parallel polarizers.

$\psi$  is the angle between the input light optical vector and the projection of the director onto the cell walls.

$d$  is the cell thickness.

$\lambda$  is the wavelength of the incident light.

$\Delta n_{\max}$  is the maximum birefringence.

$$\delta = [2\pi d \Delta n_{\max} \sin^2 \theta(V)] / \lambda$$

$\theta(V)$  is the voltage variable angle between the direction of propagation of light through the cell and the direction of the long axes of the liquid crystal directors.

$I$  is a maximum when  $\psi = 45^\circ$ , but  $\psi$  is not normally uniquely defined in an untreated cell. However, in a cell where the glass has been treated (see Section 2.10), the liquid crystal can be made to deform with a well-defined direction for its director. This preferred direction can be set at a  $45^\circ$  angle to the crossed polarizer and analyser by rotating the SLM through  $45^\circ$ .

An alternative arrangement is to view the SLM in a reflective mode. Here the mirror replaces the input polarizer giving results that will be identical to those of the transmissive case.

### 3.3.3 Twisted Nematic Effect

In the twisted nematic arrangement shown in Figure 3.3, a thin layer of nematic liquid crystal is orientated homogeneously at the cell walls, but with a twist of  $90^\circ$  introduced between the two surfaces. The bulk fluid adapts itself to the boundary conditions by distorting to form a continuous rotation from one cell wall to the other. Thus, the twisted layer rotates the plane of polarization of incident linearly polarized light. If viewed through crossed polarizers, the incident light

is transmitted. The twist can be altered by applying a voltage to the cell. Since the liquid crystal in this example exhibits PDA, the applied voltage, if above the threshold region, causes a molecular re-alignment and thereby reduces the optical transmission of the device to a minimum. The threshold voltage in this situation is,<sup>64</sup>

$$V_{TH}^2 = \left( \frac{1}{\Delta\epsilon\epsilon_0} \right)^2 [K_{11}\pi^2 + (K_{33} - 2K_{22})\omega^2] \quad [3.3]$$

where  $K_{11}$ ,  $K_{22}$ , and  $K_{33}$  are the elastic constants, and  $\omega$  is the twist angle.

The equation can further be reduced for the 90° twisted case,

$$V_{TH} = \pi \left( \sqrt{\frac{[K_{11} + \frac{1}{4}(K_{33} - 2K_{22})]}{\Delta\epsilon\epsilon_0}} \right) \quad [3.4]$$

The data presented in Figure 3.4 show the transmission and optical rotation versus voltage characteristics for such a device.<sup>64</sup>

So far in the discussion of electro-optic effects, attention has been focussed on nematic liquid crystal. The following subsections describe some of the effects which are observable in other types of liquid crystals including doped nematics.

### 3.3.4 Cholesteric to Nematic Transition

If a small amount of cholesteric material is added to a nematic liquid, the result is a cholesteric liquid with a large pitch. On application of an electric field to thin layers of this material, the helical pitch ordering can be increased or decreased, and can even tip over entire helical regions. Wysocki *et al*<sup>65</sup> observed that a phase transition from cholesteric back to nematic occurs if a sufficiently high electric field is applied to the mixture.

In the zero field state (Figure 3.5), the cholesteric planes are approximately perpendicular to the cell walls, and the helical axes have a random orientation. This gives rise to the weak scattering texture known as Grandjean or planar texture. As the electric field increased above a threshold value the helical axes

become distorted. These distortions grow as the field is further increased until the helical axes become approximately parallel to the cell walls. This is a strongly scattering texture called focal conic.

Continuing to increase the electric field causes the helices to begin to unwind and dilate, until well above threshold all the molecules, apart from the surface layers, are aligned parallel to the electric field (homogeneous), and a transparent texture results. This is the nematic mesophase.

When the field is lowered the focal conic texture returns. This is in fact a metastable state and cannot remain stable without an applied field. The field at which the helical axes start to distort is proportional to  $(1/P_0^2)^{66}$  where  $P_0$  is the undeformed helix pitch. When the field is lowered below the weak scattering state returns. This is the stable state. De Gennes<sup>67</sup> calculated the following expression for the threshold field,

$$V_{TH} = \frac{\pi^2}{P_0} \sqrt{\frac{K_{22}}{\Delta\epsilon\epsilon_0}} \quad [3.5]$$

### 3.3.5 Absorption Effects

#### 3.3.5.1 Guest-Host Effect

The guest-host or colour-switching reaction<sup>68–69</sup> is an effect in which a small amount (0.1%) of ‘guest’ pleochroic dye is incorporated within a nematic ‘host’ material. These pleochroic molecules can be aligned co-operatively by the host liquid crystal. The dye has different absorption coefficients parallel and perpendicular to its axis. Taking the arrangement shown in Figure 3.6, with zero electric field, the liquid crystal is in the homogeneous orientation, and the dye molecules are aligned with their long axes parallel to the electric vector of the linearly polarized light. In this configuration, the dye molecules have absorption bands in the visible. Above the threshold voltage, the PDA nematic fluid aligns parallel to the field and the dye changes



direction also, causing a drop in the amount of light absorbed. Consequently, an intensity change is observed in passing between the two states. These intensity variations have been used to represent the levels of grey in some of the current commercial miniature liquid crystal televisions.<sup>13</sup>

#### **3.3.5.2 Dyed Phase Change Effect**

After Heilmeyer and Zanoni<sup>68</sup> discovered the effect of adding a pleochroic dye to a nematic host, White and Taylor<sup>70</sup> discovered the use of the cholesteric-nematic phase transition as the host liquid crystal effect. Adding the pleochroic dye to the mixture, and applying the field off state, the dye molecules absorb all polarizations of incident light. Above the threshold, the cholesteric unwinds to form a pseudo-nematic fluid in the homeotropic state. Oriented this way, the dye molecules absorb little of the incident light. The dyed phase change effect has several advantages, some of these include: increased brightness—no polarizer is required; no stringent surface requirements; and a wide angle of view. The disadvantages are: high operating voltage requirements; hysteresis effects; and the critical voltage is dependent on the cell thickness (cell thickness must be uniform across the entire surface area of the device).

### **3.4 Conduction Induced Effects**

In nematic materials with an electrical conductivity greater than  $10^{-11}(\Omega\text{cm})^{-1}$ , conduction induced flow occurs during the application of a voltage. Conductive nematics show two hydrodynamic instability thresholds as the voltage across the layer is increased: firstly domains appear; secondly at higher voltages turbulence sets in. The instabilities can be produced by a.c. or d.c. excitation, with differing mechanisms occurring for each. The mechanism covering the d.c. case was described by Felici,<sup>71</sup> whilst the a.c. effect follows the Carr-Helfrich model.<sup>72-73</sup> Initially it was thought that only a material with NDA could produce turbulence, but De Jeu

*et al*<sup>74</sup> showed that this was not a prerequisite by producing effects in a mesogen having PDA.

Most applications involve induction of fluid flow by alternating currents, and this effect is illustrated in Figure 3.7. In considering the nematic material, it is assumed that the ordering is initially homogeneous and that the applied field produces a sinusoidal perturbation of the director. Due to anisotropic conductivity, a space charge accumulates at the distortion maxima and minima when the field is applied. The applied field produces a force on the liquid crystal because of the space charge and this stimulus drags the fluid towards the walls. The cell walls impose boundary conditions which give rise to a vortical flow of the fluid (Figure 3.7a). The fluid shear torque aligns the director in the direction of fluid flow, while opposing this are the dielectric and fluid forces. At the threshold voltage (Figure 3.7b) the fluid becomes unstable and a periodic distortion occurs (these are referred to as domains or Williams stripes<sup>75</sup>). Further increases in field strength cause the cellular pattern to subdivide, undulate, and eventually fracture into the turbulence shown in Figure 3.7c.

The instability threshold voltage increases as the a.c. frequency increases, and rises dramatically as the critical frequency  $f_c$  is approached. At frequencies above  $f_c$ , the space charge does not oscillate; ions do not have sufficient time to move during the half cycle of the excitation waveform, and the liquid is no longer operating in a conducting regime. Also observable is the fact that at field strengths above the threshold, the microscopic texture of the nematic material changes into an arrangement of herring-bone pattern striations ('chevrons') that scatter light.

### **3.4.1 Dynamic Scattering**

The term 'dynamic scattering' is used to refer to the intense wide angle light scattering that accompanies electro-hydrodynamic turbulence in liquid crystals.

The turbulent mesophase contains moving birefringent regions of the order of

several microns in size. The refractive index gradients produced as a result cause the diffuse optical scattering. Heilmeyer's discovery<sup>76</sup> in 1968 of domain scattering in liquid crystals led to the production of the first electro-effect liquid crystal displays.

In operation, application of a d.c. or low frequency a.c. signal across the plates of the cell changes the appearance of the material from clear to milky white. On removal of the voltage, the liquid gradually reverts back to its transparent state.

### **3.4.2 Optical Storage**

The optical storage phenomenon can be demonstrated in a nematic-cholesteric mixture (90% nematic by weight). Besides increasing the resistivity of the nematic, the addition of the cholesteric gives the mixture many of the properties of a cholesteric. Optical storage effects in mixtures with negative dielectric anisotropy were first observed by Heilmeyer and Goldmacher in 1969.<sup>77</sup> Their research (depicted in Figures 3.8a → 3.8d) showed the following effects. In going from the zero applied field state to the application of a d.c. or low frequency a.c. signal, the sample changed from a weakly scattering state to a dynamic scattering state. On removal of the field, the dynamic scattering disappeared, but a semi-permanent forward scattering state remained. The time constant for the decay of this state was shown to be minutes, hours or even days, dependent on the materials and fabrication techniques chosen. Alternatively, the scattering state could be returned to the initial weakly scattering texture by applying a signal in the audio frequency range of 500→1000 Hz.

Further investigation by other researchers<sup>78-79</sup> suggested that the mechanism of this process involves the formation of scattering centres in which the helical axes of the cholesteric molecules have a distribution of angles with respect to the electrode surfaces. This arises from the strong fluid deformations associated with dynamic scattering. The audio frequency erasure effect is due to the mixture

having NDA; the applied audio frequency field aligns the molecular long axes parallel to the electrodes, which returns the mixture to the Grandjean texture. If the helix pitch is carefully chosen, the reflection colours occur outside the visible spectrum and the liquid crystal appears transparent. The advantage of the effect, which can be operated in transmissive or reflective modes, is that a means of storing binary information using no additional power to maintain the state is facilitated optically.

### **3.5 Thermo-Optic Effects**

#### **3.5.1 Cholesteric Temperature Sensors**

The well-defined colour changes of cholesteric liquid crystals with small changes in temperature can be utilized in a variety of ways. Already commercially available is a 'thermal mapping kit' which allows integrated circuit (i.c.) designers to determine the regions of the chip that overheat in operation. This is achieved by coating the i.c. with a cholesteric compound and noting the colour change. Another commercial application is to monitor skin temperature. By applying a specially fabricated band of liquid crystal material around the suspect area of skin, the potentially tumourous areas are located by a sharp colour change. Disposable liquid crystal thermometers have also been developed.

#### **3.5.2 Thermal Smectic Effects**

Thermo-optic storage effects in liquid crystals were first reported by Soref<sup>80</sup> for nematic-cholesteric mixtures. The effect was extended to cover smectic liquid crystals and Hareng and Le Berre<sup>81</sup> reported a laser-addressed smectic storage device in 1975. In this arrangement, a transparent, homeotropically aligned smectic is heated by an infrared laser beam. The localized heating effect causes a change in transition to the isotropic state. Removal of the beam allows the material to cool from the isotropic to the smectic phase. The result is an area which contains a scattering texture, and is stable within the homeotropic state.

The display is erased by a field assisted thermal process.

### **3.6 Summary of Liquid Crystal Electro-Optic Effects**

From an analysis of current commercially available liquid crystal-based SLMs, and also taking into consideration the successful experimental SLMs covered by Fisher,<sup>11</sup> it is clear that nematic-filled SLMs are the most versatile and adaptive in use. Historically, the range of electro-optic effects reproducible in nematic mesogens, was a strong influencing factor on the designers of liquid crystal SLMs.

For the same reasons, the author chose to employ nematic liquid crystals in the experimental cells. In order to determine the diffraction efficiency of the liquid crystal experimental cell, measurements would be made on the cells in three modes of operation,

1. Electrically controllable birefringence
2. As 1. but with the experimental cell rotated through  $45^\circ$  between crossed polarizers.
3. Guest-host dye

Coupled with the descriptions of the alignment techniques put forward in chapter 2, the nematic liquid crystal was pre-tilted to  $2^\circ$  and aligned in separate parallel and antiparallel homogeneous configurations. [Note: details of cell fabrication and assembly are given in chapter 5]

Before discussing the experimental arrangements for measuring diffraction efficiency from the above configurations, it is necessary to first consider the theoretical aspects of liquid crystal director movement in response to an electric field. By considering the arrangements relevant to the experimental 'set-up', a better understanding of the liquid crystal's response to a voltage can be obtained. The remainder of this chapter is therefore devoted to considering two forms of parallel and tilted homogeneous liquid crystal filled cells using the elastic continuum theory of liquid crystals postulated by Frank<sup>86</sup> in 1958.

### 3.7 The Elastic Continuum Theory of Liquid Crystals

In terms of molecular theories of liquid crystals,<sup>82-83</sup> it is possible to calculate and successfully explain various properties of mesophase transitions. However, in describing the large-scale phenomena involving the response of bulk liquid crystal samples to external disturbances, it is more convenient to regard the liquid crystal as a continuous medium with a set of elastic constants, than to treat it on a molecular basis. Zocher,<sup>84</sup> Oseen<sup>85</sup> and Frank<sup>86</sup> developed a general theory of curvature elasticity in molecularly uniaxial liquid crystals, which was successful in explaining various electric and magnetic field-induced effects. In thin films of a nematic substance contained between two surfaces, orientations are imposed at the surface which, if not parallel, induce a curved transition from one orientation to the other. A similar curvature can be introduced by the orientating effect of an electric or magnetic field.

Frank postulated that the total free energy  $G$  of a liquid crystal specimen in any particular configuration, relative to its free energy in the state of uniform orientation (this being the equilibrium or minimum free energy state), could be expressed as the volume integral of a free energy density  $g$  which was a function of the differential coefficients which measured curvature,

$$G = \int_V g \, dv \quad [3.6]$$

Under external fields,  $g$  is given by,

$$g = g_D + g_E + g_M \quad [3.7]$$

where  $g_D$  is the change in free energy density due to the distortion of the liquid crystal director pattern due to surface effects, and  $g_E$ ,  $g_M$  are respectively the contributions to the free energy density due to electric and magnetic fields. If the vector  $\vec{L}$  represents the unit director field, then the expression obtained by Frank for  $g_D$  in the nematic state is,

$$g_D = \frac{1}{2} \{ K_{11} [\nabla \cdot \vec{L}]^2 \} + \frac{1}{2} \{ K_{22} [\vec{L} \cdot \nabla \times \vec{L}]^2 \} + \frac{1}{2} \{ K_{33} [\vec{L} \times \nabla \times \vec{L}]^2 \} \quad [3.8]$$

where  $K_{11}$ ,  $K_{22}$  and  $K_{33}$  are the nematic director elastic constants for ‘splay’, ‘twist’ and ‘bend’ respectively. Incorporating the expressions for  $g_E$  and  $g_M$  equation [3.8] becomes,

$$g = \frac{1}{2} \left\{ K_{11} [\nabla \cdot \vec{L}]^2 + K_{22} [\vec{L} \cdot \nabla \times \vec{L}]^2 + K_{33} [\vec{L} \times \nabla \times \vec{L}]^2 \right\} - \frac{1}{2} \Delta \epsilon \epsilon_0 (\vec{E} \cdot \vec{L})^2 - \frac{1}{2} \Delta \chi (\vec{H} \cdot \vec{L})^2 \quad [3.9]$$

where  $\Delta \epsilon = \epsilon_{\parallel} - \epsilon_{\perp}$  is the difference between the local relative dielectric constants in directions parallel and perpendicular to the local nematic director,  $\epsilon_0$  is the dielectric permittivity of free space, and  $\Delta \chi = \chi_{\parallel} - \chi_{\perp}$  is the difference in parallel and perpendicular values of the diamagnetic susceptibility.

Equations [3.6] and [3.9] are the fundamental equations of the elastic continuum theory of nematic liquid crystals.

### 3.8 Electric Field Deformations of various configurations

The following sections deal with the electric field deformation of the liquid crystal directors in parallel homogeneous and tilted homogeneous cells. They are adaptations of work carried out by Deuling<sup>87</sup> and Simon<sup>88</sup> respectively.

#### 3.8.1 A Parallel homogeneous liquid crystal cell

Consider the case of a nematic liquid crystal with PDA, enclosed between two transparent conductive glass plates a distance  $d$  apart (Figure 3.9). The molecules in this arrangement are orientated parallel to the containing walls. On the application of an electric field  $\vec{E}$ , perpendicular to the cell walls, the molecules will tilt relative to the plates due to the positive dielectric anisotropy.

The angle  $\theta$  is a function of  $z$ , assuming a value of  $\theta_m$  at  $z = d/2$ , and being zero at the boundaries ( $z = 0, d$ ). Assuming that all director movement is in the  $x$ - $z$  plane, then it can be seen that  $\vec{L}$ , the unit director vector, has components  $\vec{L}_z$ ,  $\vec{L}_y$  and  $\vec{L}_x$ , where,

$$\begin{aligned}\vec{L}_x &= \cos \theta(z), \\ \vec{L}_y &= 0,\end{aligned}$$

and,

$$\vec{L}_z = \sin \theta(z). \quad [3.10]$$

Accordingly, it can be shown that,

$$\text{i)} \quad [\nabla \cdot \vec{L}]^2 = \cos^2 \theta \left( \frac{d\theta}{dz} \right)^2, \quad [3.11]$$

$$\text{ii)} \quad [\vec{L} \cdot \nabla \times \vec{L}]^2 = 0, \quad [3.12]$$

$$\text{iii)} \quad [\vec{L} \times \nabla \times \vec{L}]^2 = \sin^2 \theta \left( \frac{d\theta}{dz} \right)^2. \quad [3.13]$$

From symmetry considerations, only the  $z$  component of  $\vec{E}$  is non-zero,

$$\text{hence iv)} \quad [\vec{E} \cdot \vec{L}]^2 = E_z^2 \sin^2 \theta \quad [3.14]$$

If  $G'$  represents the increase in free energy per unit area, then equation [3.6] can be modified to,

$$G' = \int_0^d g \, dz \quad [3.15]$$

Substituting equations [3.11–3.14] into [3.9] and hence into [3.15] leads to,

$$G' = \frac{1}{2} \int_0^d \left\{ (K_{11} \cos^2 \theta + K_{33} \sin^2 \theta) \left( \frac{d\theta}{dz} \right)^2 - \Delta \epsilon \epsilon_0 E_z^2 \sin^2 \theta \right\} dz \quad [3.16]$$

Application of the Euler-Lagrange equation to equation [3.22] leads to an equation for  $\theta$  which minimizes the value of the integral above, that is,

$$\begin{aligned} \left\{ (K_{11} \cos^2 \theta + K_{33} \sin^2 \theta) \left( \frac{d^2 \theta}{dz^2} \right) + (K_{33} - K_{11}) \sin \theta \cos \theta \left( \frac{d\theta}{dz} \right)^2 \right. \\ \left. - \Delta \epsilon \epsilon_0 E_z^2 \sin \theta \cos \theta \right\} = 0 \end{aligned} \quad [3.17]$$

If  $\vec{D}$  represents the dielectric displacement then,

$$D_x = \epsilon_0 \epsilon_r E_x \quad [3.18]$$

$D_x$  can be split into components  $D_{\parallel}$  and  $D_{\perp}$ , respectively parallel and perpendicular to the director,

$$D_{\parallel} = \epsilon_0 \epsilon_{\parallel} E_x \sin \theta, \quad [3.19]$$

and,

$$D_{\perp} = \epsilon_0 \epsilon_{\perp} E_x \cos \theta \quad [3.20]$$



Thus,

$$D_z = D_{\parallel} \sin \theta + D_{\perp} \cos \theta \quad [3.21]$$

or

$$D_z = \epsilon_0 E_z (\epsilon_{\parallel} \sin^2 \theta + \epsilon_{\perp} \cos^2 \theta) \quad [3.22]$$

and

$$E_z = \frac{D_z}{\epsilon_0 (\epsilon_{\parallel} \sin^2 \theta + \epsilon_{\perp} \cos^2 \theta)} \quad [3.23]$$

Substituting equation [3.23] into [3.17] and putting

$$K = \frac{(K_{33} - K_{11})}{K_{11}}, \quad \text{and} \quad M = \left( \frac{\epsilon_{\parallel} - \epsilon_{\perp}}{\epsilon_{\perp}} \right) \quad \text{yields,}$$

$$\begin{aligned} K_{11} \left[ (1 + K \sin^2 \theta) \left( \frac{d^2 \theta}{dz^2} \right) + K \sin \theta \cos \theta \left( \frac{d\theta}{dz} \right)^2 \right] \\ - \frac{M D_z^2 \sin \theta \cos \theta}{\epsilon_0 \epsilon_{\perp} (1 + M \sin^2 \theta)^2} = 0 \end{aligned} \quad [3.24]$$

Multiplying [3.24] by  $2 \left( \frac{d\theta}{dz} \right)$  and integrating once yields,

$$K_{11} (1 + K \sin^2 \theta) \left( \frac{d\theta}{dz} \right)^2 = C + \frac{D_z^2}{\epsilon_0 \epsilon_{\perp} (1 + M \sin^2 \theta)} \quad [3.25]$$

At  $z = d/2$ ,  $\left( \frac{d\theta}{dz} \right) = 0$  and  $\theta = \theta_m$ , thus  $C$  becomes,

$$C = \frac{-D_z^2}{\epsilon_0 \epsilon_{\perp} (1 + M \sin^2 \theta_m)} \quad [3.26]$$

and from equations [3.25] and [3.26],

$$\begin{aligned} \left( \frac{d\theta}{dz} \right) &= D_z \sqrt{\frac{M}{\epsilon_0 \epsilon_{\perp} K_{11}}} \\ &\times \left\{ \frac{\sin^2 \theta_m - \sin^2 \theta}{(1 + K \sin^2 \theta)(1 + M \sin^2 \theta)(1 + M \sin^2 \theta_m)} \right\}^{1/2} \end{aligned} \quad [3.27]$$

Integrating the inverse of [3.27] gives,

$$\begin{aligned} z &= \left( \frac{1}{D_z} \right) \sqrt{\frac{\epsilon_0 \epsilon_{\perp} K_{11} (1 + M \sin^2 \theta_m)}{M}} \\ &\times \int_0^{\theta} \left\{ \frac{(1 + K \sin^2 \theta)(1 + M \sin^2 \theta)}{(\sin^2 \theta_m - \sin^2 \theta)} \right\}^{1/2} d\theta \end{aligned} \quad [3.28]$$

If  $U$  represents the voltage applied to the liquid crystal, then,

$$U = 2 \int_0^{d/2} E_z dz \quad [3.29]$$

and substituting for  $E_z$  from equation [3.23],

$$U = 2 \int_0^{d/2} \frac{D_z dz}{\epsilon_0(\epsilon_{\parallel} \sin^2 \theta + \epsilon_{\perp} \cos^2 \theta)} \quad [3.30]$$

Changing the variable  $dz$  to  $d\theta$  via [3.27] gives,

$$U = 2 \sqrt{\frac{K_{11}(1 + M \sin^2 \theta_m)}{\epsilon_0 \Delta \epsilon}} \times \int_0^{\theta_m} \left\{ \frac{(1 + K \sin^2 \theta)}{(1 + M \sin^2 \theta)(\sin^2 \theta_m - \sin^2 \theta)} \right\}^{1/2} d\theta \quad [3.31]$$

Making the substitution,  $\sin \theta = \sin \theta_m \sin \phi$ , and  $N = \sin^2 \theta_m$ , then,

$$d\theta = \sqrt{\left[ \frac{N(1 - \sin^2 \phi)}{(1 - N \sin^2 \phi)} \right]} d\phi \quad [3.32]$$

and equation [3.31] becomes,

$$U = 2 \sqrt{\frac{K_{11}(1 + MN)}{\epsilon_0 \Delta \epsilon}} \times \int_0^{\pi/2} \left\{ \frac{(1 + KN \sin^2 \phi)}{(1 + MN \sin^2 \phi)(1 - N \sin^2 \phi)} \right\}^{1/2} d\phi \quad [3.33]$$

The threshold voltage  $U_0$ , is defined as the voltage at which the angle  $\theta_m$  becomes non-zero, that is, the maximum value at which  $\theta_m = 0$ . Thus,

$$U_0 = 2 \sqrt{\frac{K_{11}}{\epsilon_0 \Delta \epsilon}} \int_0^{\pi/2} d\phi = \pi \sqrt{\frac{K_{11}}{\epsilon_0 \Delta \epsilon}} \quad [3.34]$$

Combining equations [3.33] and [3.34] yields,

$$\frac{U}{U_0} = \frac{2}{\pi} \sqrt{(1 + MN)} \times \int_0^{\pi/2} \left\{ \frac{(1 + KN \sin^2 \phi)}{(1 + MN \sin^2 \phi)(1 - N \sin^2 \phi)} \right\}^{1/2} d\phi \quad [3.35]$$

and from equation [3.28],

$$\frac{2z}{d} = \frac{\int_0^{\alpha} \left\{ \frac{(1 + KN \sin^2 \phi)(1 + MN \sin^2 \phi)}{(1 - N \sin^2 \phi)} \right\}^{1/2} d\phi}{\int_0^{\pi/2} \left\{ \frac{(1 + KN \sin^2 \phi)(1 + MN \sin^2 \phi)}{(1 - N \sin^2 \phi)} \right\}^{1/2} d\phi} \quad [3.36]$$

where  $\alpha = \sin^{-1}(\sin \theta / \sin \phi_m)$ .

For a given value of  $U/U_0$  (or  $U$ ), the corresponding value of  $\theta_m(N)$  is found from equation [3.35]. Equation [3.36] is then used to calculate the angle of deformation  $\theta$ , as a function of  $z$ .

The electro-optic response of a nematic layer can be calculated once the deformation of the liquid crystal director is known at every point in the layer for any given applied field. For a layer of an initially homogeneous orientation, the optical quantity of interest is the retardation,  $R$ , given by the equation,

$$R = (n_{eff} - n_o)d, \quad [3.37]$$

where,

$$n_{eff} = \frac{n_e n_o}{d} \int_0^d (n_e^2 \sin^2 \theta + n_o^2 \cos^2 \theta)^{-1/2} dz,$$

$n_e$  = extraordinary liquid crystal refractive index, and,  
 $n_o$  = ordinary liquid crystal refractive index.

Equation [3.37] can be rewritten as,

$$R = \left\{ [n_e 2 \int_0^{d/2} (1 + V \sin^2 \theta)^{-1/2} dz - n_o d] \right\} \quad [3.38]$$

$$\text{where } V = (n_e^2 - n_o^2)/n_o^2.$$

Combining equations [3.27] and [3.38] gives,

$$\left\{ \frac{R + dn_o}{dn_e} \right\} = \frac{2}{D_z d} \sqrt{\frac{\epsilon_0 \epsilon_{\perp} K_{11} (1 + M \sin^2 \theta_m)}{M}} \times \int_0^{\theta_m} \left\{ \frac{(1 + K \sin^2 \theta)(1 + M \sin^2 \theta)}{(1 + V \sin^2 \theta)(\sin^2 \theta_m - \sin^2 \theta)} \right\}^{1/2} d\theta \quad [3.39]$$

Substituting  $D_z d/2$  from equation [3.28] into [3.39] and again putting,  $\sin \theta = \sin \theta_m \sin \phi$ , and  $N = \sin^2 \theta_m$ ,

$$\left\{ \frac{R + d n_o}{d n_e} \right\} = \frac{\int_0^{\pi/2} \left\{ \frac{(1 + KN \sin^2 \phi)(1 + MN \sin^2 \phi)}{(1 + V N \sin^2 \phi)(1 - N \sin^2 \phi)} \right\}^{1/2} d\phi}{\int_0^{\pi/2} \left\{ \frac{(1 + KN \sin^2 \phi)(1 + MN \sin^2 \phi)}{(1 - N \sin^2 \phi)} \right\}^{1/2} d\phi} \quad [3.40]$$

The integrals in equations [3.35],[3.36] and [3.40] were calculated by a 96-point Gaussian quadrature method.<sup>89</sup> Using data for a PDA liquid crystal,<sup>90</sup> the above equations<sup>†</sup> can be used to predict,

- a) the variation of  $\theta_m$  as a function of  $U/U_0$ , and
- b) the angle of deformation  $\theta$  as a function of  $z/d$  for values of  $U/U_0$ .

From Figures 3.10 and 3.11 it can be seen that quite small increases in the applied voltage just above the threshold, cause a large change in the value of  $\theta_m$ , and that at higher voltages  $\theta_m$  saturates slowly to a value  $\pi/2$ . This is verified in Figure 3.12 where there is a large decrease in cell retardation as the voltage increases above threshold, but at large values of  $U/U_0$ , little change occurs in the retardation, indicating that most of the liquid crystals are aligned with the applied field.

### 3.8.2 Tilted Homogeneous Cell

The cross section of a tilted homogeneous cell is shown in Figure 3.13. It is assumed that a nematic liquid crystal with PDA is enclosed between two conducting glass plates a distance  $d$  apart, and that the tilt angle,  $\theta_T$ , is constant (in the equilibrium state) throughout the cell. Also, it is assumed that all the director movement is in the  $x$ - $z$  plane, then by analogy with the homogeneous case above, the relationship between the applied voltage  $U$  and the maximum tilt angle  $\theta_m$  can be written as,

$$U = 2\sqrt{\frac{K_{11}(1 + M \sin^2 \theta_m)}{\epsilon_0 \Delta \epsilon}} \times \int_{\theta_T}^{\theta_m} \left\{ \frac{(1 + K \sin^2 \theta)}{(1 + M \sin^2 \theta)(\sin^2 \theta_m - \sin^2 \theta)} \right\}^{1/2} d\theta \quad [3.41]$$

Making the substitution  $\sin \theta = \sin \theta_m \sin \phi$  and  $N = \sin^2 \theta$  then,

$$U = 2\sqrt{\frac{K_{11}(1 + MN)}{\epsilon_0 \Delta \epsilon}}$$

---

<sup>†</sup> A Pascal program is listed in the Appendix which calculates the integrals in equations [3.35], [3.36] and [3.40]

$$\times \int_{\beta}^{\pi/2} \left\{ \frac{(1 + KN \sin^2 \phi)}{(1 + MN \sin^2 \phi)(1 - N \sin^2 \phi)} \right\}^{1/2} d\phi \quad [3.42]$$

where  $\beta = \sin^{-1} (\sin \theta_T / \sin \theta_m)$ .

Equations [3.36] and [3.40] can be modified to,

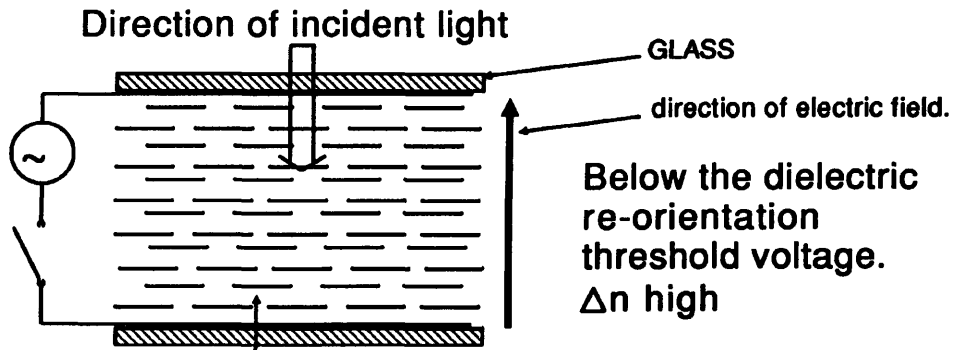
$$\frac{2z}{d} = \frac{\int_{\beta}^{\alpha} \left\{ \frac{(1 + KN \sin^2 \phi)(1 + MN \sin^2 \phi)}{(1 - N \sin^2 \phi)} \right\}^{1/2} d\phi}{\int_{\beta}^{\pi/2} \left\{ \frac{(1 + KN \sin^2 \phi)(1 + MN \sin^2 \phi)}{(1 - N \sin^2 \phi)} \right\}^{1/2} d\phi} \quad [3.43]$$

and,

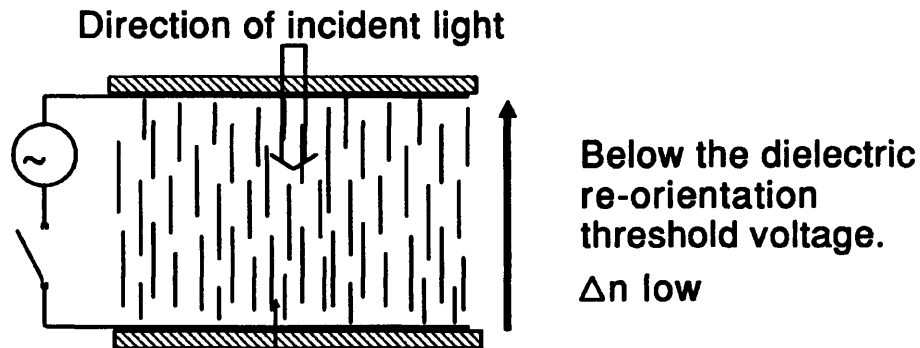
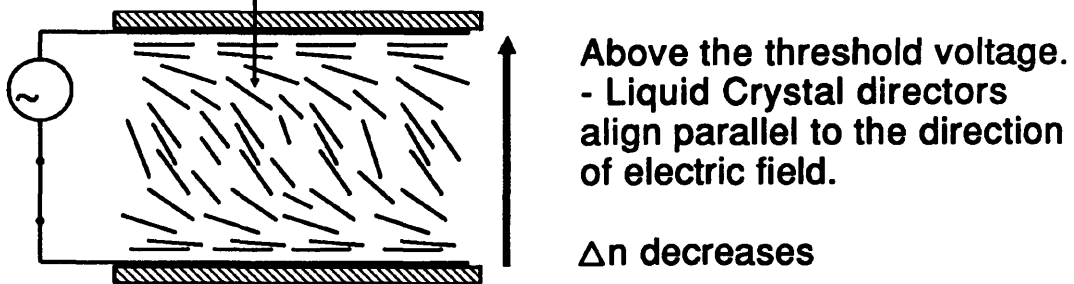
$$\left\{ \frac{R + d n_o}{d n_e} \right\} = \frac{\int_{\beta}^{\pi/2} \left\{ \frac{(1 + KN \sin^2 \phi)(1 + MN \sin^2 \phi)}{(1 + VN \sin^2 \phi)(1 - N \sin^2 \phi)} \right\}^{1/2} d\phi}{\int_{\beta}^{\pi/2} \left\{ \frac{(1 + KN \sin^2 \phi)(1 + MN \sin^2 \phi)}{(1 - N \sin^2 \phi)} \right\}^{1/2} d\phi} \quad [3.44]$$

For given values of  $\theta_T$ , equation [3.42] was solved to give the relationship between  $\theta_m$  and  $U$ . Equation [3.43] could then be evaluated to give the variation in tilt,  $\theta$ , with the coordinate  $z$  at any particular value of  $\theta_T$ . Finally, equation [3.44] gave the relationship between cell retardation and  $\theta_m$  (and hence  $U$ ). Figure 3.14 plots the calculated variation of  $\theta_m$  with applied voltage and Figure 3.15 gives the relation of percentage retardation to applied voltage at selected values of  $\theta_T$ .

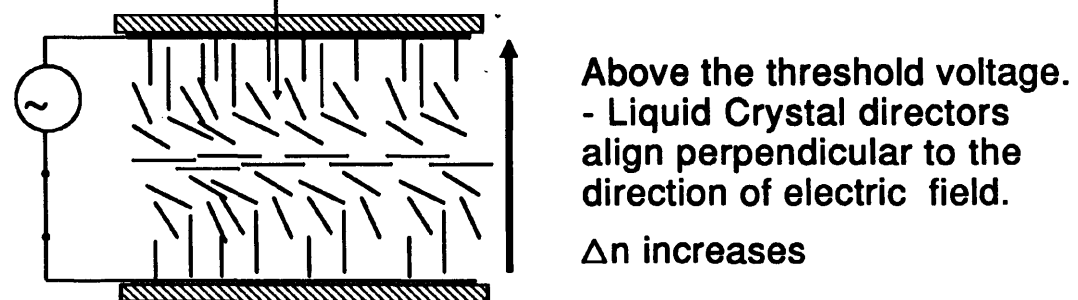
From equation [3.42] it can be seen that the voltage at which  $\theta_m$  tends to  $\theta_T$  (threshold) is essentially zero for all non-zero values of  $\theta_T$ , which is verified for different values of  $\theta_T$  in Figure 3.15.



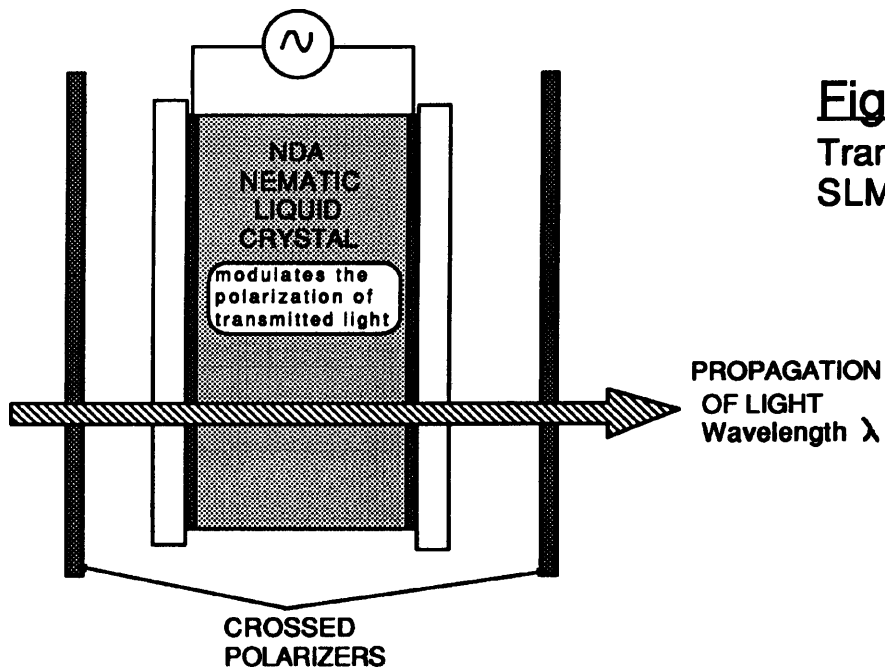
### 3.1a Nematic Liquid Crystal with PDA-Homogeneous alignment



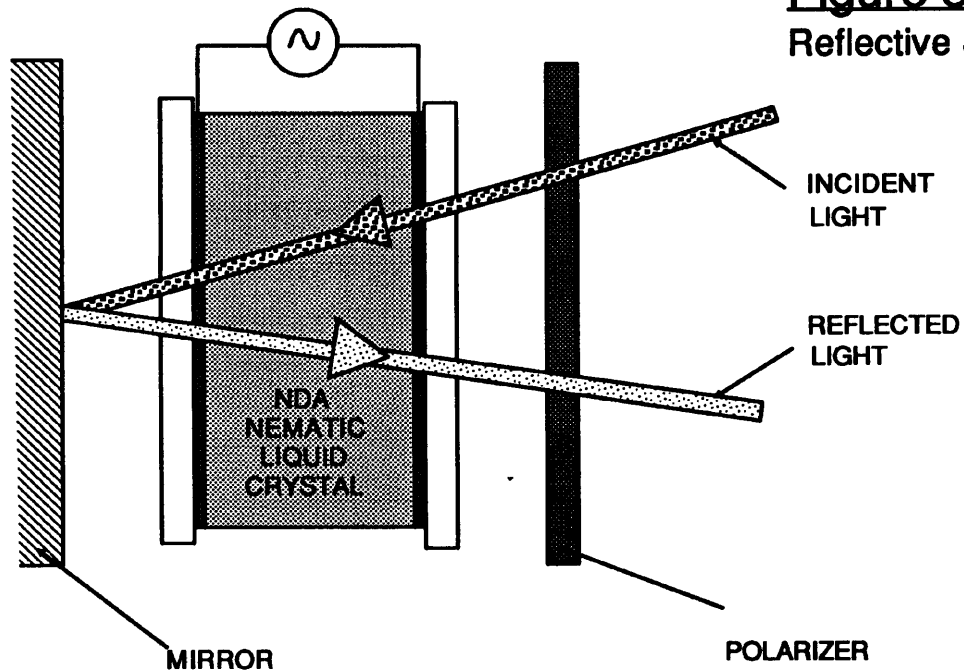
### 3.1b Nematic Liquid Crystal with NDA-Homeotropic alignment



**Figure 3.1** Electrically controllable birefringence effect above and below the voltage threshold in NDA and PDA nematic liquid crystals.

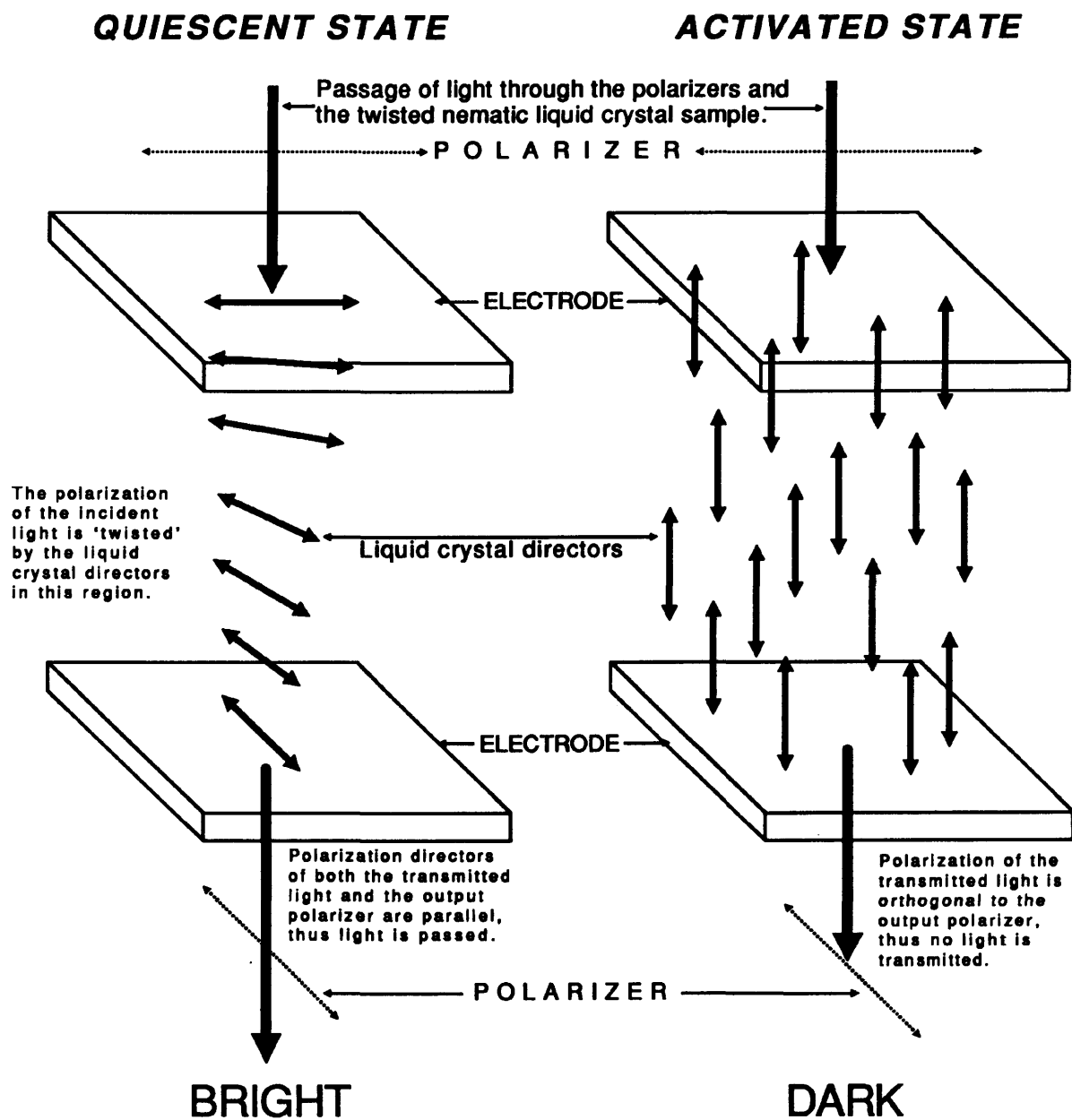


**Figure 3.2a**  
Transmissive SLM.



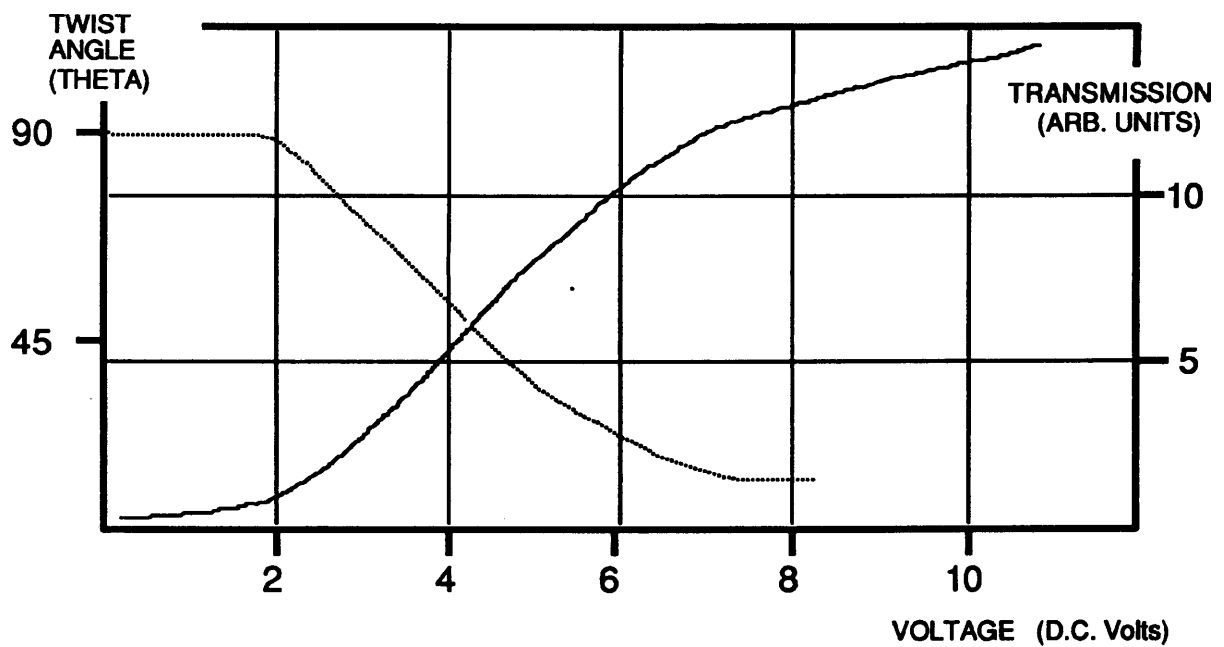
**Figure 3.2b**  
Reflective SLM

Two types of nematic liquid crystal filled Spatial Light Modulator



**Figure 3.3** TWISTED NEMATIC EFFECT  
(For crossed polarizers and a liquid crystal with PDA)

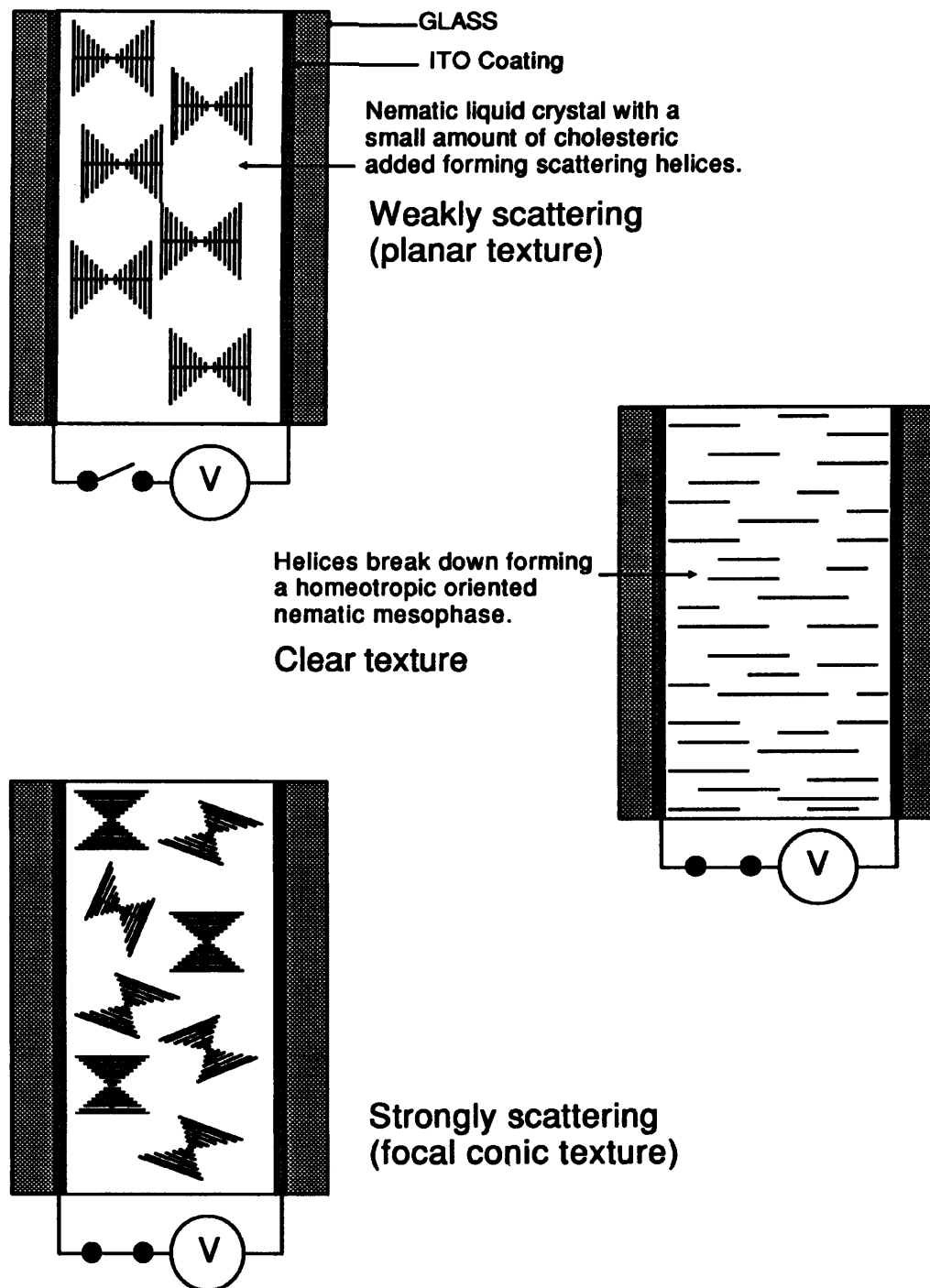




**Figure 3.4**

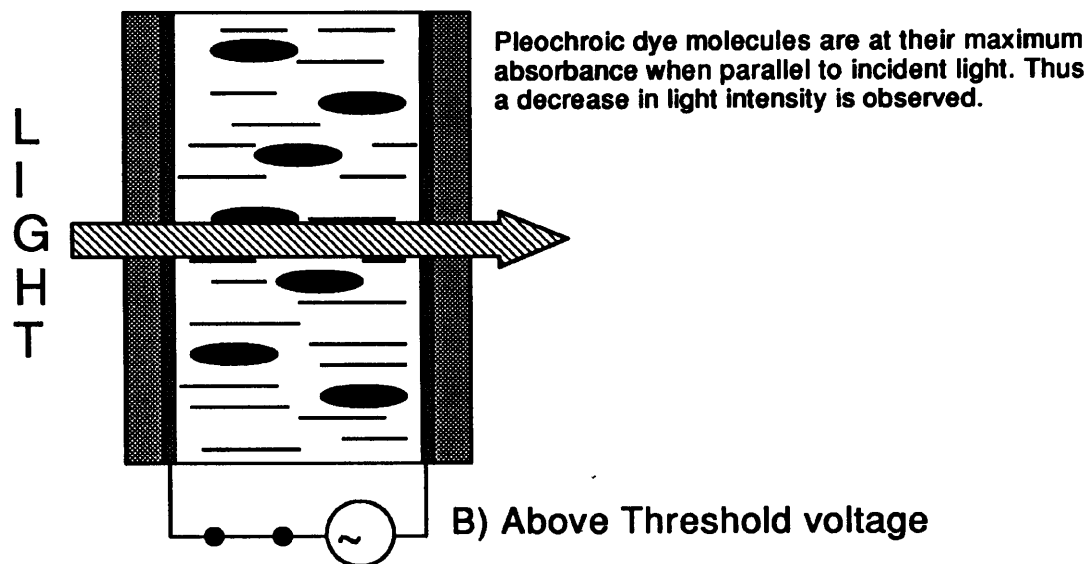
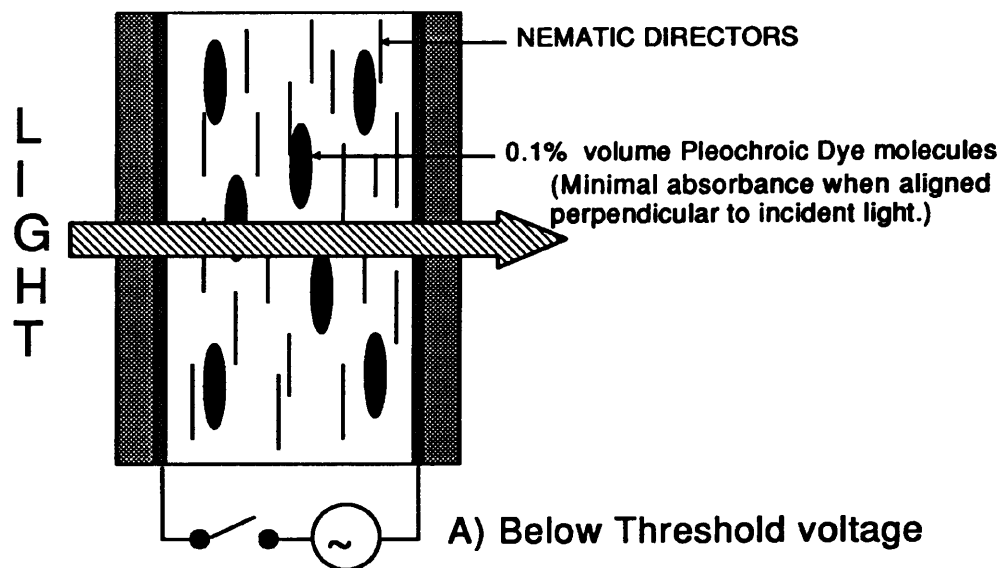
..... ROTATION ANGLE OF LINEAR POLARIZED LIGHT vs. VOLTAGE  
 — TRANSMISSION vs. VOLTAGE FOR A TWISTED NEMATIC LIQUID CRYSTAL CELL BETWEEN ALIGNED POLARIZERS.

Graphs showing the Transmission & Optical Rotation vs Voltage for a Twisted Nematic Liquid Crystal with PDA.



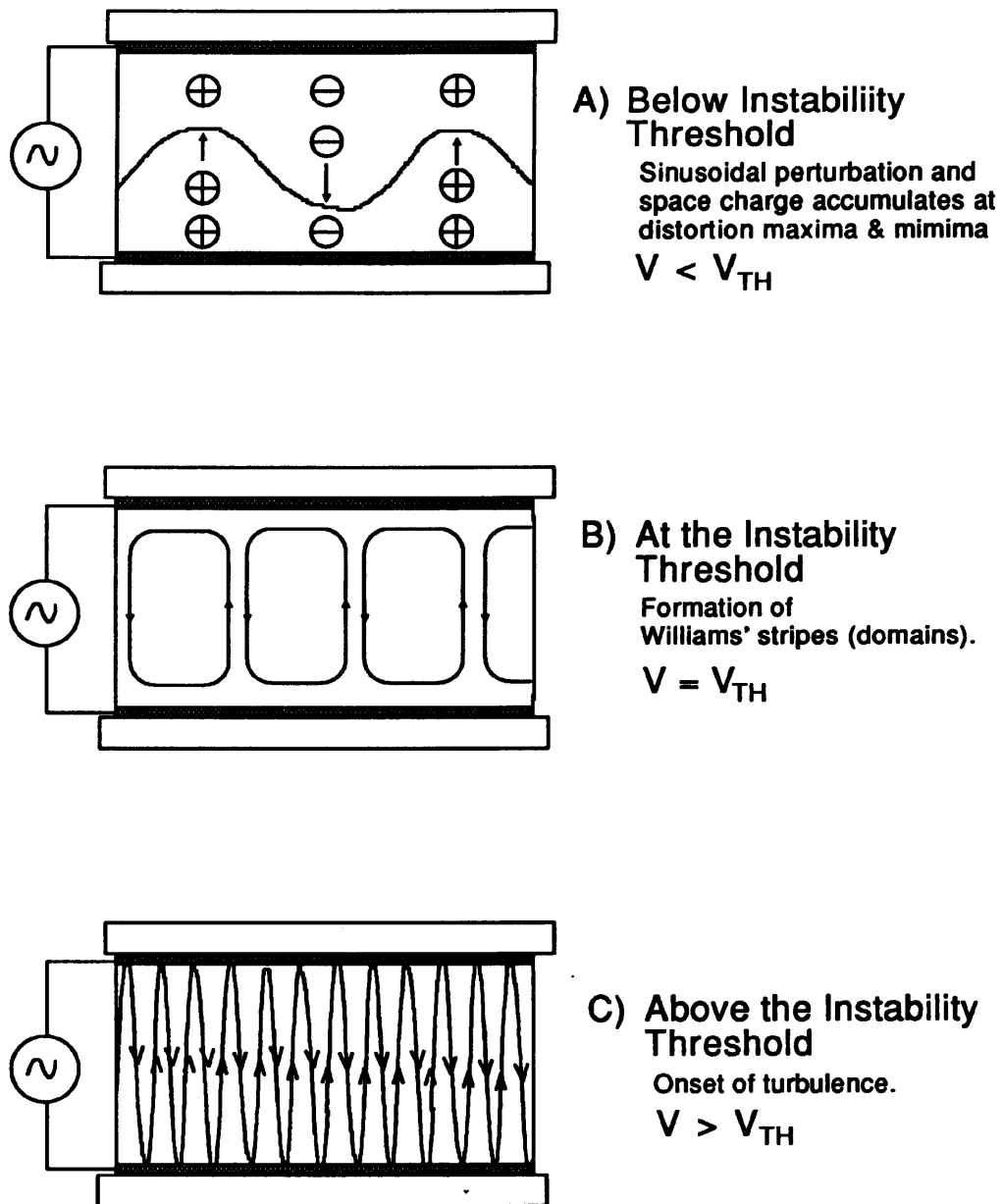
**Figure 3.5**

Electric field induced Cholesteric to Nematic Phase Change.



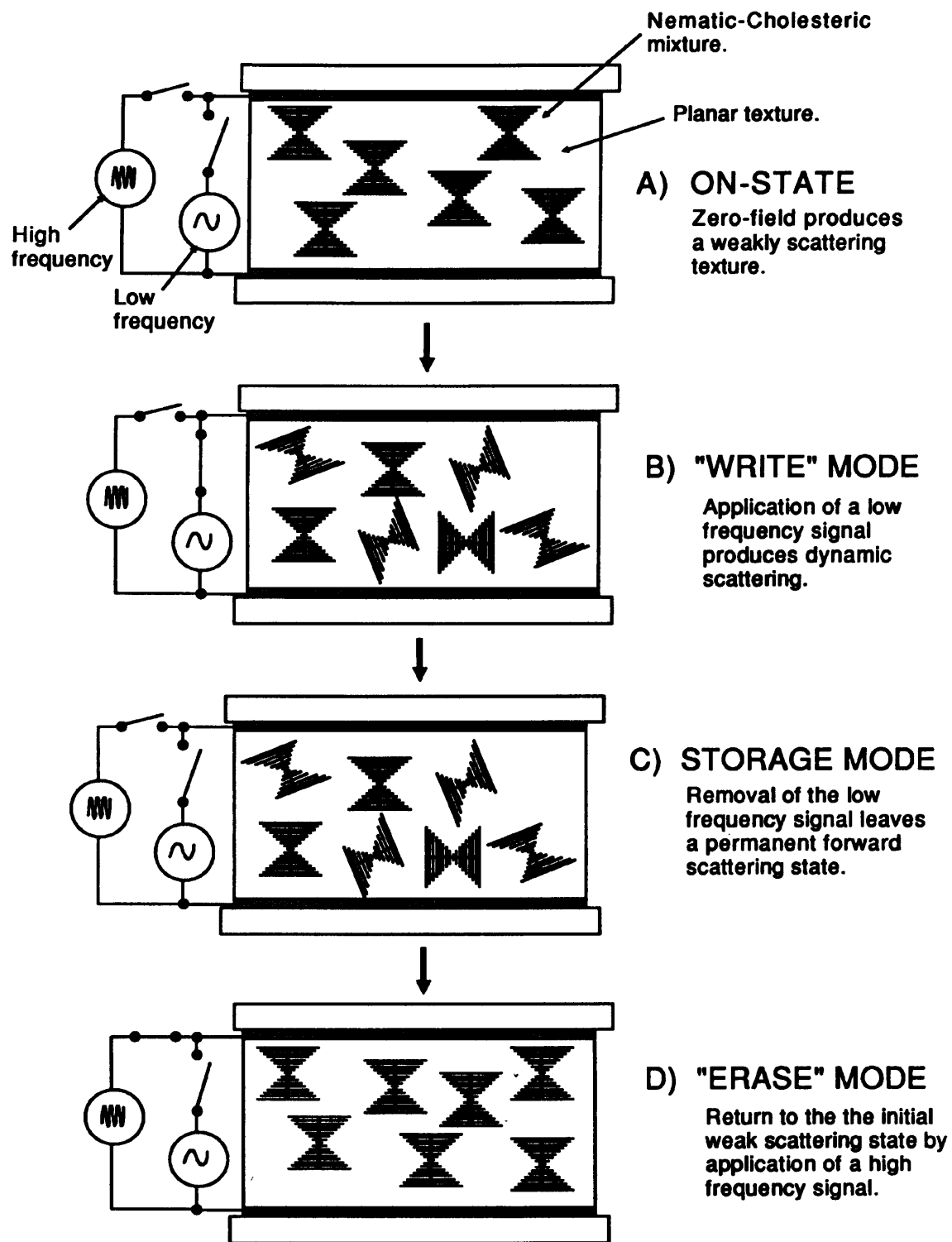
**Figure 3.6**

Guest-Host Effect in a nematic liquid crystal cell.



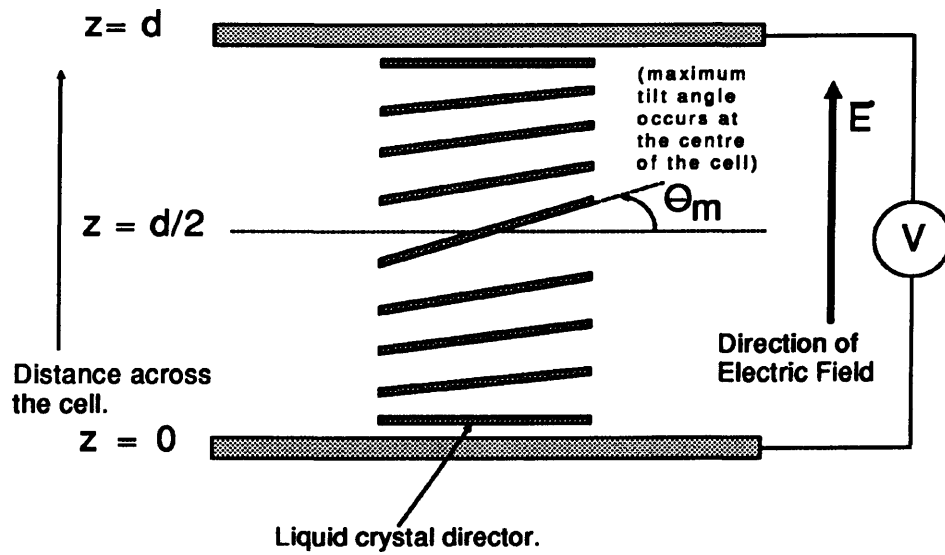
**Figure 3.7**

Induction of fluid flow in a Nematic liquid crystal by alternating currents below the critical frequency.



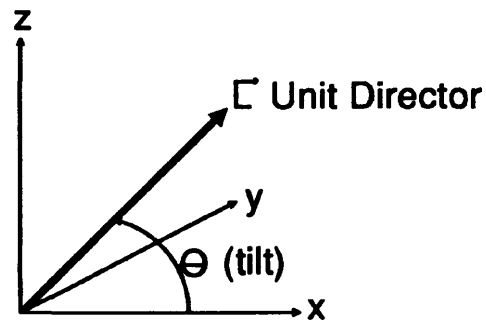
**Figure 3.8**

Optical storage effect of a nematic-cholesteric mixture using high and low frequency signals.



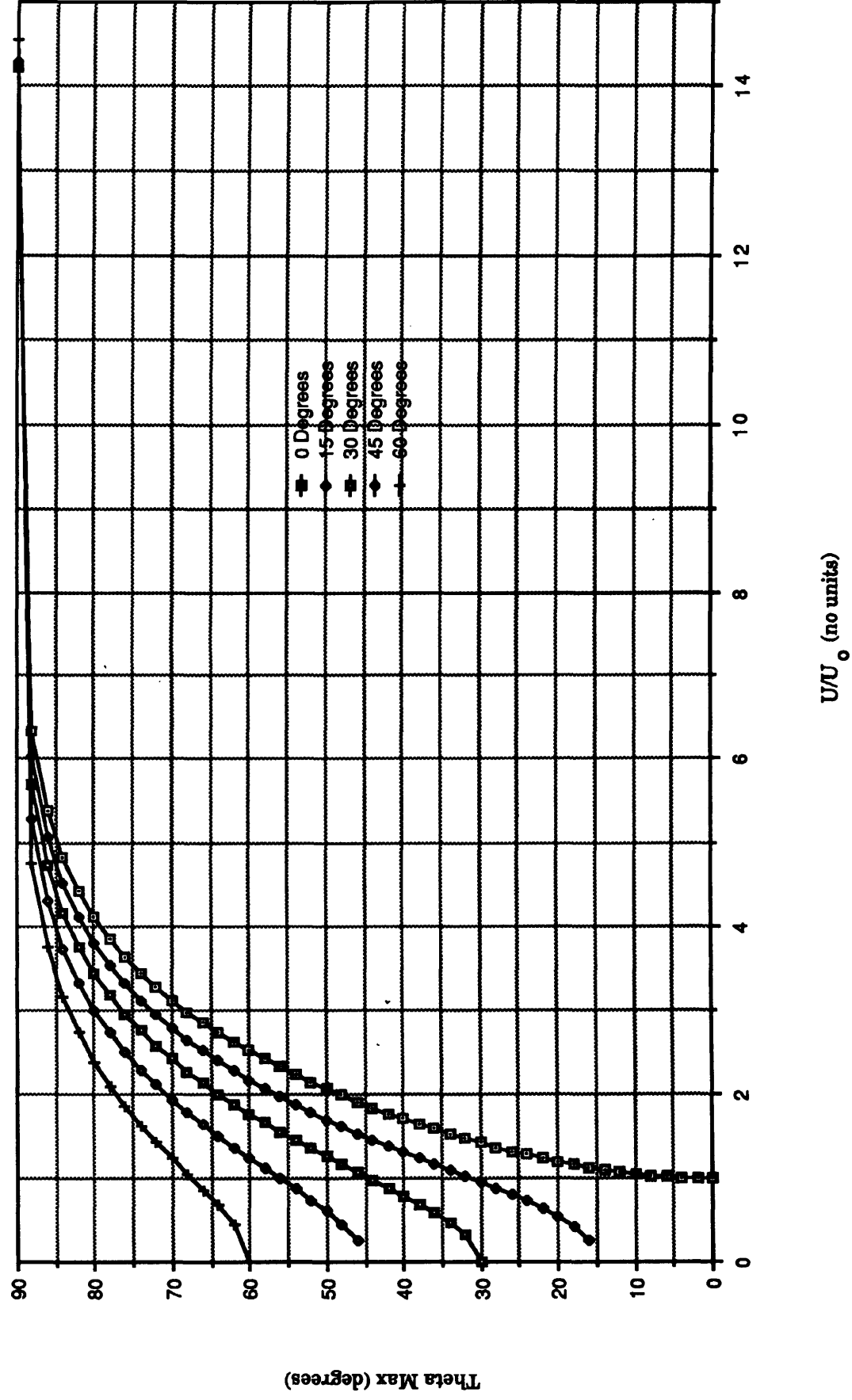
**Figure 3.9**

A Parallel Homogeneous Liquid Crystal Cell (PDA nematic)



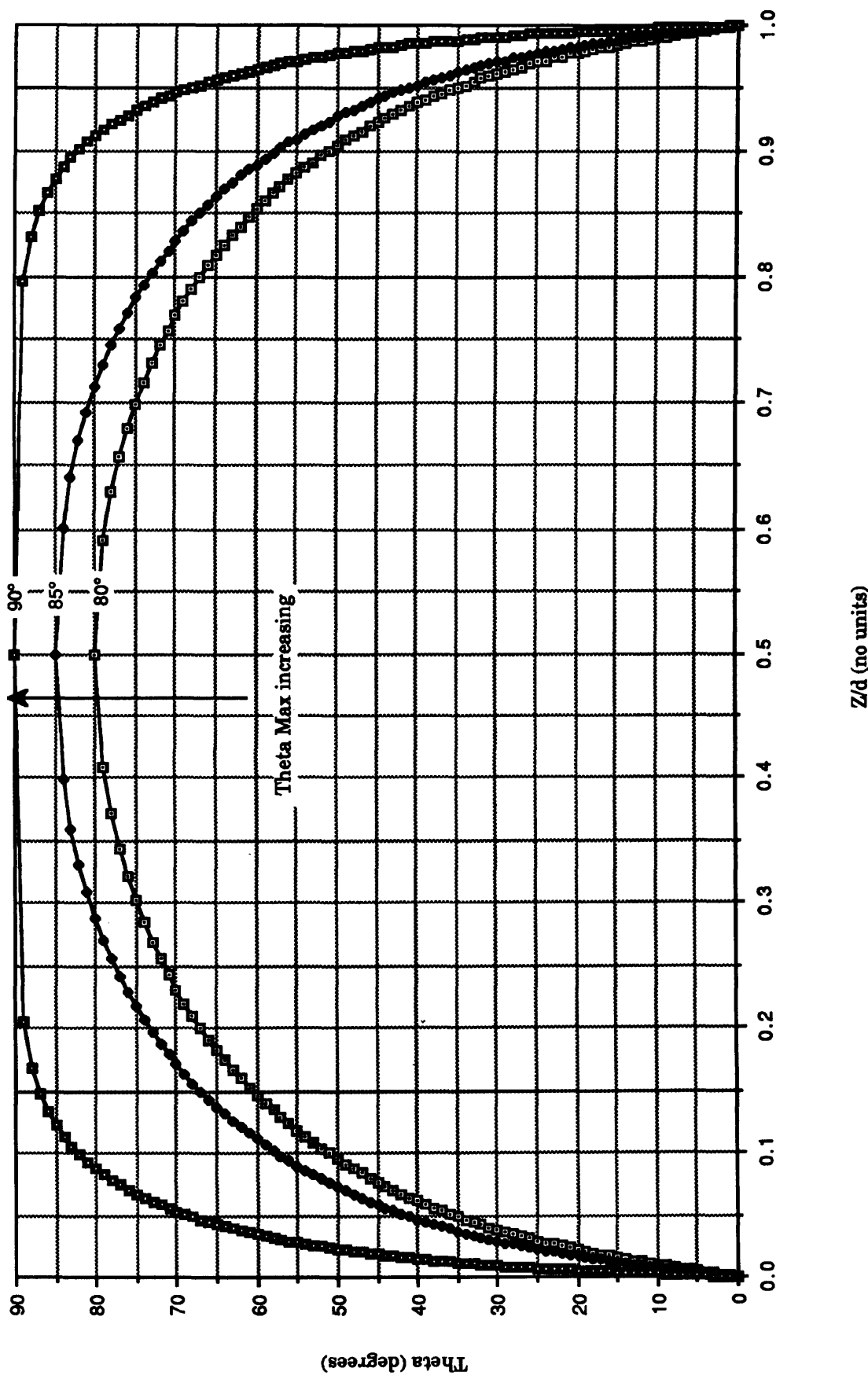
**Figure 3.10**

Graph of Theta Max vs.  $U/U_0$   
for different values of tilt angle



**Figure 3.11**

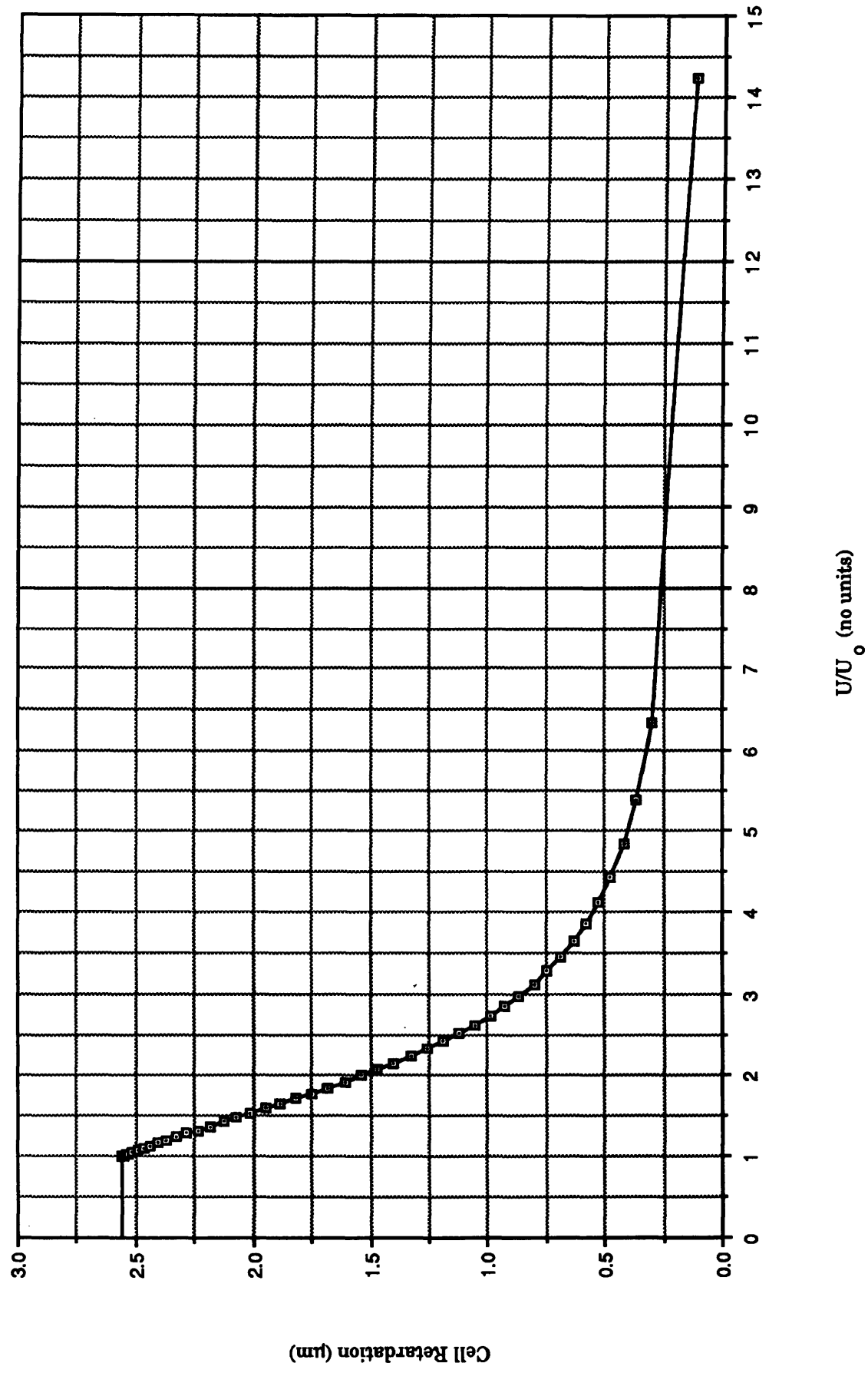
Graph showing values of director orientation (theta) across the cell at different values of Theta Max





**Figure 3.12**

Graph of Retardance vs.  $U/U_0$   
for a parallel homogeneous cell



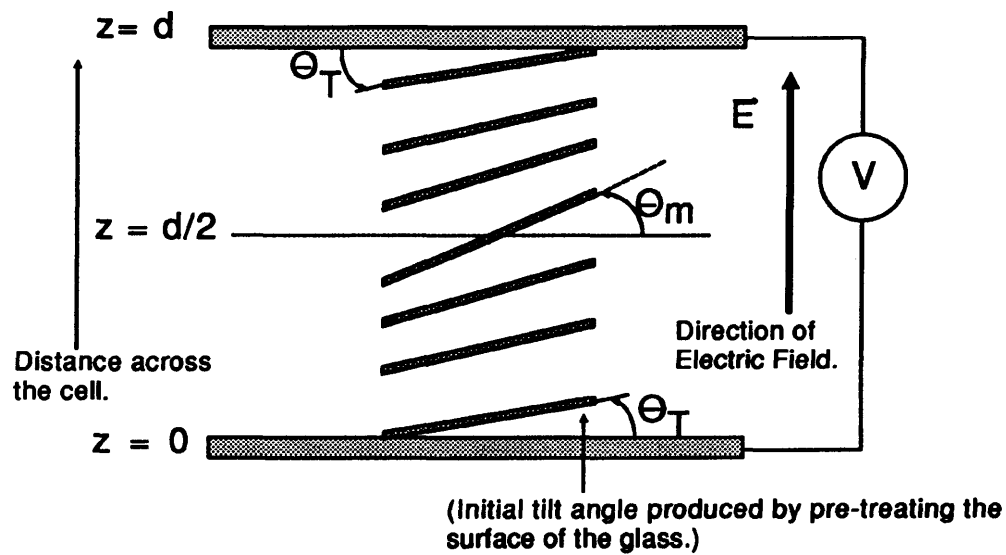


**Figure 3.13**

A Tilted Homogeneous Liquid Crystal Cell (PDA nematic)

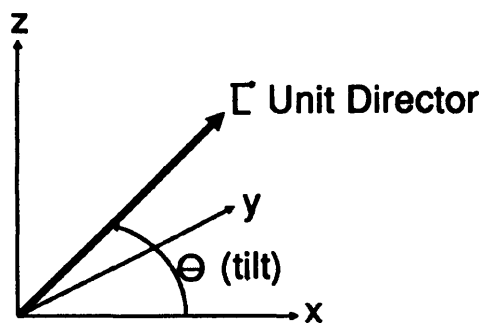


**Figure 3.14**

Graph of Theta Max versus U  
for different values of tilt angle

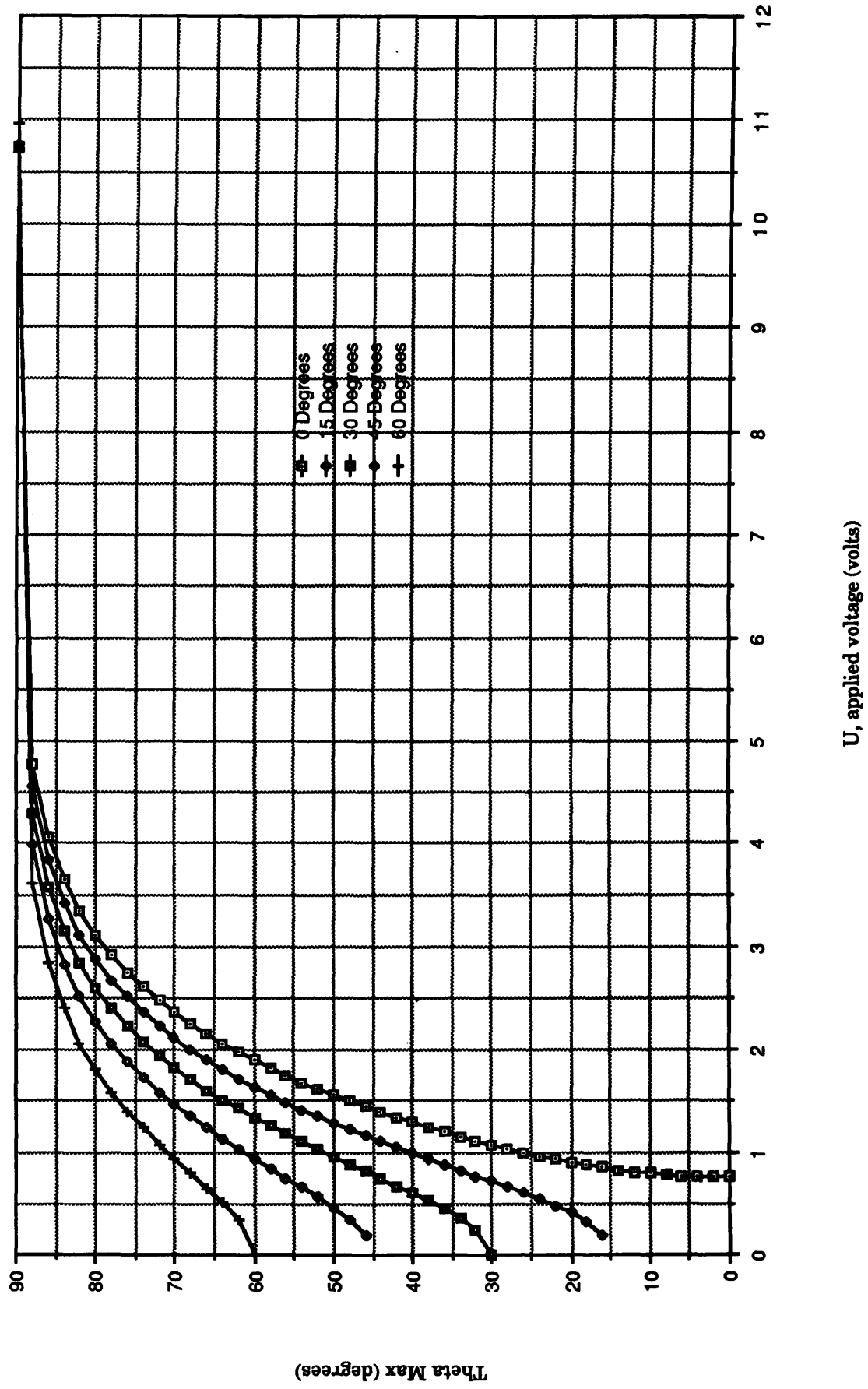
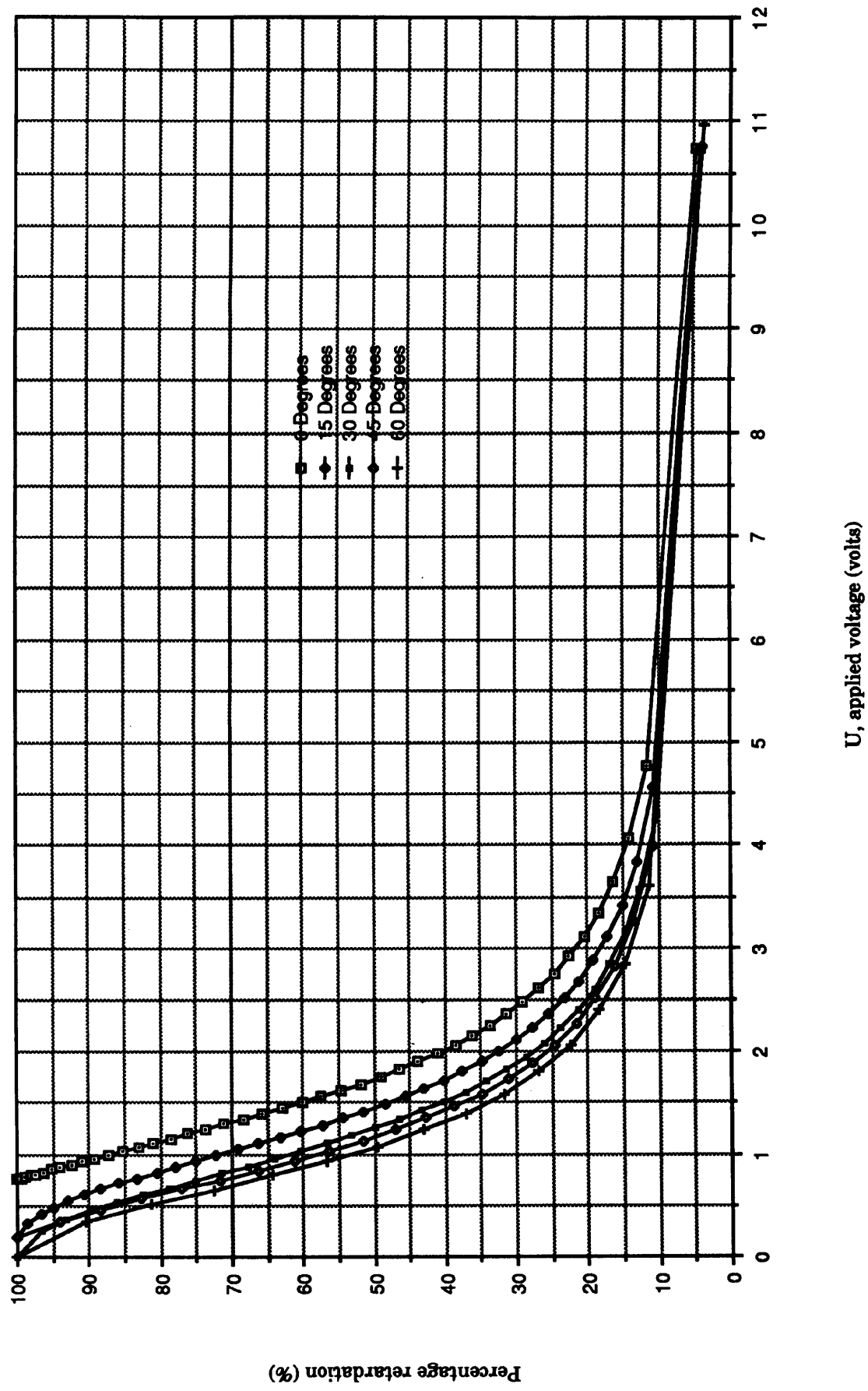


**Figure 3.15**

Graph of Percentage retardation vs. U  
for different values of tilt angle



# 4

## Theory of Phase and Amplitude Diffraction Gratings

### 4.1 Chapter Summary

In chapters 2 and 3 it was established that a treated, that is to say aligned, nematic liquid crystal would be the most appropriate liquid crystal to assess a new technique for determining its 'suitability' in a SLM. Previous suitability measurements have been based on the evaluation of transmission properties of a liquid crystal. Here however, the diffraction efficiency of a square wave grating electrically written onto the liquid crystal was chosen as the property to be evaluated; the diffraction efficiency of a liquid crystal is directly proportional to its spatial modulation efficiency. The theoretical aspects of diffraction efficiency for a two-dimensional square wave grating (both Ronchi and non-Ronchi) are discussed in this chapter. The data produced from these theoretical equations will be compared with the experimental results in chapter 6.

### 4.2 Introduction

In order to 'tune' the spatial light modulator for optimum performance in a coherent optical processor, where precise phase modulation of the light beam is required, it is essential to have detailed knowledge of the optical behaviour of the chosen nematic liquid crystal layer. Previous measurement techniques to ascertain the liquid crystal optical properties have centred around the evaluation of relative transmission, ON/OFF contrast ratio *et cetera*. Historically these measurements descended from the appraisal of liquid crystal cells used as display panels. To 'update' the techniques it was decided to measure the diffraction efficiency (D.E.) of the liquid crystal layer.

The equation for diffraction efficiency is given by,

$$\text{D.E.} = \frac{\text{Intensity of first diffracted order}}{\text{Intensity of light incident on diffraction grating}} \times 100\% \quad [4.1]$$

One way of obtaining a diffraction pattern and hence the diffraction efficiency of a liquid crystal layer is to electrically 'write' a square wave grating pattern onto the layer. In this way, coherent light shone through the layer and brought to focus by a lens will produce a detectable diffraction pattern in the Fourier plane. By measuring the intensity of the diffracted orders in the pattern at different applied voltages, and substituting them into equation [4.1] above, the D.E. of the liquid crystal can be determined for a given voltage range. Examining the initial portion of the resultant D.E. versus applied voltage curve from the point of liquid crystal 'turn-on' to the top of the first diffraction efficiency peak<sup>†</sup> indicates the liquid crystal's linearity—the more linear the curve over the stated portion, the better the liquid crystal's spatial modulation properties. This initial portion of the curve must also be considered from a manufacturer's point of view, that is, the curve could exhibit the desired linearity of response but only over a small voltage range. The voltage range of this initial linear portion dictates the number of differentiable grey levels using this liquid crystal, that is, the larger the range, the greater the number of grey levels. Thus an image with a greater number of grey levels can be represented by the liquid crystal SLM and subsequently input into the correlator.

Attention can now be focussed on the mathematical descriptions of such structures. It is intended that the theoretical descriptions of gratings will produce data which can be compared with the equivalent experimental readings in chapter 6.

The following sections (4.3 & 4.4) mathematically describe two types of grating: a Ronchi grating and a non-Ronchi grating. [Note: the term 'Ronchi' is used here to refer to a structure with an equal mark/space ratio, and non-Ronchi refers to a

---

<sup>†</sup> See discussion in section 6.5 on the choice of D.E. peak

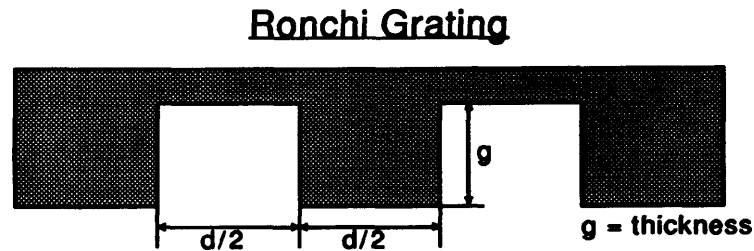
structure with an unequal mark/space ratio]. The 'non-Ronchi' grating is considered due to the potential difficulties of fabricating a perfect Ronchi grating.

### 4.3 Mathematical Description of a Ronchi Grating

Two types of Ronchi grating are available for consideration: firstly, the phase grating and secondly, the amplitude grating. Several mathematical treatments of gratings are available in the literature,<sup>91-95</sup> however the author found the treatment given in Sommerfeld<sup>96</sup> to be the most comprehensive.

#### 4.3.1 Ronchi Phase Grating

Consider the profile depicted below,



For small angles of incidence, the wave falling on half of the grating element  $d$  is retarded by,

$$\Theta(v) = [n(v) - n(0)]kg = kg\Delta n \quad [4.2]$$

where,

$g = \text{thickness},$

$k = 2\pi/\lambda,$

$n(v) = \text{Refractive index at } v \text{ volts},$

$n(0) = \text{Refractive index at zero volts},$

$\Theta(v) = \text{Phase retardance as a function of voltage}$

At a large distance from the grating the amplitude distribution  $f(\Phi)$  arising from a grating element from  $-d/2$  to  $+d/2$  is given by,

$$f(\Phi) = \frac{1}{d} \int_{-d/2}^0 e^{i(\Phi x - [\Theta/2])} dx + \frac{1}{d} \int_0^{+d/2} e^{i(\Phi x + [\Theta/2])} dx \quad [4.3]$$

$$= \frac{\sin(\Phi d/2 + \Theta/2) - \sin \Theta/2}{\Phi d/2} \quad [4.4]$$

where  $\Phi$  is a function of the order number  $h$  and thickness  $g$ .

The asymmetry of this function with respect to the direction  $\Phi = 0$  averages out in the spectrum produced by the whole grating; with perpendicular incidence (which will be applicable in the practical arrangements), the directions  $\Phi d/2 = \pm h\pi$  which match the two spectra of equal order ( $\pm h$ ) always produce the same contribution.<sup>†</sup>

$$f(\Phi) = \frac{1}{h\pi} [(-1)^h - 1] \sin \Theta/2 \quad [4.5]$$

And for  $h = 0$  that is, the d.c. term, the limit as  $\Phi \rightarrow 0$  must be taken, which yields  $f(0) = \cos \Theta/2$ . For all even numbered values of  $h$ , the square bracketed central expression in equation [4.5] is zero. Thus there are no even numbered orders present in the diffraction pattern and they can be ignored in further ideal grating considerations. Furthermore, only the equations pertaining to the first and third orders of the diffraction grating will be shown—additional odd orders (5,7,9 etc.) are not considered due to their relatively small contribution (with respect to the first & third orders) to the total intensity of the diffraction pattern. The intensity of the diffracted orders is given by  $f(\Phi) \times f(\Phi)^*$ , where “\*” denotes the complex conjugate of the function.

Figure 4.1 shows the diffraction efficiency versus phase retardance for the first and third orders of a Ronchi phase grating using equation [4.5]. The shape of the curve is in the form of a squared sine wave for both orders. The difference in magnitude between the two orders is approximately 10. The peaks and troughs of the diffraction efficiencies for both orders occur at regular  $2\pi$  radian intervals. The first peak occurs at  $\pi$  radians giving a maximum value for the diffraction efficiency of 40%, which is maintained in all the following peaks thereafter. The first trough occurs at zero radians and exhibits zero diffraction efficiency which remains unchanged for all subsequent troughs. Again like the peaks these troughs

---

<sup>†</sup> In the following calculations only the positive term will be considered



are at  $2\pi$  radian intervals. It is interesting to note that had the corresponding zero order (d.c. term) been plotted on the same graph, then it would have formed a squared cosine pattern, with its troughs occurring at the same positions as the peaks of the odd-numbered orders. This phenomenon arises due to the fact that the zero order has its energy 'dissipated' into the odd ordered 'side lobes' at certain liquid crystal phases.

#### 4.3.2 Ronchi Amplitude Grating

Sommerfeld adjusts the phase grating formula to account for amplitude gratings by letting  $\Theta = i\Theta'$  ( $\Theta'$  is real). The ratio of the transmissivities of the two halves of a grating element is then  $e^{2\Theta'}$ , and  $\Theta'$  is directly proportional to the thickness of the absorbing layer.

Thus from equation [4.3] above,<sup>†</sup>

$$\begin{aligned} f(\Phi) &= \frac{1}{d} \int_{-d/2}^0 e^{i(\Phi x + i\Theta')} dx + \frac{1}{d} \int_0^{+d/2} e^{i(\Phi x)} dx \\ &= e^{-\Theta'} \left[ \frac{1 - e^{-i\Phi d/2}}{i\Phi d} \right] + \frac{e^{i\Phi d/2} - 1}{i\Phi d} \end{aligned} \quad [4.6]$$

Taking  $\Phi = 0$ , that is ( $h = 0$ ),

$$f(0) = \frac{(1 + e^{-\Theta'})}{2}$$

$$\text{Therefore, Intensity} = (f(0))^2 = \frac{(1 + e^{-\Theta'})^2}{4}$$

Similarly, for  $\Phi = \pm 2\pi/d$ , that is ( $h = 1$ ),

$$f(\pm \frac{2\pi}{d}) = \frac{(1 - e^{-\Theta'})}{i\pi}$$

$$\text{Therefore, Intensity} = \frac{1}{\pi^2} (1 - e^{-\Theta'})^2$$

To verify that the second and all other even numbered orders do not contribute to the diffraction pattern,  $\Phi = \pm 4\pi/d$ , that is ( $h = 2$ ),

$$f(\pm \frac{2\pi}{d}) = e^{-\Theta'} \left[ \frac{1 - e^{-i2\pi}}{i2\pi} \right] + \frac{e^{i2\pi} - 1}{i2\pi}$$

---

<sup>†</sup> The  $e^{\Theta'}$  factor is placed in the first term, and not split equally between the two integrals because of the nonexistence of negative absorption.

Since  $e^{\pm i2\pi} = 1$ , both terms become zero.

Finally, for  $\Phi = \pm 6\pi/d$ , that is ( $h = 3$ ),

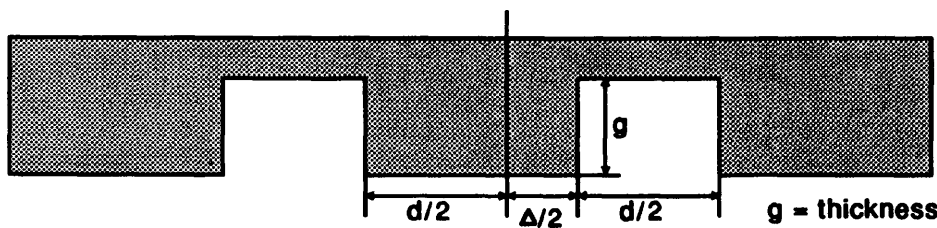
$$\text{Intensity} = \frac{1}{9\pi^2} (1 - e^{-\Theta'})^2$$

Figure 4.2 shows the graph of diffraction efficiency versus grating thickness for the first and third orders of an ideal Ronchi amplitude grating. In contrast to the phase grating the D.E. values for both orders rise to an almost constant value and remain there. This effect can be attributed to the presence of squared exponential values in the formulæ. The maximum values reached are approximately 10.1% for the first order and 1.1% for the third order, which indicates that the 10× difference mentioned previously for the ideal Ronchi phase grating is also applicable to the ideal Ronchi amplitude grating.

#### 4.4 Treatment of Non-Ronchi Gratings

Having considered Ronchi phase and amplitude gratings, it is now possible to extend Sommerfeld's work to cover the case of non-Ronchi gratings. As for Ronchi gratings, the non-Ronchi phase grating will be considered first, followed by the non-Ronchi amplitude grating. Without encroaching on the details of the cell fabrication, which are discussed in the following chapter, it is necessary to explain why the experimental cells are considered to be non-Ronchi gratings. There is a small gap present in the cells between each of the 'ON' and 'OFF' grating strips. As these 'interline' strips do not have any voltage applied to them, it can be assumed that they do not contribute to the electro-optic movement of the liquid crystal and as such can be considered to be part of the 'OFF' strip. These are shown in the diagram below.

#### Non-Ronchi Grating



By adjusting the limits of integration in equation [4.3] to account for the increased width of the OFF strip in the non-Ronchi grating, the equation can be rewritten as,

$$f(\Phi) = \frac{1}{d} \int_{-(d/2-\Delta/2)}^0 e^{i(\Phi x - [\Theta/2])} dx + \frac{1}{d} \int_0^{d/2+\Delta/2} e^{i(\Phi x + [\Theta/2])} dx \quad [4.7]$$

$$= \frac{e^{-i\Theta/2} [1 - e^{-i[\Phi(d/2-\Delta/2)]}]}{i\Phi d} + \frac{e^{i\Theta/2} [e^{i[\Phi(d/2+\Delta/2)]} - 1]}{i\Phi d} \quad [4.8]$$

#### 4.4.1 Non-Ronchi Phase Grating

For  $\Phi = 0$ , ( $h = 0$ ), using equation [4.8],

$$\begin{aligned} f(0) &= \frac{e^{-i\Theta/2(d/2-\Delta/2)}}{d} + \frac{e^{i\Theta/2(d/2+\Delta/2)}}{d} \\ &= \cos \Theta/2 + \left(\frac{\Delta}{d}\right) i \sin \Theta/2 \\ \text{Intensity} &= \cos^2 \Theta/2 + \left(\frac{\Delta}{d}\right)^2 \sin^2 \Theta/2 \end{aligned}$$

This equation for the d.c. term in a non-ideal grating reveals an additional term involving the ratio of the interline strip width  $\Delta/2$  and the electrode width  $d/2$ . This squared ratio of  $\Delta/d$  is multiplied by a  $\sin \Theta/2$  term. The resultant effect of this extra term is that the  $f(\Phi)$  function never reaches a point of zero intensity. The minimum value of  $f(\Phi)$  is thus dependent on the magnitude of  $\Delta/d$ .

When  $\Phi = \pm \frac{2\pi}{d}$ , ( $h = 1$ ),

$$\begin{aligned} f\left(\pm \frac{2\pi}{d}\right) &= \frac{-\sin \Theta/2}{\pi} [1 + e^{i(\pi\Delta/d)}] \\ \text{Intensity} &= \frac{\sin^2 \Theta/2}{\pi^2} [2 + 2 \cos\left(\frac{\pi\Delta}{d}\right)] \end{aligned}$$

Previously, when considering Ronchi gratings it was discovered that the even numbered orders made no energy contribution to the diffraction pattern. This condition can be used to test the non-Ronchi equations. Thus by setting  $h$  equal to an even number it is possible to investigate additional effects of the  $\Delta/d$  ratio.

Thus, for  $\Phi = \pm \frac{4\pi}{d}$ , ( $h = 2$ ),

$$\begin{aligned} f\left(\pm \frac{4\pi}{d}\right) &= \frac{-\sin \Theta/2}{2\pi} [1 - e^{i2\Delta\pi/d}] \\ \text{Intensity} &= \frac{\sin^2 \Theta/2}{4\pi^2} [2 - 2 \cos\left(\frac{2\pi\Delta}{d}\right)] \end{aligned}$$

If the ratio of  $\Delta/d$  is reasonably small (that is  $< 0.05$ ) the resultant intensity will be very close to zero. However, for larger values of  $\Delta/d$  the intensity is non-zero and the second order contribution increases.

Finally, for the third order ( $h = 3$ ),  $\Phi = \pm \frac{6\pi}{d}$ ,

$$\text{Intensity} = \frac{\sin^2 \Theta/2}{9\pi^2} [2 + 2 \cos(\frac{3\pi\Delta}{d})]$$

The overall effect of the  $\Delta/d$  ratio in the non-ideal grating formulæ is to reduce the intensity values of the odd numbered orders and increase the values of the even numbered orders. The larger the value of  $\Delta/d$ , the more the even numbered orders contribute to the diffraction intensity and correspondingly, the less the odd numbered orders contribute. The  $\Delta/d$  ratio for the cells was measured using a microscope and was found to be 0.25 ( $\pm 5\%$ ). Substituting the ratio of  $\Delta/d = 0.25$  into the above formulæ, it can be seen in Figure 4.3 that the maximum D.E. for the first order is 34% and the second order exhibits a maximum D.E. of 5%. However, the maximum D.E. for the third order is only 0.7% which can be ignored in the experimental analysis as its contribution is negligible with respect to the first and second orders. The 0.25 ratio is a direct result of using experimental cells designed for display purposes. The reasons for employing such cells are discussed in chapter 5, however it is sufficient to note at this point that experimental readings will be taken from the first and second diffracted orders.

For comparison, Figure 4.4 shows a graph of D.E. versus phase retardance for a non-Ronchi grating with  $\Delta/d = 0.04$ . It can be seen that the maximum D.E. increases for the first and third orders to 40% and 5% respectively, but for the second order the D.E. decreases to 0.16% which can be considered to make a negligible contribution.

#### 4.4.2 Non-Ronchi Amplitude Grating

Using the same theoretical consideration as in the Ronchi amplitude case, the ratio of transmittances between the ON and OFF strips is  $e^{\Theta'}$ . Thus equation [4.8] becomes,

$$f(\Phi) = e^{-\Theta'} \left[ \frac{1 - e^{-i[\Phi(d/2 - \Delta/2)]}}{i\Phi d} \right] + \left[ \frac{e^{i[\Phi(d/2 + \Delta/2)]} - 1}{i\Phi d} \right] \quad [4.9]$$

For  $\Phi = 0$ , ( $h = 0$ ),

$$f(0) = \left[ \frac{1 + e^{-\Theta'}}{2} \right] + \left[ \frac{(1 - e^{-\Theta'})}{2} \left( \frac{\Delta}{d} \right) \right]$$

$$\text{Intensity} = \left[ \left[ \frac{1 + e^{-\Theta'}}{2} \right] + \left[ \frac{(1 - e^{-\Theta'})}{2} \left( \frac{\Delta}{d} \right) \right] \right]^2$$

For  $\Phi = \pm \frac{2\pi}{d}$ , ( $h = 1$ ),

$$f\left(\pm \frac{2\pi}{d}\right) = (e^{-\Theta'} - 1) \left[ \frac{1 + e^{i\pi\Delta/d}}{2\pi i} \right]$$

$$\text{Intensity} = \frac{(e^{-\Theta'} - 1)^2}{4\pi^2} [2 + 2\cos\left(\frac{\pi\Delta}{d}\right)]$$

Once again, examining the contribution of the even numbered harmonics,

For  $\Phi = \pm \frac{4\pi}{d}$ , ( $h = 2$ ),

$$f\left(\pm \frac{4\pi}{d}\right) = (e^{-\Theta'} - 1) \left[ \frac{1 - e^{i2\pi\Delta/d}}{4\pi i} \right]$$

$$\text{Intensity} = \frac{(e^{-\Theta'} - 1)^2}{16\pi^2} [2 - 2\cos\left(\frac{2\pi\Delta}{d}\right)]$$

Finally for  $\Phi = \pm \frac{6\pi}{d}$ , ( $h = 3$ ),

$$\text{Intensity} = \frac{(e^{-\Theta'} - 1)^2}{36\pi^2} [2 + 2\cos\left(\frac{3\pi\Delta}{d}\right)]$$

Figure 4.5 shows the graph of diffraction efficiency versus grating thickness for the first, second and third orders of a non-Ronchi amplitude grating with a  $\Delta/d$  ratio of 0.25. The maximum D.E. of the first order is 8.6% which is less than the Ronchi amplitude grating first order maximum (10.1%). The second order maximum is 1.2% and the third order is a negligible 0.2% compared to the Ronchi third order maximum of 1.1%. However, as for the Ronchi amplitude

gratings, the shape of the non-Ronchi curves are not sinusoidal but take the shape of a squared exponential function rising to a constant maximum value.

The general points to note from the theoretical formulæ describing Ronchi and non-Ronchi gratings in this chapter are as follows,

1. The phase gratings produce results for the first and third orders which are sinusoidal. This point is also valid for even numbered orders in the non-Ronchi case.
2. The peaks and troughs occur at regular  $2\pi$  radian intervals for phase gratings (the first peak occurs at  $\pi$  radians, and the first trough at zero radians).
3. For the Ronchi phase gratings, the peaks have a maximum D.E. of 40% and the troughs a minimum of 0%.
4. The amplitude grating results have a squared exponential profile with the maximum D.E. results approximately 4 times less than the corresponding phase grating.
5. Results for the odd-numbered orders in both types of non-Ronchi grating (for  $\Delta/d = 0.25$ ) are less than their Ronchi counterparts.
6. An increase in the  $\Delta/d$  ratio causes the D.E. of the odd-numbered orders to decrease and the D.E. of the even numbered orders to increase.

**Figure 4.1**

Graph of Diffraction Efficiency vs. Phase Retardance for  
a Ronchi phase grating

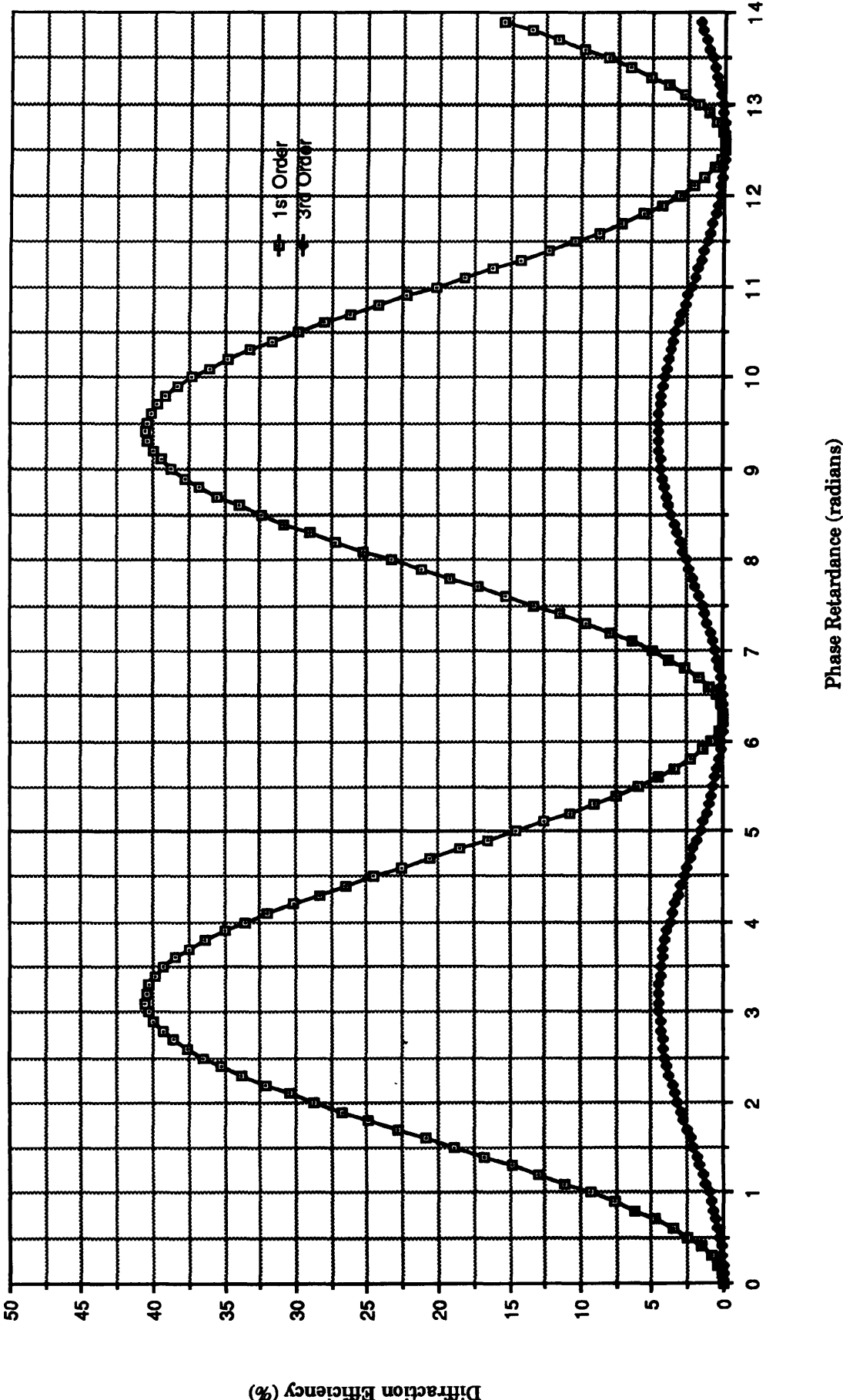


**Figure 4.2**

Graph of Diffraction Efficiency vs. Grating Thickness for  
a Ronchi amplitude grating

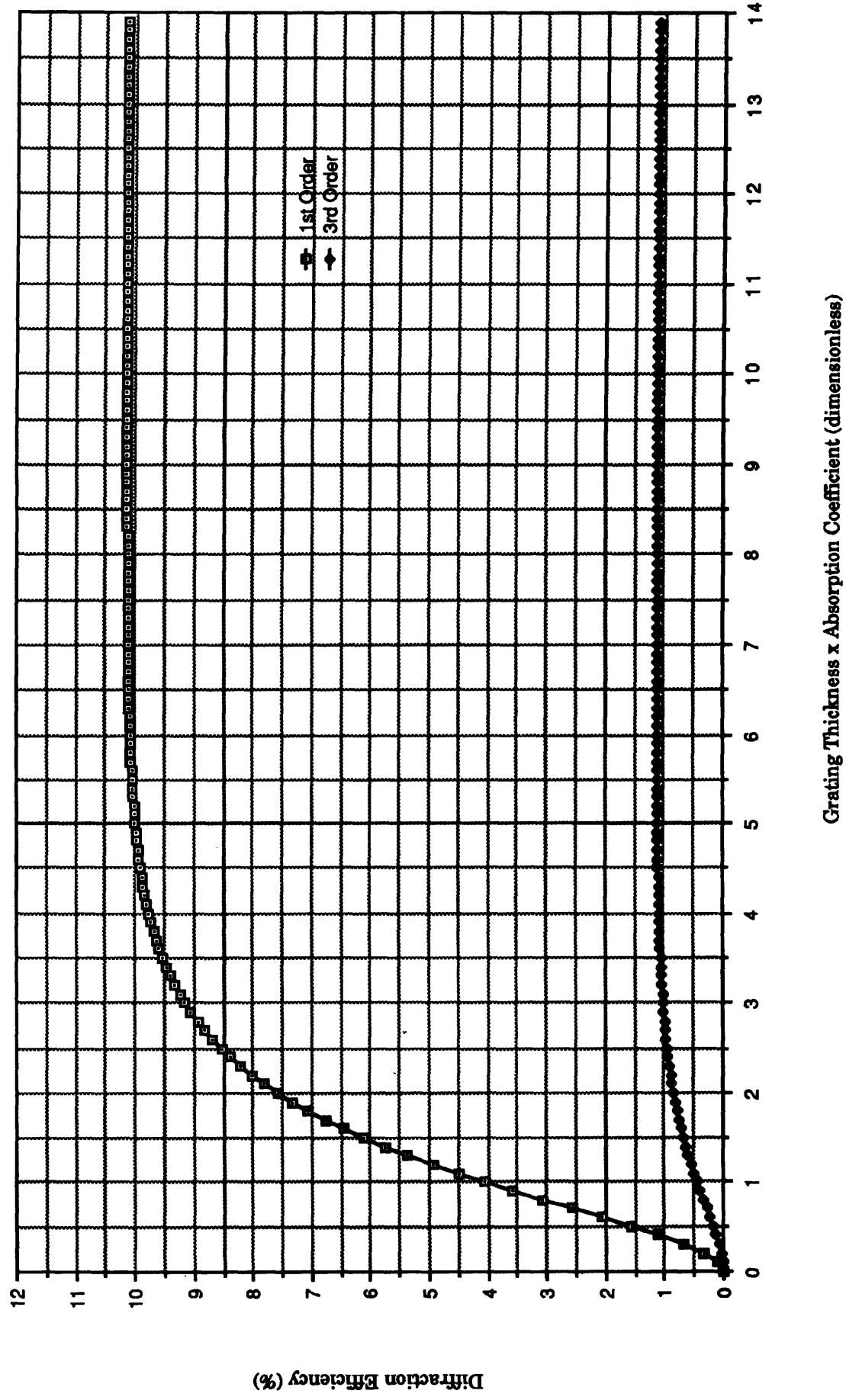




**Figure 4.3**

Graph of Diffraction Efficiency vs. Phase Retardance for  
a Non-Ronchi phase grating with  $\Delta/d = 0.25$

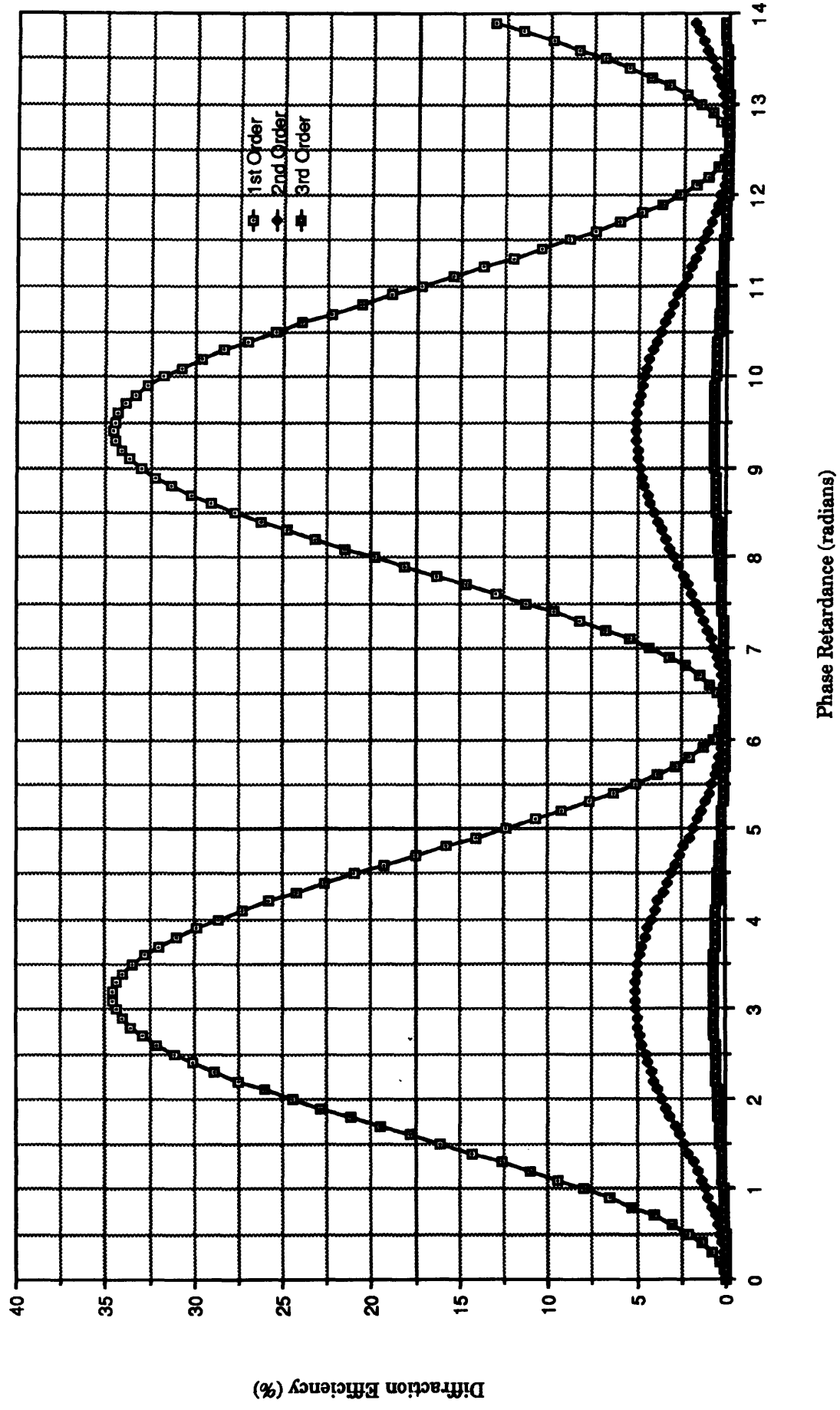


**Figure 4.4**

Graph of Diffraction Efficiency vs. Phase Retardance for  
a Non-Ronchi phase grating with  $\Delta/d = 0.04$

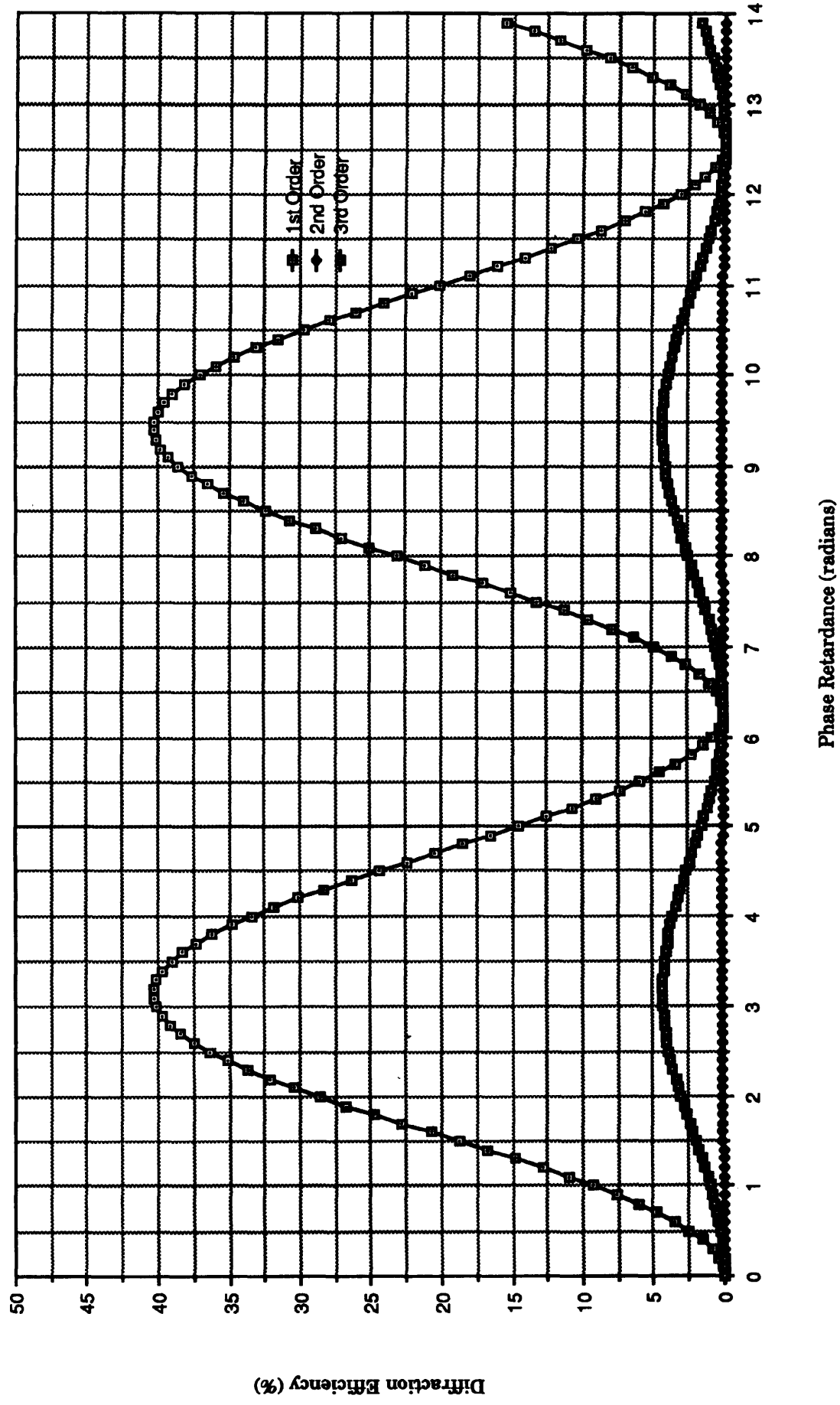
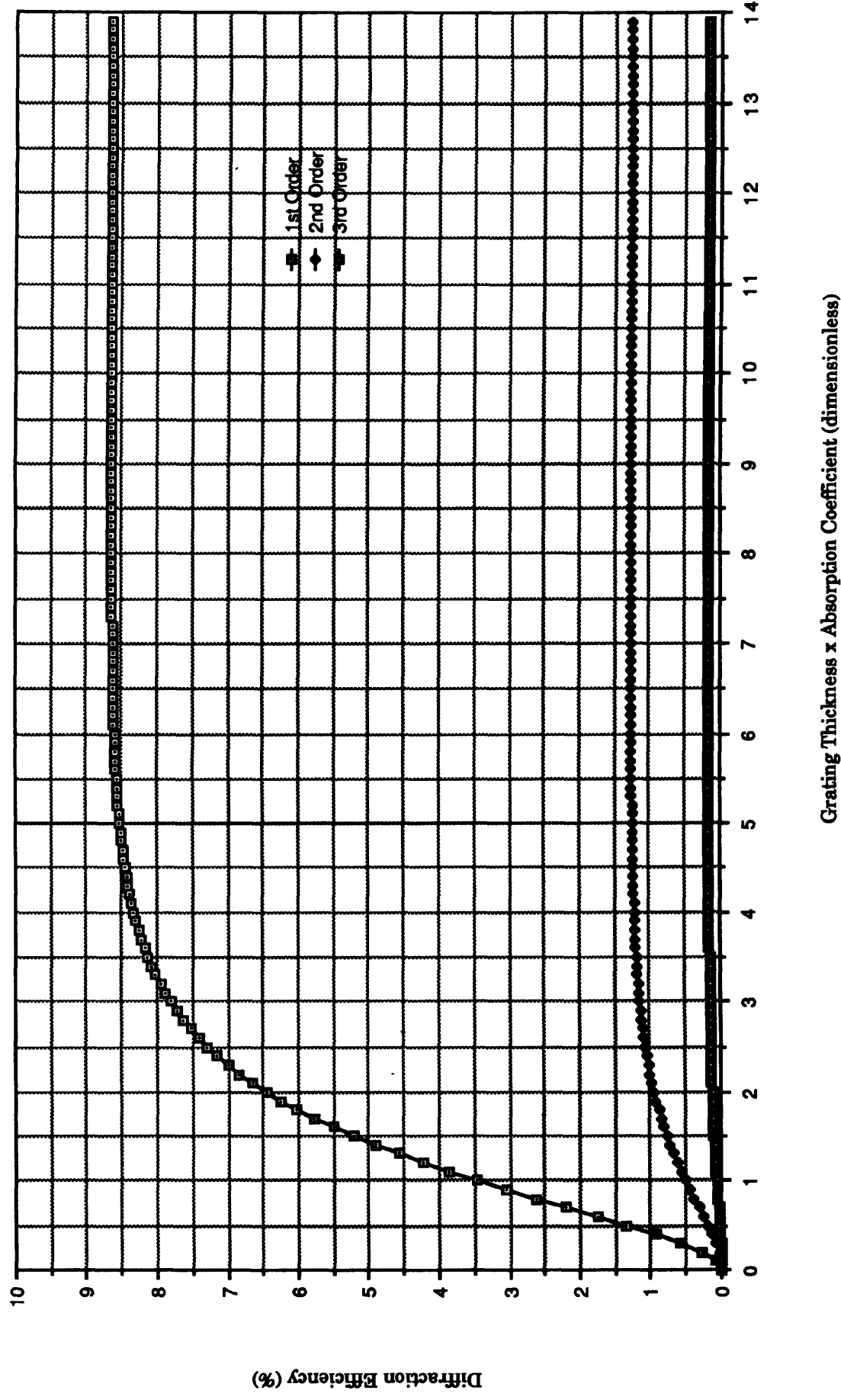


**Figure 4.5**

Graph of Diffraction Efficiency vs. Grating Thickness for  
a Non-Ronchi amplitude grating with  $\Delta/d = 0.25$



# 5

## Experimental Details

### 5.1 Chapter Summary

In chapter 4 the intensity formulæ of both phase and amplitude gratings were derived for several diffracted orders. In this chapter attention is focussed on the experimental arrangements used to measure the intensity of these diffracted orders. However before giving details of the experimental arrangement, the fabrication of the liquid crystal cells is described; this fabrication is based on the suggestions put forward in chapters 2 & 3. A description of the experimental arrangement for measuring the phase retardance of the liquid crystal follows; it is necessary to establish that the liquid crystal does not exhibit non-linearities over a given voltage range before measuring its diffraction efficiencies. The arrangement for measuring the diffraction efficiency of the liquid crystal is discussed at the end of the chapter.

### 5.2 Introduction

The intention of this chapter is to collate all the ideas, suggestions and theoretical derivations proposed in chapters 2, 3 and 4, and to put forward,

- 1) A design for an experimental cell which will give a reproducible voltage-controllable diffraction pattern.
- 2) An experimental arrangement which can measure the intensity of various orders of this diffraction pattern.

### 5.3 Construction of the Experimental Liquid Crystal Cells

In order to appreciate the decisions made by the author in choosing the types of experimental cell to construct, it must be noted that their fabrication was to be carried out in the Displays Division at S.T.L. Ltd., Harlow. Therefore, rather than incurring the expense of constructing a new set of photolithographic masks solely for

this research, the author chose to adopt an existing set of masks. The masks chosen had a conducting strip width of  $380\mu\text{m}$  and an interline gap (space between the conducting strips) of  $16\mu\text{m}$  width, permitting an ideal  $\Delta/d$  ratio of 0.04. However, during fabrication the width of the interline strip increased due to 'undercutting' of the conducting strip by the etching fluid. This decrease in width led to the practical  $\Delta/d$  ratio of 0.25 (conducting strip width  $318\mu\text{m}$ , interline gap  $78\mu\text{m}$ ). The theoretical implications of this ratio have been dealt with in the previous chapter. The cells were assembled as shown in Figure 5.1. The faces of each glass plate in contact with the liquid crystal had a grating etched onto them. The plates were arranged with the gratings orthogonal to one another. In this way further experimentation could be carried out on the cells when the author had completed his studies. By earthing all of the strips on one of the glass plates it is possible to make its grating structure redundant and thereby produce the same effect as having a single grating.

Listed below is an account of the procedures performed in order to produce a single experimental cell.

1. The commercial ITO (indium tin oxide) coated glass is cut to size (approximately 10cm square). [Note: the ITO is an electrically conductive layer coated onto the glass by the manufacturer.]
2. The glass is cleaned. This cleaning process is complicated, involving the use of ion exchanges and heated baths of weak acid, as detailed below. [Note: All temperatures are at room temperature ( $20^{\circ}\text{C}$ ) unless stated otherwise.]
  - 1) Boiled-in trichloroethane bath for 5 minutes then left in vapour for a further 5 minutes.
  - 2) Rinsed in de-ionized water.
  - 3) Detergent Cleaner (D.Con) for 5 minutes.
  - 4) Rinsed in de-ionized water.
  - 5) Rinsed in a 1% solution of HCl (Hydrochloric acid) to remove the detergent
  - 6) Rinsed in de-ionized water.
  - 7) Dried in a stream of I.P.A. vapour.
3. The conductive strips are then etched into the ITO by a photolithographic process. (This deposits a mask pattern on the surface of the ITO strips that

will be used to conduct). The unwanted ITO is stripped away by etching the glass plate in a solution of 50/50 HCl/Water at 58°C.

4. The glass plates are then re-cleaned by the same process as listed in 2. above.
5. The first stage of aligning the liquid crystal is to deposit, by the process of spin coating, a layer of polyimide onto the glass plate. Polyimide is a very stable polymer. The film is formed by depositing a filtered (millipore super)  $1/10$  diluted solution onto the spinning glass substrate (4000 rpm) at room temperature. The resulting deposit is dried at 80°C for 30 minutes. The thickness of the polyimide layer is approximately 100nm. This soft prepolymer is then rubbed evenly across the whole surface by a rotating drum covered with velvet. Full polymerization is achieved by curing in two steps; 130°C for 30 minutes, followed by 200°C for a further 30 minutes.
6. The glass plates are separated by employing 13 $\mu$ m diameter glass fibre pieces (blown over one of the plates using a nitrogen line). The two glass plates are then assembled. This is achieved by using an in-house screen printed epoxy seal ring. Essentially, this is a thin layer of special epoxy deposited around the perimeter of the plates apart from one small area, which is used as a fill hole. The epoxy is cured in a two stage process. It is heated to 70°C for 45 minutes and further heated to 130°C for an hour.

[Note: The separation of the glass plates was measured using the shifting fringe technique. In this method the coherent sources of white light are shone through the cell and at each frequency of illumination the central fringe moves. This shift is measured, the value of which can be used to determine the thickness of the cell.]

7. The assembled cell is then vacuum filled with liquid crystal. The cell is held in a cradle inside an evacuated chamber which has been lowered to  $10^{-2}$  Atm. pressure. The boat containing the liquid crystal is suspended below the fill hole of the cell and then raised up. The cell is immersed in the liquid crystal, and fills up through the fill hole. After filling, normal pressure is obtained by allowing the jar to refill with nitrogen. The cell is then removed from the apparatus and the fill hole sealed with another epoxy which cures at room temperature. [Note: when a dyed cell was made, the pleochroic dye was weighed into the liquid crystal before filling began.]

From the discussion of aligning liquid crystals on grooved surfaces in section 2.10, it was decided to assemble cells in two batches. The first batch had the rubbed glass plates aligned antiparallel to each other, whilst the other batch was assembled with the rubbed plates aligned parallel. In addition, the suggestions in section 3.3.5.1

regarding the addition of pleochroic dyes to the liquid crystal, prompted the author to fill half of the assembled cells with 2% (weight/volume) of the pleochroic dye DC-5 in the liquid crystal. These variations in the method of fabrication produce four different types of cell for each variety of liquid crystal employed. A comparison between the following cell types is therefore possible,

- a) A cell filled with a nematic liquid crystal and having the glass walls aligned parallel to each other.
- b) The same cell as a) above but having the pleochroic dye DC-5 added to the liquid crystal.
- c) A cell filled with a nematic liquid crystal and having the glass walls aligned antiparallel to each other.
- d) The same cell as c) above but having the pleochroic dye DC-5 added to the liquid crystal.

Thus, with respect to sections 4.4.1 & 4.4.2 covering non-Ronchi gratings, a) and c) above represent non-Ronchi phase gratings since they contain a phase modulating liquid crystal. Both b) and d) represent non-Ronchi amplitude gratings due to the addition of the dye which aligns parallel to the liquid crystal director and absorbs light.

The remaining sections in this chapter detail the experimental arrangements for measuring the phase retardance and the diffraction efficiency parameters of the different aligned and treated liquid crystal cells. [Note: all measurements made on the liquid crystal cells were at room temperature, 20°C]

#### **5.4 Phase Retardance**

As explained in chapter 4 it was decided to measure the diffraction efficiency in order to ascertain the suitability of a liquid crystal for use in a SLM. However it is first necessary to establish that the liquid crystal's response to an applied voltage is linear between the threshold and saturation values. This was achieved by measuring the phase retardance versus applied voltage characteristic. If any 'abnormal' responses to the applied voltage are found then the liquid crystal would be rendered unsuitable

for use in an EASLM and there would be little point in measuring its diffraction efficiency.

The phase retardance  $\phi$  of a liquid crystal is defined as,

$$\phi = \left( \frac{2\pi d \Delta n}{\lambda} \right) \quad [5.1]$$

where,

$d$  = thickness of liquid crystal sample,

$\Delta n$  = birefringence of crystal,

$\lambda$  = wavelength of incident light.

### 5.5 Experimental arrangement for measuring Phase retardance

There are several methods for measuring the phase retardance of a liquid crystal of which two will be discussed here.

The first method involves measuring the retardance directly by passing the light beam through an accurately variable phase rotator. The second method requires the use of electronic photodetectors to measure the parallel and perpendicular intensity components of the transmitted light beam. These methods shall be referred to as Method A and Method B respectively.

#### 5.5.1 Method A

Since this experiment uses a Soleil Babinet compensator it would seem appropriate at this point to give a brief description of this phase rotator. The compensator is comprised of two wedges and one parallel slab. Their optic axes are orientated as indicated in Figure 5.2. The quantity  $d_1$  corresponds to the total thickness of both wedges for any given setting of the micrometer screw. When the compensator is inserted between crossed polarizers through which a laser beam is passing the micrometer is adjusted to give two adjacent intensity nulls. The difference  $D$ , between the two micrometer readings is calculated, and the compensator can be said to have moved  $D$  micrometer units to retard the beam



by  $2\pi$  radians. Thus one micrometer unit represents  $2\pi/D$  radians. The value  $D$  will be used in subsequent calculations for phase retardance when a liquid crystal is present.

The experimental arrangement for measuring phase retardance with a Soleil Babinet compensator is shown in Figure 5.3. The compensator is positioned in the arrangement shown in such a way that its optical axis is aligned parallel to the direction of rubbing of the liquid crystal cell. The polarizer and analyser are crossed and placed in the arrangement so that they are at  $45^\circ$  to the liquid crystal cell. A diaphragm is used to filter out the unwanted extraneous laser light and pass the retarded beam into the light detector.

The experimental procedure for measuring the phase retardance versus voltage characteristic of a liquid crystal is as follows. First the liquid crystal is omitted from the arrangement and the S-B compensator adjusted to find the two adjacent micrometer positions giving the minimum reading (intensity nulls) on the light detector. The difference between the two positions will be referred to as  $D$  (as mentioned above). Next, the cell is inserted into the arrangement; the electrodes on one cell plate are connected to a variable square wave voltage generator whilst the electrodes on the other plate are earthed. An incremental voltage is applied to the electrodes until an appropriate limit is reached (in this case 10 volts peak-to-peak). After each voltage increment the liquid crystal is allowed to 'settle' for a few seconds before the S-B compensator is adjusted to find the new intensity null position.

The procedure is then reversed by applying the voltage initially at 10 volts peak-to-peak and successively decrementing it. This is performed to take into account the 'hysteresis' effect of the liquid crystal; the average of both sets of results is taken.

The readings are then analysed by substituting them into the following equation,

$$\phi_E = 2n\pi + \frac{x-y}{D} \quad [5.2]$$

where,

$\phi_E$  = experimental phase retardance,

$D$  = difference between the micrometer readings for the intensity nulls when no liquid crystal is present,

$n$  = number of  $2\pi$ 's that the liquid crystal directors rotate over the given voltage range.

$x$  = micrometer reading at 0 volts,

$y$  = micrometer reading taken at a voltage  $V$ .

The phase difference  $\Delta\phi$  is then calculated from,

$$\Delta\phi = \phi_{\max} - \phi_E \quad [5.3]$$

where  $\phi_{\max}$  is the maximum phase retardance obtained by substituting the characteristics of the liquid crystal into equation [5.1].

### 5.5.2 Method B

As mentioned in section 5.3, there is an alternative method, for measuring the phase retardance.<sup>97</sup> The experimental arrangement is similar to that above except that the S-B compensator is omitted and the light detector is replaced by a Fourier plane spectrometer complete with its own wavelength adjustable light source.

In this method the intensity readings for the parallel ( $I_{\parallel}$ ) and perpendicular ( $I_{\perp}$ ) components of the beam are measured. These intensity values are then inserted into the following equations,<sup>97</sup>

$$\begin{aligned} |\phi| &= N\pi + 2 \tan^{-1} \sqrt{\frac{I_{\perp}}{I_{\parallel}}} & \text{For } N = 0, 2, 4 \dots \\ |\phi| &= (N+1)\pi - 2 \tan^{-1} \sqrt{\frac{I_{\perp}}{I_{\parallel}}} & \text{For } N = 1, 3, 5 \dots \end{aligned}$$

where,

$\phi$  = phase retardance, (the modulus sign permits both PDA and NDA types of liquid crystal to be considered)

$N$  = determined from counting number of peaks in the transmission versus voltage curves over a given voltage range (in a similar principle to the  $n$  reading in equation [5.2]).

However there are several drawbacks to this method, namely that it requires costly equipment (spectrometer) and only permits an indirect measurement of the Fourier plane pattern to be taken. Method A on the other hand makes a direct measurement, the S-B compensator having two important features; the input retarded beam path is not deviated and a uniform retardance is produced over the whole surface of the compensator.

## **5.6 Experimental Arrangement for measuring Diffraction Efficiency**

The experimental arrangement for measuring the diffraction efficiency of the liquid crystal is shown in Figure 5.4. The arrangement consists of a linearly polarized laser which is shone through a beam expander. The outer lobes of the resultant Airy pattern are removed by a diaphragm, allowing the central portion to pass through the liquid crystal cell which has an electrically driven grating written on it. The resulting modulated beam is then focussed by a high quality achromatic doublet, the focal plane of which is the Fourier plane of the grating. Two measurement techniques were devised to record the diffraction pattern in this plane. Initially, measurements were made by photographing the diffraction pattern falling on the plane at incremental cell voltages. The developed film was subsequently analysed using a microdensitometer. The second approach used a computer controlled data logging system developed by the author. This latter technique proved to be much faster than the photographic method. The following sections describe in more detail the techniques employed.

### **5.6.1 The Photographic Method**

This method allows a 'single-shot' measurement of the diffraction pattern to be recorded which then can be examined at leisure. The procedure was initiated

by calibrating the film used for recording the diffraction pattern. The particular film chosen for the experiments was a 35mm holographic film (Agfa Gevært 10E75). The relevant properties of this film are,

- a) High resolution—greater than 2000 line pairs per millimetre.
- b) Its peak spectral response was to red laser light (632.8nm—which was used throughout all the experiments).

#### **5.6.1.1 Calibration of 10E75 Film**

The calibration process entailed photographing a 'raw' (unexpanded) laser beam transmitted through a variable neutral density filter. This varies the intensity of the laser light but leaves its wavelength unchanged. The intensity of this beam was measured by an accurate photometer. The film was then processed by developing in a 66% solution of Millimask G282c developer for 4 minutes at 20°C, followed by a one minute wash in de-ionized water and finally fixing in a 20% solution of G321 fixer for a further 4 minutes at 20°C. After rinsing in water for 15 minutes, the film was air dried. A dual-beam Joyce Loebel microdensitometer (MDM), the main operating components of which are shown in Figure 5.5, was employed to analyze the film. Referring to Figure 5.5, the intensities of the reference and sample beams are sequentially compared. The electronic controlling system causes the reference wedge to be moved in or out of the reference beam until the two intensities are equal. The position of the reference wedge gives a measure of the density of the sample and this is recorded on a plotting table by a pen having a mechanical linkage to the wedge. Since the reference wedge is linear in density along its length the readings are obtained directly in density units without any need for special circuitry. Wedges are chosen according to the scale required, a range of 0.02 → 0.25 density units per centimetre is available. Also, linear magnifications of up to 1000 are possible with this system since the MDM uses an adjustable lever arrangement for linking the plotting table to the sample stage. Thus a 1mm movement on the plotting

stage is equivalent to a  $1\mu\text{m}$  movement on the sample.

Analyzing the calibration film under the MDM yields its characteristic curve. The curve relates the (output) film density to the exposure (logarithm of the sample beam's energy) and is shown in Figure 5.6. A developed layer which has not been exposed will always have a small residual density above that of the base on which the layer is coated. This is known as the 'fog level' and the difference between the maximum density,  $D_{max}$ , and the fog density, is known as the density scale. The exposure scale is defined as the  $\log E$  ( $E$  for energy in Joules) range over which the process shows a change in density scale. The slope of the  $D$  vs  $\log E$  curve, that is  $\Gamma = dD/d(\log E)$ ,<sup>98</sup> is used as a measure of image contrast. In the case of the 10E75 film this slope is fairly linear over a large exposure range thus making it suitable for recording the diffraction pattern.

#### 5.6.1.2 Diffraction Efficiency Measurement

Once the photographic film is calibrated, measurement of the liquid crystal's diffraction efficiency may commence. A voltage is applied to alternate conducting strips on one of the cell's plates thus forming a grating (the other plate is earthed). When light is shone through this grating a diffraction pattern appears in the Fourier plane. A photograph is taken of this pattern for every voltage increment, a typical example of which is shown in Figure 5.7. Note that the faint diffraction spectra in the vertical plane are due to the pixelation effect of the liquid crystal cell. The film is processed as described in the previous section and then placed on the MDM table. The scanning slit is moved along the row of horizontal diffracted orders (the line 'X' in Figure 5.7) producing a trace of each spot's density as illustrated in Figure 5.8. By referring to the  $D$  vs  $\log E$  calibration curve, the energy of each order may be calculated and hence its diffraction efficiency at this voltage.

Thus, by photographing each cell over a range of voltages, a set of graphs of diffraction efficiency versus applied voltage is obtained. Figure 5.9 shows the sequence of events required to obtain diffraction efficiency versus voltage readings using the photographic method.

In summary, the photographic method has several associated problems. The linearity of the  $D$  vs  $\log E$  curve was dependent on the the 'freshness' of the film and the developing fluid, the latter needed to be kept in dark air-tight containers. Also the limited linearity of the  $D$  vs  $\log E$  curve caused problems when photographing the high dynamic intensity range of the diffraction pattern—in some cases the central order was so intense that it saturated the film but on the other hand the lower orders were not intense enough to expose the film. The mechanical chain linkage in the MDM proved to be a source of further error. In some situations the wedge following the exposed film moved so rapidly that the linkage could not respond fast enough, giving rise to poor results. To conclude, the whole process was time consuming and potentially error prone unless precautions were taken. A typical 'turn-around' time for calibrating, shooting, developing, analyzing and plotting 45 items of data was three days under optimal conditions. Consequently the following procedure was adopted.

### **5.6.2 Computer Controlled Data Logger**

An alternative method of determining the diffraction efficiency was devised by the author to speed-up the process of result taking and to improve the accuracy. This method involved developing a computer controlled data logger system, the aims of the system being,

- 1) To automate as far as possible the data-logging procedure, thus permitting inexperienced users to operate the system at a future date.
- 2) To obtain more readings per liquid crystal cell (approximately 100 or more per spectral order—compared with 45 or less from the photographic method).

- 3) Whilst carrying out measurements for the photographic method, it was found that a great deal of effort was required to adjust the voltage source driving the liquid crystal cell. Thus the final aim of the system was to provide a more stable and accurate computer controllable voltage supply to drive the cell.

It was decided to base the design around the software and hardware of the BBC Model B microcomputer as the author was familiar with this system and most laboratories possess this type of micro. The hardware and software components of the logger are described below.

#### **5.6.2.1 Hardware Components of the Data Logger**

To make the design as simple as possible, it was decided to employ the USER - PORT on the BBC micro to control all of the external hardware operations. The USER PORT has eight general purpose parallel input/output (I/O) lines (PB0-PB7) and two programmable lines (CB1 & CB2). Apart from CB1, they were all used to control the digital input to a  $3\frac{1}{2}$  digit binary-coded-decimal (B.C.D.) potentiometer integrated circuit (i.c.). Essentially, the potentiometer i.c. operated like a conventional 10-turn potentiometer except that the output was adjusted digitally rather than mechanically. Nine output lines from the USER PORT were configured to drive the two and a half most significant digits of the i.c. A maximum of 199 readings could be taken in this fashion. The four unused inputs to the least significant digit of the potentiometer i.c. were connected to zero volts potential. A 0→10 volts, equal mark space ratio, 50Hz square wave generated by a simple astable 555 timer circuit, was fed to the analogue input of the potentiometer chip.

Before installing the photodetector in the system its response was checked for linearity by using a rotatable polarizer/analyser combination (Malus' Law). The detector was then mounted at the end of a short length of glass fibre-optic cable and held in position by a clamp fixed on a XYZ translational stage. This arrangement permitted accurate manual positioning of

the detector along the diffraction pattern. Once positioned, the intensity of the diffracted order was measured by converting the analogue photodiode signal to a digital signal; one channel of the 12-bit analogue to digital converter (ADC) on the BBC microcomputer was used. Figure 5.10 shows the sequence of events performed by the user in order to obtain the diffraction efficiency versus voltage characteristic for the experimental cells. The circuit diagrams for the component parts of the data logging system are shown in Figure 5.11.

#### **5.6.2.2 Software Components of the Data Logger**

All of the controlling software was written using the Acornsoft ISO Pascal package. The reasons for using Pascal as a control language were,

- 1) The author was more proficient in the use of Pascal as opposed to BBC BASIC.
- 2) The ISO Pascal Stand Alone Generator (SAG) package was readily available. This enabled a compiled p-code Pascal program to be re-compiled into native 6502 machine code and transferred into an EPROM. The advantages gained by using an EPROM (erasable programmable read only memory) were that,
  - a) if the EPROM was transferred to another BBC micro, it would not require a ROM resident Pascal p-code interpreter, and
  - b) more of the computer's memory was available to store data.
- 3) The language was easier to debug, and in a compiled machine code format operated 30% faster than interpreted BBC Basic.

The flowchart in Figure 5.12 shows the operation of the controlling software. (The resultant source code is listed in Appendix B). On running the program, a 'user-friendly' interface prompts the user with a menu of options from which he or she can select the appropriate action. If the calibration option is chosen the procedure invoked permits the intensity of the laser beam to be digitized and then measured independently with an accurate photometer, thus verifying the accuracy of the digital measurement. The data logger

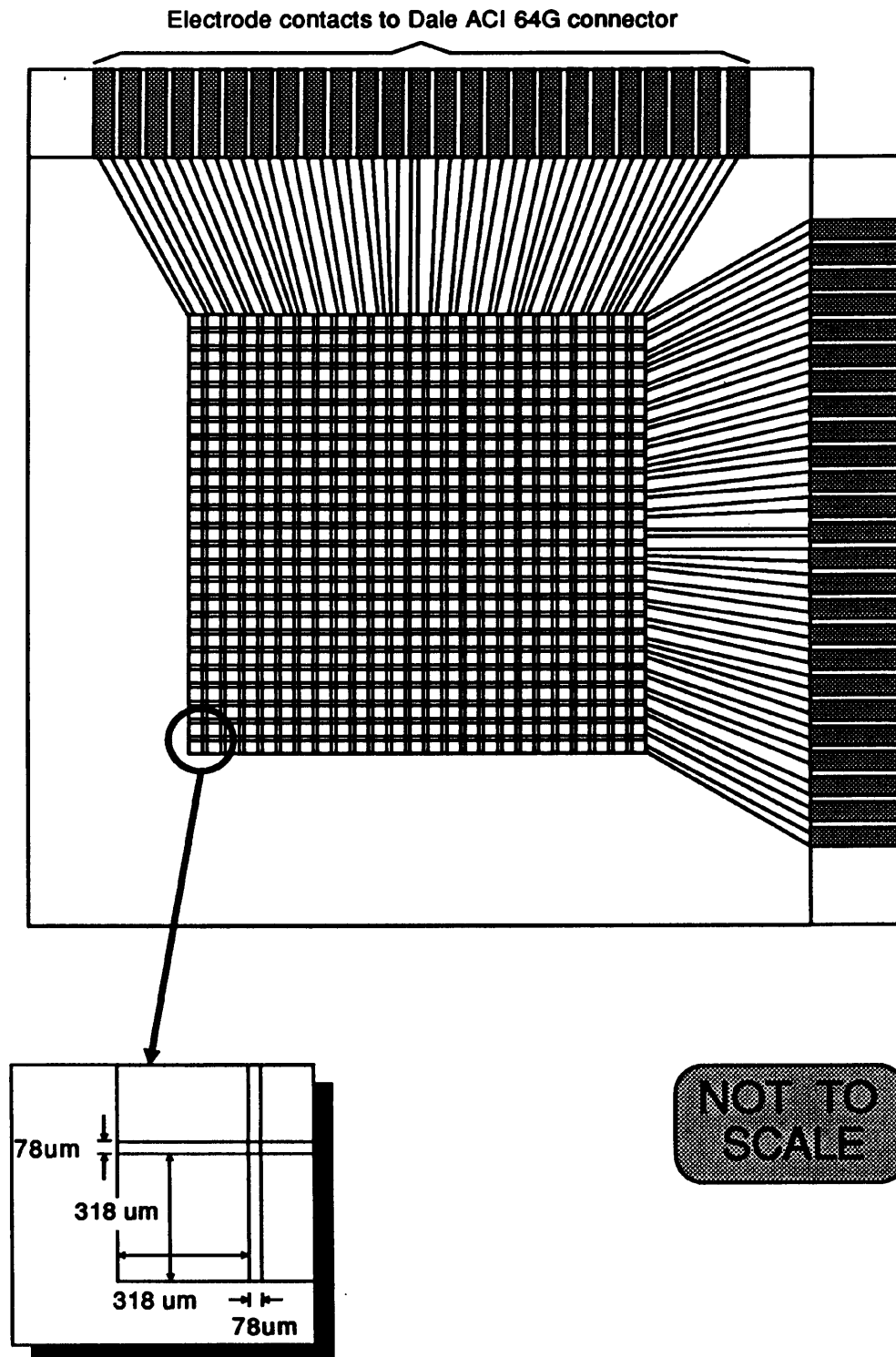


option first prompts the user for the specific details of the cell and then continues by giving directions as to which spectral order it wants to measure ( $0, \pm 1, \pm 2$ ); the user is required to move the micrometer laterally to the next spectral position, the peak intensity of this order is located with the aid of another procedure. After all the orders have been measured, the data is saved to disk using a user specified file name and date stamp. In this manner several sets of readings could be taken for each cell and the results printed out later for comparison and statistical analysis.

The design, assembly and test of the data logger took the author six weeks. In operation the computer controlled data logger performed well. Having spent several arduous months obtaining results by the photographic method it was interesting and pleasing to discover that the results from the data logger were to within  $\pm 5\%$  of those from the photographic method. This confirmed the accuracy of the data logger and consequently, the results presented in the following chapter are those obtained from the data logger.

**Figure 5.1**

**Experimental Cell Dimensions**



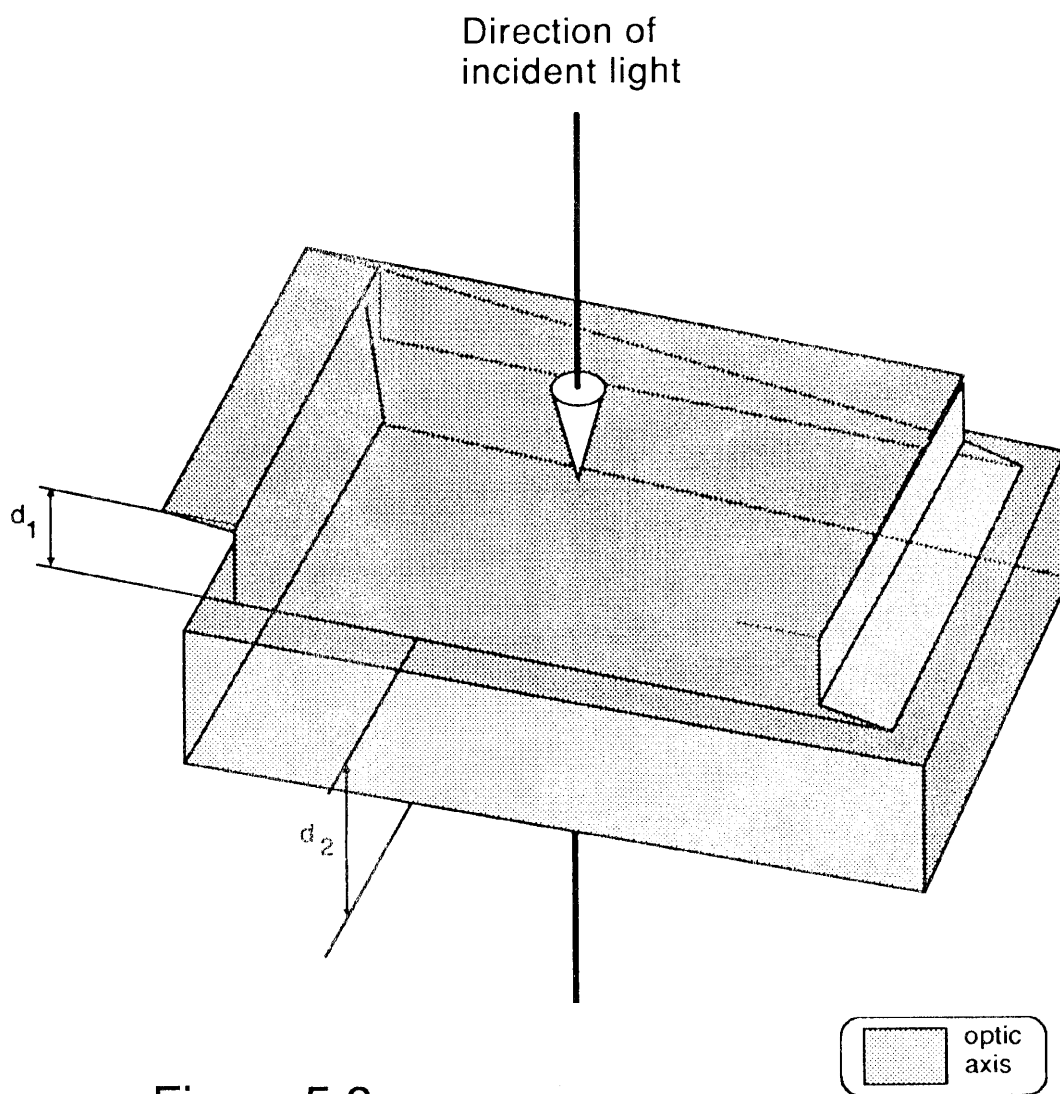


**Figure 5.2**

Schematic diagram of a Soleil Babinet Compensator.

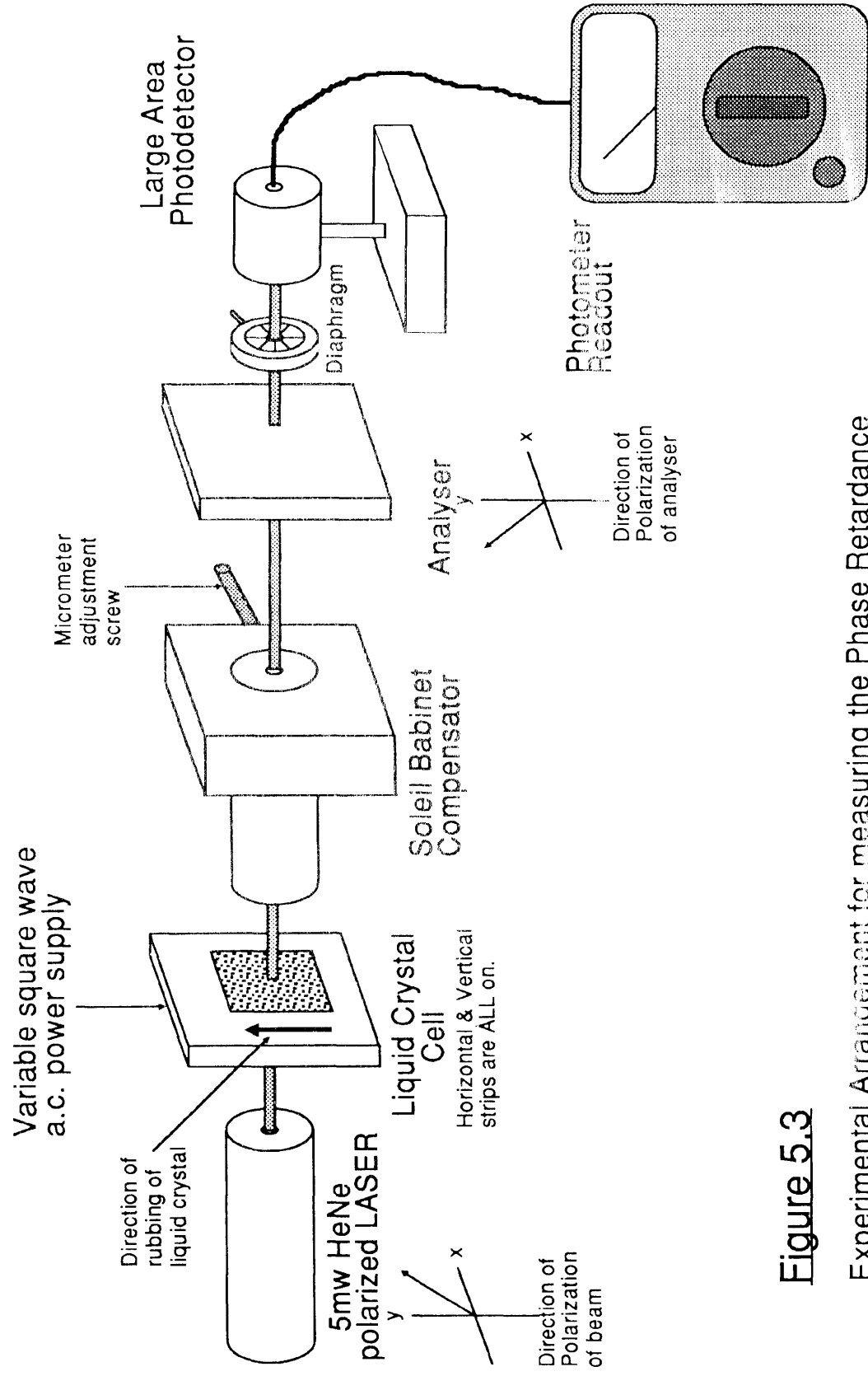


**Figure 5.3**

Experimental Arrangement for measuring the Phase Retardance of the liquid crystal in the cell.

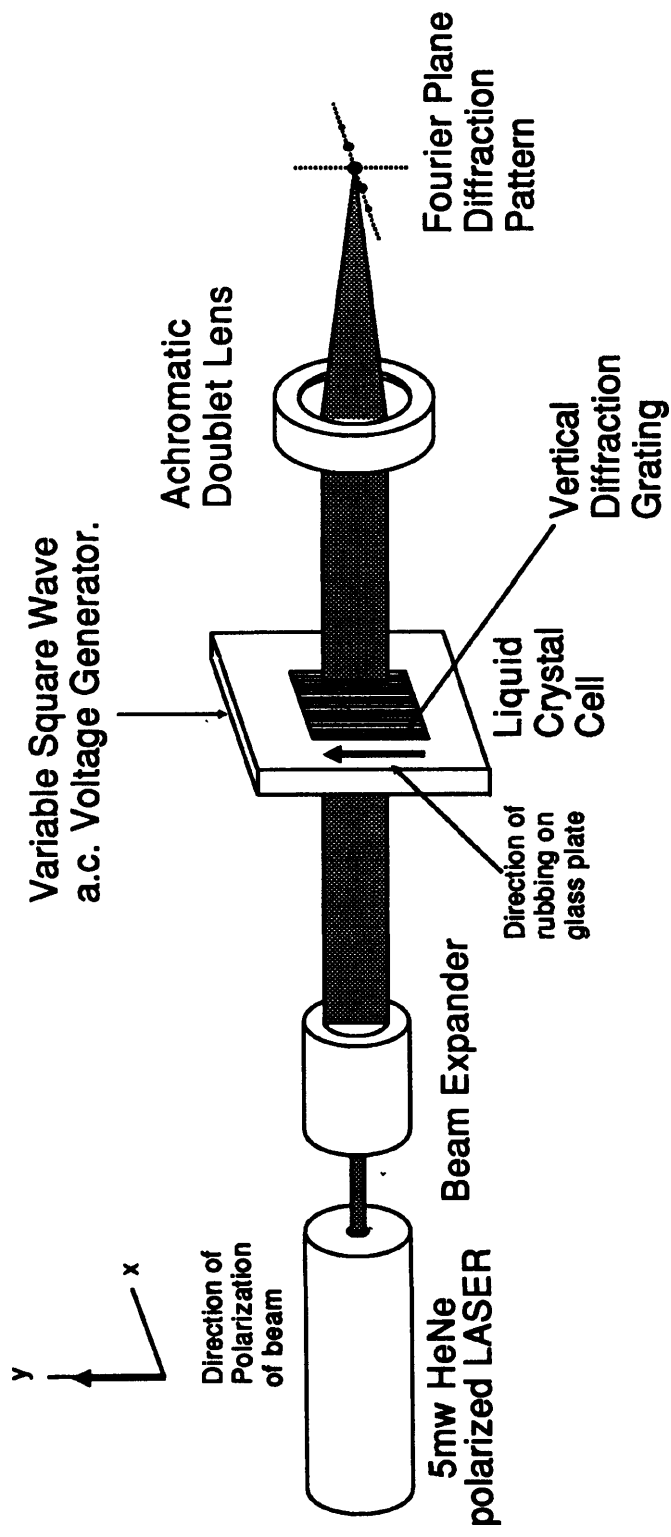


**Figure 5.4**

Experimental Arrangement for measuring the Diffraction Efficiency of the liquid crystal in the cell.

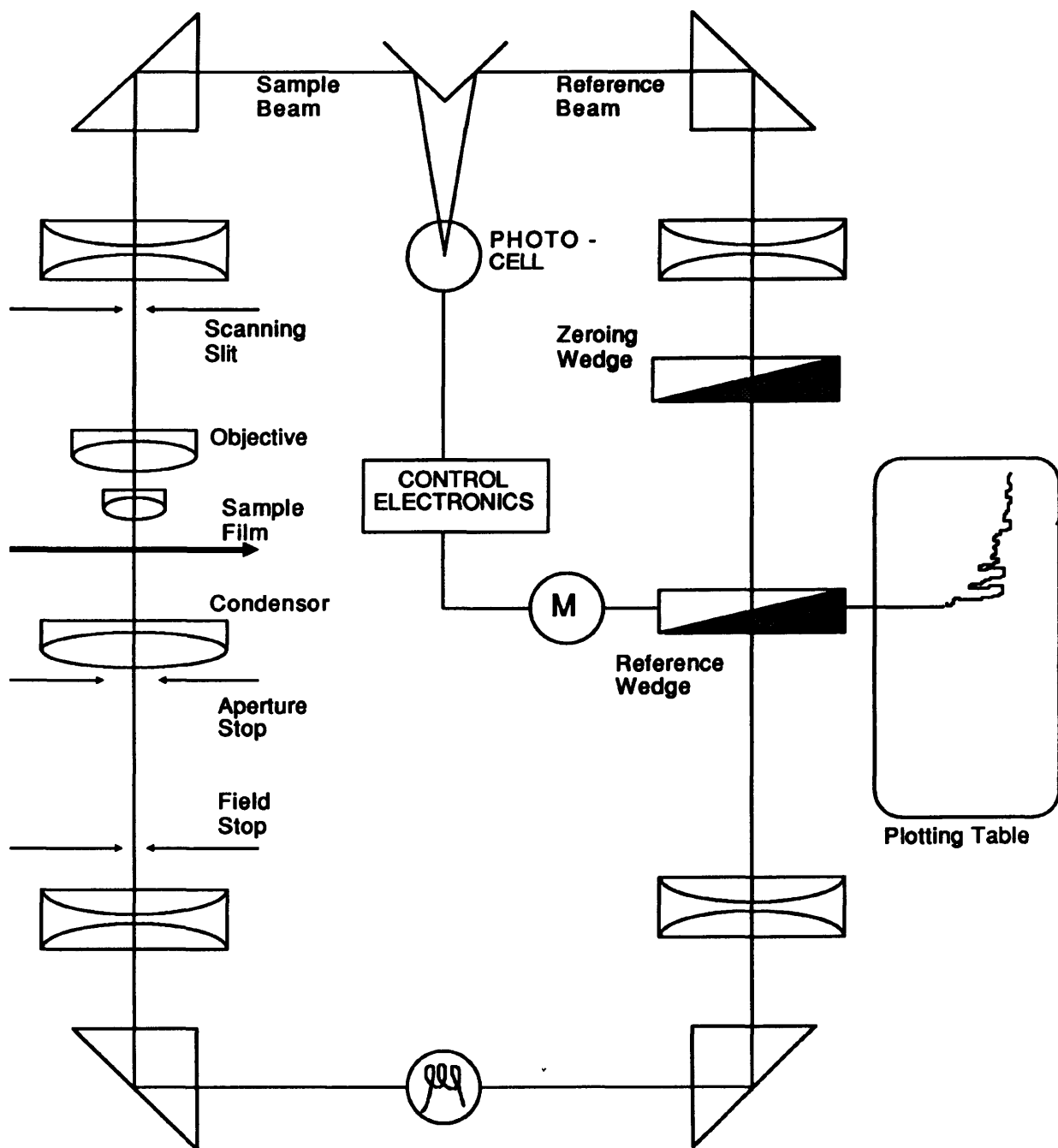


**Figure 5.5**

Schematic diagram of a dual-beam Joyce Loebel Microdenistometer (MDM).

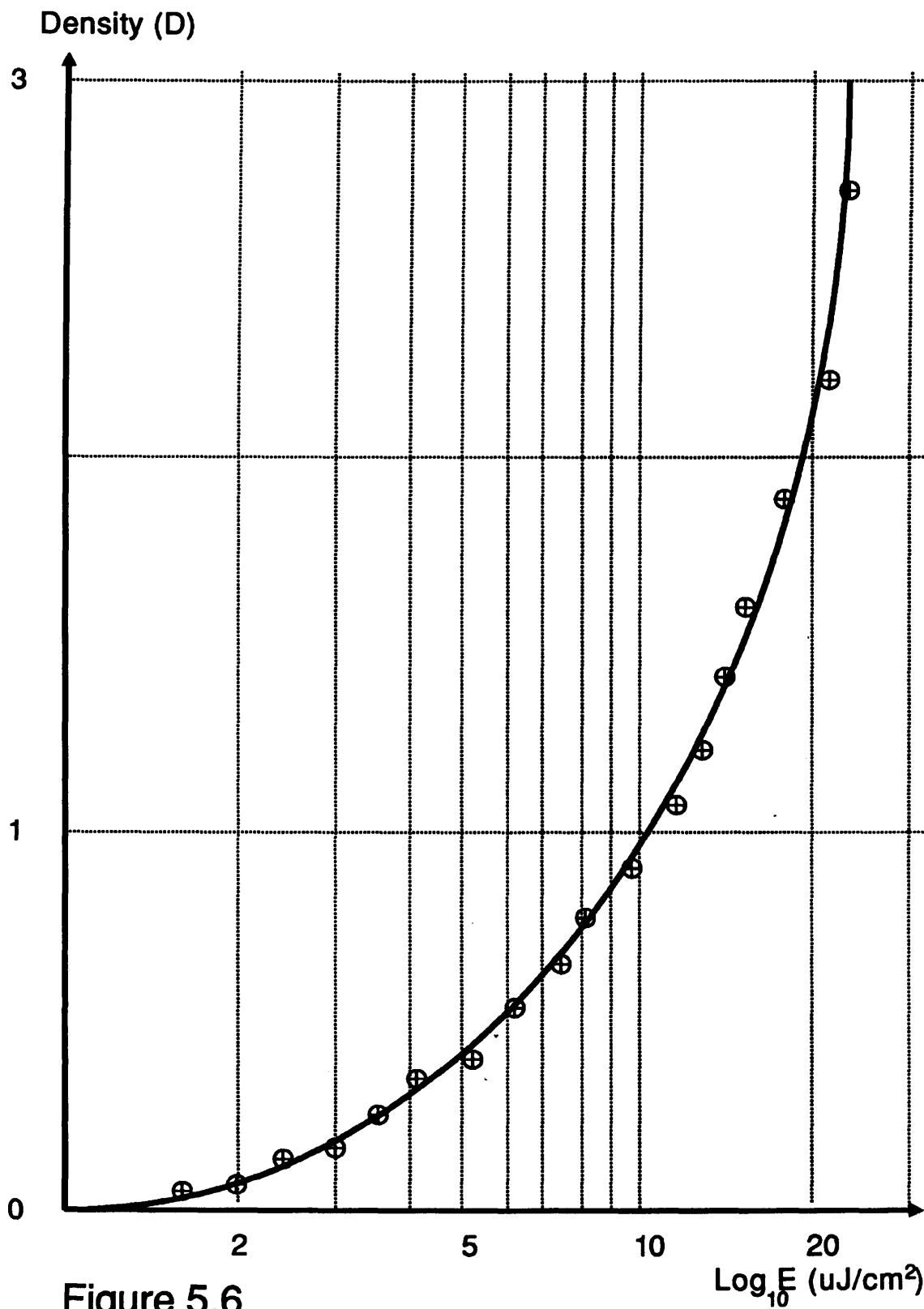


**Figure 5.6**

Characteristic D vs logE curve for the 10E75 Agfa Gevaert Film.

**Figure 5.7** Typical Diffraction Pattern from Experimental Cell.

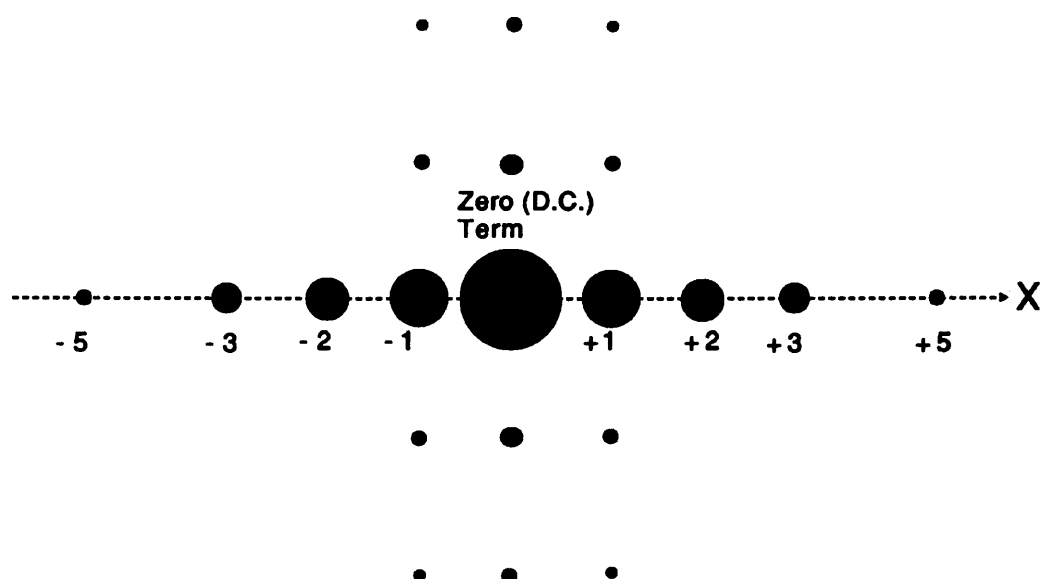


**Figure 5.8** Microdensitometer trace of the horizontal diffraction pattern along X

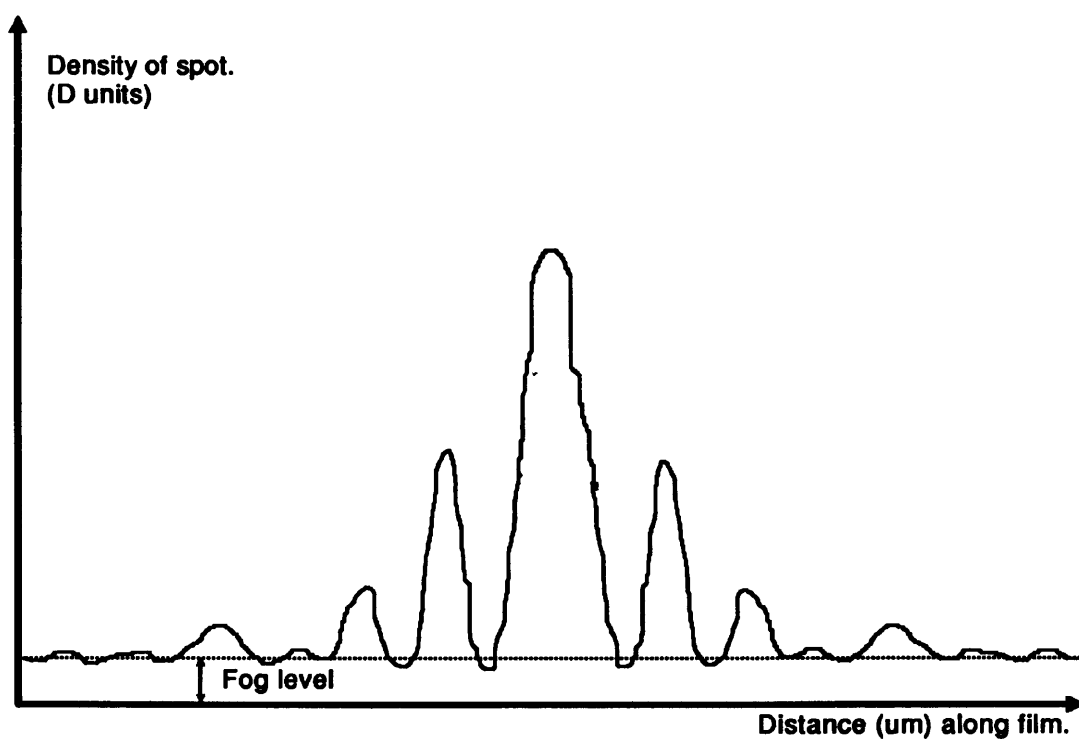




**Figure 5.9** Sequence of events necessary to produce  
Diffraction Efficiency versus voltage readings

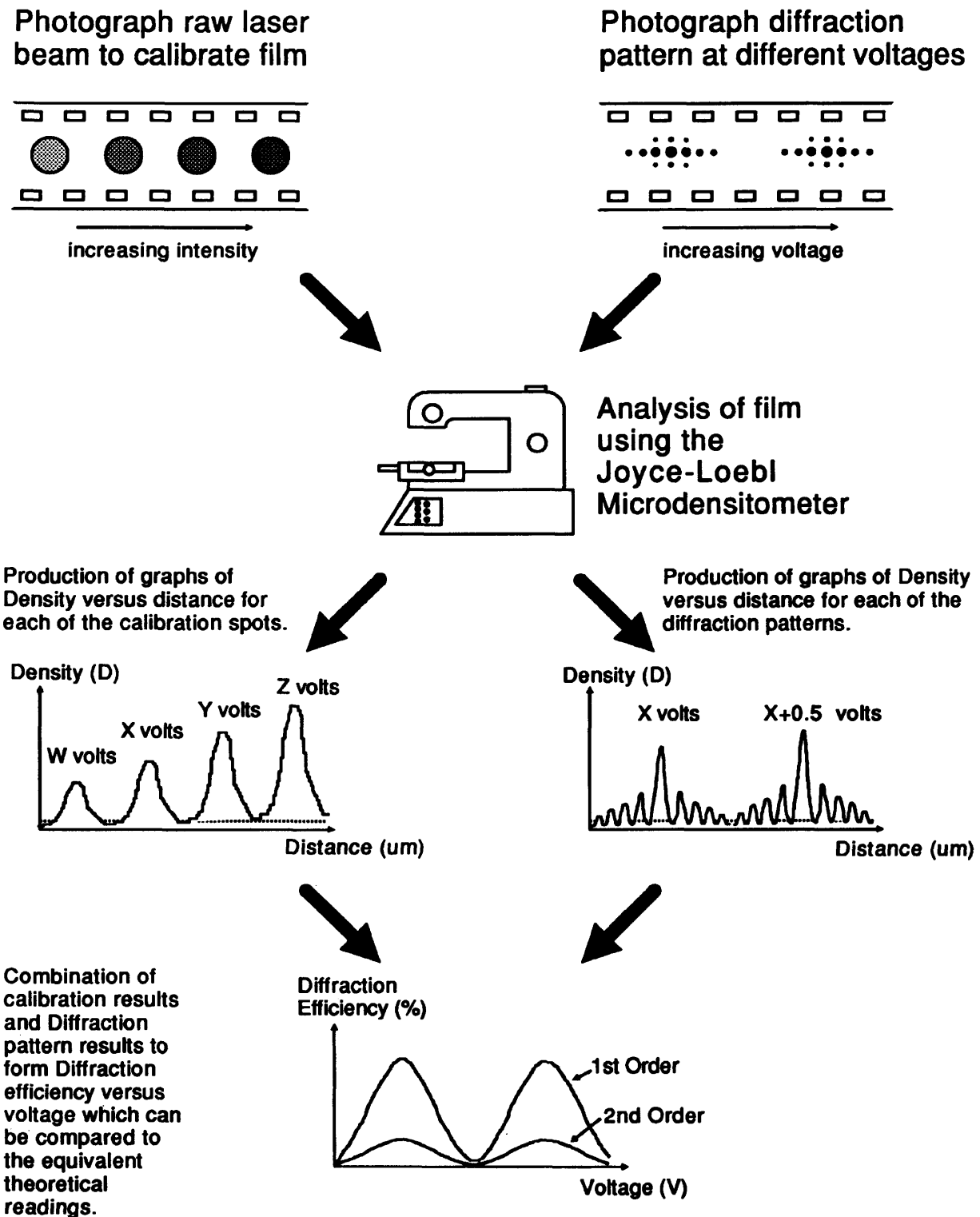
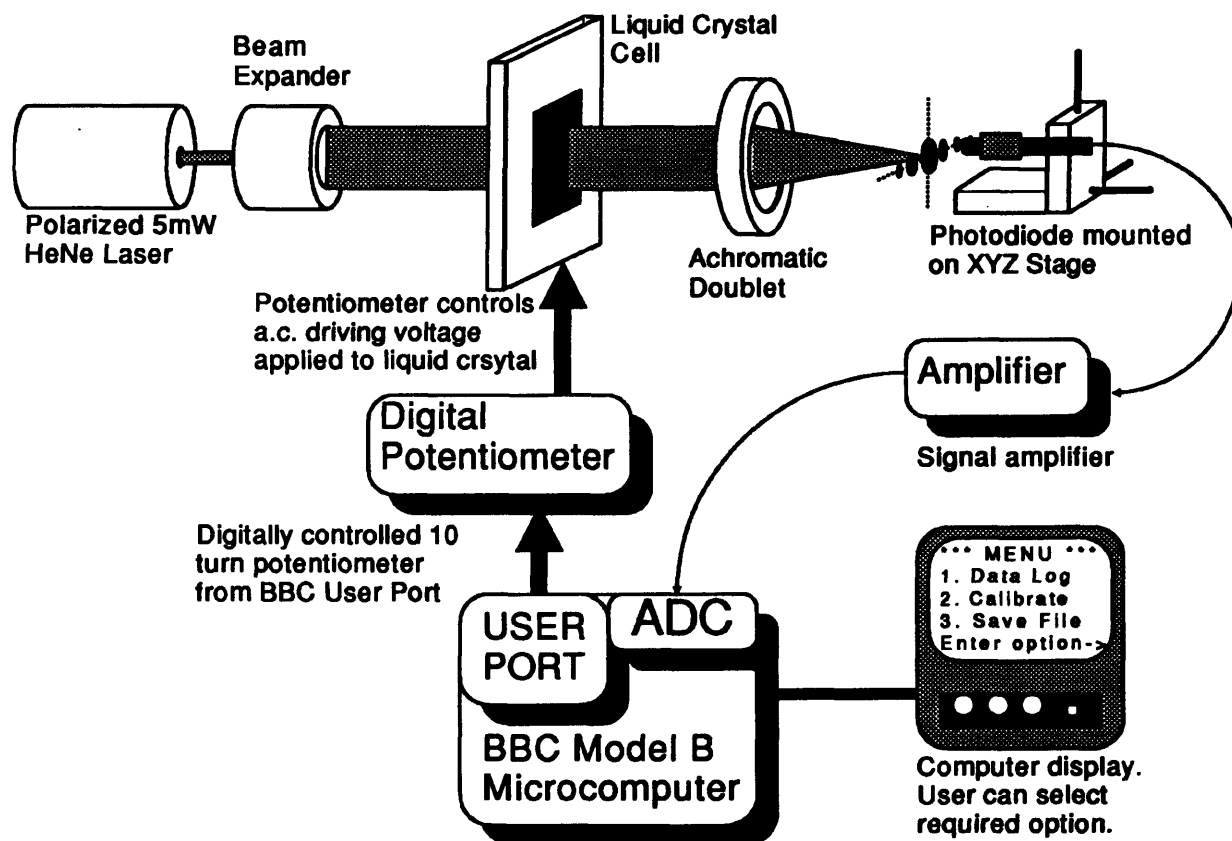


**Figure 5.10** Sequence of events performed by the computer controlled data logger in order to obtain D.E. versus voltage results.



#### Operating sequence for Data Logger

1. Calibrate photodiode using configuration with no applied voltage.
  - i) Select the calibrate option
  - ii) Move photodiode to brightest point
  - iii) Record digitised result
2. Remove photodiode equipment & measure the spot with a photometer
3. Replace photodiode equipment & select data log option from menu
  - i) Enter date, time & cell type in response to prompts
  - ii) Move photodiode to required diffraction order using peak location method.
  - iii) Data logger will automatically step the driving voltage to liquid crystal by the required number of steps. At each step the intensity of the order is digitised and the result stored on disk.
  - iv) Use XYZ stage to move photodiode to other orders
  - v) Items iii) and iv) are repeated with the voltage stepping down.
4. Steps 1 through 3 are repeated for all other cells.

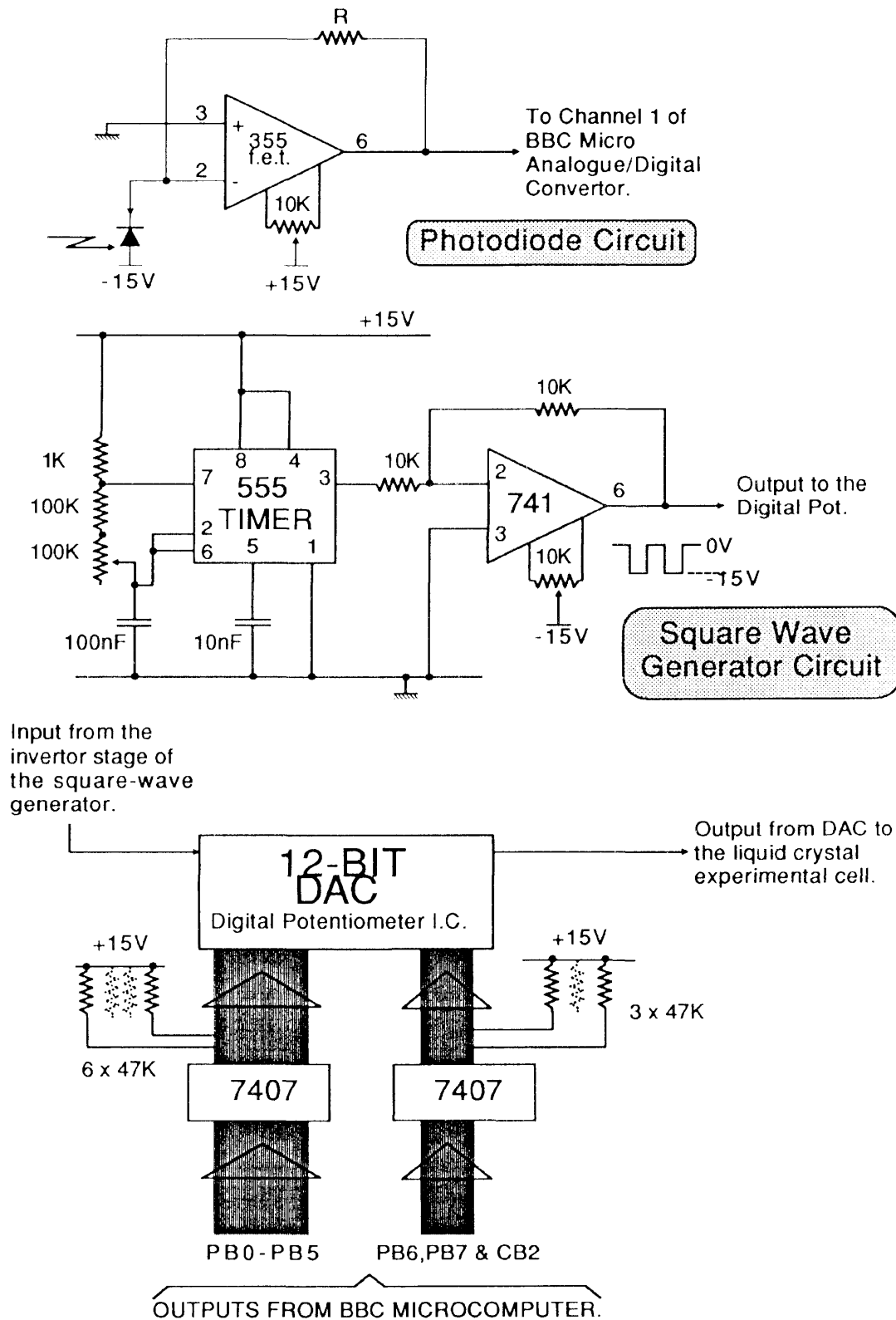
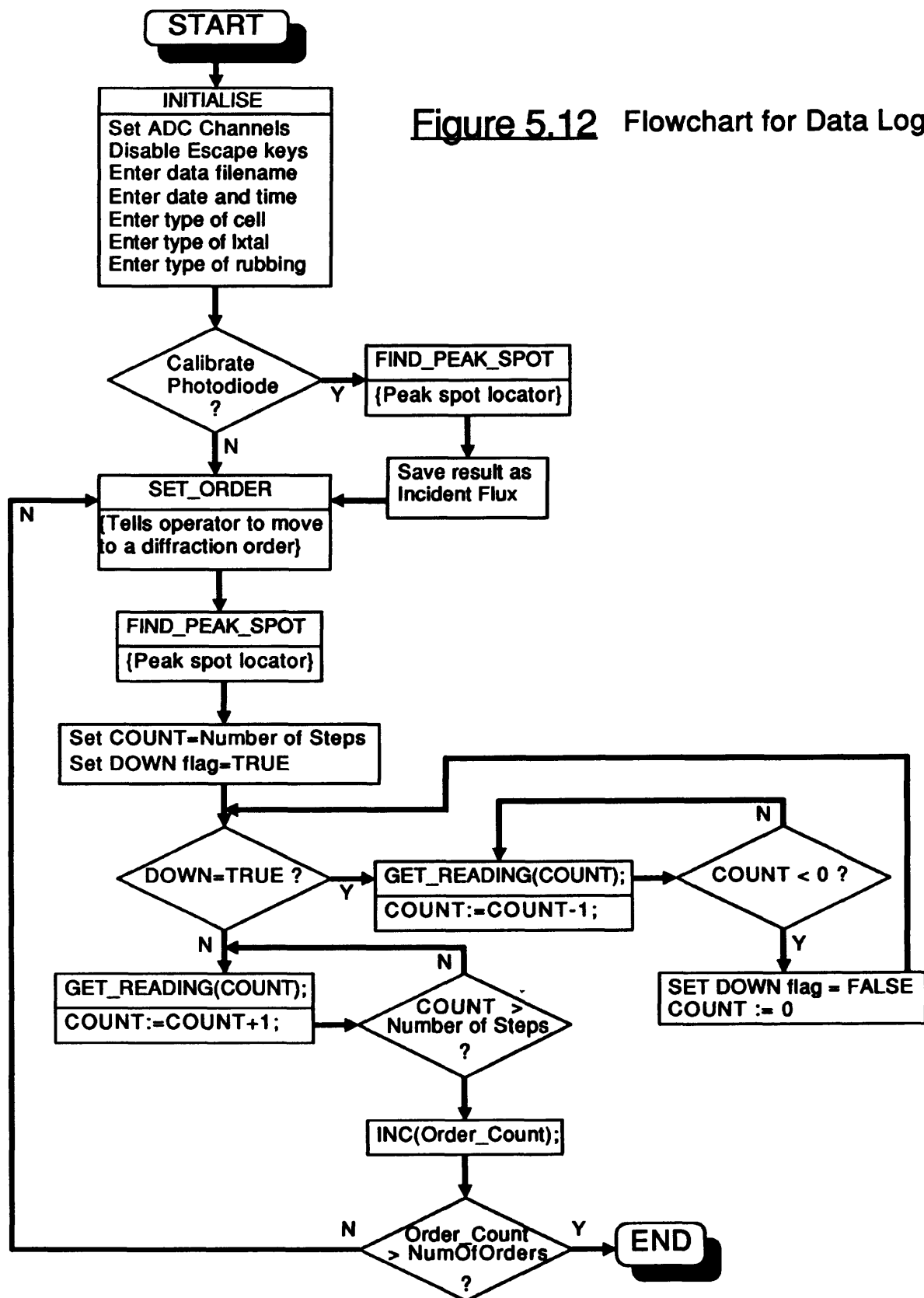


**Figure 5.11**

Circuit Diagrams of Computerized Data Logger.



# 6

## Results

### 6.1 Chapter Summary

This chapter discusses the results obtained from the experimental arrangements described in chapter 5.

The phase retardance results are considered first. The experimental maximum phase retardance (which occurs at zero volts) was lower than the theoretical maximum. However the results were in good agreement with Efron *et al's* work on voltage induced phase retardance, who proposed that the deficit was due to the non-contribution of the directors anchored to the cell walls.

The technique developed by the author, for determining the suitability of the liquid crystal for use in a SLM by measuring its diffraction efficiency properties, worked reliably giving reproducible results. These results compared favourably with the theoretical predictions made in chapter 4, exhibiting peaks and troughs at  $2\pi$  intervals.

### 6.2 Introduction

The preceding chapter established the experimental arrangements for measuring both the voltage induced diffraction efficiency and phase retardance parameters of the liquid crystal cells. It is the intention of this chapter to present the results of the measurements and to discuss their properties. In doing so, it is first necessary to explain the different types of cell configurations used and their positioning in the experimental arrangement relative to the incident light.

The results are presented for two different types of PDA nematic liquid crystal which were manufactured by the Merck company. They have reference numbers Zli1982 and Zli1800, the distinguishing characteristic being their birefringence; Zli1982 has

a birefringence  $\Delta n = 0.14$  whereas Zli1800 has a  $\Delta n = 0.07$ .

From each liquid crystal a total of four different cell configurations were fabricated.

These are as follows,

- 1) Undyed cell with parallel rubbed glass plates.
- 2) Undyed cell with antiparallel rubbed glass plates.
- 3) Dyed cell (pleochroic dye was added to the liquid crystal) with parallel rubbed glass plates.
- 4) Dyed cell with antiparallel rubbed glass plates.

The phase retardance of only the undyed cells was measured; the addition of dye to the liquid crystal affects the amplitude characteristic rather than the phase. The results show the effect of the liquid crystal's birefringence on the phase characteristic by comparing Zli1982 (high birefringence) to Zli1800 (low birefringence). The phase characteristics of Zli1982 and Zli1800 were also used to interpret the differences between the diffraction efficiency results for Zli1982 and Zli1800. Finally, these results enable the effects of parallel and antiparallel rubbing on the phase retardance to be compared for the same type of liquid crystal.

The diffraction efficiency, on the other hand, was measured on all four cell configurations and the results grouped for each type of liquid crystal according to the direction of rubbing on the cell's plates. In the experimental arrangement (shown in Figure 6.1) the incident polarized light was aligned parallel to the direction of rubbing for both the dyed and undyed cells. A further measurement was then taken for the undyed cells after rotating the orientation of the incident polarized light through  $45^\circ$  so that the angle between its polarization and the direction of rubbing on the cell was then  $45^\circ$ . Thus a total of six sets of results per liquid crystal type was obtained, Figure 6.2 presents a summary of these.

From the results the relationship between a cell's configuration and diffraction efficiency could be determined by comparing,

- 1) Undyed cell at  $0^\circ$  (phase configuration)

- 2) Dyed cell at 0° (amplitude configuration)
- 3) Undyed cell at 45° (phase rotator configuration)

Again the effects of parallel and antiparallel rubbing on the diffraction efficiency can be observed in the results. Finally, by comparing as a whole the results for Zli1982 against those for Zli1800, it was possible to discover the effect of the liquid crystal's birefringence on diffraction efficiency.

### **6.3 Discussion of the Phase Retardance results**

The phase retardance versus applied voltage results for the two types of liquid crystal are shown superimposed in Figure 6.3. The figure presents two sets of results for each type of liquid crystal. One set is for an undyed cell with antiparallel rubbed plates and the other is for an undyed cell with parallel rubbed plates. Both cells are driven with all of the conducting strips on one side of a glass plate connected to a variable voltage source. In this way, the liquid crystal acts as a voltage controllable birefringent slab. The results for Zli1982 shown in Figure 6.3 are approximately twice as large as Zli1800's over the zero to 'turn-on' voltage range. This is to be expected considering their difference in birefringence;  $\Delta n_{1982} = 2\Delta n_{1800}$ .

A closer inspection of the Zli1982 phase retardance results indicates that the initial threshold or 'turn-on' of the liquid crystal is 1.2 volts for the antiparallel rubbed cell and 1.4 volts for the parallel cell. The saturation portion, where the phase retardance does not alter appreciably in relation to applied voltage, occurs at 9 volts for both types of rubbing. A similar inspection of the Zli1800 results shows that the antiparallel rubbed cell has an initial threshold of 2.3 volts, whereas the parallel rubbed cell turns-on at 2.6 volts, the saturation voltage occurs at 6.5 volts for both types.

A summary of the observations made from the phase retardance versus voltage results are listed in the points below,

- 1) The results for the Zli1982 liquid crystal are approximately twice as large as those for the Zli1800 liquid crystal in the zero to threshold voltage range.

- 2) The turn-on point for the Zli1982 liquid crystal occurs at a lower voltage than for the Zli1800 liquid crystal.
- 3) The phase retardance readings for the initial portion of the curve (from zero volts to the point of turn-on) in the parallel rubbed cells are approximately 4% higher than the corresponding antiparallel results for both types of liquid crystal.
- 4) Beyond the saturation point, the results for both types of rubbing are the same. This effect was observed in both types of liquid crystal.

Substituting the parameters for the experimental cell thickness ( $13\mu\text{m}$ ), wavelength ( $\lambda = 632.8\text{nm}$ ), and birefringence into equation [5.1], gives a theoretical phase retardance reading  $\phi$  for Zli1982 of 18.1 radians and for Zli1800 of 9.0 radians. The theoretical predictions agree with the experimental results in so far as Zli1982's phase retardance is twice that of Zli1800's. However the experimental phase retardance maxima (that is, the phase retardance at zero volts) are lower than the theoretical values. Without distinguishing between parallel and antiparallel rubbed cells, this difference is approximately 3.5 radians for Zli1982 and 2.0 radians for Zli1800. Similar findings were reported by Efron *et al*<sup>99</sup> in 1986. They observed an average phase deficit of  $4\frac{1}{2}$  radians between the maximum experimental phase retardance readings and the maximum calculated theoretical phase retardance for cell thicknesses in the range  $1\mu\text{m}$  to  $11\mu\text{m}$ . The reason for this deficit they proposed, was due to a non-contribution of the directors anchored to the cell walls. Efron *et al*'s results were made on liquid crystals with similar properties to those of Zli1982, that is, a birefringence  $\Delta n = 0.14$ ; thus by extrapolating their results to take account of the author's thicker ( $13\mu\text{m}$ ) cells, the deficit ( $18.1 - 14.6 = 3.5$  radians) was found to be in good agreement.

The difference between the parallel and the antiparallel results as stated in point 3) above can be explained with reference to Figure 6.4. It can be seen that between the zero and threshold voltage a greater percentage of the directors in the parallel rubbed cell are approximately perpendicular to the incident light than those in the



antiparallel rubbed cell. The effect of this is that the parallel rubbed cell appears 'thicker' to the incident light; hence its birefringence will be slightly higher and consequently its phase retardance also.

#### **6.4 Discussion of the Diffraction Efficiency results**

The percentage diffraction efficiency versus applied voltage results for all of the experimental arrangements are shown in Figures 6.5 to 6.12 inclusive. Figures 6.5 to 6.8 depict the results for both the first order and second order readings for the parallel and antiparallel rubbed cells filled with Zli1982 liquid crystal. Similarly, Figures 6.9 to 6.12 depict the first order and second order readings for the parallel and antiparallel rubbed cells filled with Zli1800 liquid crystal.

On inspecting these eight graphs, it is possible to note the following similar features. First, the diffraction efficiency (D.E.) results are highest for the undyed cells with the incident linearly polarized light at  $0^\circ$  to the direction of rubbing on the liquid crystal cell. The next highest D.E. readings are from the undyed cell at  $45^\circ$ , followed by the dyed cell at  $0^\circ$ . Second, it is apparent that the D.E. readings for the parallel rubbed cells are higher than those for the antiparallel rubbed cells for both the first and second orders of the two types of liquid crystal tested. Third, the D.E. readings of the first order results are all approximately ten times greater than those of the equivalent second order results. Finally, the most noticeable distinguishing feature between the results from the Zli1982 filled cells and the results from the Zli1800 filled cells is that the Zli1982 readings exhibit two diffraction efficiency peaks, whereas the Zli1800 readings exhibit only one peak over the same applied voltage range.

A summary of the main features noted from the D.E. versus voltage results is as follows,

1. Diffraction efficiency results for the experimental cells decrease in magnitude in the following order, undyed at  $0^\circ$  to undyed at  $45^\circ$  to dyed at  $0^\circ$ .
2. Parallel rubbed cell readings are higher than antiparallel readings for both the Zli1982 and Zli1800 liquid crystal filled cells.

3. First order readings are ten times greater than the equivalent second order readings.
4. The Zli1982 filled cells exhibit two diffraction efficiency peaks whereas the Zli1800 cells only exhibit one peak. This effect is observable in both the first and second order results.

#### **6.4.1 Explanation of the D.E. versus voltage results**

An explanation is put forward for each of the features noted above in the order in which they were proposed.

##### **6.4.1.1 Magnitude variations between cell types**

The explanation for the difference in magnitude between the undyed at  $0^\circ$  D.E. results and the dyed at  $0^\circ$  results is based on the theoretical analysis of phase and amplitude gratings presented in chapter 4; essentially the undyed at  $0^\circ$  experimental arrangement represents a phase grating whereas, to all intents and purposes, the dyed at  $0^\circ$  represents an amplitude grating. The theoretical graphs in Figures 4.3 and 4.5 of the phase and amplitude non-Ronchi gratings show a maximum D.E. for the first order of 34% for the phase grating, but only a maximum D.E. of 8.6% for the amplitude grating. The theoretical analysis of gratings therefore predicts an approximate factor of four difference between the phase and amplitude diffraction efficiency readings. This applies not only to the first order but also to the second order readings. The D.E. maxima of the experimental results exhibited a much greater difference; approximately a factor of ten between the undyed at  $0^\circ$  and the dyed at  $0^\circ$ . This was true for both the first and second order results and was independent of the direction of rubbing.

The factor of ten difference can be partly attributed to the behaviour of the dyed cells; they were originally chosen to exhibit the properties of an amplitude grating by way of the guest-host electro-optic effect. On closer analysis of the operation of a guest-host cell it can be seen that the cell

exhibits the properties of *both* an amplitude grating (due to the pleochroic dye absorbing incident light—the dye ‘attaches’ itself electrostatically to the nematic director and moves in unison with it) and a phase grating. Although only 2% by weight of the dye DC5 was added to the nematic liquid crystal in the experimental cells, the ratio of phase to amplitude grating effects due to this amount of dye cannot be determined theoretically. However, the transmission characteristics for the Zli1800-filled cells were investigated. The results of the percentage transmission versus voltage formed a sigmoid-shaped curve: at zero volts, the transmission was approximately 2% and above the threshold, the transmission flattened out at 20%. The author suggests that this 20% transmission factor coupled with the phase grating behaviour contributed towards the low D.E. response of the dyed cells. Further experimental investigations of different dye concentrations in the same arrangements are required before the ratio of added dye to amplitude effect can be stated.

In the case of the undyed at 45° cell, the D.E. maxima are all approximately four times lower than the equivalent undyed at 0° results. The reason for the difference is due to the orientation of the cell at 45° to the input and output polarizers. Application of Malus’s Law twice (once at output of liquid crystal cell and again after the output polarizer) gives the following expression,

$$I_{out} = \frac{I_{in} \sin^2(2\theta)}{4} \quad [6.1]$$

where,

$I_{out}$  &  $I_{in}$  are the output and input light intensities respectively.

$\theta$  is the angle between the direction of input polarized light and the direction of rubbing on the cell.

Thus in the arrangement being considered,  $\theta = 45^\circ$ , which when substituted into equation [6.1] gives  $I_{out} = I_{in}/4$ .

Hence, the output light intensity from the undyed at 45° arrangement will be 4 times less than that of the undyed at 0° case (assuming that the undyed at 0° is not measured between crossed polarizers). Thus the experimental results follow the theoretical expectations and justify using the undyed at 45° experimental arrangement as a means of 'checking' the undyed at 0° results.

Overall, the first order readings are approximately 40% less than their theoretically derived counterparts, whereas the second order readings are approximately 60% less. The exact reasons for these anomalies are unknown and further research is required to identify the causes. The following list gives an indication as to what the author believes are the factors contributing to the deficits,

1. Non-ideal grating. As discussed in chapter 4, an increase in the  $\Delta/d$  ratio causes a marked decrease in the D.E.
2. Internal reflections of light within liquid crystal cell.
3. Refraction at boundaries (for example, glass/ITO interface and the ITO/ liquid crystal interface).
4. Inadequacy of the theoretical non-Ronchi grating equations. Sommerfeld's grating theory covers materials with a constant refractive index. The liquid crystal grating exhibits a voltage variable refractive index.

#### **6.4.1.2 Parallel readings > Antiparallel readings**

From Figures 6.5 to 6.12, it can be seen that the diffraction efficiency results for the parallel rubbed cells are greater (by as much as 25%) than their corresponding antiparallel rubbed results. Having proposed in the theoretical derivations that the maximum diffraction efficiency for the first order of a phase grating is 34%, it is not certain what factors (apart from voltage) affect the antiparallel rubbed cells as opposed to the parallel rubbed cells. Further research is required to determine the effects on diffraction efficiency of the different types of rubbing. However, what is more certain is that the

antiparallel rubbing causes the liquid crystal to turn-on at a lower voltage than the parallel rubbed cell. The phenomenon is summarized in Figure 6.4 for voltages below, at, and above the threshold field for a PDA liquid crystal. In the parallel rubbed cell the majority of the liquid crystal directors are aligned perpendicular to the direction of the applied electric field until the threshold voltage is reached. The liquid crystal directors in the antiparallel rubbed cell are aligned evenly across the thickness of the cell in a tilted configuration with respect to the direction of the electric field. Hence the liquid crystal directors in this configuration require a smaller amount of voltage to cause them to move than for the directors in the parallel rubbed cell.

#### **6.4.1.3 First order readings > second order readings**

Chapter 4 presented equations to determine the diffraction efficiencies of phase and amplitude gratings. The mathematical formula for a non-Ronchi phase grating was given in equation [4.8]. Assuming that the  $\Delta/d$  ratio is 0.25, then the diffraction efficiency for the first order is,

$$\text{D.E.}_{\text{first}} \approx \frac{3.41 \sin^2 \Theta}{\pi^2}$$

and for the second order,

$$\text{D.E.}_{\text{second}} \approx \frac{\sin^2 \Theta}{2\pi^2}$$

Hence the ratio of the first order to the second order is 1:6.8 (that is, the second order is approximately .15% of the first order). Adjusting the formula to cover the case of a non-Ronchi amplitude grating gives equation [4.9]. Again making the same assumptions, the ratio between the 1st and 2nd order terms was found to be identical. In the experimental cells there was a factor of ten difference between the first and second order results. Again, the exact causes of the difference are uncertain and cannot be attributed solely to 'experimental error'. The author feels that the reasons are similar to those put forward at the end of section 6.4.1.1 above.

#### **6.4.1.4 Number of Diffraction Efficiency peaks**

The results for the experimental cells filled with Zli1982 liquid crystal all exhibit two diffraction efficiency peaks followed by a 'tail' section which gradually increases levelling off at an almost constant value below that of the peaks. The results for the Zli1800 filled cells exhibit a single diffraction efficiency peak with a smaller tail section. The occurrence of two peaks in the Zli1982 case and a single peak in the Zli1800 case can be attributed to the phase retardance versus voltage properties of the liquid crystal. In chapter 4 it was observed that the diffraction efficiency characteristics of the orders of a phase grating exhibit peaks and troughs at  $2\pi$  radian intervals of phase retardance. Hence with reference to the phase retardance results shown in Figure 6.3, it is possible to explain the difference between the Zli1982 and the Zli1800 diffraction efficiency results in the remaining paragraphs.

Examining the Zli1982 results, the maximum experimental phase retardance occurs when no field is applied to the cell. For the parallel rubbed cell this value is 14.57 radians and for the antiparallel cell it is 14.01 radians. By adding successive multiples of  $\pi$  and substituting these values into Figure 6.3, the corresponding voltages at which the diffraction efficiency peaks and troughs occur are obtained. Thus for the parallel rubbed cell, peaks should occur at approximately 2.3 and 3.9 volts (peak-peak) and troughs at approximately 1.9 and 3.0 volts (pk-pk). Similarly for the antiparallel rubbed cell peaks should occur at 2.8 and 4.0 volts (pk-pk) and troughs at approximately 1.8 and 3.3 volts (pk-pk). Further additions of  $\pi$  beyond a phase retardance of  $4\pi$  are not possible since the maximum experimental phase retardance is 14.57 radians. Hence two peaks and two troughs are predicted for the Zli1982 liquid crystal.

The experimental diffraction efficiency results for Zli1982 (Figures 6.5 to 6.8)

match the voltage predictions for the first trough and the first peak and for the second trough. However the second peak occurs after its predicted location for the parallel cells. Also the results exhibit a second trough followed by an upwardly inclined slope which gradually levels off.

Repeating the procedure for Zli1800. The maximum experimental phase retardance for the parallel cell is 6.96 radians and for the antiparallel cell it is 6.67 radians. Adding multiples of  $\pi$  and substituting these into Figure 6.3 gives the voltages at which the peaks and troughs should occur. Thus for the parallel rubbed cell the peak should occur at 5.0 volts (pk-pk) and the trough at 3.0 volts (pk-pk). Similarly for the antiparallel rubbed cell the peak should occur at 5.0 volts (pk-pk) and the trough at 3.5 volts (pk-pk). No further additions of  $\pi$  are possible and therefore one trough and one peak are predicted.

The experimental diffraction efficiency results for Zli1800 match the voltage predictions for the peak and the trough for both parallel and antiparallel first orders. However, the peak in both second orders occurs after its predicted location, and all the results exhibit a second trough followed by a slight upward incline.

The results for the Zli1982 and Zli1800 liquid crystals appear to be 'enhanced' by some additional effect. By approximately 6.5 volts (pk-pk), the change in phase retardance per applied volt is small. This means that the voltage variable birefringence of the cell has also levelled off to an almost constant value. Thus the output from the cell is now dominated by the square wave grating effect over the now constant birefringence effect.

### **6.5 Use of the D.E. technique as a suitability criterion**

Having compared the experimental D.E. results to the the theoretical ones, attention can now be focussed on the mechanism of assessing the liquid crystal's suitability.

The assessment is subjective in that it refers only to the requirements placed on a liquid crystal for use in an electrically addressable spatial light modulator. For the sake of argument, it can be assumed that a typical EASLM will generate driving voltages of 0 to 5 volts onto the liquid crystal sandwich. As such, the liquid crystal most suited to the specification would have a turn-on voltage at 0 volts and the first diffraction efficiency peak at 5 volts. The choice of the first DE peak is deliberate since all liquid crystals used in a SLM should exhibit at least one peak. However it would be equally correct to consider additional peaks if exhibited. For example, the second peak of the parallel Zli1982 cell in Figure 6.7 exhibits a higher D.E. *vs.* voltage response than the first peak. Another alternative would be to operate the liquid crystal in reverse contrast mode by utilizing the negative sloped portion of one of the D.E. peaks. The use of any of these operating configurations is limited by the electro-optic behaviour of the liquid crystal. External factors such as temperature variation for example can enhance or inhibit the response of the liquid crystal—further research is required to determine how they affect the DE. Returning to the initial assumption, ideally the D.E. response of the liquid crystal between 0 and 5 volts should be linear, thereby enhancing the liquid crystal's ability to represent different grey levels<sup>†</sup>. It is the linearity of this portion of the D.E. versus voltage curve that determines the suitability of the liquid crystal.

Figures 6.13 and 6.14 show enlarged portions for the first order D.E. results of the parallel rubbed and the anti-parallel rubbed undyed cells for Zli1982 and Zli1800 experimental results respectively. Considering Figure 6.13 first, it can be seen that the D.E. remains zero until the liquid crystal turns on at approximately 1.5 volts. The liquid crystal then exhibits a linear response up until the first peak at 2.7 volts. Thus for a spatial light modulator having only a 1.2 volt driving range, the Zli1982 liquid crystal would be suitable. In Figure 6.14, the D.E. remains at zero until

---

<sup>†</sup> The number of representable grey levels is determined analytically. By operating the liquid crystal over the required voltage region, the intensity of the transmitted light is measured and compared to the intensity levels discernible in subsequent components of the system



approximately 3.2 volts. From this point until the first peak at 5.0 volts the D.E. curve is linear and could therefore be utilized in an EASLM having a 1.8 volt driving range.

In summary, it can be stated that the diffraction efficiency technique could be used to identify the suitability of a liquid crystal for use in a spatial light modulator. As is to be expected when designing a new measurement technique, a number of questions are produced which cannot be easily dealt with. The author feels that he has gone some way in answering the pertinent questions, but due to the short duration of the research has not been able to investigate some of the observations in greater detail. Suggestions for further research to address these questions are put forward in the concluding chapter, chapter 8.

**Figure 6.1** Experimental arrangements showing orientation of incident polarized light & liquid crystal cell.

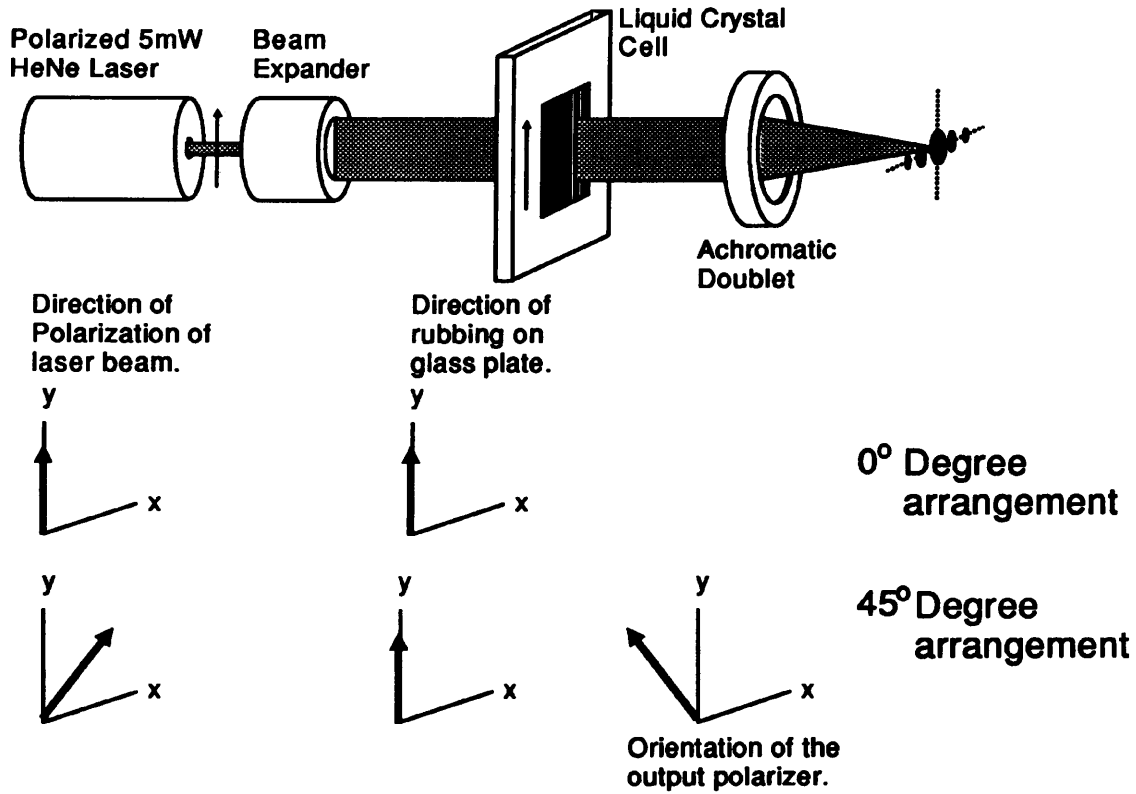
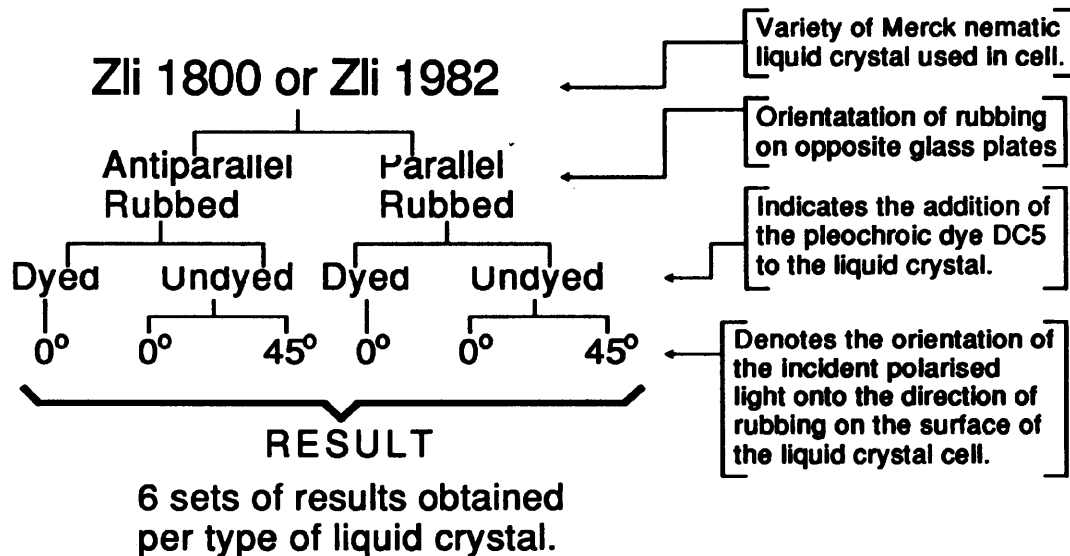


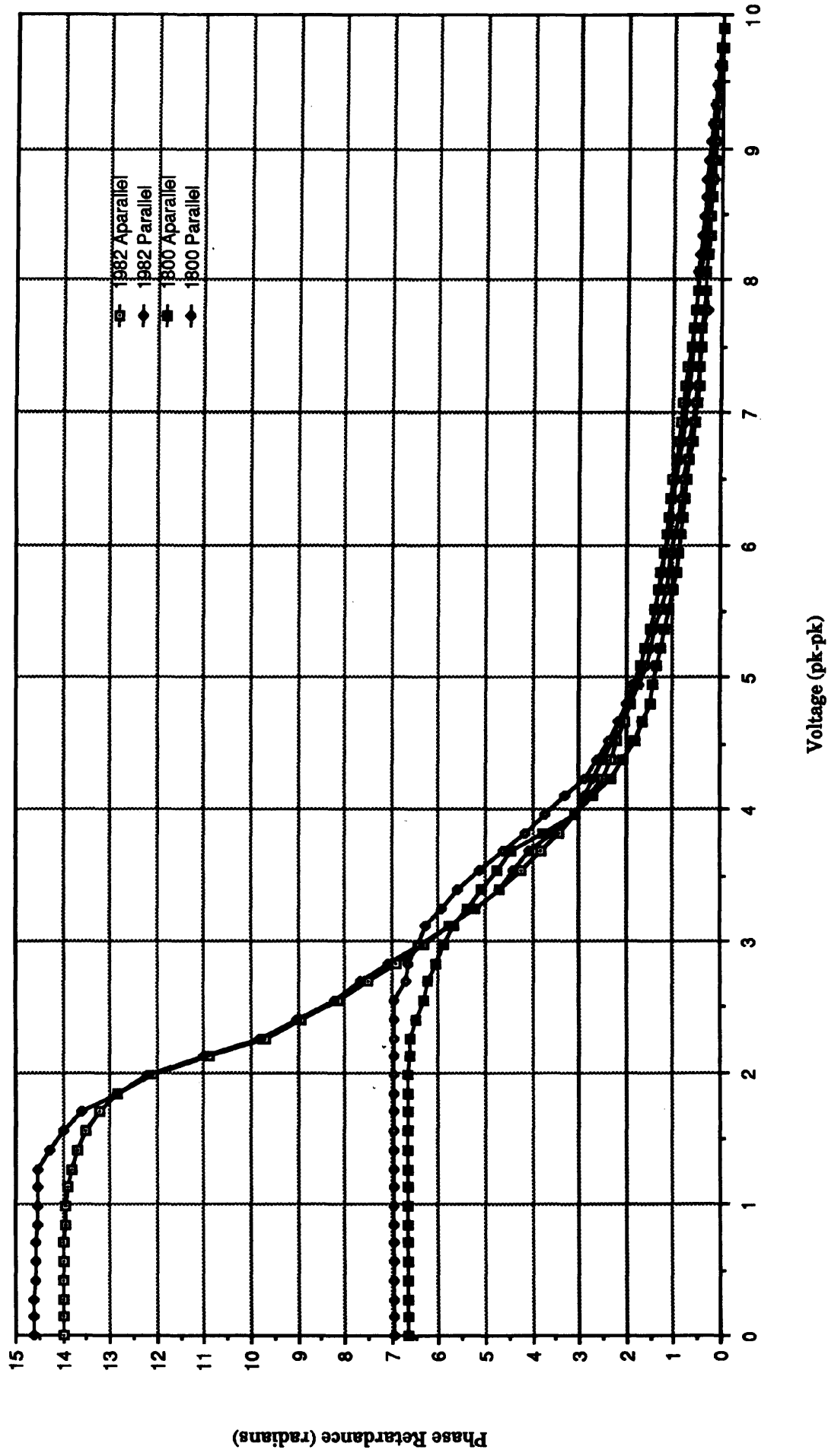
**Figure 6.2** Overview of the different types of experimental cell used to obtain the results for diffraction efficiency.



Graph of Phase retardance vs. voltage for

Zli1982 and Zli1800 type liquid crystals

**Figure 6.3**



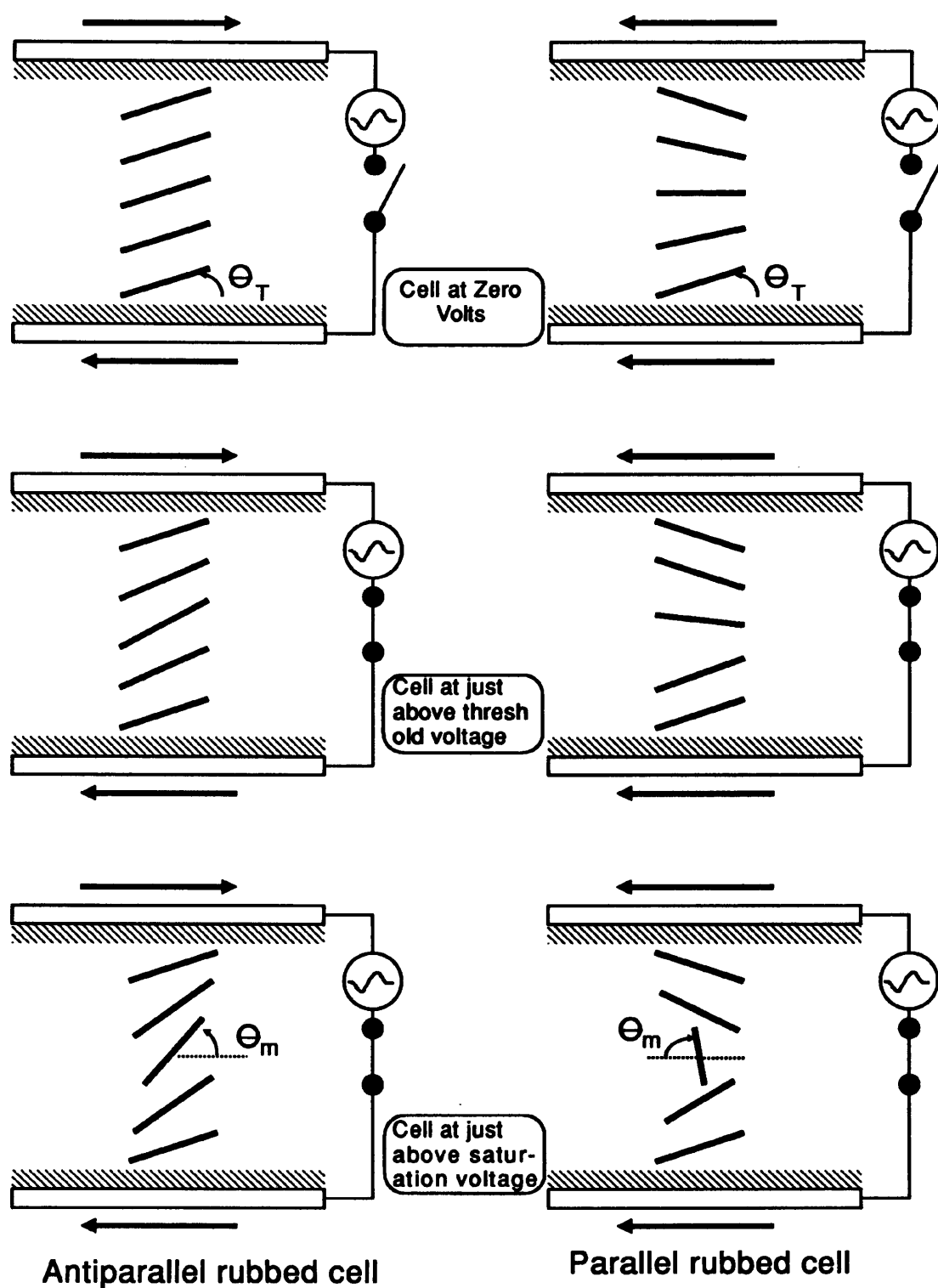


**Figure 6.4** Three stages of electrically induced director movement in Parallel and Antiparallel rubbed cells.

**Figure 6.5**

Graph of DE vs Voltage for First Order  
Antiparallel Rubbed Cell - Zli1982 liquid crystal

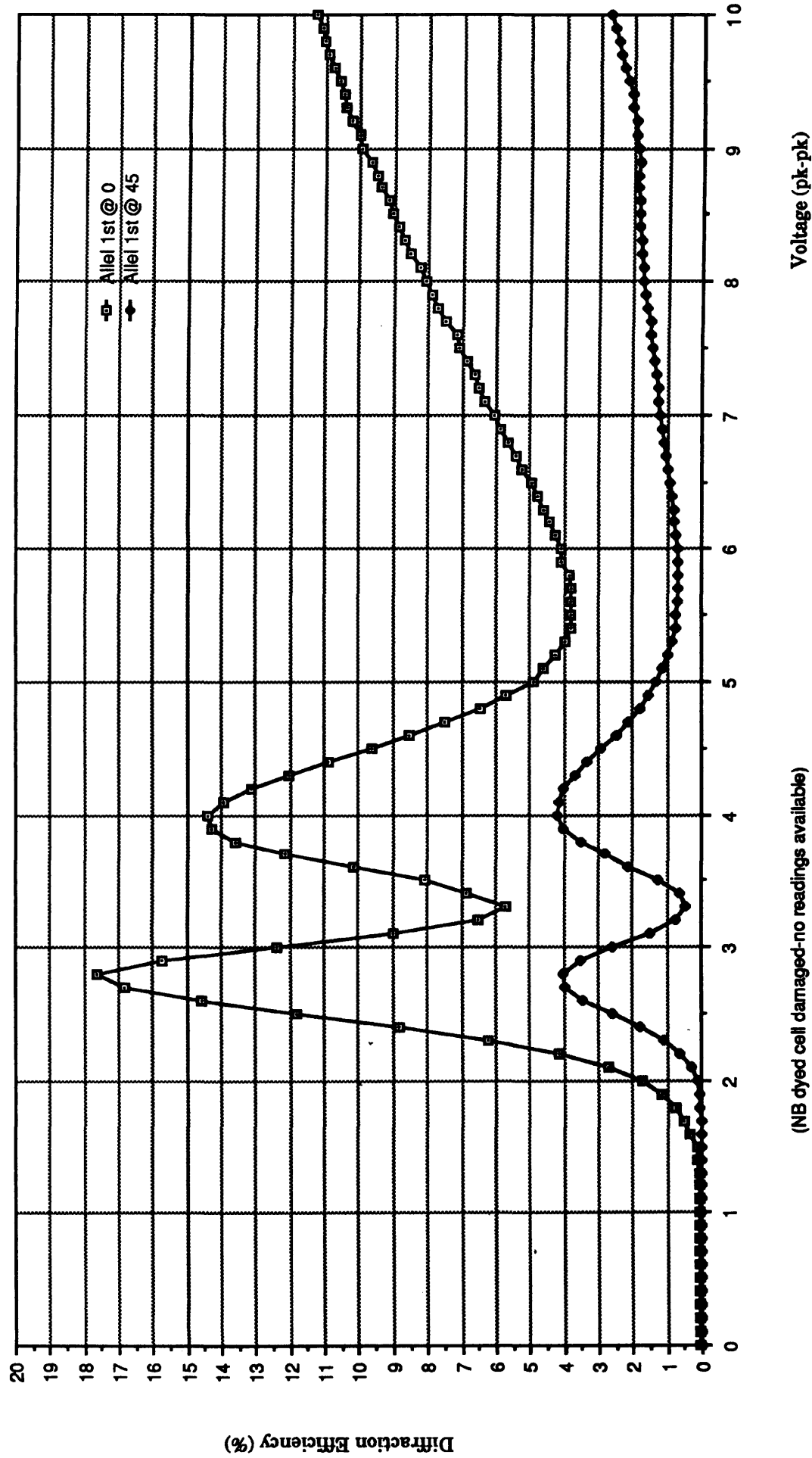


**Figure 6.6**

Graph of DE vs Voltage for Second Order  
Antiparallel Rubbed Cell - Zli1982 liquid crystal

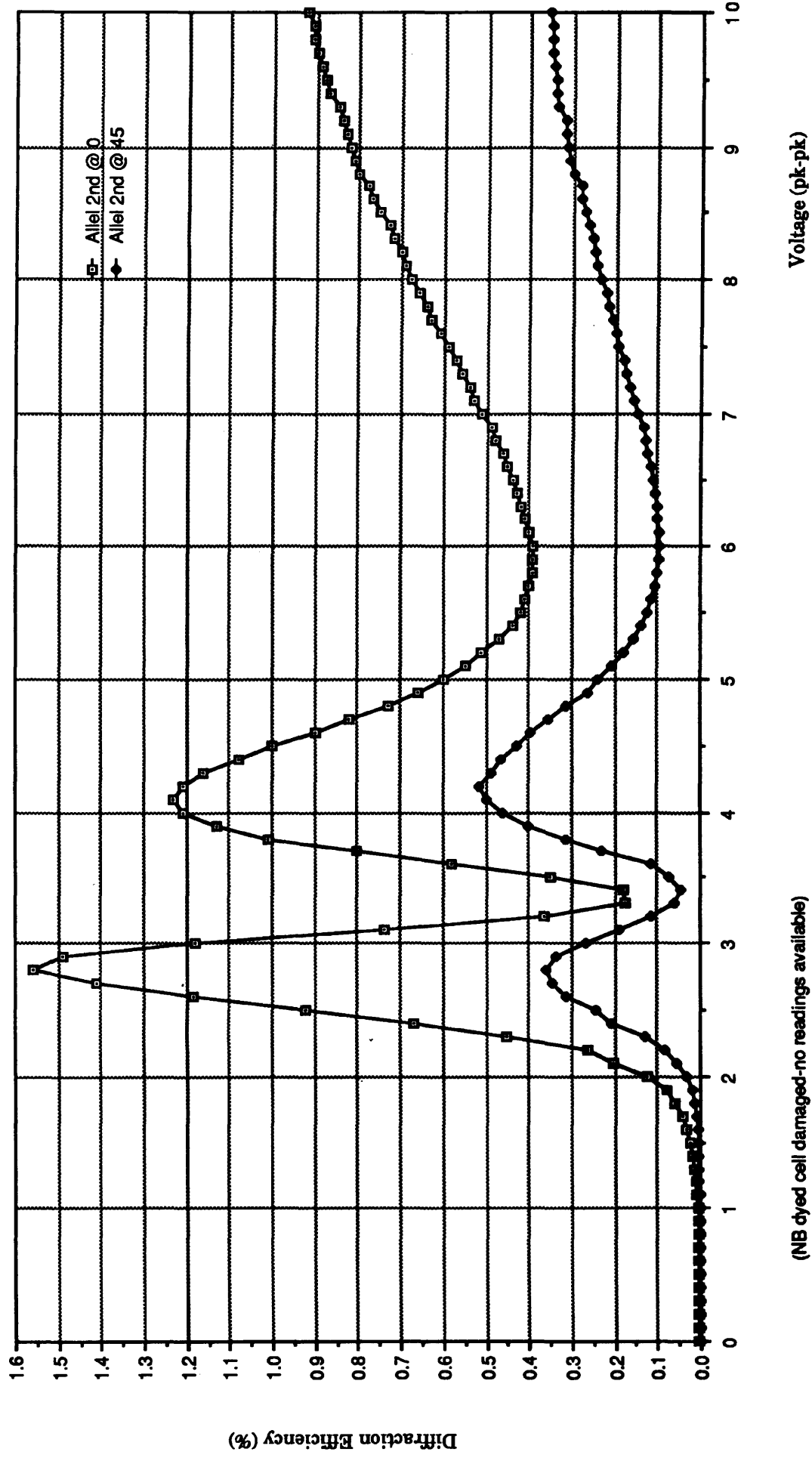


**Figure 6.7**

Graph of DE vs Voltage for First Order  
Parallel Rubbed Cell - Zli1982 liquid crystal

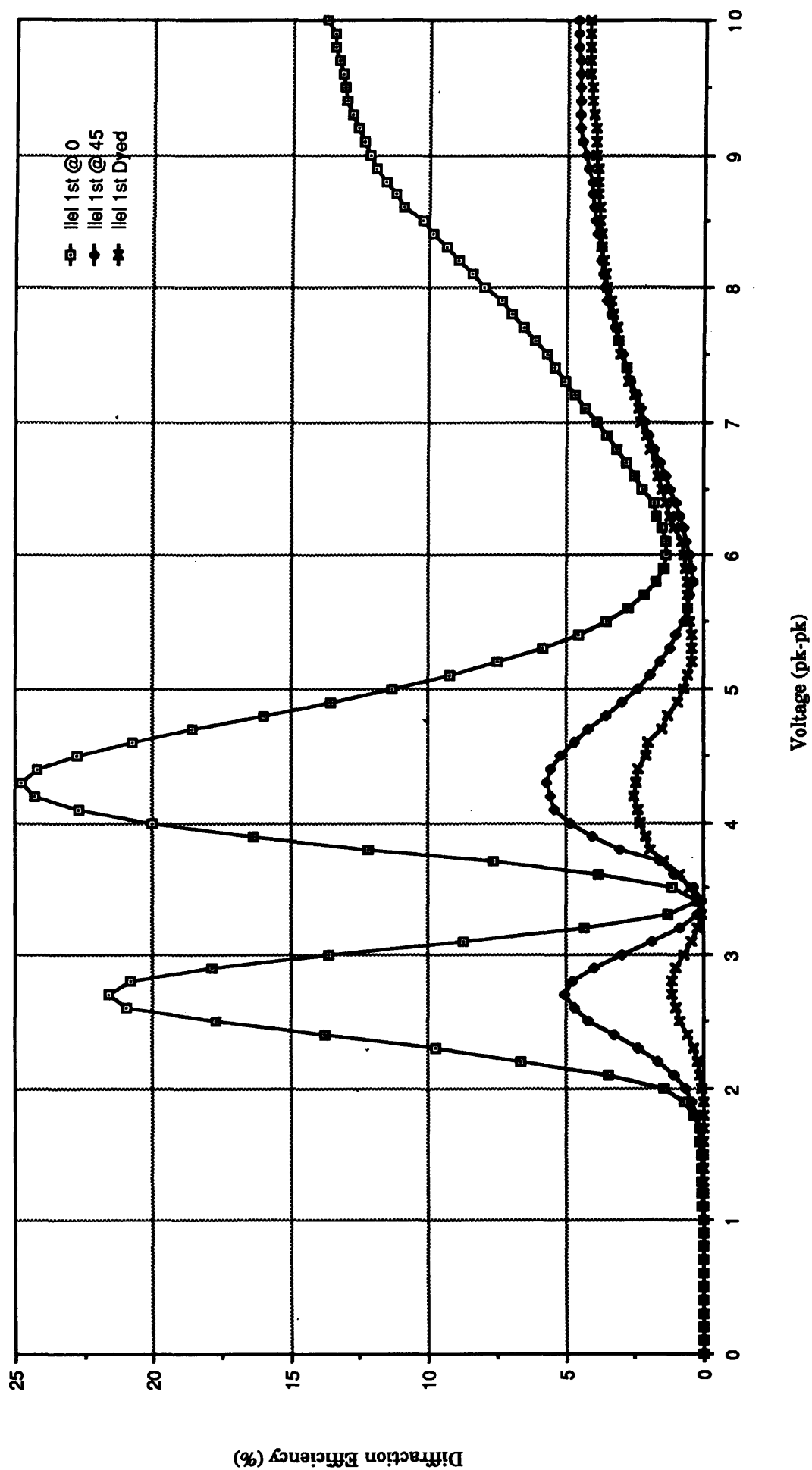


**Figure 6.8**

Graph of DE vs Voltage for Second Order  
Antiparallel Rubbed Cell - Zli1982 liquid crystal

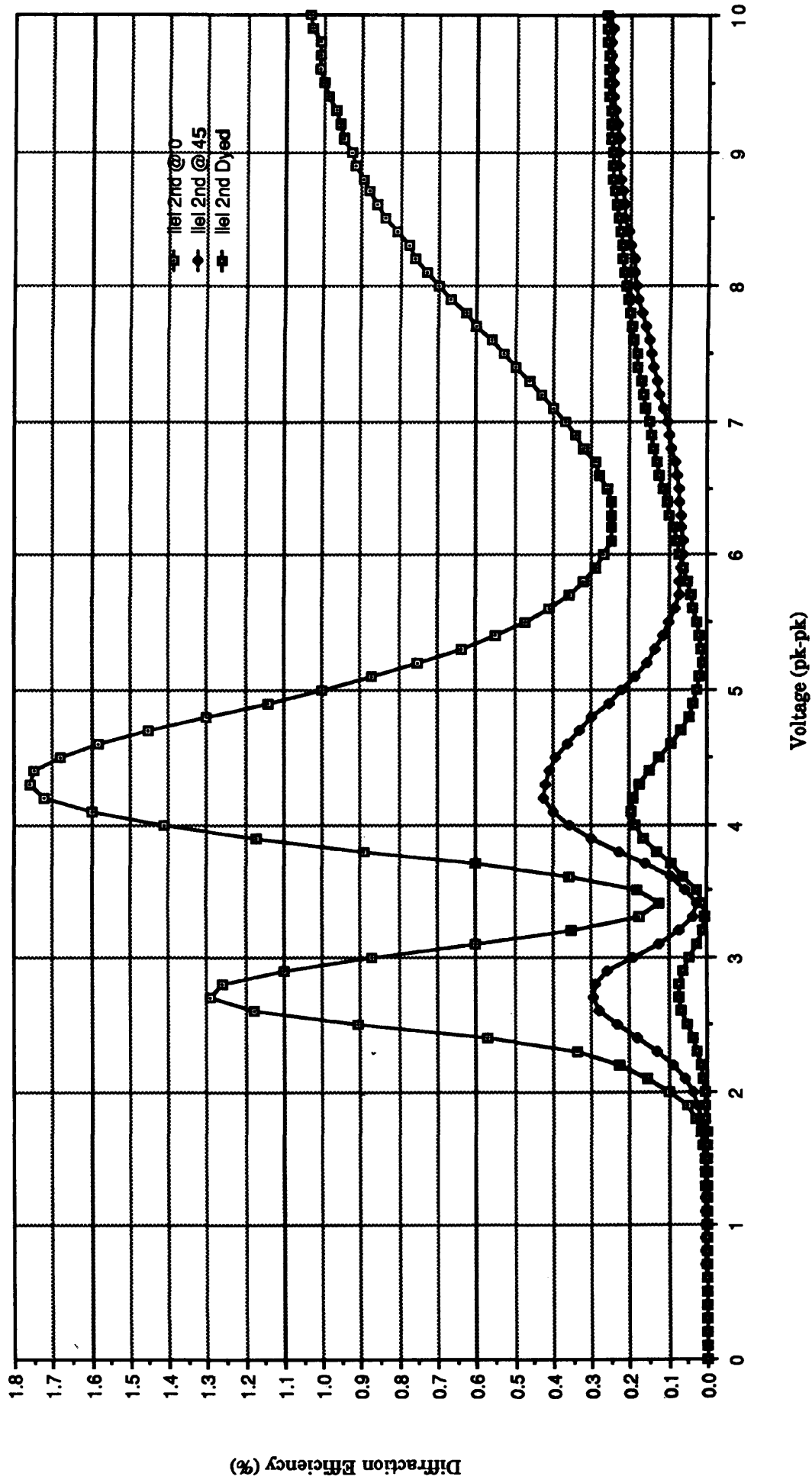




**Figure 6.2**

Graph of DE vs Voltage for First Order  
Parallel Rubbed Cell - Zli1800 liquid crystal

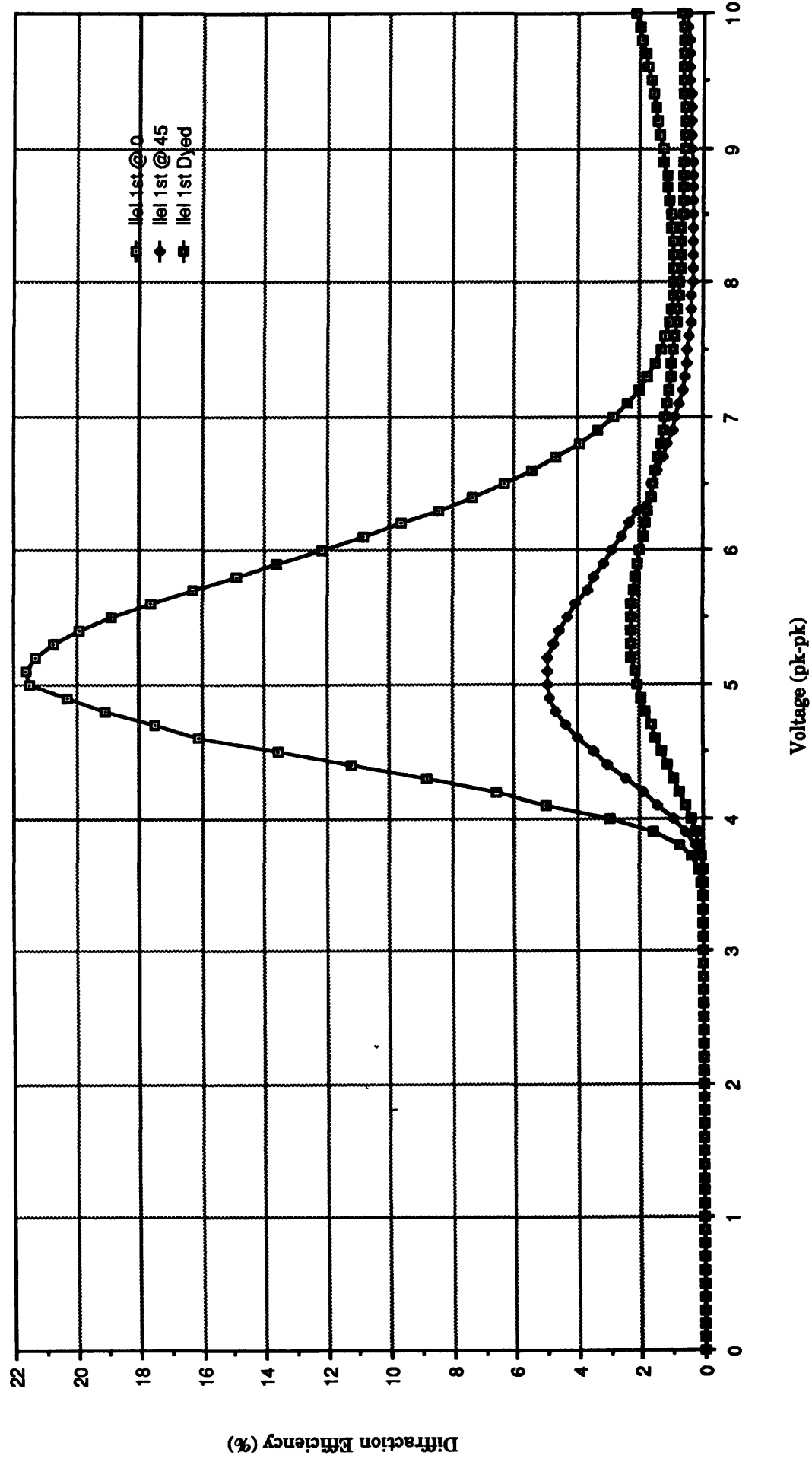


**Figure 6.10**

Graph of DE vs Voltage for Second Order

Parallel Rubbed Cell - Zli1800 liquid crystal

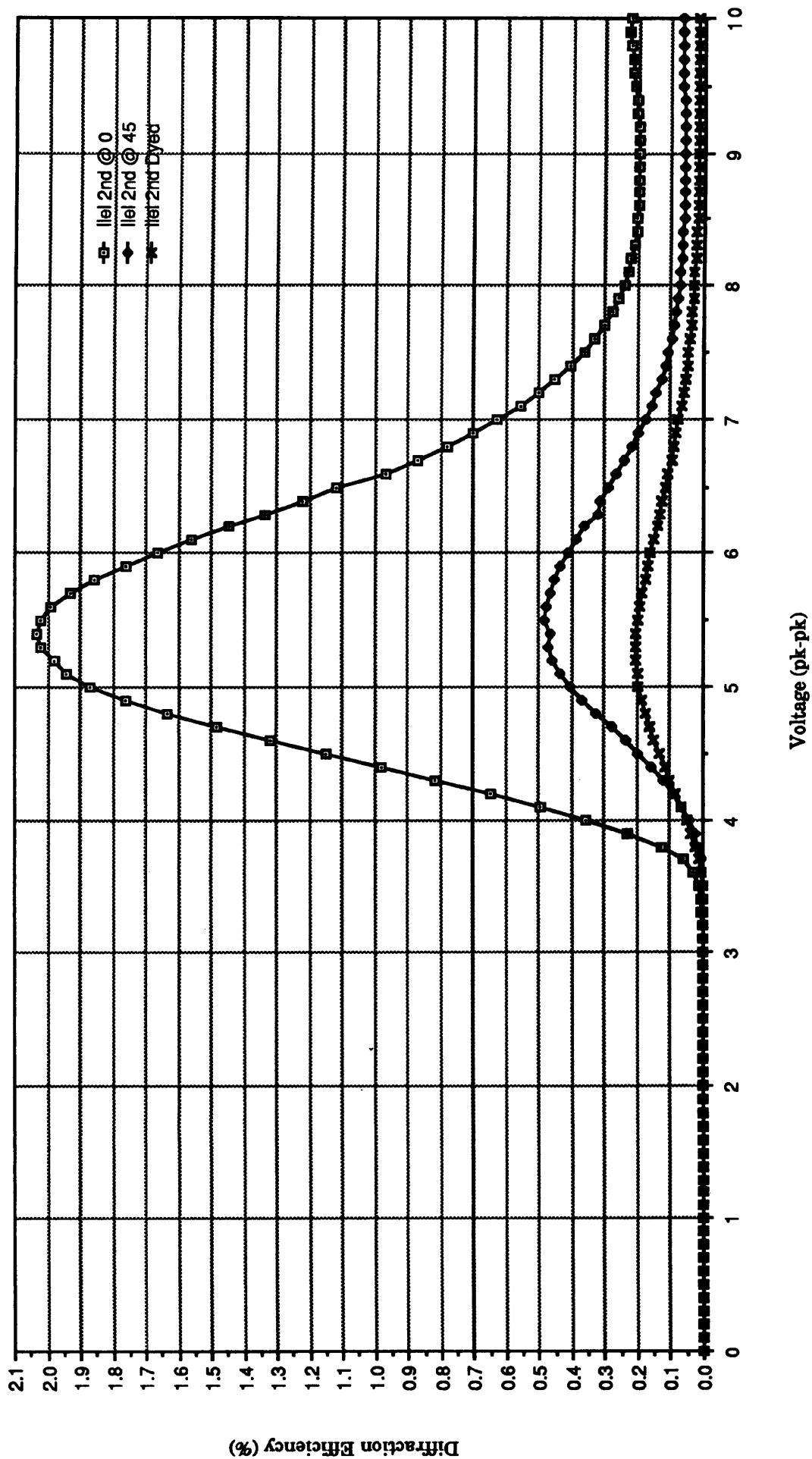


**Figure 6.11**

Graph of DE vs Voltage for First Order  
Antiparallel Rubbed Cell - Zli1800 liquid crystal

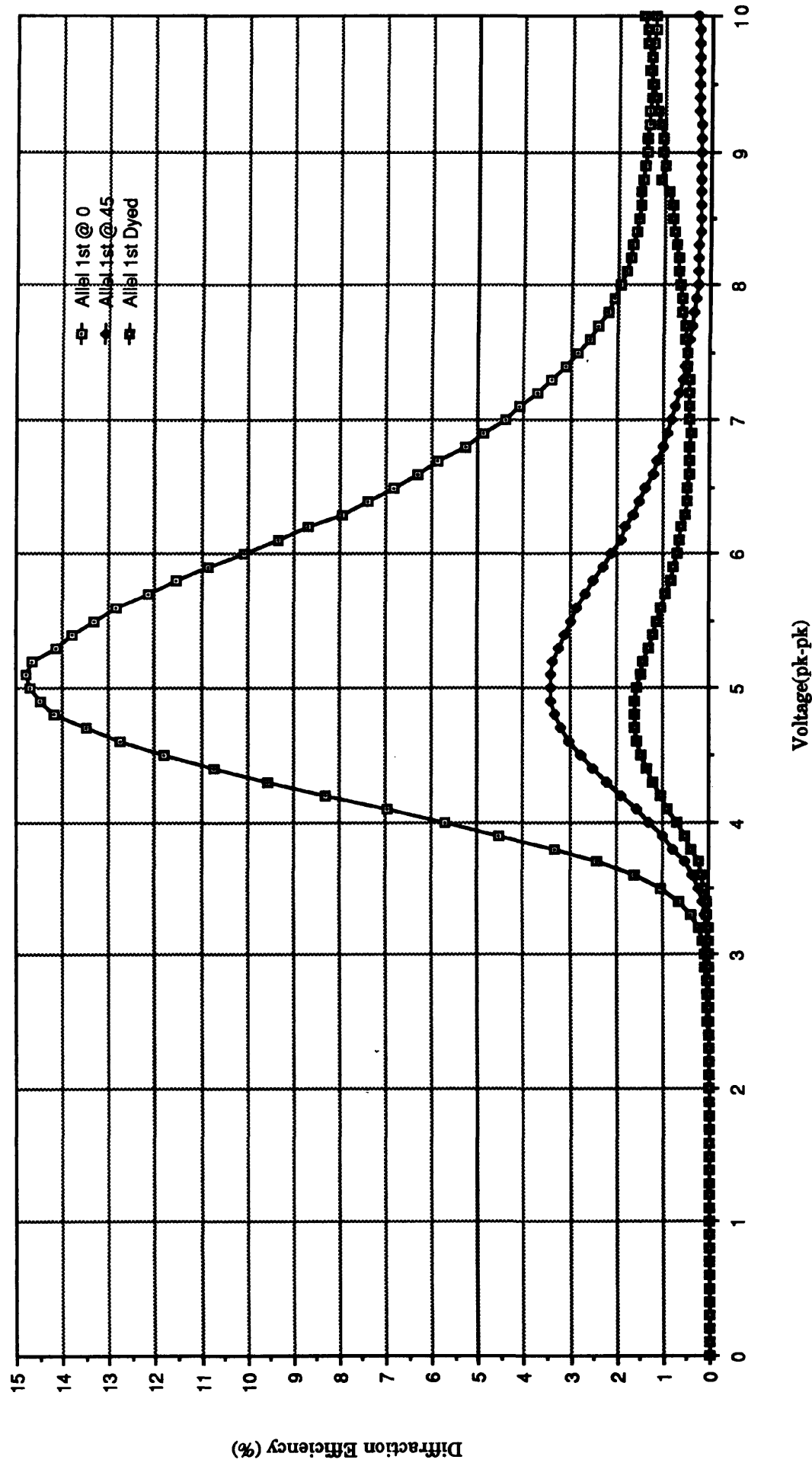


**Figure 6.12**

Graph of DE vs Voltage for Second Order  
Antiparallel Rubbed Cell - Zli1800 liquid crystal

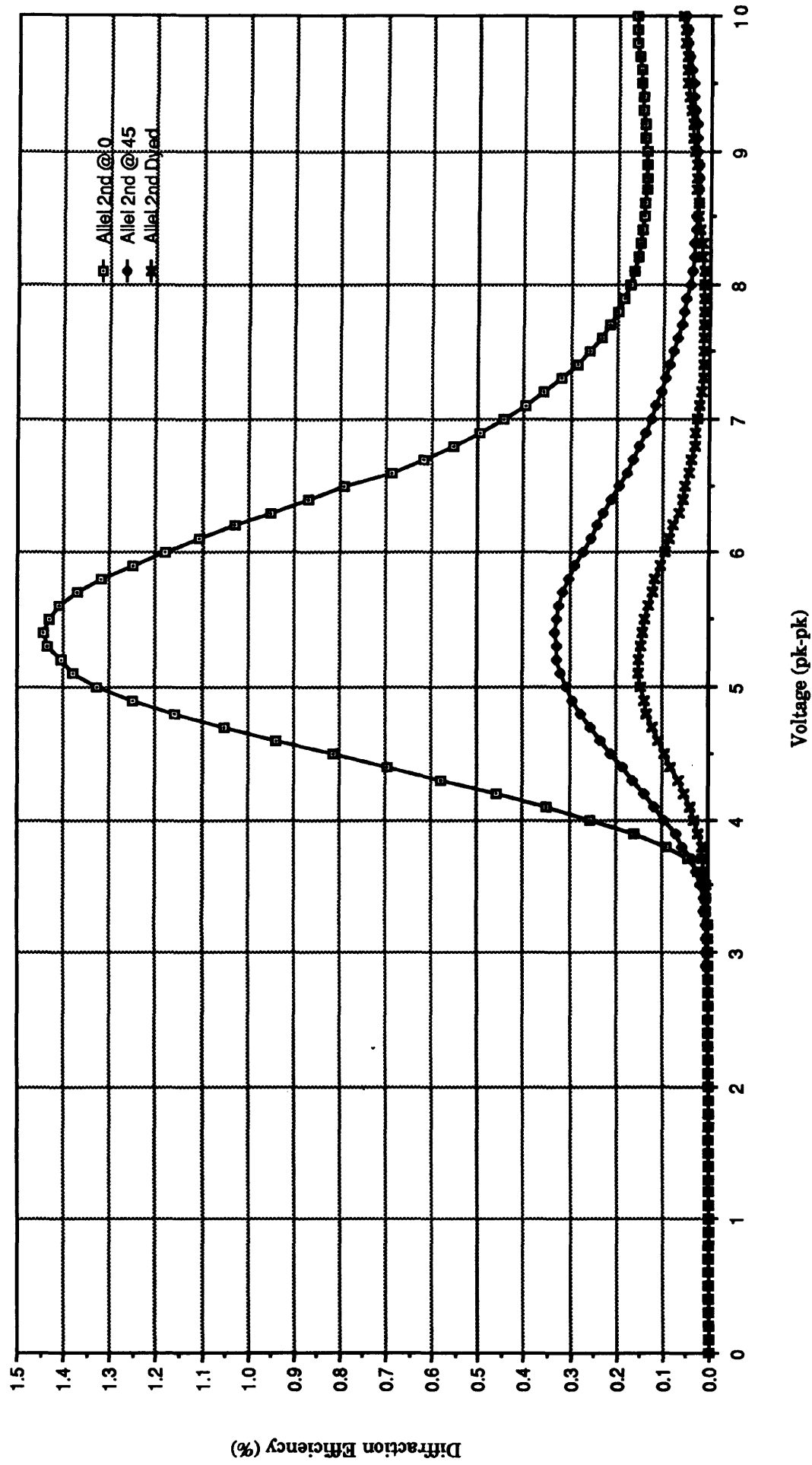


**Figure 6.13**

Enlarged graph of DE vs Voltage for First Order

Undyed @ 0° cells - Zli1982 liquid crystal

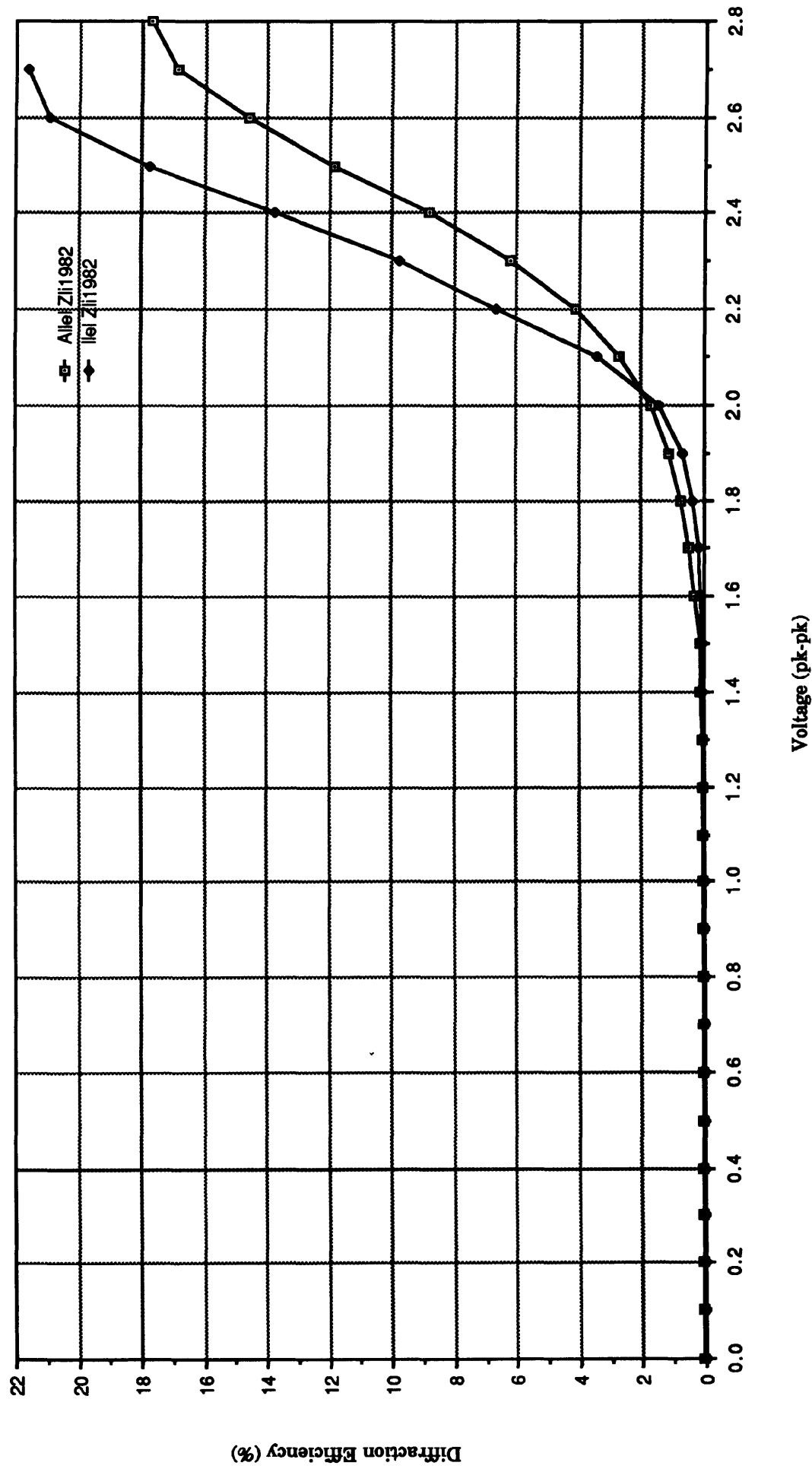
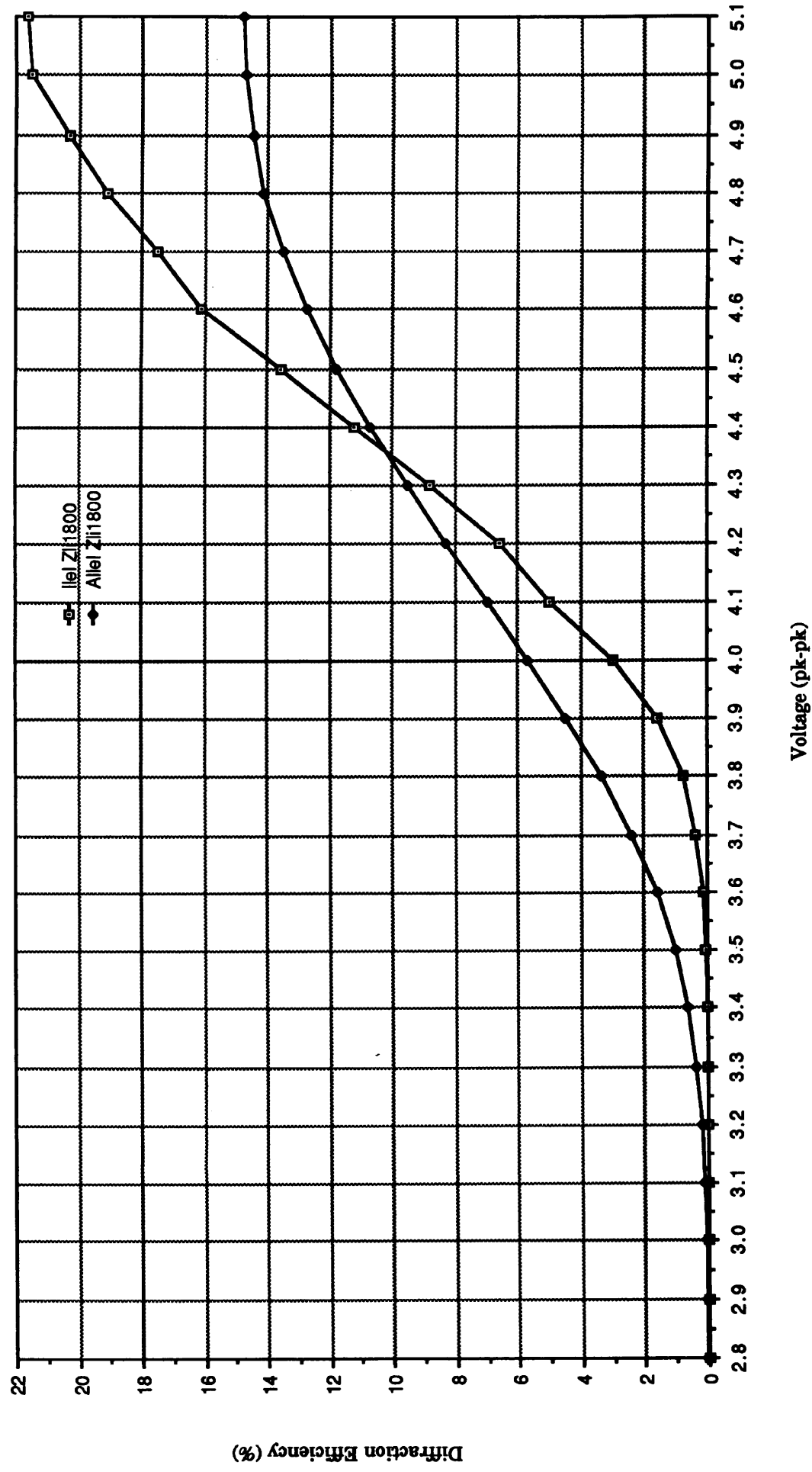


**Figure 6.14**

Enlarged graph of DE vs Voltage for First Order  
Undyed @ 0° cells - Zli1800 liquid crystal



# Total Technology Aspects of the Research.

## 7.1 Chapter Summary

As previously mentioned, the work for this Ph.D. was carried out under the auspices of the Total Technology Award Scheme. As a condition of this award the author is required to include a chapter outlining his involvement with the appointed sponsoring company. In this instance the sponsoring company was Standard Telecommunication Laboratories (S.T.L.) Ltd., based in Harlow, Essex. This establishment is the research-wing of its parent company S.T.C., the majority of its research being centred around communications. The author's liaison was with the Displays Division in S.T.L. whose particular research interest was liquid crystals. Consequently, extensive modern fabrication and testing facilities for the construction and evaluation of experimental displays were on site.

The research initiated at S.T.L. and continued at U.M.I.S.T. has been covered in the preceding chapters. Additional investigations carried out at S.T.L. as part of the Joint Opto-Electronic Research Scheme (J.O.E.R.S.) encompassed the design of a detector for use in the output section of an optical correlator (see Figure 1.1). The correlation peak detector system described in this chapter allows a correlation peak to be detected in real-time and the position of the object causing the highest peak to be optimized.

## 7.2 Introduction

The collaboration between the author and the Displays Division at S.T.L. took the following form. At present the Displays Division is actively pursuing the development

of an electrically addressed spatial light modulator (EASLM). In order to further the EASLM project, information was required about the 'suitability' of certain liquid crystals being driven by such a device—this research was performed by the author and forms the main body of the thesis.

Another aspect of this collaboration arose because both the Instrumentation Department at U.M.I.S.T. and the Displays Division were involved in the Department of Trade and Industry's J.O.E.R.S. Programmable All Optical Devices and their Applications (P.A.O.D.A.) programme. The intention of this particular programme was to amalgamate the skills and resources of the individual companies to collaborate on the design and implementation of an optical demonstrator system. The aim of the demonstrator was to show real-time optical correlation of simple objects using optical components and techniques developed by each of the collaborating companies. A detailed account of all of the collaborators contributions to the finalized demonstrator is beyond the scope of this chapter. However, a description of the author's personal contribution is given.

### **7.3 Operational Aims of the Demonstrator**

An outline of the demonstrator architecture is given in Figure 7.1. Essentially the architecture can be considered as three components. First, the input in the form of two SLMs, one for the scene information and the other to carry the reference data. Second, there is the optical correlator itself which correlates the information from the SLMs in real-time. Third, the output, which to be of any value to the operation of the former elements has to provide a feedback control path to the reference data SLM.

The most important aim laid-down by the collaborating companies is the speed of operation of the demonstrator. It was required to operate in real-time and do so with some 'corrective intelligence' so that adverse conditions could not degrade the performance. The designs of the SLMs and the correlator permitted real-time



operation so the responsibility to maintain the performance lay with the output stage.

The aim of 'intelligence' was achieved in part by attaching a motorized dove-prism to the input window of the reference data SLM. Rotating the prism caused a rotation in the reference picture imaged onto the SLM. By correlating successively rotated images with the same scene information, a sequence of varying correlation peaks could be obtained and by picking out the highest peak and moving the dove-prism back to this position an intelligent optimization of the best correlation position was facilitated.

#### **7.4 Output Detection System**

The agreed method of detecting the correlation peak was to use a charge coupled device (CCD) camera.<sup>100</sup> The camera was miniaturized to allow easy mounting to the correlator arrangement. The power supply and drive electronics were fed to the camera via screened cable from a custom-built unit. The use of a CCD device as opposed to a vidicon camera provided two advantages. First, it could be used in a space restrictive system (which this was). Second, the CCD integrated circuit did not allow 'image lag' when the correlation peak moved, to which the alternative vidicon devices are particularly susceptible.

The author's rôle in the development of the system was to design and construct a microcomputer-based device that would control the movement of the dove prism from the corresponding output of the CCD camera. Because of the limited funding and the time requirement of the project, a simple and inexpensive approach was sought. Figure 7.2 shows a typical sequence of events that the microcontroller would have to respond to in real-time.

The most time-consuming part of the cycle was the first stage; obtaining data from the camera and detecting the peak. The United Kingdom utilizes a 625-line television standard. This implies that each television frame of information contains 625 lines

of pixel data and is refreshed every  $\frac{1}{50}$ <sup>th</sup> of a second. Previous researchers<sup>101</sup> used a method of obtaining video frames ('frame grabbing') by 'picking-out' different lines from a number of consecutive frames. This approach was too slow for the J.O.E.R.S. demonstrator due to the need for the picture to remain unchanged over a number of frames, so the following technique was employed. A fast (30MHz) analogue to digital convertor (ADC) was attached to the output of the CCD camera video line. When the output of the ADC reached a preset level, that is the correlation peak, its associated controlling electronics would interrupt the microcomputer. The software routine operating in the microcomputer attended to the interrupt by accepting the data from the ADC. After waiting for a new frame signal to reset the electronic counters, the cycle was repeated (see Figure 7.3). Thus every frame produced by the camera was analysed for a correlation peak. The only disadvantage of this approach was that it would detect a single peak per frame; any peaks occurring after the first would be ignored. However, as 'simple' objects were being correlated, it was envisaged that only one correlation peak would be produced and therefore the interrupt-based ADC technique would be acceptable.

### **7.5 Operation of the Peak Detector Circuit**

A schematic diagram of the circuitry used to detect the location of the correlation peak is shown in Figure 7.4. A master clock oscillating at 8 MHz was used to drive the ADC. In this way 512 pixels could be digitized per line of video information. This 'master' or pixel clock also drove a 12-bit binary counter which counted the number of converted pixels per line. The same counter was reset at the end of each line by another synchronized 12-bit counter whose timing was derived from the divided-down pixel clock (15.625 KHz). By using the second counter, the number of lines converted could be found. Thus when a correlation peak was detected at the output of one of the ADC lines, a flip-flop was signalled which in-turn stopped the pixel and line counters and informed the host BBC microcomputer via the interrupt request signal (NIRQ) on the BBC's 1 MHz bus. The software controlled interrupt service

routine (ISR) in the BBC acknowledged the interrupt by latching the 5 bytes of data output from the ADC and the counters onto the 1 MHz data bus and thence into the computer's memory. During testing it was found that the ISR could respond to an interrupt in time to analyze the following frame of data if the correlation peak occurred in the upper two-thirds of the imaged picture. This was facilitated by moving the CCD camera to the correct position.

## 7.6 Controlling Software

Besides servicing the interrupt request from the peak-detector hardware, the software was required to perform several other functions. It was felt that a computer display of the correlation peak height and location should be displayed, as well as its numerical representation. Also, the rotation of the dove-prism was to be effected under software control using output lines from the 1 MHz bus to a stepper motor controller. The following pseudo Pascal program is a high level description of the overall requirements of the controlling software.

```
PROGRAM Pseudo PASCAL correlation peak detector;  
BEGIN { main }  
  initialise_interrupt_service_routine;  
  initialise_screen;  
  initialise_software_counters;  
  REPEAT  
    REPEAT  
      get_data_into_computer; { from ISR. Data = peak+X & Y }  
      update_display_on_monitor;  
      rotate_stepper_motor_one_division;  
      increment_step_counter;  
    UNTIL step_counter=required_number_of_steps  
    calculate_highest_peak;  
    rotate_motor_1_step_before_high_point;  
    do_fine_stepping_interval;  
  UNTIL forever  
END. { main }
```

Consideration of each of the above procedures led to the development of a 'hand-coded' machine code program to perform all the necessary operations. Each procedure was tested individually for operating faults and then added into the main program. A documented listing of the controlling software produced is given in the Appendix.

The assembled correlation peak detector system was delivered to G.E.C. Hirst Research Centre at the end of April 1986 for the final stage of the demonstrator build-up. The testing under operating conditions was supervised by Paul Waite who had been supplied with the author's documented software source listings and hardware wiring diagrams. At the time of writing, the system was reported to be working satisfactorily.

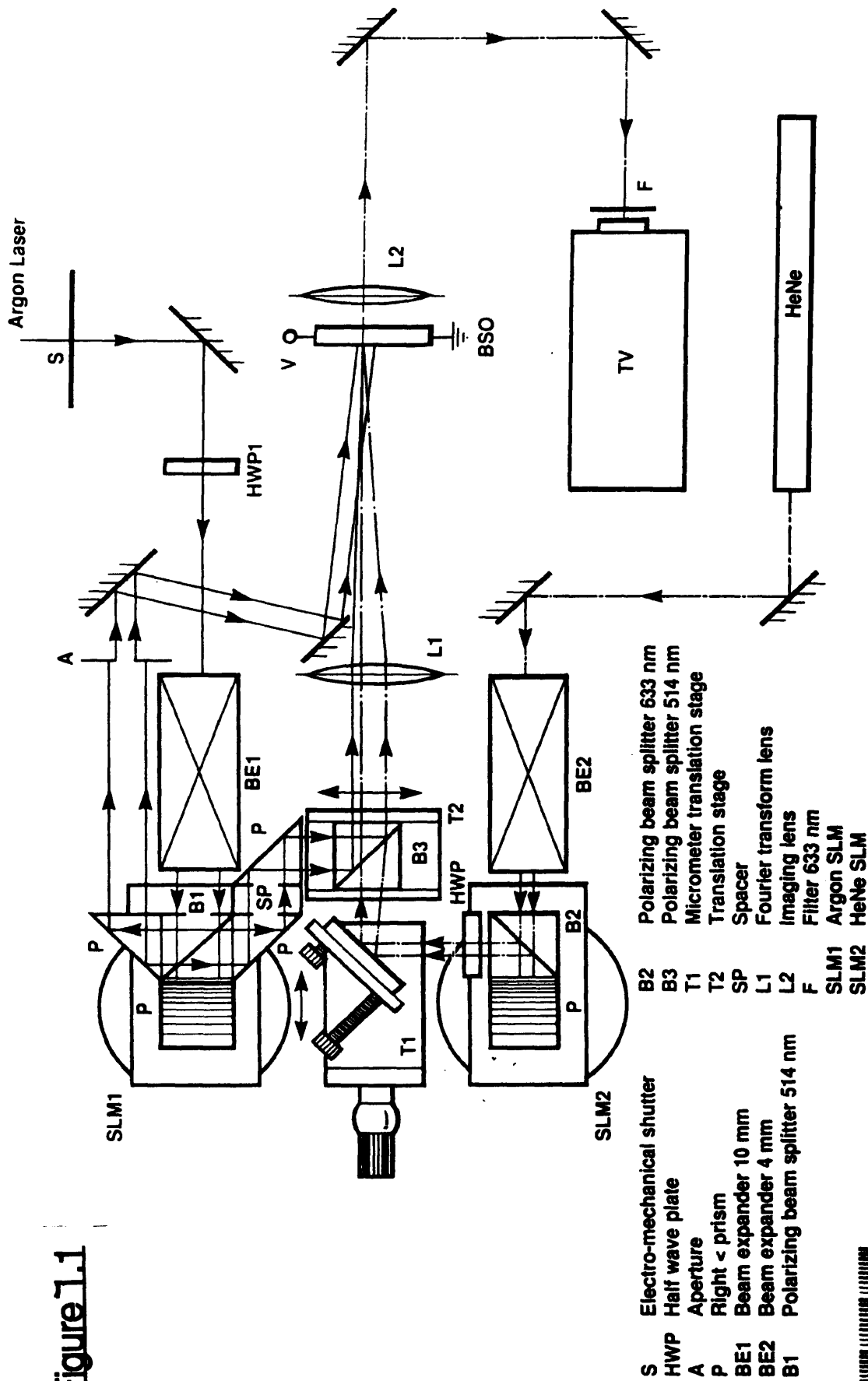
#### **7.7 Suggestions for improvements to the Peak Detector system**

After designing the correlation peak detector, the author had ideas for a more advanced 'Mark 2' system. The envisaged architecture would be more computationally intense relying on more powerful parallel computer systems and utilizing new camera designs incorporating built-in digitizer circuitry. This would 'link-up' with the research carried out by Per Lindstrøm at D.I.A.S., U.M.I.S.T. Lindstrøm<sup>102</sup> was concerned with the development of the feedback loop from the output detection system to the spatial light modulator. To this end he used a powerful single-user Motorola VME 10 minicomputer system using a multi-tasking operating system (VersaDOS) and the high level programming language Pascal to develop a series of algorithms modelling the effects of signal deterioration on the inputs to the SLMs and the output detection system. By utilizing such a configuration with additional plug-in VME-bus boards to perform video signal processing in real-time such as the Fairchild VIP100 vision interface processor,<sup>103</sup> a faster and more flexible system could be built for stand-alone or programmable applications. The ideas were discussed with members of the J.O.E.R.S. committee and a similar system is being assembled for use in the second J.O.E.R.S. demonstrator.

## **7.8 Conclusion for the Total Technology Aspects**

The knowledge and experience gained from the Total Technology involvement during the period of studentship was beneficial in providing some valuable insights. Firstly, into the short- and long-term operation of a well-established liquid crystal research establishment. Secondly, it provided the author with a reliable and accurate knowledge-base in the field of liquid crystals. Finally, the period spent developing the peak detector for the J.O.E.R.S. scheme gave the author the unique opportunity to contribute to the first collaborative demonstrator system.

Figure 1.1



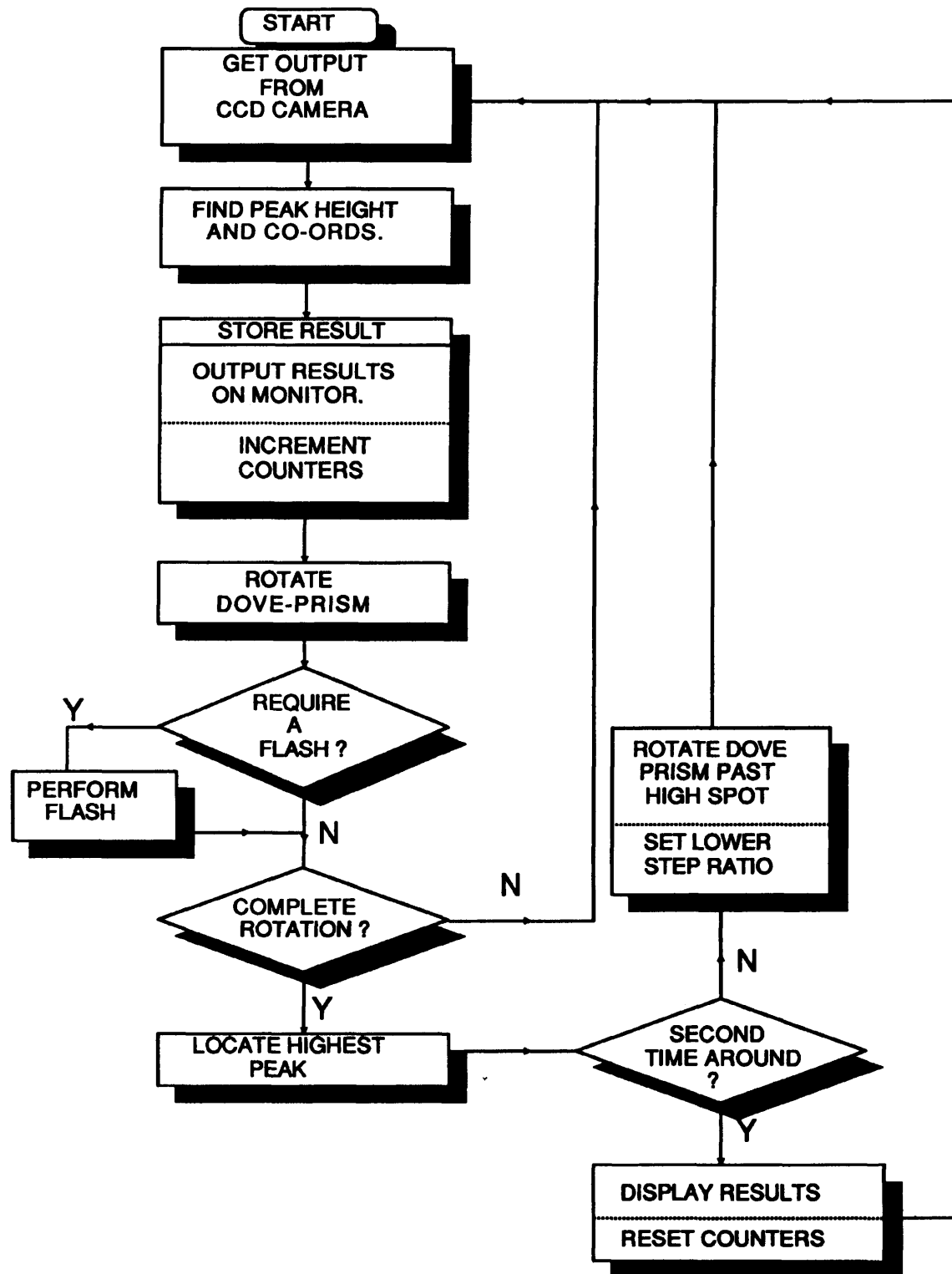


**Figure 7.2**

Flow diagram of the sequence of events controlled by the output stage.

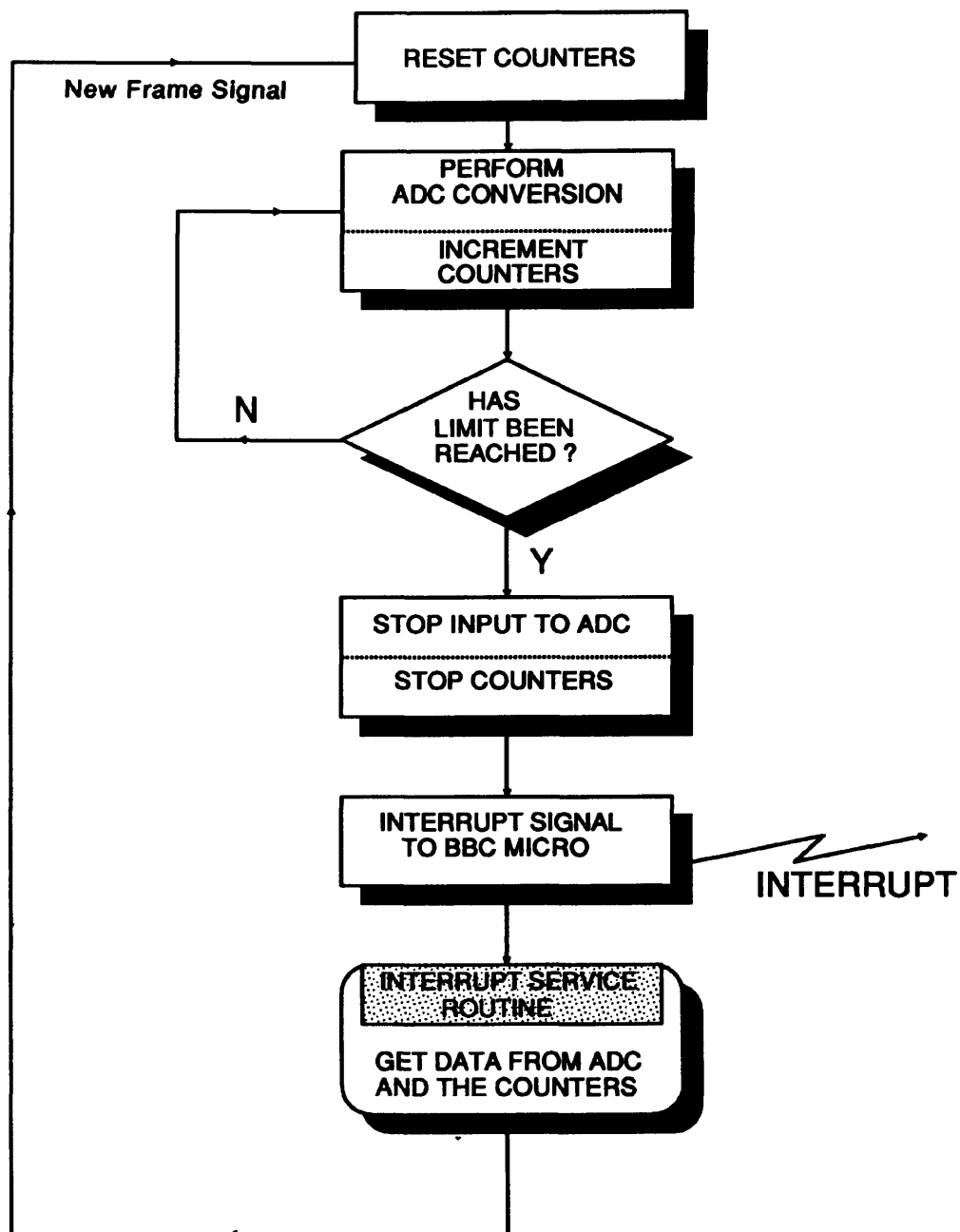


**Figure 7.3**

Flow diagram of the functions performed by the peak detector hardware.



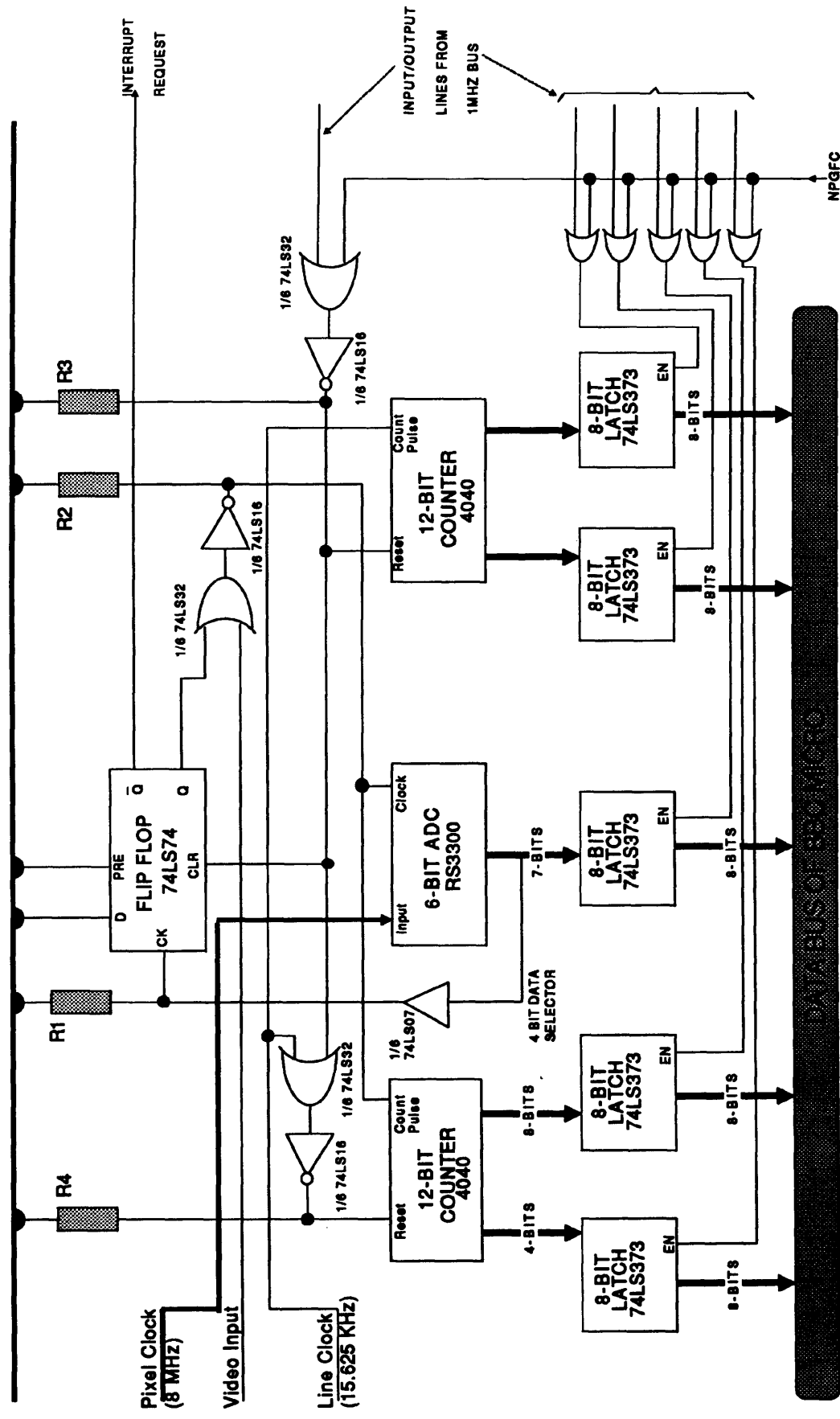


**Figure 7.4** Circuit Diagram of the correlation peak detector hardware used in the J.O.E.R.S. Demonstrator Mk. 1.

# Conclusion & Suggestions for Further Work

## 8.1 Conclusion

In conclusion to this thesis, it can be stated that the ten objectives laid out in section 1.5 were all met and the main aim of developing a new liquid crystal measurement technique was achieved. The conclusion for each objective is discussed below.

- 1) A description of the three main categories of liquid crystal was given. The nematic family was chosen as the basis upon which to evaluate the measurement technique since their characteristics were well known.
- 2) Mechanisms of aligning liquid crystal directors on different organic and inorganic surfaces were compared. Uniform alignment of the liquid crystal directors was necessary to promote a reproducible response. The rubbed polymer coating method was selected for use in the experimental cells as it was a simple but effective technique.
- 3) The tilt angle of the directors was measured with respect to the bounding glass plate using the conoscopic technique developed by Crossland *et al* within S.T.L. Ltd. and was found to be  $2^\circ$ .
- 4) Several types of electro-optic effect reproducible in nematic liquid crystals were described. The experimental cells exhibited two of these electro-optic effects, namely the guest-host effect and the controlled birefringence effect.
- 5) Mathematical descriptions of nematic liquid crystal cells were derived for directors aligned in tilted and untilted configurations. The results confirmed the validity of the mathematical model predicting the voltage induced behaviour of the liquid crystal directors in the experimental cells.

- 6) Sommerfeld's equations describing Ronchi diffraction gratings were extended to encompass non-Ronchi gratings. The experimental cells exhibited a non-Ronchi profile, and by substituting their dimensions into the extended formulæ, contributions by the zero, first and second diffracted orders were predicted.
- 7) Incorporating all of the previous suggestions, eight experimental cells were fabricated for two different types of nematic liquid crystal. In total twelve sets of diffraction efficiency results were obtained, representing measurements on the controlled birefringence effect, the guest-host effect and a phase rotation effect.
- 8) Before measuring the diffraction efficiency response of the liquid crystal in the experimental cell, it was necessary to measure its phase retardance versus voltage response to ensure that non-linearities were not present. This criterion being satisfied, the liquid crystal was mounted in the diffraction efficiency measurement apparatus and the intensities of the d.c., first and second diffracted orders measured. Two methods were used to measure the diffraction efficiencies of the orders. Initially a photographic method was employed, but this was later replaced by a faster computerized photometer system with the same accuracy.
- 9) Analysis of the phase retardance results revealed that the experimental phase retardance was lower than theoretically predicted. Efron *et al* had also observed the same effect and proposed that this deficit was due to the non-contribution of the liquid crystal directors anchored to the cell walls.

The diffraction efficiency technique worked reliably, the results matching the theoretical predictions in terms of the periodicity of their diffraction peaks and troughs ( $2\pi$  intervals) and their amplitude ratios. Thus the analysis of diffraction efficiency results from treated nematic liquid crystals gives a reliable indication of the liquid crystals suitability for use in a spatial light modulator.

- 10) A peak detector system was developed for use in the output stage of the J.O.E.-R.S. optical correlation demonstrator system. The optical correlation peak was detected at the output of the optical correlator and its location and intensity recorded electronically. This information was then used to determine the position of the object causing the highest peak and necessary action taken.

## **8.2 Suggestions for Further Work**

To extend the diffraction efficiency technique to cover not only different types of liquid crystals, but also additional types of cell configuration, further development of the measurement technique is required. These are described below,

- a) Variation in the thickness of the experimental cells. The cells used in the above configurations were all  $13\mu\text{m}$  thick. Fabrication of thinner cells would permit faster response times of the liquid crystal and highlight any irregularities present in the liquid crystal.
- b) Variation in the frequency of the applied voltage. The measurements above were made with an applied a.c. voltage at 50Hz. Readings at higher frequencies would reveal driving limitations for the particular liquid crystal under observation, thus enabling a frequency to be specified for optimum performance of the SLM.
- c) Variation of temperature. Liquid crystals have a narrow operating range. Further research at higher and lower temperatures would permit observations to be made on the stability of the D.E. peaks with respect to applied voltage.
- d) Use of different types of liquid crystal. Recent research indicates that smectic liquid crystals could also be suitable for use in mass-produced SLMs.
- e) Measurement of cells with different types of rubbing, such as  $45^\circ$  twist,  $90^\circ$  twist and  $\pi$ -twist. Also, measurement of these and other twist arrangements with different director tilt angles would be of interest. However, this would be time consuming and expensive.
- f) Investigation of liquid crystal non-linearities by using a sinusoidally driven grating. Detection of any non-linearities exhibited by the liquid crystal are difficult to identify at the output of a square-wave grating due to the large number of diffracted orders and the presence of even numbered orders from a non-Ronchi grating. The output in the Fourier plane of a sine-wave grating consists of only two diffracted orders of equal intensity. Therefore detection of non-linearities in the form of extraneous diffracted orders would be simplified in this instance.
- g) The use of a linear CCD or photodiode array in place of a single photodetector would permit measurements to be made on all of the diffraction pattern orders at

the same time for each voltage increment. One possible drawback (as observed in the photographic method) is the large dynamic range of intensity values. The d.c. central order can often 'drown-out' the other readings because of its high intensity.

- h) The diffraction efficiency measurement determines the suitability of the liquid crystal for use in a SLM. However, the ultimate test is to incorporate the liquid crystal in question into a SLM. Such a SLM has been fabricated by Marconi Research Laboratories as part of the J.O.E.R.S. scheme and could be used to assess the diffraction efficiency method of determining suitability.

# A

## References

### Chapter 1

- [1a] A.Korpel, " ", S.P.I.E, Vol. 38, p. 3, 1973.
- [1] M.Grenot *et al* , " ", Appl. Phys. Lett., Vol. 21, p. 83, 1972.
- [2] J.Grinberg *et al* , "Photoactivated Birefringent Liquid Crystal Light Valve for Colour symbology display", IEEE Trans. Elec. Dev., Vol. ED-22 No.9, p. 775, 1975.
- [3] G.H.Smith (Ed. D.Casasent), "Optical Data Processing ", Vol. 23, Springer-Verlag
- [4] N.K.Sheridon, "The RUTICON family of erasible image recording devices", IEEE Trans. Elec. Dev., Vol. ED-19, p. 1003, 1972.
- [5] K.Preston Jr., " ", Coherent Optical Computers, , p. 139, 1972.
- [6] G.O.Langer, " ", IBM Tech. Disc. Bull., Vol. 13 No. 3, p. 603, 1970.
- [7] S.L.Hou & D.S.Oliver, " ", Appl. Phys. Lett., Vol. 18, p. 325, 1971.
- [8] T.Hara *et al* , "An Improved Microchannel SLM", 8th Symp. Photo. Imag. Dev., Imp. Coll. London. Sept 1983.
- [9] D.Haven, "Electron-Beam addressed liquid crystal light valve", Int. Disp. Res. Conf. Rec., Cherryhill, N.J. 1982.
- [10] I. Ota *et al* , " ", IEEE Conf. Disp. Dev., 1972.
- [11] A.D.Fisher, "A Review of Spatial Light Modulators", Tech. Dig. Opt. Comp. Conf., Nevada, Winter 1985.
- [12] S.G.Latham & M.P.Owen, "A Silicon Liquid-Crystal Spatial Light Modulator", G.E.C. Journal of Research, Vol. 4 No. 3, p. 219, 1986..
- [13] D.Casasent & Shao-Feng Xia, "Phase Correction of Light Modulators", Opt. Lett, Vol. 11, No. 6, , 1986..
- [14] Hua-Kuang Liu *et al* , "Optical-data-processing properties of a liquid-crystal television spatial light modulator", Opt. Lett, Vol. 10, No. 12, p. 635, 1985..

### Chapter 2

- [15] F.Reinitser, " ", Wiener Monatsch., Vol. 9, p. 421, 1888.
- [16] O.Lehmann, " ", Verhandl. d. Deutschen. Phys. Ges., Vol. 5 , p. 1, 1900.
- [17] G.Friedel, "Les etats Mesomorphes de la Matiere", Ann. de Physique, Vol. 18, p. 273, 1922.
- [17a] M.Vorländer, " ", Verhandl. d. Deutschen. Phys. Ges., Vol. 3 , p. 8, 1898.
- [18] H.Sackmann & D.Demus, " ", Mol. Cryst. & Liq. Cryst., Vol. 21, p. 239 , 1973.

- [19] L.T.Creagh & A.R.Kmetz, "*Mechanism of surface Alignment in Nematic Liquid Crystals*", Mol. Cryst. & Liq. Cryst., Vol. 24, p. 59, 1973.
- [20] J.C.Dubois *et al* , " ", J. Appl. Phys., Vol. 47, p. 1270 , 1976.
- [21] F.J.Kahn *et al* , "*Surface produced Alignment of Liquid Crystals*", Proc. I.E.E., Vol. 61, p.823, 1973.
- [22] H.Zocher & Z.Coper, "*Ueber die Erzeugung des Anisotropie von Oberflächen*", Phys. Chem., Vol. 132, p. 295, 1928.
- [23] J.F.Dreyer, U.S. Patent Number 2-400-877, " ", 1946.
- [24] G.Porte, "*Tilted Alignment of MBBA Induced by short-chain surfactant*", J. Phys. (Paris), Vol. 37, p. 1245, 1976.
- [25] T.Uchida *et al* , "*Molecular Arrangement of Nematic LCs*", Jap. J. App. Phys., Vol. 11, p. 1559, 1972.
- [26] J.E.Proust *et al* , "*Orientation of a Nematic LC by suitable boundary surfaces*", Solid State Commun., Vol. 11, p. 1227, 1972.
- [27] J.C.Dubois *et al* , "*Plasma-polymerized films as orientating layers for LCs*", Appl. Phys. Lett., Vol. 24, p. 297, 1974.
- [28] P.Chatelain, "*Sur l'orientation des cristaux liquides par les surfaces frottées*", Bull. Soc. Fr. Min., Vol. 66, p. 105, 1943.
- [29] L.A.Goodman *et al* , "*The Effect of surface orientation on the operation of multiplexed twisted-nematic devices*", I.E.E.E. , Vol. ED-23, p. 1176, 1976.
- [30] J.F.Dreyer, "*Orientation of the surface of Glass*", Glass. Ind., Vol. 29, p. 197, 1948.
- [31] W.A.Weyl, "*Structure of subsurface layers and their role in glass technology*", J. Non-Cryst. Solids, Vol. 19, p. 1, 1975.
- [32] J.L.Janning, "*Thin Film surface Orientation for liquid crystals*", Appl. Phys. Lett., Vol. 41, p. 73, 1972.
- [33] E.Guyon *et al* , "*On different boundary conditions of Nematic film deposited on oblique-ly evaporated plates*", Appl. Eng. Sci. Lett., Vol. 119, , 1973.
- [34] G.A.Dir *et al* , "*A vacuum deposition alignment technique for tilt control in LCs*", SID Digest, Vol. 66, , 1978.
- [35] N.A., Swiss Patent Number CH-590-490, "*Flussigkristallzelle*", 1974.
- [36] F.J.Haas *et al* , "*New Electro-Optic Effect in a Room- temperature Nematic LC*", Phys. Rev. Lett., Vol. 25, p. 1326, 1970.
- [37] K.Hiltrop & H.Stegenmeyer, "*Contact angles and alignment of LCs on lecithin monolayers*", Mol. Cryst. Liq. Cryst., Vol. 49 , p.61, 1973.
- [38] F.J.Kahn., U.S. Patent Number 369-405-3, "*A Nematic Liquid Crystal Device.*", 1972.
- [39] Haller *et al* ., U.S. Patent Number 365-683-4, "*An Additive for LC Material.*", 1972.
- [40] G.J.Sproxel., French Patent Number 743-974-4, "*Dispositif d'affichage a cristaux liquides.*", 1974.
- [41] W.M.Schwartz & H.W.Moseley, "*The surface tension of liquid crystals*", J. Phys. Coll. Chem., Vol. 51, p. 826, 1947.

- [42] B.Ackles, "*Tailoring surfaces with silanes*", Chem. Technol. , Vol. 766, , 1977.
- [43] K.L.Mittal & D.F.O'Kane, "*Vapour deposited silane & other coupling agents*", J. Adhesion, Vol. 8, p. 98, 1976.
- [44] J.Cognard *et al* , "*Alignment of Nematic liquid crystals and their mixtures*", Supp. Sers. 1 of Mol. Cryst. Liq. Cryst., , , 1982.
- [45] R.W.Gurtler & J.W.Casey, "*Surface tilt distributions of homogeneously aligned LCs*", Mol. Cryst. Liq. Cryst., Vol. 35, , p. 275, 1976.
- [46] T.J.Scheffer & J.Nehring, "*Accurate determination of LC tilt bias angles*", J. Appl. Phys., Vol. 48, p. 1783, 1977.
- [47] F.Muller, "*Deposition oblique de couches minces de SiO et orientation des molecules dans des affichages a cristaux liquides*", Helv. Phys. Acta., Vol. 51, p. 59, 1978.
- [48] W.A.Crossland *et al* , "*Tilt angle measurements of nematic phases of cyanobiphenyls aligned by obliquely evaporated films* ", J. Phys. D., Vol. 9, p. 2001, 1976.
- [49] N.A., Swiss Patent Number CH-619-052, "*Procede de fabrication d'une cellule d'affic-hage electro-optique passif*.", 1979.
- [50] J.H.Morrisy, B.Needham & W.A.Crossland, " ", Bordeaux Conf. , Bordeaux 1978
- [51] E.P.Raynes, "*Improved contrast uniformity in twisted nematic LC electro-optic display devices*", Electr. Lett., Vol. 10, p. 141, 1974.
- [52] D.M.Buscek, "*A thin film process to improve off axis viewing of LC Displays*", Mol. Cryst. Liq. Cryst., Vol. 47, p. 145, 1978.
- [53] D.Meyerhofer, "*New technique of aligning liquid crystals on surfaces*", Appl. Phys. Lett., Vol. 29, p. 691, 1976.
- [54] M.R.Johnson & R.A.Penz, "*Low-tilt angle nematic alignment compatible with frit sealing*", IEEE., Vol. ED-24, p. 805, 1977.
- [55] E.P.Raynes *et al* , "*LC surface alignment treatment giving controlled low tilt angle*", Mol. Cryst. Liq. Cryst. Lett. , Vol. 34, p. 105, 1976.
- [56] L.Roussille & J.Robert, "*Liquid crystal quasihomotropic orientation induced by a polymer deposited on a SiO surface* ", J. Appl. Phys., Vol. 50 No. 6, p. 3975, 1979.
- [57] N.A., British Patent Number GB-2007-865, "*Liquid Crystal Displays.*", 1978.
- [58] R.Chabickovsky & G.Kocmann, "*LC Cells with special electrodes for the generation of uniform colours by optical birefringence*", IEEE, Vol ED-24, p. 807, 1977.
- [59] N.H.Hartshorne and A.Stuart, "*Crystals and the polarising microscope.*", ,

### Chapter 3

- [60] V.K.Freederickss & V.Zolina, "*Forces causing the orientation of anisotropic liquid*", Trans. Faraday Soc., Vol. 29, p. 919, 1943.
- [61] H.Gruler & G. Meier, "*Electric field induced deformations in Oriented Liquid Crystals of the Nematic type*", Mol. Cryst. & Liq. Cryst., Vol. 16, p. 299, 1972.
- [62] H. Deuling, "*Deformation of Nematic Liquid Crystals in an Electric Field*", Mol. Cryst. & Liq. Cryst., Vol. 19, p. 123, 1972.



- [63] R.A.Soref & M.J.Rafuse, "*Electrically Controlled Birefringence of thin Nematic films*", J. Appl. Phys., Vol. 43 , p. 2029, 1972.
- [64] M.Schadt & W.Helfrich, "*Voltage Dependent Optical Activity of a twisted Nematic Liquid Crystal*", Appl. Phys. Lett., Vol. 18 , p.127, 1971.
- [65] J.J.Wysocki, J.Adams & W.Haas, "*Electric field induced Phase Change in Cholesteric Liquid Crystals*", Phys. Rev. Lett. , Vol. 20, p. 1024, 1968.
- [66] G.H.Heilmeyer & J.E.Goldmacher, "*Electric Field Induced Cholesteric-Nematic Phase Change in Liquid Crystals*", J. Chem. Phys., Vol. 51, p. 1258, 1969.
- [67] P.G.deGennes, "*Calcul de la Distortion D'une Structure Cholesterique Par un Champ Magnetique*", Sol. St. Commun., Vol. 6 , p. 163, 1968.
- [68] G.H.Heilmeyer & L.A.Zanoni, "*Guest-Host Interactions in Nematic Liquid Crystals—A New Electro-Optic Effect*", Appl. Phys. Lett., Vol. 13, p. 91, 1968.
- [69] G.H.Heilmeyer, J.A.Castellano & L.A.Zanoni, "*Guest-Host Interactions in Nematic Liquid Crystals*", Mol. Cryst. & Liq. Cryst., Vol. 8, p. 293, 1969.
- [70] D.L.White & G.N.Taylor, "*A new absorptive mode reflective Liquid crystal display device*", J. Appl. Phys., Vol. 45, p. 4718, 1974.
- [71] N.Felici, "*Phenomenes Hydro et Aerodynamiques dans la Conduction des Dielectrique Fluide*", Rev. Gen. Elec., Vol. 78 , p. 717, 1969.
- [72] E.F.Carr, "*Ordering in Liquid Crystals owing to Electric and Magnetic fields*", Advan. Chem. Ser., Vol. 63, p. 76, 1967.
- [73] W.Helfrich, "*Conduction-Induced alignment of Nematic Liquid Crystals: Basic Model and Stability considerations*", J. Chem. Phys., Vol. 51, p. 4092, 1969.
- [74] W.H.de Jeu, C.J.Gerritsma & A.M.VanBortel , "*Electro-hydrodynamic Instabilities in Nematic Liquid Crystals*", Phys. Lett., Vol. 34A, p. 203, 1971.
- [75] R.Williams, "*Domains in Liquid Crystals*", J. Chem. Phys. , Vol. 39, p. 384, 1963.
- [76] G.H.Heilmeyer, L.A.Zanoni & L.A.Barton, "*Dynamic Scattering: A new Electro-Optic Effect in Certain classes of nematic liquid crystals*", Proc. IEEE., Vol. 56, p. 1662, 1968.
- [77] G.H.Heilmeyer & J.E.Goldmacher, "*A New Electric Field controlled Reflective Optical Storage Effect in Mixed Liquid Crystal Systems*", Proc. IEEE, Vol. 57, p. 34, 1969.
- [78] G.Dir et al , "*Cholesteric Liquid Crystal Texture Displays*", Proc. SID, Vol. 13, p. 105, 1972.
- [79] W.Haas, J.Adams & G.Dir, " ", Chem. Phys. Lett., Vol. 14 , p. 95, 1972.
- [80] R.A.Soref, "*Thermo-Optic Effects in Nematic-Cholesteric Mixtures*", J. Appl. Phys., Vol. 41, p. 3022, 1970.
- [81] M.Hareng & S.le Berre, " ", Electron. Lett., Vol. 11, p. 73 , 1975.
- [82] P.J.Wojtowics, " ", R.C.A. Rev., Vol. 35, pages a) 105, b) 108, c) 462., 1974.
- [83] Ping Sheng, " ", R.C.A. Rev., Vol. 35, p. 132., 1974.
- [84] H.Zocher, " ", Trans. Farad. Soc., Vol. 29, p. 945, 1933.
- [85] C.W.Oseen, "*The Theory of Liquid Crystals*", Trans. Faraday Soc., Vol. 2, p. 833, 1933.

- [86] F.C.Frank, "*On the Theory of Liquid Crystals*", Disc. Faraday Soc., Vol. 25, p. 19, 1958.
- [87] H.J.Deuling, "*Deformation of Nematic Liquid Crystals in an Electric Field*", Mol. Cryst. Liq. Cryst., Vol. 19, p. 123., 1972.
- [88] R.Simon, "*Electro-Optic effects in thin Films of Liquid Crystal Material*", Ph.D. Thesis, CNAA, Thames Polytechnic, 1982.
- [89] C.G.Xie, "*Computerized Guassian Quadrature*" , Private Communication, 1986
- [90] B.D.H. and Merck, "*Nematic Liquid Crystals Data Sheet*", 1985.

#### Chapter 4

- [91] J.W.Goodman, "*Introduction to Fourier Optics*", Chapter 2 , McGraw-Hill.
- [92] M.Françon, "*Optical image formation and processing*", Chapter 3 , Academic Press.
- [93] R.M.Bracewell, "*The Fourier Transform and its Applications*", Chapters 5,7 & 10., McGraw-Hill.
- [94] P.M.Duffieux, "*The Fourier Transform and its Application to Optics*", Chapter 9, Wiley.
- [95] E.Hecht & A.Zajac, "*Optics*", Chapter 10, Addison-Wesley.
- [96] A.Sommerfeld, "*'Optics'-Lectures on Theoretical Physics. Vol. 4* ", Chapter5—Theory of Diffraction,

#### Chapter 5

- [97] S.T.Wu *et al* , "*Birefringence Measurements of Liquid Crystals* ", Appl. Opt., Vol. 23 No. 21, p. 3911, 1984.
- [98] J.C.Dainty & R.Shaw, "*Image Science*", Chapter 9—Microdensitometry, Academic Press.

#### Chapter 6

- [99] U.Efron *et al* , "*Nematic liquid crystals for spatial light modulators: recent studies*", J.O.S.A., Vol. 3 No. 2, p. 247, 1986.

#### Chapter 7

- [100] Meetings of the J.O.E.R.S. working party between January and April 1986.
- [101] F.Merkle & T.Lörch, "*Hybrid Optical-Digital pattern recognition*", Appl. Opt., Vol. 23 No. 10, p. 1509, 1984..
- [102] P.G.Lindstrøm, Ph.D. Thesis. D.I.A.S., U.M.I.S.T., "*Computer Simulation of Hybrid Cross-Correlators*" , Private Communication, December 1986
- [103] Fairchild VIP 100 Data Sheet.

# B

## Data Logger Software

```
PROGRAM Liquid_Crystal_Data_Logger (INPUT,LCFILE,OUTPUT);
  {Written 2/6/86 in Acornsoft ISO Pascal Level 0 and Stand Alone Generator
  Package to produce ROM'able code.
  By Fraser Dickin
  this program is to be used for the sole purpose of getting data from the
  light sensitive device (photodiode) and converting this analogue signal
  into a digital one. The value is stored along with a value created
  by the program as the external applied voltage (DAC—2.5 digit pot.)
  Finished code in 16k ROM on 20/6/86 - Call it with '*LOG' command}
CONST
  allOut = &FF;
  zero = 0;
  one = 1;
  namelen = 10;
  max_no_readings = 100;
  channel1 = 1;
TYPE
  BYTE = 0..255;
  WORD = 0..65535;
  name = PACKED ARRAY[1..namelen] OF CHAR;
{$U-}
  fudgerec = PACKED RECORD
    CASE BOOLEAN OF
      FALSE : (addr : ↑ BYTE);
      TRUE : (int : WORD);
    END; {case}
  datatype = RECORD
    day : 1..31;
    month : 1..12;
  END;
  lxtaltype = (ZLi1800, ZLi1982);
  orte = (zero_undyed, zero_dyed, forty_5_undyed);
  rubtype = (parallel, antiparallel);
  readtype = PACKED ARRAY[0..max_no_readings] OF INTEGER;
  OrderType = INTEGER;
  data = PACKED RECORD
    date : datatype;
    lxtal : lxtaltype;
```

```

    orientation : orteype;
    rubbing : rubtype;
    incident_flux : REAL;
    plus_one ,
    minus_one ,
    plus_two ,
    minus_two : readtype;
END; {record}
{$U+}
VAR
    i : WORD;
    pi : BYTE;
    PCR_reg ,
    mode_number ,
    time_delay ,
    reading_number,
    adval_reading ,
    Address ,
    dummy : INTEGER;
    LCFILE : PACKED FILE OF DATA;
    MYdata : data;
    current_read : readtype;
    filename : name;
    today : 0...31;
    this_month : 0...12;
    this_lxtal : lxtaltype;
    this_orient : orteype;
    this_rub : rubtype;
    Temp_Addr : INTEGER;
    Rom_On : BOOLEAN;
{$U-}
FUNCTION Peek(address : WORD) : BYTE;
VAR fudge : fudgerec;
BEGIN
    fudge.int := address;
    peek := fudge.addr↑ ;
END;
PROCEDURE Poke(address : WORD; value : BYTE);
VAR fudge : fudgerec;
BEGIN
    fudge.int := address;
    fudge.addr↑ := value;
END;
{$U+}
PROCEDURE Tab (X,Y : INTEGER);
CONST TabCode = 31;
BEGIN

```

```

        VDU(TabCode,X,Y)
    END;
FUNCTION AnUpdate : INTEGER;
    BEGIN
        AnUpdate := ADVAL(0) DIV 256
    END;
PROCEDURE ForceADC;
    BEGIN
        OSCLI('FX17,1');
    END;
FUNCTION Get_Key_Press : CHAR;
CONST osrdch = & FFE0;
    BEGIN
        Get_Key_Press := CHR(CODE0(osrdch,0,0,0) MOD & 100);
    END;
PROCEDURE Out_BCD (value : INTEGER);
CONST ORB = & FE60;
VAR dummy : INTEGER;
    FUNCTION Convert_BCD (number : INTEGER):INTEGER;
    VAR Tens ,
    Units : INTEGER;
        FUNCTION mcAddr : INTEGER;
        CONST mcoffset = 3;
        osbyte = & FFF4;
        VAR oshwm : INTEGER;
            BEGIN
                IF Rom_On = FALSE THEN mcAddr := & 8163
                ELSE mcAddr := Address;
                { BEGIN
                    oshwm := CODE0(osbyte,131,0,0)MOD & 1000000 DIV & 100;
                    mcAddr := oshwm + mcoffset;
                END; }
            END;
        FUNCTION Shift_Left (value : INTEGER) : INTEGER;
        CONST bits_rotation = 4;
        VAR dummy : INTEGER;
            BEGIN
                dummy := CODE1(mcAddr, bits_rotation, value);
                Shift_Left := value;
            END;
        BEGIN {Convert}
            Temp_Addr := mcAddr;
            Tens := number DIV 10;
            Units := number MOD 10;
            Tens := Shift_Left(Tens);
            Convert_BCD := Tens + Units;

```

```

    END; {Convert}
BEGIN {Out_BCD}
    dummy := Convert_BCD(value);
    Poke(ORB,dummy);
END; {Out_BCD}
PROCEDURE Set_CB2 (value : INTEGER);
    CONST PCR = &FE6C;
    filter = & 1F;
    VAR PCR_reg : INTEGER;
    BEGIN
        CASE value OF
            1 : value := &E0;
            0 : value := &C0;
        END
        OTHERWISE WRITELN('Error in the Set_CB2 routine ');
        PCR_reg := Peek(PCR);
        PCR_reg := PCR_reg MOD filter;
        PCR_reg := PCR_reg + value;
        Poke(PCR, PCR_reg);
    END;
PROCEDURE fSet_Port (fvalue : INTEGER);
fCONST fDDRB = &FE62;
fBEGIN
    fPoke(fDDRB, fvalue);
fEND;
PROCEDURE fOut_Port (value : INTEGER);
    CONST fORB = &FE60;
    BEGIN
        fPoke(fORB, value);
    END;
PROCEDURE Find_Peak_Spot;
    VAR exit ,
        val ,
        count ,
        maxval ,
        average_val : INTEGER;
    BEGIN
        Set_Port(allOut);
        Out_BCD(zero);
        Set_CB2(one);
        maxval := 0;
        count := 0;
        average_val := 0;
        Tab(20,12); WRITE('Remember that 4096 is the MAX value');
        Tab(10,15); WRITE('ADC Value = ');
        Tab(40,15); WRITE('MAX value so far = ');

```

```

Tab(25,18); WRITE('Press Q to Quit');
REPEAT
  ForceADC;
  REPEAT
    SETTIME(zero);
    REPEAT
      {do nothing}
    UNTIL TIME < 10; {tenth of a second}
  UNTIL AnUpdate = channel.1;
  val := (ADVAL(1) DIV 16);
  count := count + 1;
  IF count = 1 THEN average_val := val;
  average_val := (average_val + val) DIV 2;
  IF maxval < val THEN maxval:=val;
  Tab(22,15); WRITE(' ');
  Tab(59,15); WRITE(' ');
  Tab(22,15); WRITE(average_val:5);
  Tab(59,15); WRITE(maxval:5);
  exit := INKEY(10); { half a second }
UNTIL exit = ORD('Q'); { capital Q }
END;
PROCEDURE Readname (VAR filename : name);
  VAR i : 1...namelen;
  BEGIN
    FOR i:=1 to namelen DO filename[i]:= ' ';
    WHILE INPUT↑ = ' ' DO GET(INPUT);
    i:=1;
    REPEAT
      READ(filename[i]);
      i:=i+1;
    UNTIL EOLN OR (filename[i-1]=' ');
    IF EOLN THEN READLN;
  END;
PROCEDURE Load_Data;
  VAR count : INTEGER;
  response : CHAR;
  BEGIN
    PAGE;
    WRITE('Enter a data filename to load -> ');
    Readname(filename);
    RESET(LCFIL, filename);
    READ(LCFIL, MYdata);
    WRITE('Hardcopy Y/N ');
    READLN(response);
    IF (response = 'Y') OR (response = 'y') THEN VDU(2,1,15);
    WRITELN('File = ', filename:7);
  END;

```

```

WITH Mydata.date DO
BEGIN
    WRITE('day = ',day:2);
    WRITELN(' month = ',month:2);
END;
WRITE(' lxtal type = ');
CASE ORD(MYdata.lxtal) OF
    0 : WRITELN('ZLi1800');
    1 : WRITELN('ZLi1982');
END;
WRITE(' orientation = ');
CASE ORD(MYdata.orientation) OF
    0 : WRITELN('Zero undyed');
    1 : WRITELN('Zero dyed');
    2 : WRITELN('45 degrees undyed');
END;
WRITE(' rubbing = ');
CASE ORD(MYdata.rubbing) OF
    0 : WRITELN('Parallel');
    1 : WRITELN('Anti parallel');
END;
WRITELN(' incident flux = ',MYdata.incident_flux:10:3);
WRITELN;
WRITELN('Number':15,'Plus One':15,'Minus One':15,'Plus Three':15,
    'Minus Three':15);
FOR count := 0 TO 100 DO
WITH MYdata DO
    WRITELN(count:15,plus_one[count]:15,minus_one[count]:15,
        plus_two[count]:15,minus_two[count]:15);
    VDU(3);
END;
PROCEDURE Do_Data_Log;
VAR No_of_Times,
    Reading ,
    Count : INTEGER;
    flux : REAL;
PROCEDURE Get_Reading (Count : INTEGER);
CONST channel1 = 1;
VAR answer : CHAR;
PROCEDURE Wait;
BEGIN
    SETTIME(zero);
    REPEAT
        { do nothing }
    UNTIL TIME < (time_delay*50);

```



```

    END;
BEGIN { get_reading}
    { Wait;
    ForceADC;
    REPEAT
        do nothing
    UNTIL AnUpdate = channel_1;
    reading := ADVAL(channel_1);
    current_read[Count] := reading;}
    Tab(26,8); WRITE(' ');
    Tab(26,8); WRITE(Count:3);
    REPEAT
        answer := Get_Key_Press;
    UNTIL answer = ' ';
END; { get_reading}
PROCEDURE Set_Order (value : INTEGER);
VAR answer : CHAR;
BEGIN
    PAGE;
    WRITE('Please make sure you are working on ');
    CASE value OF
        1 : WRITE('PLUS FIRST');
        2 : WRITE('MINUS FIRST');
        3 : WRITE('MINUS THIRD');
        4 : WRITE('PLUS THIRD');
    END;
    WRITELN(' order');
    WRITELN;
    WRITE('Press any key to continue');
    answer := Get_Key_Press;
END; { set_order}
PROCEDURE Change (value : INTEGER);
BEGIN
    CASE value OF
        1 : MYdata.plus_one := current_read;
        2 : MYdata.minus_one := current_read;
        3 : MYdata.minus_two := current_read;
        4 : MYdata.plus_two := current_read;
    END;
END;
PROCEDURE Save_Data;
BEGIN
    WITH MYdata DO
        BEGIN
            lxtal := this_lxtal;
            orientation := this_orient;

```

```

        rubbing := this_rub;
        date.day := today;
        date.month := this_month;
    END;
    REWRITE(LCFILE,filename);
    WRITE(LCFILE,MYdata);
END;
PROCEDURE Initialise;
VAR response : INTEGER;
BEGIN
    PAGE;
    OSCLI('FX 200,1'); { clear escape key action}
    OSCLI('FX 16,1'); { select channel 1 to be used }
    WRITE('Enter a filename to save data as -l ');
    Readname(filename);
    Writeln;
    Writeln('Enter the time delay between readings');
    WRITE(' in units of half a second -l ');
    READLN(time_delay);
    Writeln;
    WRITE('Enter day and month "DD MM" ');
    READLN(today,this_month);
    Writeln;
    Writeln('Enter the type of liquid crystal cell ');
    Writeln;
    WRITE('1 = Zli1982 LXtal, 2 = Zli1800 LXtal : ');
    READ(response);
    CASE response OF
        1 : this_lxtal := Zli1982;
        2 : this_lxtal := Zli1800;
    END {case}
    OTHERWISE Initialise;
    Writeln;Writeln;
    Writeln('Enter the type of cell orientation ');
    Writeln;W
    WRITE('1 = Undyed @ 0, 2 = Dyed @ 0, 3 = Undyed @ 45 : ');
    READ(response);
    CASE response OF
        1 : this_orient := zero_undyed;
        2 : this_orient := zero_dyed;
        3 : this_orient := forty_5_undyed;
    END
    OTHERWISE Initialise;
    Writeln;
    Writeln('Enter type of rubbing');
    Writeln;

```

```

WRITE('1 = Parallel, 2 = Antiparallel : ');
READ(response);
CASE response OF
  1 : this_rub := parallel;
  2 : this_rub := antiparallel;
END {case}
  OTHERWISE Initialise;
END;
BEGIN { Do_Data_Log}
  { Initialise; }
  FOR No.of_Times := 1 TO 4 DO
    BEGIN
      PAGE;
      Set_Order(No.of_Times);
      {Tab(30,10); WRITE('PEAK SPOT LOCATOR');
      Find_Peak_Spot; }
      Tab(0,0);
      Set_Port(allOut);
      Out_BCD(zero);
      Set_CB2(one);
      Out_Port(zero);
      Tab(10,8); WRITE('Data Number -l ');
      {Tab(26,8); WRITE('100':3); }
      Get_Reading(100);
      FOR count:= 99 DOWNT0 0 DO
        BEGIN
          {Tab(26,8); WRITE(' ');
          Tab(26,8); WRITE(count:3); }
          IF count = 99 THEN BEGIN
            Out_BCD(count);
            Set_CB2(zero);
            Get_Reading(count);
          END;
          Out_BCD(count);
          Get_Reading(count);
          {Tab(22,15); WRITE(' ');
          Tab(22,15); WRITE(reading:4); }
          END;
          Change(No.of_Times);
        END; {1 to 4 loop}
      PAGE;
      { Tab(15,10); WRITE('Enter the incident flux -l ');
      Find_Peak_Spot;
      Tab(43,10); READLN(flux);
      MYdata.incident_flux := flux;

```

```

    Save_Data; }
END; {Do_Data_Log}
PROCEDURE Options; FORWARD;
PROCEDURE Test_ADC;
VAR response : CHAR;
    dummy : INTEGER;
    BEGIN
        PAGE;
        Tab(20,5); WRITELN('ADC TEST PROGRAM');
        Find_Peak_Spot;
        Options;
    END;
PROCEDURE Test_User_Port;
VAR answer : CHAR;
count ,
dummy ,
value : INTEGER;
BEGIN
    IF Rom_On = FALSE THEN Temp_Addr := & 8163
    ELSE Temp_Addr := Address;
    PAGE;
    Tab(20,5); WRITE('USER PORT Test Program');
    Tab(10,10); WRITE('Please connect the USER PORT lead');
    Tab(10,11); WRITE('to the interface board');
    Tab(12,13); WRITE('Press any key to step through');
    Set_Port(allOut);
    value:=1;
    Tab(15,15); WRITE('Bit ',value:1,' should now be ON');
    Out_Port(value);
    answer := Get_Key_Press;
    FOR count := 2 TO 8 DO
    BEGIN
        Tab(19,15); WRITE(' ');
        dummy := CODE1(Temp_Addr,one,value);
        Out_Port(value);
        Tab(19,15); WRITE(count:1);
        answer := Get_Key_Press;
    END;
    TAB(15,15); WRITE(' ');
    Tab(15,15); WRITELN('CB2 should now be ON');
    Set_CB2(one);
    TAB(20,19); WRITE('Press any key to continue');
    answer := Get_Key_Press;
    Set_CB2(zero);
    Set_Port(zero);
    Options;

```

```

END;
PROCEDURE Options;
VAR selection : CHAR;
BEGIN
    PAGE;
    Tab(25,5); WRITELN('M-A-I-N M-E-N-U');
    Tab(20,10); WRITELN('A - Test the USER PORT');
    Tab(20,12); WRITELN('B - Test the ADC');
    Tab(20,14); WRITELN('C - Run the Data Logging Program');
    Tab(5,20); WRITE('Please choose the option you require :- ');
    READ(selection);
    CASE selection OF
        'a','A' : Test_User_Port;
        'b','B' : Test_ADC;
        'c','C' : Do_Data_Log;
        'l','L' : BEGIN
            Load_Data;
            Selection := Get_Key_Press;
            Options;
        END;
        'r','R' : BEGIN
            PAGE;
            Rom_On := TRUE;
            WRITE('Input ROM address in decimal ! -> ');
            READLN(Address);
            WRITELN;
            WRITELN('Address being called is and ',Address:4);
            Selection := Get_Key_Press;
            Options;
        END;
    END
    OTHERWISE Options;
END;
BEGIN { main}
    MODE(0);
    OSCLI('FX119'); { close any open files }
    REPEAT
        Rom_On := FALSE;
        Options;
    UNTIL 1<0; { c/o Per Lindstrom ! }
END. { main }

```

# C

## Peak Capture Software

### { Peak Capture Software

Written using the SYSTEM ADE Assembler/Editor Package  
in 6502 machine-code for the BBC Model 'B' microcomputer.  
The 'SYSLIB' is a proprietary macro package of SYSTEM Ltd.  
This software produces a pseudo-3D colour image on the computer  
monitor along with the numerical height and positional information  
of the digitised correlation peak.  
Original material by Fraser Dickin at S.T.L. Ltd., January 1986.  
Additional material by Paul Waite at G.E.C. HRC., April 1986. }

ORG &1902

EXEC VIDIG

; Machine Operating System addresses

OSCLI EQU &FFF7  
OSBYTE EQU &FFF4  
OSWORD EQU &FFF1  
OSWRCH EQU &FFEE  
OSNEWL EQU &FFE7  
OSRDCH EQU &FFE0  
OSFILE EQU &FFDD  
OSARGS EQU &FFDA  
OSBGET EQU &FFD7  
OSBPUT EQU &FFD4  
OSGBPB EQU &FFD1  
OSFIND EQU &FFCE  
OSRDRM EQU &FFB9

;Digitiser latch addresses

HPIXEL EQU &FC7F  
LPIXEL EQU &FCBF  
HLINE EQU &FCDF  
LLINE EQU &FCEF  
ADC EQU &FCF7  
VRESET EQU &FCFB

;O.S. Vectors

USERV EQU &200  
BRKV EQU &202  
IRQ1V EQU &204  
IRQ2V EQU &206  
EVENTV EQU &220

;Various addresses

LATCH EQU &FE30  
ROMREC EQU &F4  
ROMTAB EQU &2A1  
ROMORG EQU &8000  
ROMTYP EQU &8006  
ERRPTR EQU &FD

```

ASTRPT EQU &F2
;Various constants
BELL EQU 7
SPACE EQU &20
CR EQU &0D
LF EQU &0A
EOS EQU &F3
RCSR EQU &89
LCSR EQU &88
UCSR EQU &8B
DCSR EQU &8A
DEL EQU &7F
COPY EQU &87
;OSFILE codes
SAVE EQU 0
WRPARM EQU 1
RDPARM EQU 5
DELETE EQU 6
LOAD EQU &FF
;User zero page addresses
DSECT
    ORG &70
STRPTR DS 2
PTR1 DS 2
PTR2 DS 2
PTR3 DS 2
PTR4 DS 2
PTR5 DS 2
PTR6 DS 2
PTRX DS 2
;General user storage space
    ORG &700
OLDIRQ DS 2
OLDEVE DS 2
ESCFLG DS 1
POS DS 1
VPOS DS 1
HXD DS 2
HXDFLG DS 1
TENUNI DS 1
HUNDS DS 1
TEMP1 DS 1
TEMP2 DS 1
TEMP3 DS 1
CHGFLG DS 1
MCAND DS 2
MLIER DS 2
HIPROD DS 2
DVSOR DS 2
DVEND DS 4
RETADR DS 2
DEND
;Strings
SCRN1 DFB 22,1

```

```

DFB 23,1,0,0,0,0,0,0
DFB 19,0,3,0,0,0
DFB 19,1,128,0,0,0
DFB 19,2,2,0,0,0
DFB 19,3,4,0,0,0
DFB 18,0,0
DFB 25,4,0,0,0,0
DFB 25,5,0,0,&FF,3
DFB 25,5,&FF,4,&FF,3
DFB 25,5,&FF,4,0,0
DFB 25,5,0,0,0,0
DFB 25,4,0,0,&87,0
DFB 25,5,&FF,4,&87,0
DFB 31,2,29
ASC 'Position ( , )'
DFB 31,24,29
ASC 'Threshold'
DFB EOS
;Pseudo 3-D Grid Pattern
SCRN2 DFB 18,0,3
DFB 25,4,0,0,0,0
DFB 25,4
DW 208,234
DFB 25,85
DW 689,234
DFB 25,4,0,0,0,0
DFB 25,4
DW 480,0
DFB 25,85
DW 689,234
DFB 18,0,2
DFB 25,4,0,0,0,0
DFB 25,5
DW 480,0
DFB 25,5
DW 532,59
DFB 25,5
DW 52,59
DFB 25,5
DW 104,117
DFB 25,5
DW 584,117
DFB 25,5
DW 636,176
DFB 25,5
DW 156,176
DFB 25,5
DW 208,234
DFB 25,5
DW 689,234
DFB 25,5
DW 480,0
DFB 25,5
DW 360,0

```



```

    DFB 25,5
    DW 568,234
    DFB 25,5
    DW 448,234
    DFB 25,5
    DW 240,0
    DFB 25,5
    DW 120,0
    DFB 25,5
    DW 328,234
    DFB 25,5
    DW 208,234
    DFB 25,5
    DW 0,0
    DFB 18,4,0
    DFB 17,2
    DFB EOS
PLOTST DFB &19
PCODE DFB 4
PX DW 0
PY DW 0
DECSTR ASC '000'
    DFB EOS
YORN ASC 'Y/N'
    DFB EOS
,*****
;Load Macros from System Library
    GET SYSLIB,VDU,FX,ERROR,OSW,STAR,CRLF
    GET SYSLIB,MODE,CLS,CLG,COLOUR,GCOL,SETCOL,RESTOR
    GET SYSLIB,GWIN,PLOT,TWIN,OFFSET
    GET SYSLIB,HOME,CURSOR,INKEY
    GET SYSLIB,TV,PAGE,INPUT
    GET SYSLIB,TIME,SOUND,ENVELO
    GET SYSLIB,OPENIN,OPENOU,OPENUP
    GET SYSLIB,CLOSE,BPUT,BPUTA,BGET
    GET SYSLIB,WRSTR,WRITE,INCW,DECW
    GET SYSLIB,STORAD,STORPT,TAB
,*****
;Main routine
VIDIG JSR SETUP
VIDLP JSR DISP
; JSR KEYS
    JSR CHKESC
    BCC VIDLP
EXIT JSR RESET
    FX 4,0,0
    TAB 0,23
    JSR RDLANG
SELLNG LDA #&8E
    JMP OSBYTE
;Check for Escape key pressed
;C=0 if not.
CHKESC LDA ESCFLG
    BEQ NOESC

```

```

    SEC
    RTS
NOESC CLC
    RTS
;Get keys and alter counters if reqd.
KEYS LDA  #&FF
    STA  CHGFLG
    JSR  GETKEY
    CMP  #LCSR
    BNE  NLEFT
    JMP  PIXDEC
NLEFT CMP  #RCSR
    BNE  NRIGHT
    JMP  PIXINC
NRIGHT CMP #UCSR
    BNE  NUP
    JMP  LININC
NUP CMP  #DCSR
    BNE  NDOWN
    JMP  LINDEC
NDOWN CMP #'A'
    BNE  NADCUP
    JMP  ADCINC
NADCUP CMP #'Z'
    BNE  NOWT
    JMP  ADCDEC
NOWT LDA  #0
    STA  CHGFLG
    RTS
;Get socket of current language
;in X
RDLANG LDA #&FC
    LDY  #&FF
    LDX  #0
    JMP  OSBYTE
;Tab the cursor to X,Y
TABIT LDA #31
    JSR  OSWRCH
    TXA
    JSR  OSWRCH
    TYA
    JSR  OSWRCH
    RTS
;Increment Pixel counter by 1 (PTR1)
PIXINC LDA PTR1+1
    BEQ  PIXOKI
    CMP  #2
    BCS  PXERRI
    LDA  PTR1
    CMP  #&E1
    BCS  PXERRI
PIXOKI JMP INCPT1
PXERRI RTS
;Decrement Pixel counter by 1 (PTR1)

```

```

PIXDEC LDA  PTR1
      BNE  PIXOKD
      LDA  PTR1+1
      BEQ  PXERRD
PIXOKD JMP  DECPT1
PXERRD RTS
;Increment Line counter by 1 (PTR2)
LININC LDA  PTR2+1
      BEQ  LINOKI
      CMP  #2
      BCS  LNERRI
      LDA  PTR2
      CMP  #39
      BCS  LNERRI
LINOKI JMP  INCPT2
LNERRI RTS
;Decrement Line counter by 1 (PTR2)
LINDEC LDA  PTR2
      BNE  LINOKD
      LDA  PTR2+1
      BEQ  LNERRD
LINOKD JMP  DECPT2
LNERRD RTS
;Increment ADC by 1 (PTR3)
ADCINC LDA  PTR3
      CMP  #65
      BCS  ADCERI
      JMP  INCPT3
ADCERI RTS
;Decrement ADC by 1 (PTR3)
ADCDEC LDA  PTR3
      BEQ  ADCERD
      JMP  DECPT3
ADCERD RTS
;Display numeric values and plot
;the correlation peak
DISP JSR  XPLOT
      TAB  12,29
      LDA  PTR1
      LDX  PTR1+1
      JSR  PRTDEC
      TAB  16,29
      LDA  PTR2
      LDX  PTR2+1
      JSR  PRTDEC
      TAB  36,29
      LDA  PTR3
      LDX  PTR3+1
      JSR  PRTDEC
      RTS
;Plot correlation peak
XPLOT LDA  #5
      JSR  DOPLOT
      LDA  PTR1

```

```

STA PX
LDA PTR1+1
STA PX+1
LDA PTR2
STA PY
LDA PTR2+1
STA PY+1
JSR TRANSF
LDA #4
JSR DOPLOT
LDA PY+1
PHA
LDA PY
PHA
LDA PTR3
PHA
ASL PTR3
ROL PTR3+1
ASL PTR3
ROL PTR3+1
CLC
LDA PTR3
ADC PY
STA PY
LDA PTR3+1
ADC PY+1
STA PY+1
LDA #5
JSR DOPLOT
PLA
STA PTR3
LDA #0
STA PTR3+1
PLA
STA PY
PLA
STA PY+1
PLOTX RTS
;Print out the plot string
;Plot code in A on entry
DOPLOT STA PCODE
LDX #0
PLOTLP LDA PLOTST,X
JSR OSWRCH
INX
CPX #6
BNE PLOTLP
RTS
;*****
;SET-UP AND INITIALISATION
;Set up vector intercept (IRQ1), set
;variables & screen mode etc.
SETUP JSR SETVEC
JSR INIT

```

```

        JSR  SETSCR
        RTS
;Set IRQ1V, EVENTV and BREAK intercept
SETVEC SEI
; JMP  DEBUG1
        LDA  IRQ2V
        STA  OLDIRQ
        LDA  IRQ2V+1
        STA  OLDIRQ+1
        LDA  #>IRQ
        STA  IRQ2V
        LDA  #<IRQ
        STA  IRQ2V+1
DEBUG1 LDA  EVENTV
        STA  OLDEVE
        LDA  EVENTV+1
        STA  OLDEVE+1
        LDA  #>EVENT
        STA  EVENTV
        LDA  #<EVENT
        STA  EVENTV+1
        LDA  #&0E
        LDX  #6
        JSR  OSBYTE
        LDY  #0
        LDA  #&F7
        LDX  #&4C
        JSR  OSBYTE
        LDA  #&F8
        LDY  #0
        LDX  #>BREAK
        JSR  OSBYTE
        LDA  #&F9
        LDY  #0
        LDX  #<BREAK
        JSR  OSBYTE
        CLI
        RTS
;Initialise variables, status
INIT LDA  #0
        STA  ESCFLG
        LDA  #&FF
        STA  CHGFLG
        LDA  #0
        LDX  #5
INITLP STA  PTR1,X
        DEX
        BPL  INITLP
        FX  4,1,0
        LDA  #&10
        LDX  #0
        JSR  OSBYTE
        RTS
;Set up the screen

```

```

SETSCR TV 0,1
    WRITE SCRN1
    OFFSET 300,300
    WRITE SCRN2
    RTS
;*****
;RESET PRIOR TO EXIT
;Clear buffers, reset mode and reset
;the vectors and BREAK handler.
RESET JSR CLRBUF
    TAB 0,23
    JSR RSTVEC
    RTS
;Reset IRQ1V, EVENTV and BREAK
;intercept
    JMP DEBUG2
RSTVEC SEI
    LDA OLDIRQ
    STA IRQ2V
    LDA OLDIRQ+1
    STA IRQ2V+1
DEBUG2 LDA OLDEVE
    STA EVENTV
    LDA OLDEVE+1
    STA EVENTV+1
    LDA #&0D
    LDX #6
    JSR OSBYTE
    LDA #&F7
    LDY #0
    LDX #0
    JSR OSBYTE
    CLI
    RTS
;Delay loop
DELAY LDY #&30
DELP1 LDX #&FF
DELP2 DEX
    BNE DELP2
    DEY
    BNE DELP1
    RTS
;*****
;INTERRUPT, EVENT & BREAK PROCESSING
;Break key intercept handler
BREAK BCS ENTRY2
    RTS
ENTRY2 JMP EXIT
;Event vector processor
EVENT CMP #6
    BNE NOTESC
    LDA #&FF
    STA ESCFLG
NOTESC JMP (OLDEVE)

```

;IRQ processing routine

```
IRQ LDA  &FC
    PHA
    TXA
    PHA
    TYA
    PHA
    LDA  LPIXEL
    STA  PTR1
    LDA  HPIXEL
    STA  PTR1+1
    LDA  LLINE
    STA  PTR2
    LDA  HLINE
    STA  PTR2+1
    LDA  ADC
    STA  PTR3
    LDA  VRESET
    PLA
    TAY
    PLA
    TAX
    PLA
    STA  &FC
    JMP  (OLDIRQ)
```

;\*\*\*\*\*

;POINTER ARITHMETIC

```
INCPT1 INCW  PTR1
    RTS
DECPT1 DECW  PTR1
    RTS
INCPT2 INCW  PTR2
    RTS
DECPT2 DECW  PTR2
    RTS
INCPT3 INCW  PTR3
    RTS
DECPT3 DECW  PTR3
    RTS
INCPT4 INCW  PTR4
    RTS
DECPT4 DECW  PTR4
    RTS
```

;Decrement PTRX. On exit C=1 if the  
;contents were at zero on entry.

```
DECPTX LDA  PTRX
    BNE  DLB
    LDA  PTRX+1
    BNE  DHB
    SEC
    RTS
DHB DEC  PTRX+1
DLB DEC  PTRX
    CLC
```

```

    RTS
;Increment string pointer
INCSTR INCW  STRPTR
    RTS
;*****
;VARIOUS SUBROUTINES
;Print string pointed to by X,Y.
;Stop on EOS char &F3.
PRTSTR STX  STRPTR
    STY  STRPTR+1
    LDY  #0
PRINT LDA  (STRPTR),Y
    CMP  #EOS
    BEQ  PRTEND
    JSR  OSWRCH
    JSR  INCSTR
    JMP  PRINT
PRTEND RTS
;Get the current cursor position and
;store in POS and VPOS.
SVCPOS PHA
    TYA
    PHA
    TXA
    PHA
    LDA  #&86
    JSR  OSBYTE
    STX  POS
    STY  VPOS
    PLA
    TAX
    PLA
    TAY
    PLA
    RTS
;Set cursor to position POS,VPOS
LDCPOS LDA  #31
    JSR  OSWRCH
    LDA  POS
    JSR  OSWRCH
    LDA  VPOS
    JSR  OSWRCH
    RTS
;Step the cursor down one line
STEPDN INC  VPOS
    JSR  LDCPOS
    RTS
;Poke a value into OS variables
;A=Osbyte code, X=Value
OSVWR LDY  #0
    JSR  OSBYTE
    RTS
;Peek a value from OS variables
;A=Osbyte code
OSVRD LDY  #&FF
    LDX  #0
    JSR  OSBYTE
    RTS

```



# D

## Gaussian Quadrature Programs

```
PROGRAM Gaussian_Quadrature_1 (INPUT, DataFile, OUTPUT);
(* This program is used to calculate the retardation of the cells
   thickness in microns for given values of U/U0.
   Calculates data for equations [3.35], [3.40], [3.42] and [3.44]
*)
CONST
  QuadSize = 96; (*size of the Gaussian quadrature*)
  K33 = 10.67; (*These four are the data for the liquid crystal*)
  K11 = 7.08;
  Epar = 20.1;
  Eperp = 6.228;
  n0 = 1.5335;
  ne = 1.7304;
  Esc = 27;
  Pi = 3.141592654;
TYPE
  QuadArray = ARRAY [1..QuadSize] OF REAL;
VAR
  Phi : QuadArray;
  X : QuadArray;
  C : QuadArray;
  PhiAlpha : QuadArray;
  I : INTEGER;
  ThetaMax : INTEGER;
  dummy : INTEGER;
  Top : REAL;
  Bottom : REAL;
  K,M,V : REAL;
  LeaveC : CHAR;
  DataFile : TEXT;
  FileName : STRING;
FUNCTION RAD (Degrees : REAL) : REAL;
CONST Radians = 180;
BEGIN
  RAD := ((Degrees*Pi)/Radians);
END;
FUNCTION ASN (x:REAL) : REAL;
BEGIN
  IF x = 1.0 THEN ASN := Pi/2
  ELSE ASN := ARCTAN(x/SQRT(1-x*x));
END;
PROCEDURE InitArrays;
VAR i : INTEGER;
BEGIN
  K := K33 - K11;
```

```

M := (Epar-Eperp)/Eperp;
V := (SQR(ne)-SQR(n0))/SQR(n0);
(* data for a 96-point Gaussian quadrature - FIRST HALF *)
(* X data Constant data *)
WRITELN('Got first half of data.');
```

X[1]	:= 0.01627675;	C[1]	:= 0.03255061;
X[2]	:= 0.04881299;	C[2]	:= 0.03251612;
X[3]	:= 0.08129749;	C[3]	:= 0.03244716;
X[4]	:= 0.1136959;	C[4]	:= 0.03234382;
X[5]	:= 0.1459737;	C[5]	:= 0.0322062;
X[6]	:= 0.1780969;	C[6]	:= 0.03203446;
X[7]	:= 0.2100313;	C[7]	:= 0.03182876;
X[8]	:= 0.2417432;	C[8]	:= 0.03158933;
X[9]	:= 0.2731988;	C[9]	:= 0.03131643;
X[10]	:= 0.3043649;	C[10]	:= 0.03101033;
X[11]	:= 0.3352085;	C[11]	:= 0.03067138;
X[12]	:= 0.3656968;	C[12]	:= 0.03029991;
X[13]	:= 0.4797639;	C[13]	:= 0.02989634;
X[14]	:= 0.425479;	C[14]	:= 0.02946109;
X[15]	:= 0.4547094221;	C[15]	:= 0.02899461;
X[16]	:= 0.4834579739;	C[16]	:= 0.02849741;
X[17]	:= 0.5116941771;	C[17]	:= 0.02797001;
X[18]	:= 0.5393881083;	C[18]	:= 0.02741296;
X[19]	:= 0.5665104185;	C[19]	:= 0.02682687;
X[20]	:= 0.5930323647;	C[20]	:= 0.02621234;
X[21]	:= 0.6189258401;	C[21]	:= 0.02557004;
X[22]	:= 0.6441634037;	C[22]	:= 0.02490063;
X[23]	:= 0.66871831;	C[23]	:= 0.02420484;
X[24]	:= 0.6925645366;	C[24]	:= 0.0234834;
X[25]	:= 0.7156768123;	C[25]	:= 0.02273707;
X[26]	:= 0.7380306437;	C[26]	:= 0.02196664;
X[27]	:= 0.7596023411;	C[27]	:= 0.02117294;
X[28]	:= 0.7803690483;	C[28]	:= 0.0203568;
X[29]	:= 0.8003087441;	C[29]	:= 0.01951908;
X[30]	:= 0.8194003107;	C[30]	:= 0.01866068;
X[31]	:= 0.8376235112;	C[31]	:= 0.0177825;
X[32]	:= 0.8549590334;	C[32]	:= 0.01688548;
X[33]	:= 0.8713885059;	C[33]	:= 0.01597056;
X[34]	:= 0.8868945174;	C[34]	:= 0.01503872;
X[35]	:= 0.9014606353;	C[35]	:= 0.01409094;
X[36]	:= 0.9150714231;	C[36]	:= 0.01312823;
X[37]	:= 0.9277124567;	C[37]	:= 0.0121516;
X[38]	:= 0.9393703397;	C[38]	:= 0.0111621;
X[39]	:= 0.9500327177;	C[39]	:= 0.01016077;
X[40]	:= 0.9596882914;	C[40]	:= 0.009148671;
X[41]	:= 0.9683268284;	C[41]	:= 0.008126877;
X[42]	:= 0.9759391745;	C[42]	:= 0.007096471;
X[43]	:= 0.9825172635;	C[43]	:= 0.006058545;
X[44]	:= 0.9880541263;	C[44]	:= 0.005014203;
X[45]	:= 0.9925439003;	C[45]	:= 0.003964555;
X[46]	:= 0.9959818429;	C[46]	:= 0.002910732;
X[47]	:= 0.9983643758;	C[47]	:= 0.001853961;
X[48]	:= 0.9996895038;	C[48]	:= 0.000796792;

```

FOR i := 1 TO 48 DO

```

```

        BEGIN
        X[i+48] := -X[i];
        C[i+48] := C[i];
        END;
        WRITELN('Got second half of data.');
```

END;

```

PROCEDURE TheCore;
VAR
    ThetaMax : INTEGER;
    N : REAL;
    I : INTEGER;
    IAns1, IAns2 : REAL;
    IAns3 : REAL;
    Result : REAL;
    U : REAL;
    Beta : REAL;
    MaxPercent : REAL;
    Step : INTEGER;
    tilt : INTEGER;
    UpperLimit : INTEGER;
    LowerLimit : INTEGER;
    d : INTEGER;
    times : INTEGER;
BEGIN
    WRITE('Input the number of degree increments -> ');
    READ(Step);
    UpperLimit := (90 DIV Step);
    WRITELN('Upper Limit =', UpperLimit:4);
    WRITE('Input thickness in microns (default=100) -> '); READ(d);
    IF d = 0 THEN d := 100; (*Thickness in microns*)
    WRITE('Enter the initial tilt angle (in degrees) -> ');
    READ(tilt);
    WRITE('Enter filename with extension -> '); READLN(FileName); WRITELN;
    IF FileName="" THEN FileName := 'MYDATA.DAT';
    REWRITE(DataFile, FileName);
    IF tilt = 0 THEN LowerLimit := 0
    ELSE BEGIN
        IF tilt MOD Step <> 0 THEN LowerLimit := (tilt DIV Step) + 1
        ELSE LowerLimit := tilt DIV Step
    END;
    FOR I:= 1 TO QuadSize DO BEGIN
        Phi[I] := SQR(SIN((((Pi/4)-(Beta/2))*X[I])+(Pi/4)+(Beta/2)));
    END;
    FOR times:= 1 TO 4 DO BEGIN (*New bit is here-for VAX FITZ file plot*)
        WRITELN(DataFile, 'Num points =', (UpperLimit+1):2,
        'ThetaMax start =', LowerLimit:3);
        FOR ThetaMax := LowerLimit TO UpperLimit DO (*loop1*)
            BEGIN
                IF tilt > 0 THEN Beta := ASN(SIN(RAD(tilt))/SIN(RAD(ThetaMax*Step)))
                ELSE Beta := 0;
                N := SQR(SIN(RAD(ThetaMax*Step)));
                IAns1:=0; IAns2:=0; IAns3:=0; Result:=0; (*Initialising the variables*)
                WRITE('Theta Max = ', ThetaMax*Step:2, ' ');
                (* WRITE(DataFile, 'ThetaMax =', ThetaMax*Step:2); *)
            END
        END
    END

```

```

FOR I := 1 TO QuadSize DO (*loop2*)
BEGIN
    Bottom := ((1+K*N*Phi[I])*(1+M*N*Phi[I]))/(1-N*Phi[I]);
    U := ((1+K*N*Phi[I])*(1+M*N))/((1+M*N*Phi[I])*(1-N*Phi[I]));
    Top := Bottom/(1+V*N*Phi[I]);
    IAns1 := IAns1+(C[I]*SQRT(Top));
    IAns2 := IAns2+(C[I]*SQRT(Bottom));
    IAns3 := IAns3+(C[I]*SQRT(U));
END; (*loop2*)
Result := ((IAns1/IAns2)*d*ne)-(d*n0); (*The external summators cancel*)
IAns3 := ((2/Pi)*((Pi/4)-(Beta/2)))*IAns3;
IF ThetaMax = LowerLimit THEN MaxPercent := Result;
CASE times OF
1 : BEGIN
    WRITELN(' U/U0 = ',IAns3:7:4);
    WRITELN(DataFile, IAns3:7:4);
END;
2 : BEGIN
    WRITELN(' U = ',IAns3*Pi*SQRT(K11/(8.854191*(Epar-Eperp))):7:4);
    WRITELN(DataFile, IAns3*Pi*SQRT(K11/(8.854191*(Epar-Eperp))):7:4);
END;
3 : BEGIN
    WRITELN(' Retd = ',Result:7:4);
    WRITELN(DataFile,Result:7:4);
END;
4 : BEGIN
    WRITELN('          WRITELN(DataFile,(Result/MaxPercent)*100:6:2);
END;
END; (*case*)
END; (*loop1*)
END; (*The new bit*)
END; (*TheCore*)
BEGIN (*main*)
    WRITE(CHR(Esc),'E'); (*Clearscreen*)
    InitArrays;
    TheCore;
    WRITE('Done — Press SPACE to continue -> ');
    REPEAT
        READ(LeaveC)
    UNTIL LeaveC = ' ';
    WRITELN;
END. (*main*)
(*****
PROGRAM Gaussian_Quadrature_2 (INPUT, DataFile, OUTPUT);
(* This program is similar to gauss1.pas above except it calculates data
for equations [3.36] & [3.43]
Purpose : To calculate the equations relating s/d to Theta and Theta max
Input : User is asked for the start value of theta max and the value
by which to increment it (until > 90 degs). Initial tilt angle
of liquid crystal at glass surface. Filename by which to save the
data as.
Output : The data is written to the screen and the disk A:
Data Format : Value of ThetaMax, Theta, s/d, Alpha, Beta (on screen)
*)

```

```

CONST
  QuadSize = 96; (*size of the Gaussian quadrature*)
  K33 = 10.67; (*These four are the data for the liquid crystal*)
  K11 = 7.08;
  Epar = 20.1;
  Eperp = 6.228;
  n0 = 1.5335;
  ne = 1.7304;
  Eac = 27;
  Pi = 3.141592654;
TYPE
  QuadArray = ARRAY [1..QuadSize] OF REAL;
VAR
  Phi : QuadArray;
  X : QuadArray;
  C : QuadArray;
  PhiAlpha : QuadArray;
  I : INTEGER;
  ThetaMax : INTEGER;
  dummy : INTEGER;
  Top : REAL;
  Bottom : REAL;
  K,M,V : REAL;
  LeaveC : CHAR;
  DataFile : TEXT;
  FileName : STRING;
FUNCTION RAD (Degrees : REAL) : REAL;
CONST Radians = 180;
BEGIN
  RAD := ((Degrees*Pi)/Radians);
END;
FUNCTION ASN (x:REAL) : REAL;
BEGIN
  IF x = 1.0 THEN ASN := Pi/2
  ELSE ASN := ARCTAN(x/SQRT(1-x*x));
END;
PROCEDURE InitArrays;
VAR i : INTEGER;
BEGIN
  K := K33 - K11;
  M := (Epar-Eperp)/Eperp;
  V := (SQR(ne)-SQR(n0))/SQR(n0);
  (* data for a 96-point Gaussian quadrature - FIRST HALF *)
  (* X data Constant data *)
  WRITELN('Got first half of data.');
```

i	X[i]	C[i]
1	0.01627675	0.03255061
2	0.04881299	0.03251612
3	0.08129749	0.03244716
4	0.1136959	0.03234382
5	0.1459737	0.0322062
6	0.1780969	0.03203446
7	0.2100313	0.03182876
8	0.2417432	0.03158933
9	0.2731988	0.03131643

```

  X[1] := 0.01627675; C[1] := 0.03255061;
  X[2] := 0.04881299; C[2] := 0.03251612;
  X[3] := 0.08129749; C[3] := 0.03244716;
  X[4] := 0.1136959; C[4] := 0.03234382;
  X[5] := 0.1459737; C[5] := 0.0322062;
  X[6] := 0.1780969; C[6] := 0.03203446;
  X[7] := 0.2100313; C[7] := 0.03182876;
  X[8] := 0.2417432; C[8] := 0.03158933;
  X[9] := 0.2731988; C[9] := 0.03131643;

```

```

X[10] := 0.3043649; C[10] := 0.03101033;
X[11] := 0.3352085; C[11] := 0.03067138;
X[12] := 0.3656968; C[12] := 0.03029991;
X[13] := 0.4797639; C[13] := 0.02989634;
X[14] := 0.425479; C[14] := 0.02946109;
X[15] := 0.4547094221; C[15] := 0.02899461;
X[16] := 0.4834579739; C[16] := 0.02849741;
X[17] := 0.5116941771; C[17] := 0.02797001;
X[18] := 0.5393881083; C[18] := 0.02741296;
X[19] := 0.5665104185; C[19] := 0.02682687;
X[20] := 0.5930323647; C[20] := 0.02621234;
X[21] := 0.6189258401; C[21] := 0.02557004;
X[22] := 0.6441634037; C[22] := 0.02490063;
X[23] := 0.66871831; C[23] := 0.02420484;
X[24] := 0.6925645366; C[24] := 0.0234834;
X[25] := 0.7156768123; C[25] := 0.02273707;
X[26] := 0.7380306437; C[26] := 0.02196664;
X[27] := 0.7596023411; C[27] := 0.02117294;
X[28] := 0.7803690483; C[28] := 0.0203568;
X[29] := 0.8003087441; C[29] := 0.01951908;
X[30] := 0.8194003107; C[30] := 0.01866068;
X[31] := 0.8376235112; C[31] := 0.0177825;
X[32] := 0.8549590334; C[32] := 0.01688548;
X[33] := 0.8713885059; C[33] := 0.01597056;
X[34] := 0.8868945174; C[34] := 0.01503872;
X[35] := 0.9014606353; C[35] := 0.01409094;
X[36] := 0.9150714231; C[36] := 0.01312823;
X[37] := 0.9277124567; C[37] := 0.0121516;
X[38] := 0.9393703397; C[38] := 0.0111621;
X[39] := 0.9500327177; C[39] := 0.01016077;
X[40] := 0.9596882914; C[40] := 0.009148671;
X[41] := 0.9683268284; C[41] := 0.008126877;
X[42] := 0.9759391745; C[42] := 0.007096471;
X[43] := 0.9825172635; C[43] := 0.006058545;
X[44] := 0.9880541263; C[44] := 0.005014203;
X[45] := 0.9925439003; C[45] := 0.003964555;
X[46] := 0.9959818429; C[46] := 0.002910732;
X[47] := 0.9983643758; C[47] := 0.001853961;
X[48] := 0.9996895038; C[48] := 0.000796792;
FOR i := 1 TO 48 DO
  BEGIN
    X[i+48] := -X[i];
    C[i+48] := C[i];
  END;
  WRITELN('Got second half of data.');
```

```

END;
PROCEDURE TheCore;
VAR ThetaMax : INTEGER;
    Theta : INTEGER;
    ThetaInc : REAL;
    N : REAL;
    I : INTEGER;
    IAns1, IAns2 : REAL;
    IAns3 : REAL;
```

```

Result : REAL;
U : REAL;
Beta : REAL;
Alpha : REAL;
MaxPercent : REAL;
Step : INTEGER;
ThetaTilt : INTEGER;
UpperLimit : INTEGER;
LowerLimit : INTEGER;
d : INTEGER;
times : INTEGER;
ZoverD : REAL;
TMStart, TMInc : INTEGER;
BEGIN (* The new Core *)
  WRITE('Input Theta Max start AND step values (e.g. 86,1) -> ');
  READLN(TMStart, TMInc); Put pratt proofing in here at a later date
  WRITE('Enter the initial tilt angle (in degrees) -> ');
  READ(ThetaTilt);
  WRITE('Enter filename with extension -> ');
  READLN(FileName); WRITELN;
  IF FileName="" THEN FileName := 'FIG3.11.DAT';
  REWRITE(DataFile, FileName);
  IF ThetaTilt = 0 THEN BEGIN LowerLimit := 0; Beta := 0.0; END
    ELSE LowerLimit := ThetaTilt;
  ThetaMax := TMStart;
  WHILE ThetaMax /= 90 DO BEGIN
    WRITELN(DataFile, 'Theta max =', ThetaMax:3,
      ' Num points =', ((ThetaMax-LowerLimit)+1):3,
      ' Start Theta =', LowerLimit:3);
    FOR I:= 1 TO QuadSize DO
      Phi[I] := SQR(SIN((((Pi/4)-(Beta/2))*X[I])+(Pi/4)+(Beta/2)));
      N := SQR(SIN(RAD(ThetaMax)));
      IF ThetaTilt <> 0 THEN Beta := ASN(SIN(RAD(ThetaTilt))/SIN(RAD(ThetaMax)));
      Bottom := 0.0; IAns2 := 0.0;
      FOR I := 1 TO QuadSize DO BEGIN
        Bottom := ((1+K*N*Phi[I])*(1+M*N*Phi[I]))/(1-N*Phi[I]);
        IF Bottom /= 0 THEN WRITELN('Negative bottom at I =', I:3);
        IAns2 := IAns2+(C[I]*SQRT(Bottom)*((Pi/4)-(Beta/2)));
      END;
      FOR Theta := LowerLimit TO ThetaMax DO BEGIN (* loop1 *)
        Alpha := ASN(SIN(RAD(Theta))/SIN(RAD(ThetaMax)));
        FOR I := 1 TO QuadSize DO
          Phi[I] := SQR(SIN((((Alpha-Beta)/2)*X[I])+((Alpha+Beta)/2)));
          Top := 0.0; IAns1 := 0.0;
          FOR I := 1 TO QuadSize DO BEGIN
            Top := ((1+K*N*Phi[I])*(1+M*N*Phi[I]))/(1-N*Phi[I]);
            IF Top /= 0 THEN WRITELN('Negative Top at I =', I:3);
            IAns1 := IAns1+(C[I]*SQRT(Top)*((Alpha-Beta)/2));
          END;
          ZoverD := (IAns1/IAns2)/2;
          WRITELN('Theta Max =', ThetaMax:3, ' Theta =', Theta:3,
            ' ZoverD =', ZoverD:7:4, ' Alpha =', Alpha:5:2,
            ' Beta =', Beta:5:2);
          WRITELN(DataFile, ZoverD:7:4);
        END;
      END;
    END;
  END;

```

```

    END; (* loop1 *)
    ThetaMax := ThetaMax + TMInc;
  END; (* WHILE ThetaMax *)
END; (* new Core *)
BEGIN (*main*)
  WRITE(CHR(Esc),'E'); (*Clearscreen*)
  InitArrays;
  TheCore;
  WRITE('Done — Press SPACE to continue -> ');
  REPEAT
    READ(LeaveC)
  UNTIL LeaveC = ' ';
  Writeln;
END. (*main*)

```



# E

## Liquid Crystal Parameters

E. Merck, Darmstadt		ZLI -	1646	1695	1800		2244		2359	2363
					- 000	- 100	- 000	- 100		
Melting point	/ °C		- 7	(S-S) +6	- 9	- 7	- 5	- 6	- 9	- 21
Transition S - N	/ °C		< - 20	+ 13	< - 20	< - 20	< - 20	< - 20	< - 20	< - 30
Clearing point	/ °C		+ 60	+ 72	+ 60	+ 61	+ 85	+ 94	+ 68	+ 89
Viscosity $\nu$	/ mm <sup>2</sup> · s <sup>-1</sup>									
	at 20 °C		26	62	29	23	36	31	28	36
	at 0 °C		88		105	75	135	108	93	130
	at -20 °C						870		520	835
Dielectric anisotropy	$\epsilon_{  }$		10,6	7,8	11,8	3,9	11,7	6,4	7,1	11,9
	$\epsilon_{\perp}$		4,6	3,6	4,8	1,6	5,3	4,0	4,5	5,4
	$\Delta\epsilon = \epsilon_{  } - \epsilon_{\perp}$		+ 6,0	+ 4,2	+ 7,0	+ 2,3	+ 6,4	+ 2,4	+ 2,6	+ 6,5
Optical anisotropy	$\Delta n = n_e - n_o$		0,08	0,06	0,08	0,07	0,076	0,075	0,05	0,081
Threshold voltage	$V_{10(0,20)} / V$		1,88	2,3	1,72	2,53	1,96	3,02	2,32	2,04
Saturation voltage	$V_{90(0,20)} / V$		2,59	3,3	2,21	3,34	2,71	4,13	3,43	2,90
Temp. dependence (0 °C to 40 °C)	$dV / dT / mV \cdot \text{grad}^{-1}$		11,1		10,0	14,9	8,3	13,1	14,8	9,4
	$\delta / \% \cdot \text{grad}^{-1}$		0,60		0,59	0,59	0,42	0,43	0,82	0,45
Sharpness	$(V_{s0} / V_{i0} - 1) \cdot 100$		13,3	17,0	14,5	13,0	13,8	12,9	19,0	14,2
	$(V_{s0} / V_{i0} - 1) \cdot 100$		37,8	45,2	28,5	36,0	38,3	36,8	47,8	42,1
Margin	$M_{20}$		1,78		1,63	1,67	1,94	1,85	1,88	2,04
	$M_{0-40}$		2,21		2,15	2,04	2,28	2,15	2,33	2,34
	$M'_{0-40}$		1,66		1,60	1,57	1,69	1,63	1,75	1,70

E. Merck, Darmstadt		ZLI -	1221	1612	1840	1982	2061	2214	2392	2892
Melting point	/ °C		- 11	- 11	- 15	- 15	- 10	- 10	- 20	- 17
Transition S - N	/ °C		< - 30	< - 20	< - 20	< - 20	< - 20	< - 10	< - 20	< - 30
Clearing point	/ °C		+ 90	+ 90	+ 90	+ 91	+ 91	+116	+105	+ 86
Viscosity $\nu$	/ mm <sup>2</sup> · s <sup>-1</sup>									
	at 20 °C		40	40	31	26	41	37	38	18
	at 0 °C		170	168	118	95	204	152	158	56
	at -20 °C		1800		975	630			1300	292
	at -30 °C		10000		3670	2330			12000	1017
Dielectric anisotropy	$\epsilon_{  }$		12,6	14,7	16,8	14,4	23,8	15,5	18,1	9,0
	$\epsilon_{\perp}$		4,6	4,8	4,6	4,2	5,5	4,2	5,0	3,6
	$\Delta\epsilon = \epsilon_{  } - \epsilon_{\perp}$		+ 8,0	+ 9,9	+ 12,2	+ 10,2	+ 18,3	+ 11,3	+ 13,1	+ 5,4
Optical anisotropy	$\Delta n = n_e - n_o$		0,13	0,18	0,15	0,14	0,18	0,16	0,15	0,125
Threshold voltage	$V_{10(0,20)} / V$		1,93	1,83	1,92	1,82	1,64	2,17	1,91	2,53
Saturation voltage	$V_{90(0,20)} / V$		2,89	2,69	2,64	2,71	2,24	2,90	2,82	3,44
Temp. dependence (0 °C to 40 °C)	$dV / dT / mV \cdot \text{grad}^{-1}$		8,0	7,4	9,0	8,8	7,1	6,8	7,1	11,6
	$\delta / \% \cdot \text{grad}^{-1}$		0,41	0,40	0,47	0,45	0,43	0,31	0,37	0,45
Sharpness	$(V_{s0} / V_{i0} - 1) \cdot 100$		15,0	17,5	15,1	16,1	15,2	13,8	16,8	14,2
	$(V_{s0} / V_{i0} - 1) \cdot 100$		39,4	47,0	37,5	41,7	36,6	33,6	47,6	36,0
Margin	$M_{20}$		1,85	2,00	1,92	1,92	1,88	1,77	2,07	1,71
	$M_{0-40}$		2,11	2,30	2,24	2,23	2,21	1,97	2,38	1,94
	$M'_{0-40}$		1,57	1,65	1,68	1,62	1,66	1,51	1,68	1,47

ProQuest Number: 29223012

INFORMATION TO ALL USERS

The quality and completeness of this reproduction is dependent on the quality and completeness of the copy made available to ProQuest.



Distributed by ProQuest LLC (2022).

Copyright of the Dissertation is held by the Author unless otherwise noted.

This work may be used in accordance with the terms of the Creative Commons license or other rights statement, as indicated in the copyright statement or in the metadata associated with this work. Unless otherwise specified in the copyright statement or the metadata, all rights are reserved by the copyright holder.

This work is protected against unauthorized copying under Title 17,  
United States Code and other applicable copyright laws.

Microform Edition where available © ProQuest LLC. No reproduction or digitization of the Microform Edition is authorized without permission of ProQuest LLC.

ProQuest LLC  
789 East Eisenhower Parkway  
P.O. Box 1346  
Ann Arbor, MI 48106 - 1346 USA